Realistic Cellular Automaton Model for Synchronized Two-Lane Traffic

Simulation, Validation, and Applications

Vom Fachbereich Physik
der Universität Duisburg-Essen
zur Erlangung des akademischen Grades
eines Doktors der Naturwissenschaften
genehmigte Dissertation

von
Andreas Pottmeier
aus
Krefeld

Referent: Prof. Dr. Michael Schreckenberg
Korreferent: Prof. Dr. Dietrich E. Wolf
Tag der mündlichen Prüfung: 18. Dezember 2007

Contents

Abstract

An objective of current traffic-research is the realistic description of vehicular traffic by means of traffic modeling. Since no present traffic model is capable to reproduce all empirical characteristics, the development of such a model is of main interest. Thus, this thesis presents a realistic cellular automaton model for multi-lane traffic and validates it by means of empirical single-vehicle data. In contrast to present approaches a limited deceleration capability is assigned to the vehicles. Moreover, the velocity of the vehicles is determined on the basis of the local neighborhood. Therefore, the drivers are divided into optimistic or pessimistic drivers. The former may underestimate their safety distance if their neighborhood admits it. The latter always keep a safe distance. This results in a convincing reproduction of the microscopic and macroscopic features of synchronized traffic. The anticipation of the leader's velocity is thereby essential for the reproduction of synchronized traffic.

This thesis is divided into three main parts. The first one validates the single-lane model by Lee et al. by means of empirical data. This approach builds the basis for the further developments of this thesis. Then, the fundamental characteristics are summarized. This is followed by new results concerning the comparison with empirical findings that confirm the good reproduction of the reality. The analyses also show the important and fundamental property of synchronized traffic: its density dependent life-time. Nevertheless, accidents appear in the stationary state. Thus, the model approach has to be modified so that it is capable to model multi-lane traffic.

The adapted model is enhanced in the next part by a realistic lane change algorithm. A multi-lane model is formulated that reproduces the empirical data even better than the single-lane approach. Moreover, specific two-lane characteristics like the density dependent lane change frequency are reproduced as well as the coupling of the lanes. Moreover, if the velocity difference between the two lanes is too high, the lanes may decouple, i.e., different traffic states emerge on the two lanes. This is a direct consequence of the limited deceleration capability of the vehicles.

In the last part of the thesis the two-lane model is applied to open systems with bottlenecks like an on-ramp and a speed-limit. The empirically observed complex structures of the synchronized traffic are reproduced here in great detail. Thus, the approach discussed in this thesis exceeds the present in the degree of realism. Because of the reliability of the presented model it is supposed to be implemented to simulate the whole network of North Rhine-Westphalia.

1 Preface

1.1 Introduction

For many road users traffic congestions are a daily recurring experience and they spent much time on the road standing in a traffic jam although much effort is made to avoid such situations.
In particular, two factors worsen the situation: On the one hand, the amount of vehicular traffic still rises. Especially, the number of trucks increses permanently. On the other hand, the extension of the network is seldom possible although the maximum capacity of many parts of the network is reached.
One approach to improve the current situation is to provide better traffic information that can be used on different levels: The road user would appreciate to know whether he has to expect traffic congestions on his way home or has to reschedule his departure. The traffic authorities can use this information to route the traffic and reallocate it. This is especially beneficial when the road network is dense like in North Rhine-Westphalia. Here, the road user can often choose between alternative routes to his destination.
A vivid example for such a traffic information system for every road user is the Internet platform "autobahn.nrw.de". It provides the traffic state of the autobahn network of North-Rhine Westphalia on the Internet and is extended frequently, e.g, travel times are calculated for the most important meshes of the network.
This traffic information system is based on a microscopic simulation that is fed by traffic data gathered throughout the network. It enhances the quality of the pure traffic data that is acquired on the road as by this means, e.g, enhanced information like travel times can be generated. The precondition for usable information, is a simulation model that reproduces the road traffic with a high degree of realism.
Thus, it is not surprising that the simulation of vehicular traffic has risen much interest in recent years not only from the theoretical point of view but also on the application level. The advances in the modeling methodology increased the degree of realism, the fundamental relations are better understood than ever and a connection between the drivers impression and empirical observations was found. The driver faces roughly three different traffic states: He drives as fast as he wants undisturbed by the other vehicles, he moves in a great bunch of vehicles not very fast but steadily, or he stands for a long time in a dense traffic jam. These three states are found in the microscopic empirical data so that a distinction between free flow, synchronized traffic, and wide jams was proposed by Kerner [72]. The characteristics of the states were investigated and extensive knowledge on the microscopic level was gained in recent time. Nevertheless, some aspects of the microscopic behavior of the vehicles are still not known exactly. Whereas the fundamental relations in free-flow and in dense traffic of wide moving jams seem to be understood very well, the existence, the concept, and the origin of synchronized traffic is still far behind that of free-flow and traffic jams.
Nevertheless, several empirical studies [43, 67, 69, 71, 75] describe the properties of synchronized traffic, and various model approaches have been proposed [21, 48, 51, 77, 81, 91]

which try to reproduce the basic characteristics. However, the models focus on the reproduction of the microscopic [91] or the macroscopic features [81] of the traffic states proposed by the three phase traffic theory. In addition, the reproduction of the microscopic features is still limited especially for synchronized traffic.
Thus, a better understanding of the mechanisms leading to the synchronized state is still necessary not only as it may be helpful to stabilize traffic and to increase the throughput of a road, thus, to improve the efficiency of the road-infrastructure. This is especially important as in synchronized state the throughput of vehicles is very high despite the high density.
Further, most traffic disturbances happen at bottlenecks like on-ramps. Thus, if the complex features of the emerging traffic at an on-ramp are understood more deeply, new approaches to optimize the traffic at junctions are possible and the knowledge can be used to control the traffic state on the main road by controlling the inflow. In particular, theoretical observations [59] have demonstrated that the travel-time of vehicles on a highway and on the corresponding on-ramp can be optimized by means of ramp metering. The benefits of these ramp metering systems are confirmed by several empirical studies [149].
These considerations show the large interest from the traffic engineer's point of view but the microscopic features are of special interest for physicists, too. Traffic can be understood as a complex system of many interacting particles driven far from equilibrium. In this context, especially the collective behavior of the vehicles that lead to synchronized traffic arouse the curiosity of the physicists. In contrast to many other fields of physics where the dynamics can be described by physical laws this is not the case for vehicular traffic as the microscopic features are still not understood well enough. Thus, better knowledge of the processes on the microscopic level can be gained by the analysis of traffic data and the formulation of an elaborate modeling approach. Here, it is the goal of the physicist to characterize the essential parts of the model dynamics. This means, that only a few parameters have to be considered and no fine-tuning of the parameters is necessary.
One approach to reach this aim are the widely adapted cellular automaton models. Introduced by von Neumann in the 1950ies [132] it was applied to vehicular traffic firstly by Cremer and Ludwig [25]. In 1992 Nagel and Schreckenberg [126] proposed an approach that despite its simplicity was able to reproduce basic features of traffic flow like spontaneous jam formation and stop-and-go patterns. This stochastic model was used for different traffic simulations like the network of the city of Duisburg [33, 34] and the Dallas/Forth-Worth area [146]. It was also utilized during the first steps to simulate the highway traffic in North-Rhine Westphalia [66].
Nevertheless, the current model approaches describe vehicular traffic not sufficiently. They reproduce some microscopic features very well but map some macroscopic features insufficiently [91] or concentrate mainly on the reproduction of macroscopic features of the three phase traffic theory [81]. Thus a more comprehensive approach is needed that covers both aspects: the reproduction of the microscopic and macroscopic findings.
Thus, in this thesis a more realistic multi-lane model approach is presented that reproduces the empirical findings on the macroscopic as well as on the microscopic level very well. Special concern is laid hereby on the reproduction of the empirical data in an analogue system as the source of the traffic data: a two-lane road.
Therefore, this thesis further enlightens the origin and the microscopic features of synchronized traffic and provides a more realistic model as the basis for traffic simulations and forecasts.

1.2 Outline

The outline of this thesis is as follows:
In chapter 2 the measurement techniques and traffic observables that are required to describe and classify the different traffic states are presented.
The empirically observed characteristics of highway traffic are discussed in the following and the main features of free-flow, synchronized traffic, and wide moving jams are provided and fundamental empirical facts are reviewed. Finally, empirical findings of multi-lane traffic are summarized.
In chapter 3 prominent cellular automaton models are presented. Based on the model by Nagel and Schreckenberg the methodology of the modeling concept is discussed. This model and two extended variants are analyzed and their features regarding the degree of realism in modeling the different traffic states are briefly discussed.
The following chapter reviews empirical data that are used to validate the presented cellular automaton model. On the one hand, locally and globally gathered aggregated data are presented and, on the other hand, single-vehicle data of the different traffic states are shown.
The results are utilized in chapter 5 to calibrate the cellular automaton model by Lee *et al.* [107] and to validate the model on a microscopic level. Special concern is thereby paid on the reproduction of the single-vehicle data. Further, the model is analyzed in great detail with respect to the model parameters and the accidents that occur in the model. The reasons for these dangerous configurations are presented and used to enhance the model so that it can form the basis for a convenient simulation of open systems and especially of two-lane traffic. Thus, in the next chapter the model by Lee *et al.* is extended by a realistic lane change algorithm. Its high degree of realism is validated by the comparison with single-vehicle data. It is important to note that the empirical data are also acquired on a multi-lane road. Again, the model parameters are analyzed with respect to their influence on the model dynamics.
In chapter 7 the extended model by Lee *et al.* is applied to more realistic scenarios. Main concern is the analysis of the characteristics of the traffic in the vicinity of an on-ramp. The spatiotemporal structure is compared with empirical findings by Kerner [73]. He found that synchronized traffic is according to the three phase traffic theory formed in different patterns. The reproduction of this patterns and therefore the high degree of realism of the model approach is validated in this chapter for the single-lane and the two-lane system. To compare these results with other kinds of bottlenecks the influence of a velocity defect is analyzed as well. Moreover, the life-time of the synchronized traffic that is formed at an on-ramp is discussed. The results help to understand the systematics that lead to a traffic break down and hint at alternative strategies to control the inflow at an on-ramp and thus increase its capacity.

2 Measuring Traffic Observables

The quality of theoretical models for traffic flow is – like in all other fields of physics – strongly depending on a good agreement with empirical findings. With respect to the particular goal of the modeling approach the degree of the needed accordance may change. For example, the analysis of an oversimplified model approach can be used to find the reason for a particular basic phenomenon in vehicular traffic [123]. Otherwise, a model should be as precise and realistic as possible to analyze complex scenarios like the influence of a ramp metering algorithm (see e.g. [79, 103, 135, 174]), simulate the traffic in a real network [34, 41, 134, 141, 169], or even forecast it [23, 134].
Nevertheless, it is a difficult task to validate a model even when there is a consensus about the underlying empirical phenomena: On the one hand, it has to be certain which aspect of real traffic is described by the model. On the other hand, the fundamental difficulty that no laboratory experiments can be performed has to be mastered. In contrast, the empirical data that can be established is not only acquired from mostly complex networks but it is also affected by – temporal – influences like speed limits, road works, or overtake ban for trucks or regular cars that cannot always be retraced completely so that the interpretation of these data is very complicated.
Nonetheless, in recent years many investigations were carried out and led to a more profound understanding of the empirical findings [45, 70, 73, 80, 84, 110, 130].

2.1 Measurement Observables

The description and analysis of vehicular traffic is based on empirical data that gives information about the driving state of the vehicle. If the data of all vehicles in the system – the road – are available, the complete traffic state can be described. But these information are not available in real life because only a limited number of vehicles can be observed. It is not possible today to trace every single vehicle[1].
Nevertheless, there are several approaches to collect traffic data trying to overcome these problems. All of these have their advantages and disadvantages. In general, data can be collected by moving or by stationary devices.
The stationary measuring offers two different strategies: locally acquired data and global quantities. The former data source is the usual way to detect the important quantities since it is simpler to install. The detecting devices are very often inductive loops that are incorporated in the road and detect vehicles passing them by their induced electric signal. If two loop detectors are connected the velocity can also be detected via the time difference of the impulses. Other methods to acquire local traffic data are infrared or radar based detectors.
With respect to all simulations in this theses virtual inductive loops are inserted at relevant positions. Here, flow and velocity are measured to directly allow an effective comparison of

[1] This might change if more vehicles are equipped with GPS devices, but data protection has to be considered.

simulation and empirical data. This offers the opportunity that the measuring process is as close to reality as possible and the discrepancies because of different measuring methods are kept as small as possible.
The data provided by inductive loops are for the sake of storage reasons usually given as temporally aggregated data. The typical averaging intervals vary from 30 seconds up to several minutes. One disadvantage of the data aggregation – especially of speed measurements – is that important details of their distribution are hidden. The density, if it is locally measured, can only be quantified if it is averaged in time. Otherwise, in city traffic it is harder to define a sufficient aggregation interval as the traffic is affected primarily by the traffic lights. Artifacts because of the measurement interval have to be avoided.
Globally measured values cover the whole street or mostly a limited part of it. This method gives direct access to the data of several vehicles at the same time and thus the density is a direct measure. Video detection devices give a practical method to get these global measures. But only in the recent time this measuring method got more important as the image processing algorithms become more effective and processing power increases drastically. Thus, until now very limited data are available from this source.
The second class of traffic data available is from moving devices. These are measurement vehicles that act as floating cars. These vehicles record their position and velocity beside other values. Some car-following experiments were made (e.g. [97, 129, 130]) were the floating-cars try to adapt the driving behavior of the surrounding traffic. Using the acquired data one tries to describe the traffic state but no information about the density is available. A larger number of floating cars would provide a better data basis but these are not available for practical and financial reasons. Thus, alternative approaches are made to get more floating car data. For example, data is gathered by taxis as their position is usually well known via their GPS signal. This approach is investigated, e.g., in the project "traffic on-line" [60] they should know the environment very well and can use shortcuts.
A very recent approach to get floating car information is the utilization of the data acquired by cell phones [1, 164]. The phone providers are able to locate the cellular phones quite accurately, especially if these phones use the UMTS-network, which is split in much smaller cells than the GSM network. Hence, the movement of the vehicles can be traced quite correctly. By these information the traffic state of whole networks could be detected. These data can also be used to build origin-destination matrices that are very valuable in traffic planning and for traffic management.
The empirical data used in this thesis are solely locally measured data in general provided by loop-detectors. Thus, for the later discussion it should be stressed that the measurements provided by counting loops are local, which has to be taken into account when comparing empirical findings with model results.
The most important measures that are used to describe vehicular traffic are the flow, the velocity, and the density in the investigated system. Mostly these measures are aggregated but also information about single vehicles are available.
The traffic flow J gives the number N of vehicles that pass a cross section in a given time interval $[t_0, t_0 + \Delta T]$:

$$J(t) = \frac{N(t)}{\Delta T}. \tag{2.1}$$

If the detector consists of two inductive loops that are installed in a row it is also possible to measure the velocity of the vehicles. The velocity of a single vehicle n is the ratio of

the distance Δx – here the distance between the two inductive loops – passed by a vehicle and the travel time Δt the vehicle needs to pass Δx:

$$v_n = \frac{\Delta x}{\Delta t}. \tag{2.2}$$

The assumption is only valid if Δt is infinitesimal small or the velocity is constant during the passing of the detectors. The latter may not be true in congested traffic with many interactions between the vehicles and thus there are strong fluctuations of the velocity. The arithmetic mean velocity $\langle v_{v_n}(t)\rangle$ of all N vehicles n which pass the detector in the time interval $t = t_0$ and $t = t_0 + \Delta T$ is then

$$\langle v_{v_n}(t)\rangle = \frac{1}{N(t)} \sum_{t_0 \le t_n < t_0 + \Delta T} v_n(t) = \frac{1}{N(t)} \sum_{t_0 \le t_n < t_0 + \Delta T} \frac{\Delta x}{\Delta t_n}. \tag{2.3}$$

The time Δt_n is the time vehicle n needs to pass the two inductive loops of the detector and Δx is the distance between the two loops.
As stated above, the aggregation of the velocity is unfavorable and not definite. Another approach to determine the mean velocity is to use the distance Δx divided by the mean passing time:

$$\langle v_{\Delta t_n}\rangle = \frac{\Delta x}{\frac{1}{N} \sum\limits_{t_0 \le t_n < t_0 + \Delta T} \Delta t_n}. \tag{2.4}$$

Because

$$\frac{1}{N} \sum_{t_0 \le t_n < t_0 + \Delta T} \frac{1}{\Delta t_n} \ge \left[\frac{1}{N} \sum_{t_0 \le t_n < t_0 + \Delta T} \Delta t_n \right]^{-1} \tag{2.5}$$

it holds

$$\langle v_{v_n}\rangle \ge \langle v_{\Delta t_n}\rangle. \tag{2.6}$$

The difference between both definitions is, that $\langle v_{v_n}\rangle$ is the mean velocity with regard to the number of measured vehicles N whereby $\langle v_{\Delta t_n}\rangle$ is the mean velocity with regard to the measurement period. The inequality (2.6) is now equivalent to the sum of the single velocities weighted by the part of the time the vehicle is located between the two detectors:

$$\begin{aligned} \langle v_{t_i}\rangle &= \frac{\Delta x}{\frac{1}{N} \sum\limits_{t_0 \le t_n < t_0 + \Delta T} \Delta t_n} = \frac{N \cdot \Delta x}{\sum\limits_{t_0 \le t_n < t_0 + \Delta T} \Delta t_n} \\ &= \frac{\Delta t_1}{\sum\limits_{t_0 \le t_n < t_0 + \Delta T} \Delta t_n} \frac{\Delta x}{\Delta t_1} + \ldots + \frac{\Delta t_n}{\sum\limits_{t_0 \le t_n < t_0 + \Delta T} \Delta t_n} \frac{\Delta x}{\Delta t_n} \\ &= \frac{\Delta t_1}{\sum\limits_{t_0 \le t_n < t_0 + \Delta T} \Delta t_n} v_1 + \ldots + \frac{\Delta t_n}{\sum\limits_{t_0 \le t_n < t_0 + \Delta T} \Delta t_n} v_N. \end{aligned} \tag{2.7}$$

That provides an obvious interpretation of Eq. (2.6). A low velocity is weighted more on $\langle v_{\Delta t_n}\rangle$ because the vehicle spends more time to pass the detector. As $\langle v_{\Delta t_n}\rangle$ reacts more sensible to erroneous measurements for small velocities, the mean velocity is calculated by $\langle v_{v_n}\rangle$.
Another important measure is the time headway distribution, i.e., the difference of the passing times of vehicle n and its succeeding one $n-1$ $t_n^h = t_n - t_{n-1}$.

This quantity can also be detected by most inductive loops. It is a very important value to compare with simulation results as no corrections are needed and no ambiguities appear. The reproduction of this measuring method in a micro-simulation with discrete space and time like in cellular automata is problematic. Here, the temporal discretization introduces a typical time-scale that corresponds to the reaction time in other car following models. The measurement of the time headways is also affected as this reaction time is represented by a strong peak. Using a smaller discretization reduces this effect but does not eliminate it. To reduce these drawbacks and to increase the resolution the time headway is measured as follows.
The basis for a correct measurement is build on an accurate determination of the time a vehicle reaches the detector. In general, a fast vehicles passe the detector in one time-step. This means it effectively reaches the detector at a fraction of this time-step. Therefore, if the time a vehicle reaches the detector is measured accurately the time headway is simply the difference of the passing times. Thus, the time vehicle n passes the detector t_n is calculated as:

$$t_n = T_0 + \frac{x_{\text{det}} - x_n}{v_n}. \tag{2.8}$$

Here, T_0 is the time at the beginning of the update step and x_{det} the position of the detector. Now the resolution of the passing times reaches the maximum possible value, i.e., the reciprocal maximum velocity $\frac{1}{v_{\max}}$. Then the time headway is given as:

$$t_{\text{h}}^n = t_n - t_{n-1}. \tag{2.9}$$

This approach mimics the measuring method of the inductive loops very well. Different approaches like $t_{\text{n}}^{\text{h}} = \frac{x_n - x_{n-1}}{v_n}$ are less accurate.
By means of the temporal headway it is possible to calculate the net distance headway d_n – the bumper-to-bumper distance:

$$d_n = v_n \cdot t_{\text{h}}^n - l_{n-1}. \tag{2.10}$$

Using the velocity v_n is somehow arbitrary since v_{n-1} can also be taken. The latter would lead to the calculation of the headway in upstream direction rather than downstream. This distance is often called gap_n which has the same meaning.
Nevertheless, the difference between both calculations should be negligible if the distances are small and therefore the surrounding traffic upstream and downstream of the measurement location should be homogeneous. Again, the calculation of the distance headway is based on the assumption that the velocity of both vehicles does not change significantly.
In contrast to the locally measured quantities discussed up to now the density has to be measured on a section of a highway. In principle, it is not possible to measure this by means of inductive loops. A measuring method that covers an extended part of the road should be used here. Nevertheless, most of the detection is done by means of inductive loops or other local measuring devices. Thus, an approximation of the spatial density by the local measures has to be found. The idea is to utilize the hydrodynamic relation and calculate the density via

$$\rho_t = \frac{J_t}{v_t}. \tag{2.11}$$

This is a problematic approach since the detector only measures data when a vehicle passes it, which means, that it is an event driven measurement. Therefore, the velocity

is overestimated in congested traffic. This leads to an underestimation of the density. In the fundamental diagram the density approaches zero in the congested regime as only a few vehicles drive and could therefore be detected.
A different approach to derive the density by means of local counts is to measure the fraction of time the inductive loop is occupied by a vehicle. This occupation is calculated as

$$occ_t = \frac{1}{T} \sum_{t \le t_n \le t+T} \Delta t_n = \frac{1}{T} \sum_{t \le t_n \le t+T} \frac{l_n}{v_n}, \tag{2.12}$$

thereby is Δt_n the time the inductive loop – only one of the two loops measures the occupation – is covered by vehicle n in the time interval T.
The occupancy can be related to the density under the assumption that they are proportional to each other. The observations of [97] support this assumption. An occupancy of one means that vehicles are standing bumper to bumper which leads to a density $\rho_{\max}$ of

$$\rho_{\max} = \frac{N}{\sum_{n=1}^{N} l_n} = \frac{1}{\langle l \rangle}, \tag{2.13}$$

with the mean length $\langle l \rangle$ of N vehicles passing the detector in the time T. Then, the relation between the occupancy and the density is quite simple. Under the assumption of a constant velocity of the vehicles during averaging one finds:

$$\rho = occ_t \cdot \rho_{\max} = \frac{occ_t}{\langle l \rangle}. \tag{2.14}$$

Two approximations for $\rho_{\max}$ can be found in literature: $\rho_{\max} \approx 133\frac{1}{3}\,\text{veh/km}$ [126] or $\rho_{\max} \approx 140\,\text{veh/km}$ [129]. The first value is used throughout this thesis.
Using the occupation one finds now a wide range of densities with the same flow that cover a triangular region in the fundamental diagram.
In contrast to the local measures, global readings are provided by measuring the whole highway. These information are hardly to acquire. Video detection is one approach that can observe at least a part of a highway section. In contrast, in simulations global quantities can easily be calculated. These measures give a complete picture of the extended traffic state like the length of a jam or a synchronized regime and are therefore very valuable. The local measurements can only give an approximation of these extensions.
In a simulation environment the global quantities are more or less obtained directly. The occupation *occ* is just the fraction of the road with total length L that is covered by a vehicle. If N is the number of vehicles and l_n the length of the nth vehicle, the occupation is calculated as follows:

$$occ_{\text{g}} = \frac{\sum_{n=1}^{N} l_n}{L}. \tag{2.15}$$

The density ρ_{g} is simply the number of vehicles on the highway divided by the length of the latter

$$\rho_{\text{g}} = \frac{N}{L}. \tag{2.16}$$

The global mean velocity is the average of the single velocities v_n

$$v_{\text{g}} = \frac{1}{N} \sum_{n=1}^{N} v_n. \tag{2.17}$$

Using the hydrodynamical relation again the global flow can be obtained

$$\begin{aligned} J_{\mathrm{g}} &= \rho_{\mathrm{g}} \cdot v_{\mathrm{g}} \\ &= \frac{N}{L} \cdot \frac{1}{N} \sum_{n=1}^{N} v_n \\ &= \frac{1}{L} \sum_{n=1}^{N} v_n. \end{aligned} \tag{2.18}$$

With respect to cellular automata, which are of main interest in this thesis, the occupation ratio is simply the number of occupied cells divided the total number of cells L_{ca} of the system:

$$occ_{\mathrm{ca}} = \sum_{n=1}^{N} \frac{l_{n,\mathrm{ca}}}{L_{\mathrm{ca}}}. \tag{2.19}$$

If all vehicles have the same length, i.e., they cover the same number of cells this sum simplifies to:

$$occ_{\mathrm{ca}} = \frac{N \cdot l_{\mathrm{ca}}}{L_{\mathrm{ca}}}. \tag{2.20}$$

The density is calculated following Eq. (2.14). As this calculation of the occupation and the density is used throughout this thesis the index "ca" is omitted.
Besides all globally averaged data, the micro-simulations also provide measures of each individual vehicle like its length, headways, and other model specific values.
If a distribution functions p_x of an observable x with the discretization Δx are plotted from the empirical data as well as from the simulations these have been normalized such that $\sum p_x \cdot \Delta x = 1$. This guarantees that the distributions are independent from the binning of the data.
The empirically observed traffic patterns and the relation of these to the traffic data are discussed in the following section.

2.2 Experimentally Observed Traffic States

The classification of a traffic state described by its state variables is still discussed controversially. Recent analyses propose the existence of three different traffic states: free-flow, wide moving jams, and synchronized traffic. This classification of the traffic states, the so-called *Three Phase Traffic Theory* was proposed by Kerner *et al.* [73, 74, 75, 86]. In the next sections these three states are discussed briefly. Before this description was proposed different approaches were made to describe the characteristics of vehicular traffic. A first attempt was made in 1935 by Greenshields [40]. His assumptions allowed for a rough distinction between free flowing vehicles on the one hand and congested traffic on the other hand. Over the years the state of knowledge of the properties of traffic has reached a higher level. Nowadays a huge amount of traffic data are available and can serve as the basis for extensive statistical investigations. This information give also insight into the microscopic characteristics of traffic dynamics.
It is important to keep in mind that these data are nearly always acquired in a complex network and thus biased by many circumstances which makes the interpretation a complex

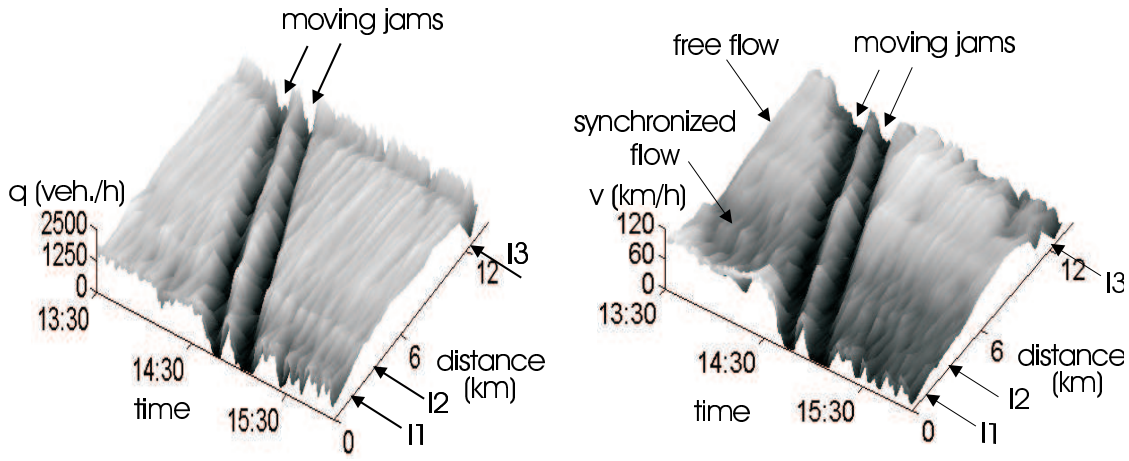

Figure 2.1: The different traffic states detected on a section of the German highway A5. In the left figure the flow vs. time is plotted and in the right the velocity vs. time. A free-flow region can be seen downstream of the on-ramp and synchronized traffic is pinned there. Two wide moving jams traverse through both regions undisturbed. The figures are taken from [71].

task. This may be one reason that the description of traffic is still under controversial discussion, especially the classification of the traffic dynamics into the three states mentioned above is subject of different opinions.
Additionally, the dynamics of the traffic is governed by country specific rules, e.g., on German highways it is not allowed to overtake on the right side and the drivers are appealed to drive on the right lane if possible. These facts have to be considered in the estimation of the empirical data. Particularly the traffic data presented here are obtained from German highways so that these restrictions have to be considered.
The mentioned traffic states are characterized by important empirical findings like the shape in the fundamental-diagram, the time headway distribution or the autocorrelation. These are considered in the following sub-sections and in chapter 4.

2.2.1 Free-Flow

The traffic theory characterizes the free-flow as a state where the vehicles can freely move with their desired speed. The interaction between the vehicles is very rare and in this state obviously no traffic jams occur. In the fundamental diagram – a theoretical one is shown in Fig. 2.2 – this state is represented by a line with positive slope at low densities. The slope is connected to the mean velocity by the hydrodynamical relation $J = \rho \cdot \langle v \rangle$. It is in general different for the distinct lanes because overtaking on the right hand side is prohibited in Germany. Thus, the slow vehicles drive on the outer right lane.
In empirical data this linear branch might end up in a finite curvature near the density slightly below the maximum flow [69, 94]. This is the result of the stronger vehicle interaction. Slightly below the maximum flow it is no longer possible for the cars to always drive with their desired speed that is faster than the maximum velocity of the trucks. The interaction with the slower trucks becomes stronger and therefore the maximum speed of the cars is affected by the slower trucks.

The importance of the trucks is supported by empirical results from a highway where the velocity is restricted by a strict speed limit that even the slower trucks can reach. The curvature at the upper limit is not observed here [130].
Furthermore, the free-flow branch of the fundamental diagram must be split into two parts. Up to densities of the jam outflow ρ_{out} no jams may evolve. Local perturbations dissolve very quickly. At higher densities above ρ_{out} the free flow branch shows metastable behavior. A local perturbation can force a breakdown of the free-flow traffic and lead to a spontaneous jam formation at homogeneous road sections or at bottlenecks [50, 68, 69, 70, 73, 83, 84]. The state of the metastable free-flow is characterized by a maximum flow J_{max} that is associated to the flow out of a jam J_{out} by $\frac{J_{\text{max}}}{J_{\text{out}}} = 1.5$.

2.2.2 Wide Moving Jams and Stop-and-Go Traffic

In contrast to free-flow traffic (jam free), congested traffic is characterized by different kinds of jams and does not belong to the free-flow line of the fundamental diagram.
One basic feature of congested traffic are stop-and-go waves which have been the subject of many different studies [30, 46, 97, 104, 118]. Some interesting empirical results have been found. The wavelength of the jams correspondent to their width is varying between 2.5 km and 5 km and the life-time – the wave period – was found to be between 4 min and up to 20 min. Recently, the origin of such waves was traced back to the so called "pinch effect" in synchronized traffic [67, 73], which implies that perturbations may lead to local compressions of the synchronized flow forming wide moving jams. For a more detailed discussion see Sec. 2.2.3.
The wide moving jams show up as compact clusters of vehicles that are moving upstream. As the velocities and the flow inside are very limited the jam is separated from the surrounding by two sharp jam fronts which are decoupled from each other. Thus, there is no correlation between the inflow into and the flow out of the jam. Moreover, wide moving jams propagate unhindered through free-flow as well as synchronized traffic [72, 73, 92].

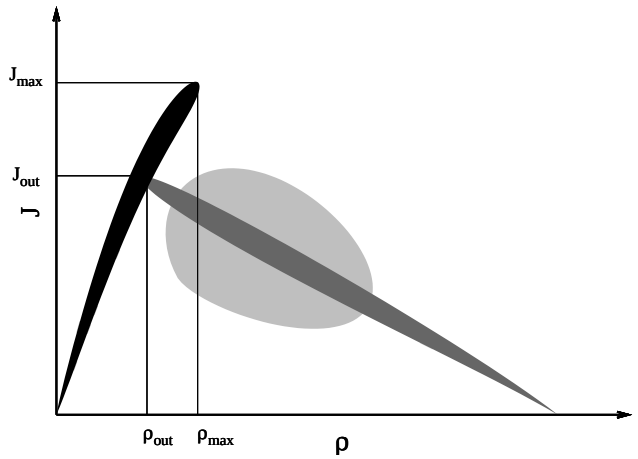

Figure 2.2: Theoretical concept of the fundamental diagram for a multi-lane road. The free-flow state is depicted by the black region and wide moving jams are represented by the dark-gray one. The two-dimensional region of the synchronized traffic is located in the light-gray area.

If the surrounding traffic is synchronized the downstream density of the jam front takes on the density of the ambient traffic. Recent investigations hint at a more complex inner structure of the moving traffic jams [80]. The microscopic features show a structure of alternating regions in which the traffic flow is interrupted by flow states of low speed which are associated with so called "moving blanks". These could be compared with electron holes in semiconductor physics as they move against the movement direction of the particles.
A different approach to describe the global features of wide moving jams was provided in [10]. Here, arguments of the random walk theory are applied to describe the jam characteristics in a cellular automaton model. This approach provides a convenient insight into the movement of the jam.
Additional universal quantities were found in [84] that do only slightly depend on the internal composition of the traffic like the fraction of trucks, the length of the vehicles or, as an example for an external factor, the weather. These quantities are the density ρ_{jam} inside the jam and when propagating through free flow the density in the outflow region ρ_{out}. The flow out of a jam J_{out} is found to be universal as well. Because of the universality of the jam outflow a sequence of coexisting jams may exist [84].
In the fundamental diagram the wide moving jams form a characteristic line with negative slope. The slope is equal to the velocity of the downstream front of the cluster. This propagation velocity seems to be an universal constant of traffic with a typical value of 15 km/h for German highways. It can easily be measured by means of the density autocorrelation [130, 139].

2.2.3 Synchronized Flow and Pinch Effect

The third common traffic state is the so-called synchronized traffic [67, 84, 85, 86, 94, 113, 130].
The notation "synchronized traffic" was chosen by Koshi [97] and reused by Kerner and coworkers [85] because of the synchronization of the velocity and the flow among neighboring lanes. But this holds true for other traffic states like wide moving jams as well where the jams and the free flow in between are also synchronized on all lanes. Thus, this characterization is not sufficient.
This form of traffic is mostly found in the vicinity of a bottleneck like an on-ramp [43, 68, 69, 70, 73, 84]. The synchronized traffic shows no functional relation between the flow and the density but it covers a 2-dimensional region in the fundamental diagram (Fig. 2.3).
The three phase traffic theory proposes three different kinds of synchronized traffic: First, homogeneous and stationary states where the flow and the velocity are almost stationary, second, homogeneous-in-speed states where only the velocity is stationary while the flow and the density strongly fluctuates and third, non-homogeneous and non-stationary states which are the most common manifestation. In this thesis the discussion is limited to the synchronized traffic of the third kind as the other two have been rarely observed [94, 130].
The region of synchronized traffic is divided by a solid line in the fundamental diagram. The line corresponds to the state of wide moving jams. It is assumed that synchronized states below the line are long-living, i.e., no transition to wide moving jams can occur. States above the line of jammed traffic are metastable. A disturbance can lead to the formation of wide moving jams. This is also the case for the free-flow phase where states above the intersection point J_{out} are metastable.
In the vicinity of a bottleneck, here an on-ramp, the local manifestation of the synchronized

state appears in three shapes [73, 78, 81]. In the first form – the localized one – the synchronized region is limited to a small region upstream of the on-ramp where it is pinned. In the second shape – the moving synchronized pattern – the region of synchronized flow grows and the upstream front moves against the driving direction with a velocity that is depending on the upstream flow. It forms a wide area of continuous synchronized traffic. Like the localized pattern it is also pinned to the on-ramp. The last observed manifestation is the moving synchronized pattern. Here, the synchronized traffic emerges at the on-ramp and a region is build where synchronized flow alternates with free-flow. These manifestations form a characteristic phase diagram that depends on the in-flow on the main road and the flux of the on-ramp [73, 77, 81]. Depending on the local topology more different forms of synchronized traffic and its forming are proposed and therefore many variations of the phase diagram exist [78, 82].
Nevertheless, the origin of the synchronized traffic or the widely scattered traffic states is still under debate. Thus, the traffic models that are capable to model this phenomena are based on different assumptions for the origin of these states. The models include anticipation effects [91, 128, 166], different kinds of vehicles (trucks and cars) [121, 165], that the dependence of the optimal velocity on distance headway shows plateaus [122, 148], and the variety of oscillating metastable states with different wavelengths [49, 163]. The influence of the lane changes on the evolution of the synchronized traffic is also still an open question. The large number of lane changes in the synchronized traffic hints at the importance of this mechanism. Thus, whether multi-lane traffic is required to describe synchronized traffic conveniently, is discussed in [55, 106, 113].
The direct formation of a wide moving jam is unlikely to be seen in free-flow [69, 70, 73] but in general it is formed indirectly namely out of synchronized traffic via a sequence of transitions from free-flow to synchronized traffic to wide moving jams. Kerner stated that these transitions could be characterized as “first order phase transition” in the physical sense as the transitions between the traffic states come along with a discontinuous change of any traffic variable [56, 67, 71, 85, 86, 106]. But the validity of this concept is not clear up to now. In this thesis the term phase is used in the sense that the traffic is realized in different states and these may change to other states.
Nevertheless, the transition between free-flow and synchronized traffic is mainly observed in the vicinity of a bottleneck like an on-ramp. Thus, here also most wide moving jams emerge in such environments. A possible interpretation of jams emerging in synchronized traffic is provided by the so called “pinch-effect”. It describes a process of local compression in the synchronized regime – the pinch region [72]. These local perturbations may form small jams. They could simply dissolve or lead to a larger disturbance like the formation of a wide jam. This perturbation of the flow can be caused by random internal fluctuations, for example in the vicinity of an on-ramp, by an upstream moving wide jam or an expanding synchronized region. Once the wide moving jams are formed they do not simply disappear but one finds a hysteresis so that the density has to be reduced to restore synchronized traffic again [56]. Recent empirical investigations try to approximate the breakdown probability [18, 103, 175] of the traffic in the vicinity of an on-ramp in dependence of the fluxes on the main road and the on-ramp.
The mechanisms of the pinch effect can be compared with the transition between a gas and a liquid. If the former is compressed beyond its critical density it becomes supercritical so that even a small fluctuation is sufficient to build a condensation nucleus that leads to a droplet formation [29, 105]. It is important to note that the often acclaimed universality

of wide moving jams (see Sec. 2.2.2) cannot be applied to these narrow jams but the latter consist of only two fronts where the vehicle speed and the density sharply changes. In addition, there are no characteristic parameters: The outflow depends on the inflow and the upstream velocity is larger compared to wide jams. Thus, the narrow jams cannot propagate undisturbed through all traffic states and without impact on the states they pass.
The wide moving jams are not pinned at the bottleneck but traverse the synchronized state unhindered and unaffected [72, 92].

2.2.4 Multi-Lane Characteristics

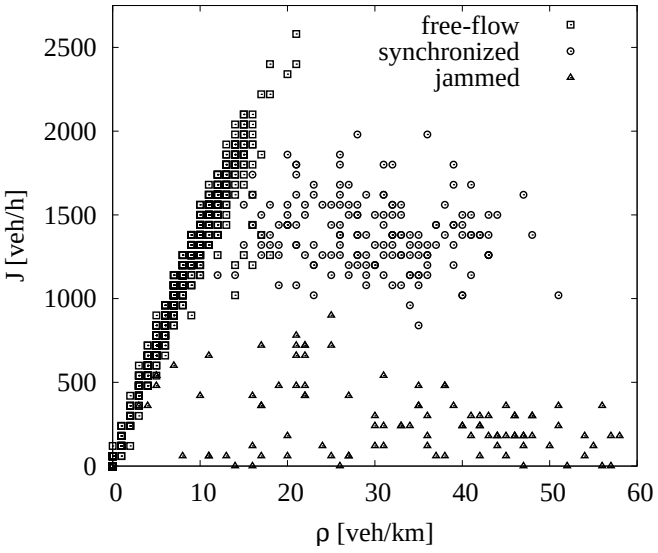

Figure 2.3: Empirical fundamental diagram of minute aggregated data from a two-lane section of the A40. Three empirical traffic states are recovered: free-flow (squares), synchronized traffic (circles), and wide moving jams (triangles). The data of the synchronized state are gathered near Moers at 2000-12-12 and that of wide moving jams stem from a detector near Bochum-Werne at 2001-02-12 (from [88]).

The empirical studies that examine the multi-lane characteristics are limited to [17, 19, 44, 159] in contrast to the broad data basis of aggregated data and single-vehicle data that provides quite good understanding of the strategies of the drivers and the resulting traffic states. Nevertheless, the influence of the lane changes seem to be very important as by these the different lanes are synchronized which means that the vehicles spread from a higher occupied lane to the less occupied. The higher occupied lane is in general the lane where the vehicles enter the road. As a consequence the vehicles are more or less uniformly distributed to all lanes and thus the velocities on the different lanes are synchronized as well [97]. Also the different patterns of synchronized flow as described in Sec. 2.2.3 are transferred from one lane to the other so that on both lanes the same pattern emerge [73]. Little differences are in general found in the neighborhood of an on-ramp. Here, the flow on the right lane of a three-lane road is slightly smaller than on the other lanes as the

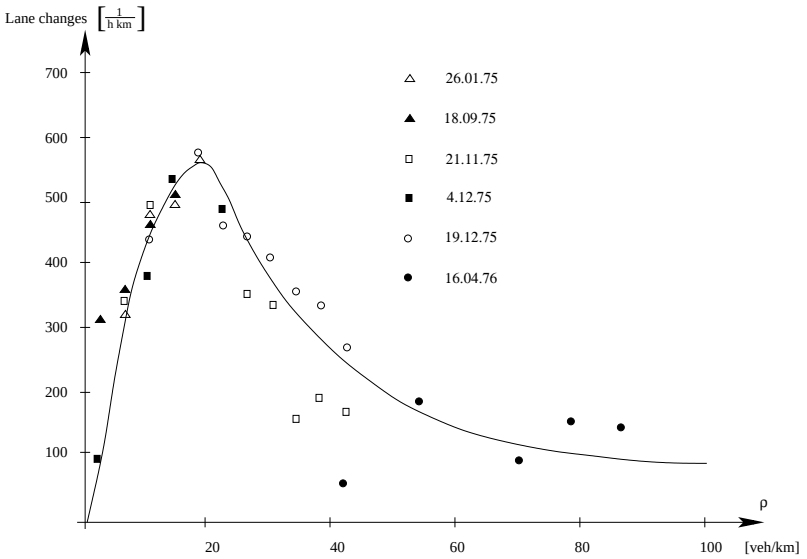

Figure 2.4: Number of lane changes versus density on different observation days (from [159]). Most lane changes are observed around $\rho \approx 20\,\text{veh/km}$. The traffic consists of cars and trucks.

drivers intend to clear space for the vehicles driving onto the road [17, 19, 44]. However, the common lane usage behavior is strongly depending on the legal restrictions.
Sparmann found in 1987 [111, 159] that the lane usage curve which shows the flow or density distribution on the lanes is different on German highways compared to countries where a symmetric lane-usage is the standard. In Germany the drivers are requested to use the right lane if possible and they are not allowed to overtake on the right side.
Here, a lane usage inversion was found which means that at low densities nearly all vehicles drive on the right lane. At higher densities this discrepancy reduces until this behavior changes and more vehicles drive on the "faster" left lane. It is called "faster" lane as it is the lane that has to be used to overtake. The flow and the occupation get asymmetric. This lane usage inversion [111, 159] starts at the upper density limit of the free flow when the vehicles start to interact with each others and thus overtaking begins to be beneficial. For higher densities this trend keeps stable. The lane usage inversion can be observed for all except very low densities. In contrast, in urban traffic or on highways without the right lane constraints, the traffic flow is evenly distributed on both lanes [17, 19, 44].
Less accurately measured is the lane-changing frequency. Here, the difficulties arise as this information cannot be measured by local detectors. Thus, the few researches are limited to [17, 19] and the only available observation for German highways can be found in [159]. Nevertheless, there are two competing mechanisms known to affect the number of lane changes: on the one hand, a driver wants to change the lane if he expects to be faster or drive more comfortable on another lane. This becomes more frequent if the density rises and the interaction between the vehicles becomes more frequent. On the other hand, there has to be enough room on the destination lane so that a save lane change is possible. Thus, it is obvious that for low densities the number of lane changes rises with increasing density until the lane changes become unsafe and uncomfortable, respectively, and decreases at high ones. The maximum is reached at mid densities near the maximum flow (Fig. 2.4).

For low densities the fraction of slow vehicle, i.e., trucks and lorries, is a crucial factor. If trucks are absent, the motivation to change the lane at low densities is low and the number of lane changes negligible. Additionally, the lane change frequency is depending strongly on the specific section of the road. If one looks at the region downstream of an on-ramp, the number of lane changes can exceed the mean [159].
A further result of the investigations of Sparmann concerning two-lane traffic describes the time a vehicle needs for a complete lane change. Whereas in general a time of 1 sec is needed to react on changes in the environment when driving straight forward, a driver needs more time to change the lane. $t_{\mathrm{lc}} = 3\,\mathrm{sec}$ are noted for the whole maneuver [159].

3 Modeling Vehicular Traffic

Modeling vehicular traffic and the description of its properties is the content of various analyses during the last half of the 20th century. These approaches can be separated into two classes. First, coarse grained macroscopic models and, second, microscopic models. In this thesis a special emphasis is laid on members of the second class, the cellular automaton models. These are investigated here and thus discussed in greater detail in this chapter. The exemplary approaches show on the one hand the basics of cellular automaton models and they reproduce on the other hand some of the main features of highway traffic. Nevertheless, these models show certain limitations but their capabilities act as "ingredients" for the model by Lee *et al.* [107, 108] that is discussed in great detail in Sec. 5.1.
For an overview of other macroscopic and microscopic modeling approaches please refer to [21, 37, 42, 43, 47, 51, 58, 69, 75, 154, 157, 171]. With respect to cellular automaton models please see especially [21, 95, 114].

3.1 Simple Stochastic CA Models

Generally speaking, cellular automata are discrete dynamical systems. Their behavior is completely described by the interaction with their local neighborhood. Discrete means, that these systems are discrete in space – it consists of a grid of cells which can adopt a discrete number of states – and discrete in time. The state at one time step of the cellular automaton is transferred by an update procedure to the next one. This procedure is applied to the cells in different orders, e.g., in parallel or sequentially.
The concept of cellular automata bases on the ideas of Johann (John) von Neumann who introduced them in the 1940's [132]. In his work on a theory of self-replicating computing machines he invented an "universal" computer that could emulate any describable function of any other machine by a set of logical rules ("von Neumann architecture"). In fact cellular automaton models became very popular in the development of micro computers. In fact they are von Neumann machines. In 1970 the famous "game of live" was published by John H. Conway [38]. The game is a simple two-dimensional analogon to basic live processes. The next step to popularity was done by Stephen Wolfram [172]. He analyzed a class of deterministic one-dimensional cellular automata systematically. Each of the cells can be in two states and the evolution is only depending on the state of the nearest neighbors. Thus, there are $2^3 = 8$ possible states that could be inherited by a cell. Among the simple rule-set Wolfram nevertheless found sets that show complex behavior.
A very impressive aspect of stochastic cellular automaton models is their complex dynamic behavior, including such phenomena like *self-organized criticality* [2, 7, 160, 173], although they are only based on a set of a few simple local update rules.
In recent years, the theory of CA was extended by stochastic rule-sets in order to enlarge the concept to a wider variety of systems [20, 115, 144].
Although this concept of cellular automata is an extreme idealization of a physical system,

this concept was often successfully applied to describe physical many particle systems (See, e.g., [31] for an general overview of recent research activities). On the broad field of transportation phenomena it is for example applied to simulate pedestrian motion [16, 99, 152, 153], intracellular traffic [133], or ant trails [65].
Concerning the simulation of vehicular traffic a first approach was done by M. Cremer and J. Ludwig [25]. Due to their simplicity, cellular automaton models are predestined for simulations of systems containing a large number of particles. Especially the simulation of large scale traffic networks in real time is of main interest nowadays [23, 34, 41, 66, 134, 141, 169, 170]. Thus, this model class became very popular recently.
For the analysis of the main features of the models for vehicular traffic a simple topology is used, i.e., most simulations are performed on a periodic system consisting of an one dimensional grid or single-lane. This topology is a strong simplification and stands in strong contrast to a realistic highway section. Nevertheless, this approach is justified as it was shown for a large class of models that the different steady states are selected by the different boundary conditions [96, 138, 158] and do not change the microscopic structure of these states. This means, the knowledge of the periodic system affords to understand the dynamics of systems with other boundary conditions.
If more complex topologies or defects are concerned an open system is considered especially in Sec. 7.1 when the influence of an on-ramp is discussed in detail and the different patterns of synchronized traffic are analyzed.
Despite of the system type, cellular automaton models for vehicular traffic are in general defined as follows. The road is divided into cells that can be either empty or occupied by car n with a velocity $v_n = 0, \ldots, v_{\max}$. Vehicles move from the left to the right on a lane with – in general – periodic boundary conditions, and the system update is performed in parallel, i.e., all vehicles are faced with the same situation. However, there are a lot of possible update procedures like ordered or random sequential [123, 145, 151].
In the following, the position and velocity of the nth car at time t is denoted by x_n^t and v_n^t, respectively. Cars are numbered in driving direction, i.e., vehicle $n+1$ precedes vehicle n. A car may occupy more than a single cell[1]. Therefore, the gap between consecutive cars is given by $d_n = x_{n+1} - x_n - l_{n+1}$ where l_{n+1} is the length of the vehicle $n+1$.

3.1.1 The Cellular Automaton Model by Nagel and Schreckenberg

The prototype of the models which are discussed in this section is a cellular automaton model introduced by Nagel and Schreckenberg [126] (hereafter cited as "NaSch model"). It is a minimal model in the sense that every single simplification of the algorithm would lead to a less realistic model. Because of its simplicity it fulfills an important role as it allows for a very efficient and fast implementation.
It also mimics the basic update algorithm for all other stochastic cellular automaton models. The algorithm is divided into four sub-steps: First, the vehicle accelerates followed by the deceleration step which takes into account the distance to the leading vehicle. This again is succeeded by the randomization step. At last the vehicle is moved according to its velocity.
This approach serves as a general guideline for the velocity update and the vehicle movement [21]:

1. Step: Acceleration,

[1] If a vehicle is longer than on cell its position is denoted by the cell occupied by the front of the vehicle.

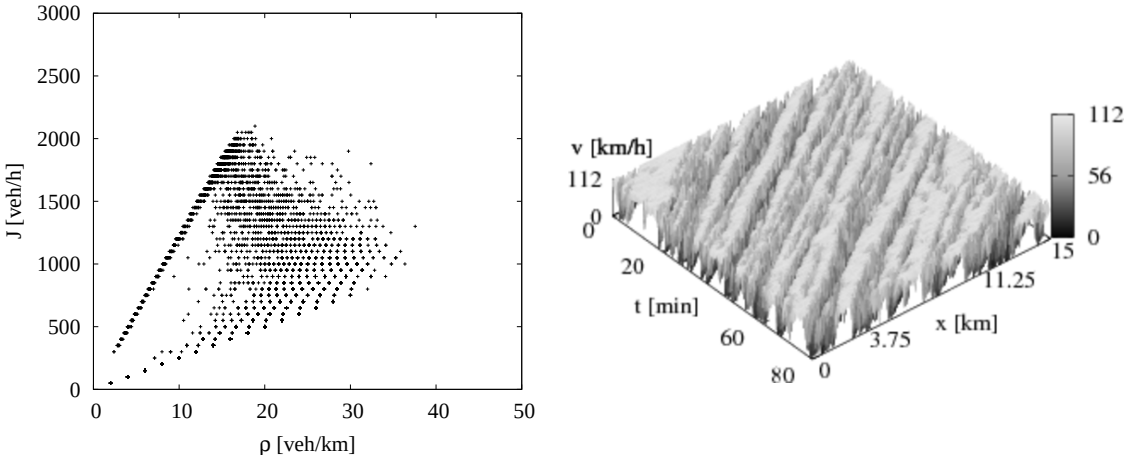

Figure 3.1: **Left**: Local fundamental diagram of the NaSch model. **Right**: Space-time plot of the NaSch model at $\rho = 29\,\text{veh/km}$. The parameters are $v_{\max} = 112\,\text{km/h} = 5\frac{\text{cells}}{\delta t}$, one time-step corresponds to $\delta t = 1.2\,\text{sec}$ and $p_{\text{d}} = 0.16$. A cell has a length of 7.5 m.

2. Step: Deceleration,

3. Step: Randomization/dawdling,

4. Step: Movement.

These steps may be preceded in enhanced models by

0. Step: Determination of meta parameters (randomization parameter, brake-light status, etc.).

For the NaSch model the system update is performed in parallel according the four following rules:

$$\begin{aligned}
&1. \quad v_n^{t+\frac{1}{3}} = \min(v_n^t + 1, v_{\max}),\\
&2. \quad v_n^{t+\frac{2}{3}} = \min(v_n^{t+\frac{1}{3}}, d_n),\\
&3. \quad v_n^{t+1} = \max(v_n^{t+\frac{2}{3}} - 1, 0) \text{ with probability } p,\\
&4. \quad x_n^{t+1} = x_n^t + v_n^{t+1}.
\end{aligned} \tag{3.1}$$

The parameters are the velocity v_n, the maximum velocity $v_{\max}$ and the position x_n of car n. d_n specifies the number of empty cells in front of a car.
In this model each vehicle occupies one cell of length 7.5 m which corresponds to the total average space a car occupies in a compact jam. This choice is in accordance with measurements on German highways on the left and middle lane, where the density of trucks is negligible [84]. The maximum velocity mainly appoints the slope of the free-flow branch whereas the congested region is depending on the value of p. Thus, by these parameters the model can be tuned.

The model results agree well with the empirical findings in the free-flow region (see left of Fig. 3.1). The fundamental diagram shows that the NaSch model reproduces the slope of the fluxes and the maximum flow very well.
Nevertheless, neither the empirically found metastability of the flow above J_{out} nor all characteristics of congested traffic can be reproduced. In congested traffic no synchronized traffic is present. This is also true for the observed parallel propagation of jam waves, as in the jam outflow regions additional jams emerge. The jammed state contains clusters of an exponential size distribution [125, 151] (right of Fig. 3.1). Parallel jams do only emerge if a disturbance exists, e.g., a speed limit or a region with higher dawdling probability [139]. Upstream of this defect sites parallel jams emerge and build a region of separated free-flow and widening jams. But these boundary induced effects are not sufficient.

3.1.2 The VDR Model

To overcome basic missing features of the NaSch model, like the nonexistence of parallel propagating jams and the metastable free-flow branch, a simple extension was proposed by [8, 9, 155, 161]. The slow-to-start rule – also known as velocity-dependent-randomization (VDR) – extends the calculation of the dawdling parameter in the update algorithm. This is now set in dependence of the current velocity v_n of the vehicle. The simplest approach just sets a different dawdling parameter p for stopped vehicles:

$$p(v) = \begin{cases} p_0, & \text{for } v = 0, \\ p_{\text{d}}, & \text{for } v > 0. \end{cases} \tag{3.2}$$

The remaining update follows that of the NaSch model.
With $p_0 > p$ the acceleration of the standing vehicles is delayed. Thus, it is possible to tune the velocity of the vehicles and the outflow of the jam separately. p_0 determines the jam velocity and is chosen such that the upstream velocity of the moving jams is in accordance with the empirical findings. p still influences the velocity of the driving vehicles. Thus, the free-flow branch of the fundamental diagram can be reproduced in good agreement with the empirical data if in addition $v_{\max}$ is chosen appropriately (left part of Fig. 3.2). Additionally, the hysteresis of the metastable free-flow branch can now be reproduced. If the system is initialized homogeneously, metastability is found.
Despite the progress of this model approach makes in simulating the free-flow region it still suffers from discrepancies in the congested region. The model fails to reproduce the congested phase correctly (see Fig. 3.2, left). Compared to the NaSch model the mismatch of the fundamental diagram in the congested regime is even more serious. Neither a regime of wide moving jams nor synchronized traffic can be identified. The reason for this is found in a strong separation between free flow and wide jams. The latter are compact so that the flux is zero in the stationary state of the periodic system. Additionally, this separation reduces the weight of the measurements that interfere between wide jams and free flow. Synchronized traffic can not be seen in the space-time plot either (right part of Fig. 3.2). Hence, no data points are measured for $\rho > 20\,\text{veh/km}$.
If the global fundamental diagram is considered, densities $\rho > 20\,\text{veh/km}$ are observed as it is accumulated over all traffic states that emerge in the whole system.
Nevertheless, a major achievement of the VDR model is a more realistic description of the dynamics of wide moving jams. Because of the delayed start of the vehicles the outflow from a jam is lower than the maximum flow and so no jams emerge in the outflow region.

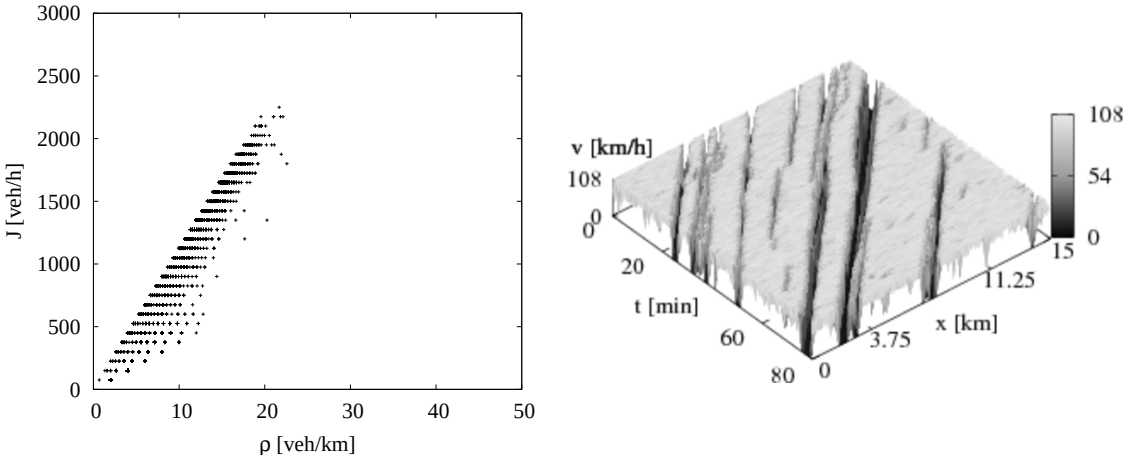

Figure 3.2: **Left:** Local fundamental diagram of the VDR model. **Right:** Space-time plot of the VDR model at $\rho = 29\,\text{veh/km}$. The parameters are $v_{\max} = 108\,\text{km/h} = 3\frac{\text{cells}}{\delta t}$, one time-step corresponds to $\delta t = 0.75\,\text{sec}$, $p_0 = 0.58$, and $p_\text{d} = 0.16$.

This effect leads to the increased stability of jams, including the empirically observed parallel upstream motion of two jams which are sharply separated from free-flow (Fig. 3.2, right).
An analytical approach in terms of random walk theory was suggested in order to determine characteristic quantities of wide jams, especially resolving probabilities and life-times [10]. It was shown that the random walk approach renders the jamming dynamics of the VDR model. Nagel and Paczuski [125] also analyzed the life-time of jams in the cruise control limit of the NaSch model and found also good agreement with random walk theory. Thus, it can be assumed that the jamming behavior is generic for a lot of stochastic cellular automaton models for traffic flow, especially model types that use the VDR slow-to-start rule for the generation of wide phase separated jams.
Nevertheless, recent studies indicate that local defects can break the strong separation in such a way that stop and go traffic can exist [139, 140].

3.1.3 The BL Model

The models presented up to now did not match the empirical results in a satisfying manner. In [91, 92] Knospe *et al.* proposed a further enhanced cellular automaton that describes the congested traffic more accurately. It uses ingredients from other model approaches like the fundamental update algorithm of the NaSch model [126] and the slow-to-start rule of the VDR model [9]. Moreover, as a further ingredients anticipation [11, 90] is included. An effective gap is used instead of the real spatial distance. In addition, the braking of a vehicle is indicated by a brake-light so that the follower can react to it [39]. An upstream moving cascade of brake-lights may follow and it generates longer ranging interactions whereas the update itself is still locally limited to the next nearest neighbor [57]. The brake-light is a binary variable, i.e., $b_n = 1$ if it is switched on and $b_n = 0$ if it is switched off.
Furthermore, a vehicle may occupy more than a single cell so that a finer discretization for a given length of a vehicle is possible. The randomization parameter p_d can adopt three

values depending on the current velocity and the brake-light status of the leader:

$$p_{\mathrm{d}} = p(v_n^t, b_{n+1}^t, t_{\mathrm{n}}^{\mathrm{h}}, t^s) = \begin{cases} p_{\mathrm{b}}, & \text{for } b_{n+1} = 1 \text{ and } t_{\mathrm{n}}^{\mathrm{h}} < l^s, \\ p_0, & \text{for } v_n = 0, \\ p, & \text{else.} \end{cases} \tag{3.3}$$

The dawdling is depending on two times $t_{\mathrm{n}}^{\mathrm{h}}$ and $l^s = \min(v_n, h)$. The former is the time headway and the latter is a cut-off time that prevents the driver to react on a brake-light too far away. h is the interaction range with the brake-light. The effective gap is denoted as $d_n^{\mathrm{eff}} = d_n + \max(v_{\mathrm{anti}} - d_{\mathrm{security}}, 0)$ where $v_{\mathrm{anti}} = \min(d_{n+1}, v_{n+1})$ is the anticipated velocity of the leading vehicle. The effectiveness of the anticipation is controlled by d_{security}. This implies that accidents are avoided only if $d_{\mathrm{security}} \geq 1\,\mathrm{cell/time\text{-}step}$. The update rules are as follows.
First the brake-light is reset and the dawdling parameter is calculated:

0. $p_{\mathrm{d}} = p_{\mathrm{d}}(v_n^t, b_{n+1}, t_{\mathrm{n}}^{\mathrm{h}}, l^s)$,
   $b_n^{t+1} = 0$.

This is followed by the update of the velocity and the movement of the vehicle:

1. if $((b_{n+1} = 0)$ and $(b_n = 0))$ or $(t_{\mathrm{n}}^{\mathrm{h}} \geq t^s)$,
   then $v_n^{t+\frac{1}{3}} = \min(v_n^t + 1, v_{\max})$,

2. $v_n^{t+\frac{2}{3}} = \min(v_n^{t+\frac{1}{3}}, d_n^{\mathrm{eff}})$,
   if $(v_n^{t+\frac{2}{3}} < v_n^t)$, then $b_n^{t+1} = 1$,

3. if $(\mathrm{rand}() < p_{\mathrm{d}})$, then $v_n^{t+1} = \max(v_n^{t+\frac{2}{3}} - 1, 0)$,
   if $(p_{\mathrm{d}} = p_{\mathrm{b}})$ then $b_n^{t+1} = 1$,

4. $x_n^{t+1} = x_n^t + v_n^{t+1}$.

In order to illustrate the update algorithm, the steps are briefly explained now.
In step 0 the dawdling parameter is calculated. It determines the upstream velocity of the downstream front of wide moving jams if it is set to p_0. Additionally, the brake light is set if the preceding vehicle is inside the interaction horizon l^s. In the next step 1 the velocity is increased if the vehicle is not driving with its maximum velocity or the brake light of the next vehicle is not on and the vehicle is within the interaction horizon. Step 2 avoids accidents as the velocity is adjusted taking into account the effective gap to the leader. If the vehicle's velocity is reduced compared to the preceding time-step the brake-light is switched on. The dawdling of the vehicle is performed in step 4. If the vehicle's dawdling parameter is p_{b}, i.e., it is set due to the leaders brake-light, the brake-light is turned on. Finally, the position of the vehicle is updated.
The rules lead to the wanted dynamics of the vehicles: In free-flow the vehicles thus drive with their desired velocity besides random fluctuations. In synchronized traffic no large velocity changes are needed and a "comfortable" driving is possible. In jammed traffic accidents are avoided.
The BL model reproduces the empirical data in great detail. In particular, three qualitatively different microscopic traffic states that are in accordance with the empirical results

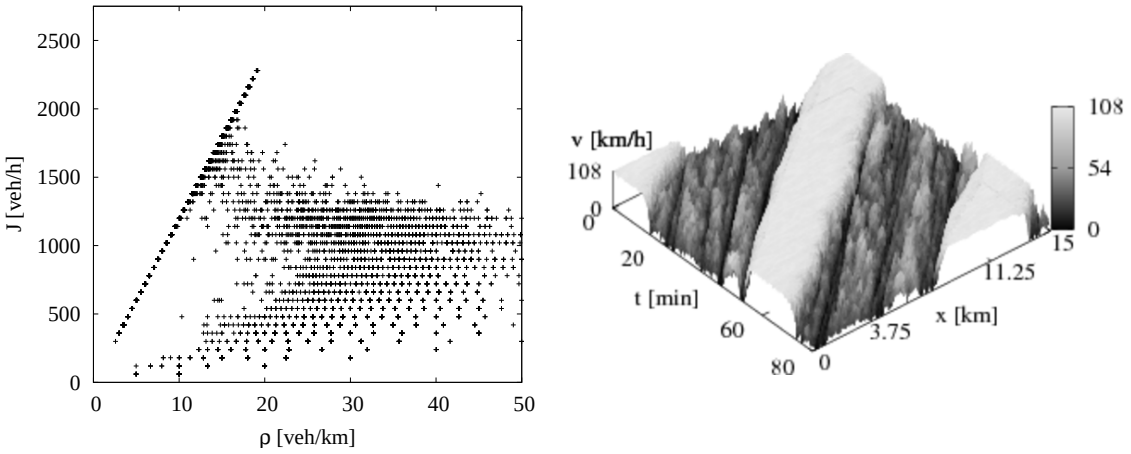

Figure 3.3: **Left:** Local fundamental diagram of the BL model. **Right:** Space-time plot of the BL model at $\rho = 29\,\text{veh/km}$. The parameters are $v_{\max} = 108\,\text{km/h} = 20\frac{\text{cells}}{\delta t}$, one time-step corresponds to $\delta t = 1\,\text{sec}$, $p_0 = 0.5$, $p_\text{d} = 0.1$, and $p_\text{b} = 0.94$. $d_\text{security} = 7\,\text{cells}$ and one cell has a length of 1.5 m. Each vehicle covers 5 cells.

can be observed. Wide moving jams move unhindered through both free flow and synchronized traffic [72] which is one important feature a model should reproduce. The fundamental diagram shows the widely scattered region (left side of Fig. 3.3) of the synchronized traffic. The free-flow branch is reproduced as well as the velocity of the downstream front of wide moving jams.
The agreement of the simulation results with empirical single-vehicle data is good in different aspects. The optimal velocity function is reproduced excellently and the autocorrelation is in good agreement as well if slow vehicles are introduced.
However, the short time headways in free flow are not reproduced. Only if vehicles with a higher maximum velocity are introduced, smaller headways than 1 sec are found. Nevertheless, the slope background signal is not reproduced, just peaks at small time headways appear. The single-vehicle data of the velocity in the synchronized region do not agree with the empirical findings. Unrealistic fluctuations are found therein.
Note, this approach is still being developed [64].
In [92, 93] Knospe *et al.* also extended the BL model with rules that allow asymmetric lane changing on a two-lane road. It incorporates a right-lane preference as well as an overtaking prohibition on the right lane. This leads to a correct reproduction of the density inversion phenomenon.

4 Model Validation

It is a difficult task to characterize the accuracy of a given model as the empirical data are strongly depending on the environment and the local conditions in which they are acquired. For example, it is strongly required to evaluate the number of regarded lanes or whether the measurements are performed on a section downstream of a bottleneck. Therefore, it is difficult to identify and extract the main properties that characterize the driving behavior of the vehicles accurately, e.g., the dependence of the velocity of individual vehicles on the distance headway or the intention to change the lane.
However, the knowledge of the different traffic states has risen in recent years so that a basis was formed to validate simulation results with different empirical data sources.
Thus, different scenarios are analyzed and their results are compared to empirical findings. Some results that are generally valid are acquired in the simulation of a periodic system. More elaborate topologies like an open system with an on-ramp are discussed separately.
A more conclusive method is to use empirical single-vehicle data to calibrate the models and evaluate the simulation results. Unfortunately, the number of such a kind of empirical investigations is very limited, so that the discussions are based on the results from [94], [162] and [130].
Most of the empirical data that serve as reference for the simulation results are acquired by inductive loops. Therefore, all measurements of single-vehicle data in the simulations are done by introducing a virtual inductive loop: Besides the local flow J, velocity v, and occupation ratios *occ*, the time headways t_h (Eq. 2.9) and distance headways d_n given by Eq. (2.10) are measured in that manner as in reality.

4.1 Aggregated Data

4.1.1 Local Measurements

The relation between the state variables that is most often used to describe road traffic is the fundamental diagram. It shows the dependence of the averaged flow J on the density ρ. In general in empirical fundamental diagrams minute-aggregated data are plotted whereas the density is calculated from the flux and the velocity via the hydrodynamical relation (Eq. 2.11).
Considering the fundamental diagram, the main characteristic of the free-flow traffic is the undisturbed movement of the vehicles, which is reflected by the high mean value of the average speed. This results in a nearly linear branch in the fundamental diagram for small densities. The slope of the free-flow branch is directly connected with the maximum velocity of the vehicles, i.e., the slope is given by v_max.
In most simulations, only vehicles with a single maximum velocity are used. The strictly linear slope of the free-flow branch should therefore be reproduced. Thus, the simulation results can easily be compared with real world data where the linear form of the free-flow branch is relevant. The curvature at the free-flow branch near the optimal flux does not appear (see discussion in 2.2.1).

When different vehicles are simulated, i.e., for example trucks, as in the analysis of two-lane traffic in Sec. 6.1, the free-flow branch gets more scattered depending on the lane and whether the trucks are allowed to change the lane as well. Nevertheless for the sake of simplicity only two maximum velocities are used in the simulations and no distribution of the maximum velocity is applied when trucks are considered.
If a highway section without a speed limit is simulated a distribution of maximum velocities has to be applied to the vehicles. The distribution can be acquired empirically from single-vehicle data [94] for very low densities where the vehicles do not interact.
The regime of congested traffic is characterized by a negative slope in the fundamental diagram. The vehicles can no longer drive with their desired velocity. It is separated into synchronized traffic and wide moving jams. In the former state, the mean velocity of the vehicles is smaller compared to that in free flow. Nevertheless, the flow can reach high values that are close to the maximum flux. Moreover if multi-lane traffic is concerned there are strong correlations between the density on the different lanes caused by the lane changes.
To identify the traffic state by means of the fundamental diagram is quite uncertain as the data points strongly depend on the measuring and averaging process. More elaborate are space-time plots of the system. These show – especially in the vicinity of a disturbance like an on-ramp – the traffic state as well as the type of synchronized traffic.
Descriptive statistics offers many other approaches to characterize time-series and thus the interaction between the vehicles. Thus, a different approach considers the autocorrelation or the cross-correlation of the traffic observables. These are valuable to characterize the time-scales of the interactions between the vehicles. The autocorrelation $\mathcal{A}_\psi(\tau)$ is defined as:

$$\mathcal{A}_\psi(\tau) = \frac{\langle\psi(t)\psi(t+\tau)\rangle - \langle\psi(t)\rangle\langle\psi(t+\tau)\rangle}{\sqrt{\langle\psi^2(t)\rangle - \langle\psi(t)\rangle^2}\sqrt{\langle\psi^2(t+\tau)\rangle - \langle\psi(t+\tau)\rangle^2}}. \tag{4.1}$$

Here, ψ represents the time-series of the state variable one is interested in and τ is the observed time slot. The autocorrelation $\mathcal{A}_\psi(\tau)$ describes the relation of the dependent variable with its history. The cross-correlation $\mathcal{C}_{\vartheta,\psi}(\tau)$ reflects in contrast the dependency between two different quantities ψ and ϑ. It is defined as follows:

$$\mathcal{C}_{\vartheta,\psi}(\tau) = \frac{\langle\vartheta(t)\psi(t+\tau)\rangle - \langle\vartheta(t)\rangle\langle\psi(t+\tau)\rangle}{\sqrt{\langle\vartheta^2(t)\rangle - \langle\vartheta(t)\rangle^2}\sqrt{\langle\psi^2(t+\tau)\rangle - \langle\psi(t+\tau)\rangle^2}}. \tag{4.2}$$

Especially, the cross-correlation $\mathcal{C}_{J,\rho}$ of the flow J and the density ρ is characteristic for the different traffic states [130]. It allows to distinguish between the two types of congested traffic, wide moving jams and synchronized traffic.
As stated in Sec. 2.2.2 wide moving jams show also some universalities that can be used to validate a model's features. Here, especially the upstream velocity of the jams has to be mentioned. The typical velocity of $v_{\text{jam}} = 15\,\text{km/h}$ [67] that seems to be a "universal constant" that is not influenced by the weather or other road conditions. Thus, it can be utilized to calibrate the propagation velocity of wide moving jams v_{jam} which can easily be measured by the density autocorrelation. The velocity of the jam is directly related to the outflow of a jam J_{out} that in general adopts a constant value as well $J_{\text{out}} \approx 1{,}800\,\text{veh/h}$. It is significantly lower than the maximum flow J_{max}. This is the reason for the coexistence of wide moving jams and free flow and the fact, that no jams emerge in the outflow region of a jam. A relation $J_{\text{max}} \approx 1.5 \cdot J_{\text{out}}$ is observed empirically.

4.1.2 Global Measurements

Beside temporally aggregated data also spatially aggregated values can serve as a valuable source to characterize and calibrate the models properties. In a simulation environment it is an easy task to acquire global values of the different traffic measures, whereas empirical data could only be measured using video detection of a part of the road. As it is a difficult and elaborate task these results are really scarce.
Nevertheless, the number of lane changes (Fig. 2.4) is a spatiotemporal measure that serves as a test to validate a lane change algorithm. Thus, it is essential for a two-lane model to reproduce the characteristic relation between the density and the number of lane changes. At low densities the number of lane changes is low as well. In this region the lane change frequency is strongly depending on the distribution of the velocities, i.e., slow trucks force lane changes even at low densities. Near the optimal flux the number approaches its maximum. In synchronized traffic the number of lane changes is high as well and decreases for higher densities.
Moreover, strong correlations between the densities on different lanes exist that are caused by the lane changes.
Note that the empirical data are very limited and therefore the validation of a two-lane model concerning the lane change frequency is very vague.
Furthermore, global measurements are especially eligible to describe the influence of the different model parameters on the dynamics of a model. For example the width of the synchronized region with respect to the density can be described very conveniently using the fundamental diagram. The slope of the free-flow branch is again a reference for the maximum velocity of the vehicles via the hydrodynamic equation (2.1).

4.1.3 Traffic Patterns

The synchronized traffic that is formed in the vicinity of an on-ramp adopts different characteristic traffic patterns. These are mainly classified by the spatiotemporal structures of the states near the ramp and collected in a complex phase diagram as a function of the inflows. Therefore, it is relevant for a traffic model to reproduce these patterns besides the microscopic findings described above. The synchronized traffic appears in different variants as shown in [73]: moving synchronized, widening synchronized, and localized synchronized pattern (see Sec. 2.2.3). So, the degree of realism of a traffic model is among other characteristics depending on the correct mapping of these traffic states. These capabilities are therefore discussed in detail when analyzing a traffic model. Especially, the transfer of the state to all lanes on a multi-lane road should be modeled correctly. This as well holds true for the correct description of the pinch effect as well as the metastability of the synchronized traffic.

4.2 Single-Vehicle Data

The measurements based on the aggregated data show qualitative differences in the three traffic states. This is correct for data from single-vehicles as well.
Especially the time headway distribution p_{t_h}, the distribution of the time that elapses between two consecutive vehicles reaching the detecting device, shows significant distinctions in each traffic state. Note, this value can be interpreted as the microscopic analogon of the reciprocal flow. In order to facilitate a comparison between the empirical time

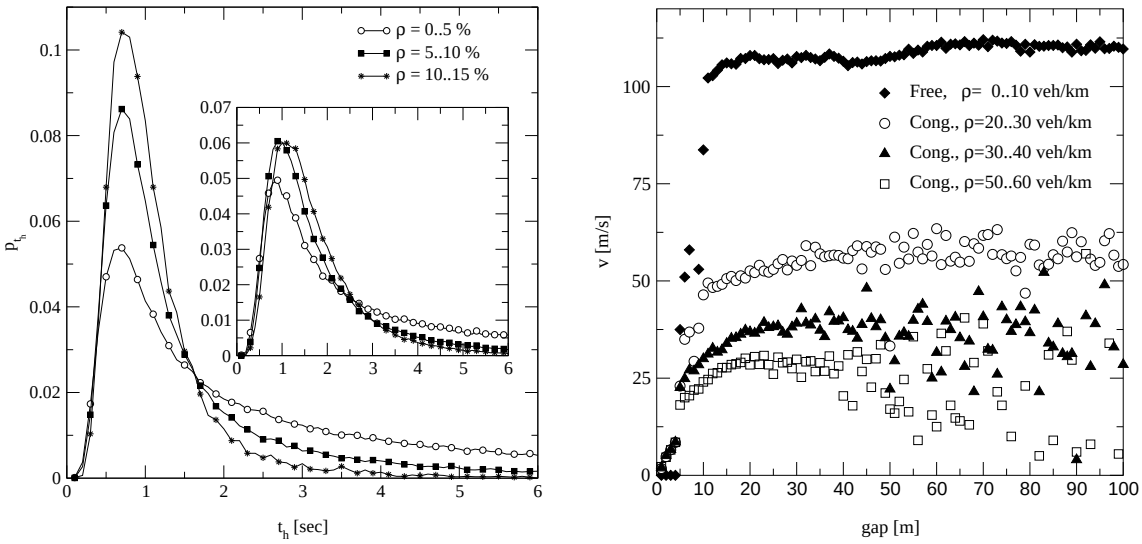

Figure 4.1: **Left:** The time headway distribution in free-flow from a section of the highway A3. Time headways smaller than one second are the most frequent ones and the maximum is independent of the density. It is reached at $t_\mathrm{h} \approx 0.75\,\mathrm{sec}$. The background signal decays exponentially. The inset shows data sets from a detector at the highway A1 near Cologne. The data show the same characteristics. The maximum is slightly shifted to $t_\mathrm{h} \approx 1\,\mathrm{sec}$. From [94]. **Right:** Empirical optimal-velocity function. The mean velocity for a given spatial headway is depicted for free-flow and congested traffic for different densities. In free-flow the asymptotic velocity is independent of the density. In congested traffic the vehicle-vehicle interaction becomes important so that the velocity is lower. The vehicles drive more slowly than the headway permits. From [95].

headways and the ones measured in the simulations, the distributions are normalized by $\sum p_{t_\mathrm{h}} \cdot \Delta t_\mathrm{h} = 1$.

In free-flow traffic the characteristic distribution of the time headway depends on the density. The position of the maximum as well as the distribution for short times is not depending on the density (Fig. 4.1). Nevertheless, the degree of realism depends on the proper reproduction of the minimal time headway or cut-off at small times and the typical shape of the time headway distribution. Slow vehicles influence this measure as they increase the interaction between the vehicles and thus the exact shape is affected by the relative frequency of slow vehicles. The characteristic exponential decay of the background signal of the time headway distribution for the undisturbed vehicles in free-flow should be reproduced accurately as well. This signal could be explained by so-called "random headway states" [116]. These characteristics have to be reproduced by microscopic models.

In synchronized traffic the time headway distribution differs strongly from that of free-flow traffic. It shows a much broader distribution and the maximum is moving significantly towards larger time headways with changing densities.

In the region of wide moving jams it is recommended to distinguish between the measures performed in the jam and that in the outflow of the jam. In the former case many different time headways are detected as the vehicles may stop for long time. In the outflow of a

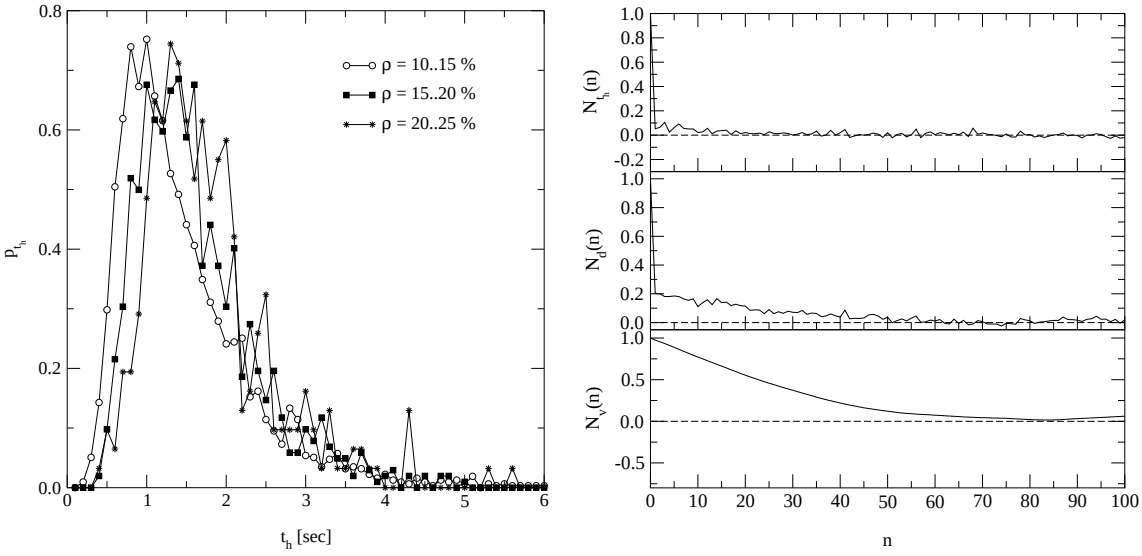

Figure 4.2: **Left:** The time headway distribution in synchronized traffic. From [94]. The maximum is reached at $t_\mathrm{h} \approx 1\,\mathrm{sec}$ for $\rho = 10 \ldots 15\%$ and declines exponentially till $\rho \approx 4\,\mathrm{sec}$. Longer time headways are rarely detected. For higher densities the maximum is shifted slightly to higher time headways. For $\rho = 20 \ldots 25\%$ the maximum is detected with $t_\mathrm{h} \approx 1.3\,\mathrm{sec}$. **Right:** Vehicle-vehicle correlation of the single-vehicle data in the synchronized state. At the top the vehicle-vehicle correlation of the time headway is shown. No correlation are found. In the middle the distance vehicle-vehicle correlation is depicted. It decays immediately to $\mathcal{N}_d \approx 0.2$ for small n and decreases further for larger n. In contrast, the velocities are highly correlated as shown at the bottom. The vehicle-vehicle correlation decays slowly and adopts values $\mathcal{N}_v > 0.25$ for $n \leq 50$. From [88].

jam a time headway of 2 sec is found in general[1].
Strength and range of the interaction between the vehicles can in the case of single-vehicle data be characterized by the vehicle-vehicle correlation $\mathcal{N}_\psi(\eta)$:

$$\mathcal{N}_\psi(\eta) = \frac{\langle \psi(n)\psi(n+\eta)\rangle - \langle \psi(n)\rangle\langle \psi(n+\eta)\rangle}{\sqrt{\langle \psi^2(n)\rangle - \langle \psi(n)\rangle^2}\sqrt{\langle \psi^2(n+\eta)\rangle - \langle \psi(n+\eta)\rangle^2}}. \tag{4.3}$$

The index ψ describes the used data set, e.g., $\psi = d_n$ or v_n. The argument η is the distance between the considered vehicles. Thus, $\eta = 1$ describes the relationship between two consecutive vehicles, $\eta = 2$ the connection to the next but one vehicle and so forth. Here, it is irrelevant at which time the vehicles pass the detector.
The vehicle-vehicle correlation (Fig. 4.2) of the single-vehicle data in the synchronized phase shows characteristic properties. Looking at the velocity correlation $\mathcal{N}_v$ one sees that there is a strong correlation for up to 50 consecutive vehicles. Whereas the vehicle-vehicle correlation of the time headways $\mathcal{N}_{t_\mathrm{h}}$ is negligible the vehicle-vehicle correlation of the gap is not zero but low with $\mathcal{N}_d \approx 0.2$ for small n.
Another test for the capabilities of microscopic models is the velocity-distance relation,

[1] This corresponds to a jam velocity of 13.5 km/h if the mean length of a vehicle is set to 7.5 m.

aka. the optimal-velocity function (cf. 4.1). By this function the microscopic structure of the different states are characterized. In free-flow traffic the asymptotic velocity is independent of the density but determined by a given speed limit. In congested traffic the vehicles interact with each other so that the asymptotic velocity is much lower than in free-flow. The vehicles drive slower than the distance headway permits.
Note, an elaborate discussion of empirical tests for cellular automaton models of vehicular traffic is given in [95].

5 The Model by Lee *et al.*

Cellular automaton models are a valuable approach to describe highway traffic in a proper manner as discussed in the preceding section. Putting together the "ingredients" that lead to a realistic model a basis for a more elaborate approach is provided. For example, the slow-to-start rule is used as the kernel for wide moving jams, and the anticipation of the leader's driving behavior allows for shorter time-headways.
Nevertheless, different approaches were made to develop a microscopic model that reproduces synchronized traffic sufficiently and to describe real world traffic more accurately [64, 81] as discussed in Sec. 2.2.3. But these approaches all suffer from deficiencies, e.g., short time headways in the free-flow regime are not reproduced correctly.
However, if such a model approach should serve as the basis for a modern traffic information system like the Internet platform *autobahn.nrw.de*, it must reproduce highway traffic in a sufficient degree of realism. Several preconditions have to be fulfilled. First, the approach has to reproduce the free-flow branch including the metastable high-flow region and the short time headways. Second, regarding congested traffic the synchronized state as well as wide moving jams and their macroscopic and microscopic attributes have to be reproduced, too. This is not only true for the undisturbed dynamics. Especially the behavior of a model in the presence of inhomogeneities or defects is of tremendous importance. In particular, these bottlenecks govern the traffic of highway networks and therefore have to be examined as well.
In this thesis special interest is laid on the formation of synchronized traffic and its properties. The different approaches to model this kind of traffic show that the origin of this phenomenon is still not finally clarified.
Therefore, the approach proposed by Lee *et al.* [107, 108] is discussed in great detail in this chapter. In the first step the basic features of the single-lane model are recapitulated and afterwards more extensive findings of the model dynamics are presented. The results and the enhancements of this chapter form the basis for the more elaborate investigations in the next chapter where the model is extended further by realistic lane changing rules. Its properties are discussed and compared to empirical findings in great detail. In a last step of the model validation different bottleneck mechanisms like on-ramps and speed limits are investigated.
But first the original single-lane model is analyzed to find the basis for the formation of synchronized traffic: The driver and its behavior that are included into the model definition. The driver evaluates its neighborhood and decides how to drive based on this observation. This can be described as an enhanced anticipation of the driving behavior of the leading vehicles. This decision is limited by mechanical capabilities of the vehicle. This means that the vehicle cannot accelerate arbitrarily and it is not able to decelerate infinitely fast. The latter has been examined for a continuous model in [98].
This approach is the basis of a simulation model that reproduces the basic features like wide-moving jams as well as the more complex dynamics of synchronized traffic in its different appearances. The next section discusses the model and shows further features as well as some limitations of this model approach.

5.1 Definition of the Single-Lane Model

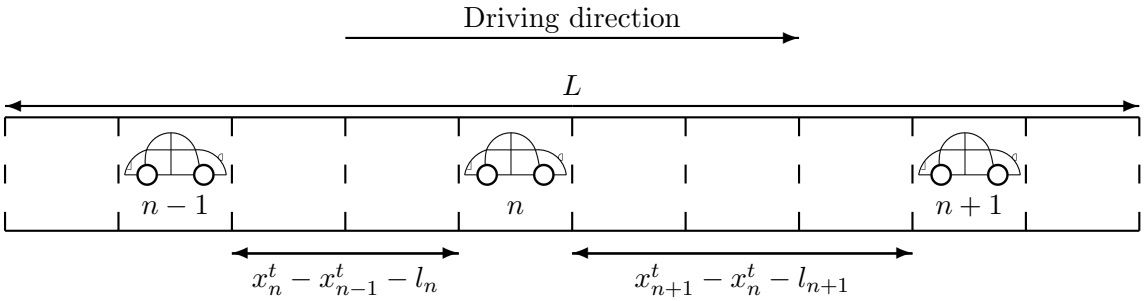

Figure 5.1: Sketch of a single-lane road that shows the configuration of the velocity update of vehicle n that drives behind vehicle $n+1$. x_n^t denotes the position of vehicle n and l_n its length. The vehicles drive from left to right.

In 2004 Lee *et al.* [107, 108] proposed a cellular automaton model that emphasizes the conflict between human overreaction and limited mechanical capabilities as the origin of congested traffic states. The limited acceleration and deceleration capabilities lead to a totally different approach to realize collision free traffic. Hard-core repulsion or unlimited deceleration as it is used in former models to ensure strict collision avoidance is not part of this model so that it is not assured directly that no collisions occur.
How this is realized is explained in the following. First, the update algorithm is presented and the particular equations are discussed. Then the dependence of the model features on the different model parameters is examined. Thus, a deep understanding is established, which is necessary for the further simulations like multi-lane traffic or open systems with an on-ramp.
In contrast to the other cellular automaton models discussed in Sec. 3.1 the calculation of the velocity of the vehicles is not accomplished as a function of different model parameters $v_n^{t+1} = f(v_n^t, gap_n^t, \ldots)$ but is written as an inequality that gives the velocity v_n^{t+1}.
The purpose of this inequality is to calculate a maximum velocity c_n^{t+1} so that the follower can drive as fast as possible but still is able to stop behind his leader. In other words, if the leader decelerates at maximum capability, the maximum velocity of the follower n is calculated so that he is able to stop bumper-to-bumper behind his leader $n+1$. This velocity is considered as a safe velocity for the vehicle n that satisfies the following condition:

$$x_n^t + \Delta + \sum_{i=0}^{\tau_f(c_n^{t+1})} (c_n^{t+1} - D \cdot i) \quad \leq \quad x_{n+1}^t + \sum_{i=1}^{\tau_l(v_{n+1}^t)} (v_{n+1}^t - D \cdot i) \tag{5.1}$$

Here, x_n^t and v_n^t are the position and the velocity of vehicle n, respectively. Δ represents the minimum gap between the vehicles that is at least the length l_{n+1} of the leading vehicle. D denotes the deceleration capability of the vehicles, $\tau_f(c_n^{t+1})$ and $\tau_l(v_{n+1}^t)$ describe the number of time-steps in which the velocity is calculated and the safety is ensured for the follower and the leader, respectively (see Eq. 5.4).
Each summation in (5.1) denotes a deceleration cascade with maximum braking capability D. As long as both $\tau_f(v)$ and $\tau_l(v)$ are set to v/D and $\Delta = L$, the deceleration would end in a bumper-to-bumper configuration. But this is weakened by the introduced human

factor that evaluates the neighborhood (see below) and acts depending on the results. Note that c_n^{t+1} is determined by the upper limit of (5.1). Nevertheless, the retarded reaction – the vehicle responds to its leader one time step later – of vehicle n is modeled by the different lower summation limits. If $\tau_l < 1$ the sum on the right is equal to zero while the left sum has always at least one term, i.e., $\tilde{c}_n$.
This inequality can easily be resolved with respect to c_n^{t+1}:

$$x_n^t + \Delta + \sum_{i=0}^{\tau_f(c_n^{t+1})} (c_n^{t+1} - D \cdot i) \quad \leq \quad x_{n+1}^t + \sum_{i=1}^{\tau_l(v_{n+1}^t)} (v_{n+1}^t - D \cdot i)$$

$$\begin{aligned} x_n^t + \Delta + (\tau_f(c_n^{t+1}) + 1)c_n^{t+1} - \frac{D}{2} \cdot (\tau_f^2(c_n^{t+1}) + \tau_f(c_n^{t+1})) \\ \leq \quad x_{n+1}^t + \tau_l(v_{n+1}^t) \cdot v_{n+1}^t - \frac{D}{2} \cdot (\tau_l^2(v_{n+1}^t) + \tau_l(v_{n+1}^t)) \end{aligned} \tag{5.2}$$

$$\begin{aligned} c_n^{t+1} \quad \leq \quad & \frac{x_{n+1}^t - x_n^t - \Delta + \tau_l(v_{n+1}^t) \cdot v_{n+1}^t}{\tau_f(c_n^{t+1}) + 1} \\ & + \frac{\frac{D}{2} \cdot [\tau_f^2(c_n^{t+1}) + \tau_f(c_n^{t+1}) - \tau_l^2(v_{n+1}^t) - \tau_l(v_{n+1}^t)]}{\tau_f(c_n^{t+1}) + 1} \end{aligned}$$

Unfortunately, the right part of equation 5.2 has still functions of the dependent variable c_n^{t+1}. Thus, this transformation does not simplify the velocity calculation so that an analytic approach could be made to find a simple connection between c_n^{t+1} and the other state variables. This fact is also important when the model is analyzed with respect to its behavior regarding accidents. Nevertheless, this formulation is valuable in numerical calculations as it can be processed faster than the original formulation[1].
In order to model the different behaviors of the drivers, not only the usual stochastic variation of the driving is applied. The model introduces an attitude of the driver and distinguishes between *optimistic* and *pessimistic* driving. The vehicles drive with respect to their neighborhood. The driver evaluates the local situation, represented by the Boolean variable γ, and decides whether he will drive optimistically $\gamma = 0$ or pessimistically $\gamma = 1$. The former controls the driving behavior in free flow. The vehicles drive unhindered and drivers accept "unsafe" gaps, i.e., gaps smaller than those allowing them to react to an emergency braking of the leading vehicle. Short time headways below one second are possible. The latter parameter governs the driving at high densities. The interaction between the cars is high and braking is likely. The vehicles drive pessimistic and remain aloof (a detailed discussion is given in Sec. 5.4.1). This leads to the following specification of γ:

$$\gamma_n^t = \begin{cases} 0, & \text{for } v_n^t \leq v_{n+1}^t \leq v_{n+2}^t \text{ or } v_{n+2}^t \geq v_{\text{fast}}, \\ 1, & \text{otherwise.} \end{cases} \tag{5.3}$$

Here, v_{fast} is a high velocity slightly below the maximum velocity: $v_{\text{fast}} = v_{\max} - 1$.
This definition gives two reasons for a driver to act optimistically: He drives in a platoon of vehicles that are driving equally fast or faster than himself, i.e., $v_n^t \leq v_{n+1}^t \leq v_{n+2}^t$, or

[1] The summation is linearized and thus one has to iterate only over the c_n^{t+1}.

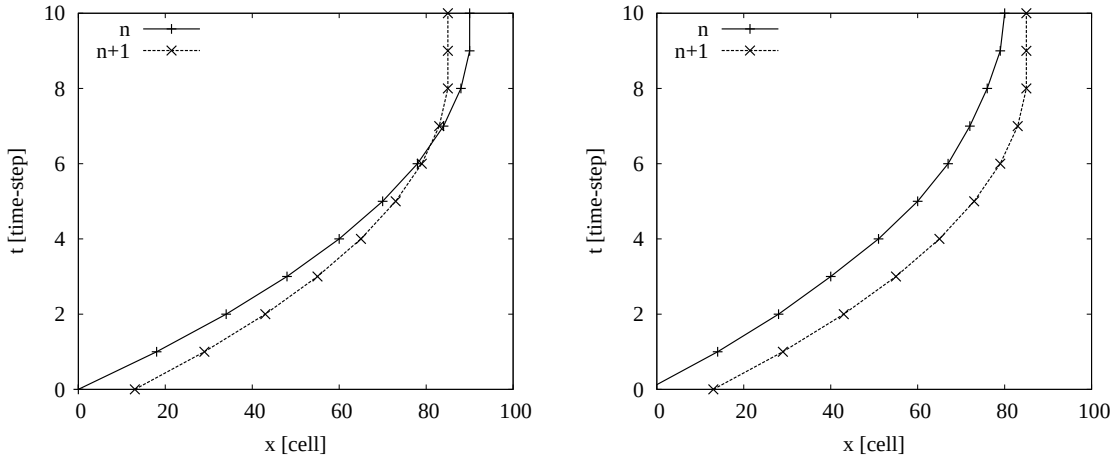

Figure 5.2: **Left:** Trajectory of vehicle n and $n+1$ during the calculation of the safe velocity. Vehicle n is optimistic so that it only assumes the safety for t_{safe} time-steps. An accident would happen in this situation if the leading vehicle continues to decelerate for 8 time-steps. **Right:** Trajectory for a pessimistic vehicle n. It is able to stop if the leading vehicle $n+1$ stops completely as well regardless of the vehicle's distance and velocity.

the next but one vehicle is speeding away with high velocity, $v_{n+2}^t \geq v_{\text{fast}}$. Both reasons describe a local situation in which the driver is not likely to be hindered by its leaders such that he has to anticipate a hard brake.
The calculation of the upper limits $\tau_l(v)$ and $\tau_f(v)$ of the summation (5.1) as well as the minimum gap between the cars are as follows:

$$\begin{aligned} \Delta &= L + \gamma_n^t \max\{0, \min\{g_{\text{add}}, v_n^t - g_{\text{add}}\}\} \\ \tau_f(v) &= \gamma_n^t \frac{v}{D} + (1-\gamma_n^t)\max\{0, \min\{\frac{v}{D}, t_{\text{safe}}\} - 1\} \\ \tau_l(v) &= \gamma_n^t \frac{v}{D} + (1-\gamma_n^t)\min\{\frac{v}{D}, t_{\text{safe}}\} \end{aligned} \tag{5.4}$$

Here, t_{safe} denotes the maximum number of time-steps for which a vehicle observes its own safety when driving optimistically. The driver monitors the safety of his situation only towards this limited "time horizon". g_{add} is an additional safety gap for the optimistic drivers ($\gamma_n^t = 0$) that drive faster than $2 \cdot g_{\text{add}}$ to avoid accidents.
In the left and right part of Fig. 5.2 the trajectories of the deceleration process of two vehicles n and $n+1$ for the optimistic and the pessimistic case are visualized, respectively. In both cases, the vehicles start with the same velocity and the leading vehicle $n+1$ starts to decelerate.
For the optimistic driver the speed and distance is considered safe for t_{safe} seconds (Fig. 5.2 left). A collision is not likely to occur in the next time-steps but it is almost sure to happen if the leading car is forced to decelerate unexpectedly without prior notice by the following car. In this example, the accident would happen when the two trajectories cross each other after 8 time-steps. Thus, it is important to choose the function that decides whether a vehicle drives optimistically or not accurately. If the time horizon is set to $t_{\text{safe}} = \frac{v}{D}$ no

accidents will occur since a complete stop of the vehicles is ensured and thus the model would be intrinsically safe. This is equivalent to the pessimistic velocity update. As Fig. 5.2 shows the pessimistic driver basically assumes that on any given moment the car in front may be forced to a complete stop. Thus, the time-interval Δt – represented by the summation index i – is dependent on the velocity of both the following and the leading vehicle. While this assumed full-stop is unlikely in the free flow, it is the sane assumption of drivers in synchronized and congested traffic to anticipate the full-stop at any moment. This rigid interaction of the cars is important for the formation of synchronized traffic.
The remaining update is as follows:

$$p = \max\{p_{\mathrm{d}}, p_0 - v_n^t(p_0 - p_{\mathrm{d}})/v_{\mathrm{slow}}\}, \tag{5.5}$$

$$\tilde{c}_n^{t+1} = \max\{c_n^{t+1} \mid c_n^{t+1} \text{ satisfies Eq. (5.1) – (5.4)}\}, \tag{5.6}$$

$$\tilde{v}_n^{t+1} = \max\{0, v_n^t + a, \max\{0, v_n^t - D, \tilde{c}_n^{t+1}\}\}, \tag{5.7}$$

$$v_n^{t+1} = \max\{0, v_n^t - D, \tilde{v}_n^{t+1} - \eta\}, \text{ where } \eta = 1 \text{ if rand}() < p \text{ or } 0 \text{ otherwise}, \tag{5.8}$$

$$x_n^{t+1} = x_n^t + v_n^{t+1}. \tag{5.9}$$

The calculation of the stochastic parameter p (Eq. 5.5) is a generalization of the slow to start rule (see [8, 9, 91]). It interpolates linearly between p_{d} and p_0 for vehicles driving slower than v_{slow} whereas slow vehicles dawdle more likely. This is important to reflect the compact jam patterns that are often found in congested traffic flow. In [10] it is shown that this ingredient produces stripped jam patterns in simple cellular automaton models. Note that the limited deceleration capability also limits the dawdling of a vehicle (Eq. 5.8), i.e., the vehicle cannot dawdle when it has reduced its velocity maximally.
The second step of the update algorithm (Eq. 5.6) calculates the maximum safe velocity $\tilde{c}_n^{t+1}$. In the next step (Eq. 5.7) the mechanical restrictions are applied and the traffic is regulated. After the dawdling step (Eq. 5.8) the vehicle is moved (Eq. 5.9).
It is important to note that in contrast to other cellular automaton models the dawdling of a vehicle may have a stronger impact on the dynamics in this model. On the one hand, dawdling just reduces the velocity of the vehicle or prevents its acceleration. This is the usual impact that dawdling has on the model dynamics. On the other hand, in this model γ – the attitude of the driver – is objective of the dawdling of a vehicle, too. To clarify that a closer look at the definition of γ is worthwhile. In the first part of the definition γ is only set to 0 if the leading vehicles are driving at least as fast as the vehicle that is concerned. For the sake of simplicity lets assume for the next considerations that these vehicles all drive with the same velocity. Thus, if one of the leading vehicles dawdles once the series of equal velocities is broken and the last vehicle of this group changes its attitude to pessimistic. Now, at least for the next time-step, the stricter driving rules of a pessimistic driver are applied: A larger gap has to be reached and the safety of the driving has to be validated so that a full-stop can be performed without an accident. This may lead to a different driving behavior if the distance of the last vehicle is small enough. The vehicle has to brake as well with the same consequences to its successors. Thus, a cascade of attitude changes may emerge inducing longer ranging interactions. Certain parallels

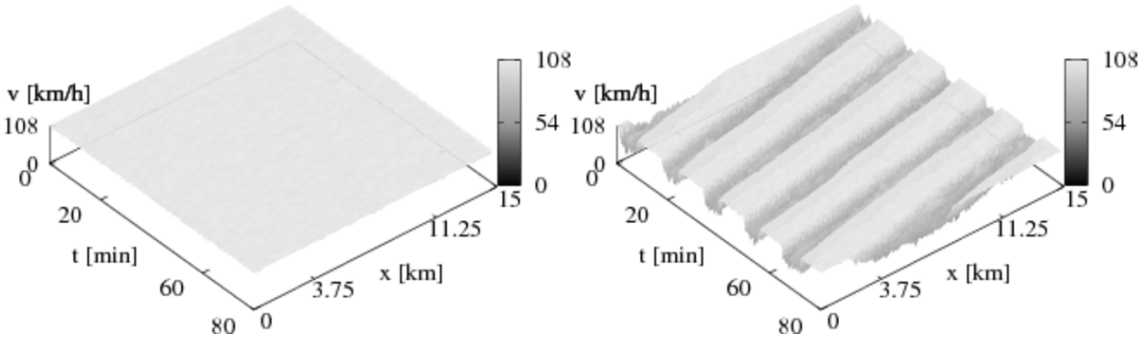

Figure 5.3: **Left:** Space-time plot of the free-flow phase of the periodic system. The initial density is $\rho = 13\,\text{veh/km}$. **Right:** Space-time plot of coexisting free-flow and synchronized traffic in the periodic system. The initial density is $\rho = 23\,\text{veh/km}$.

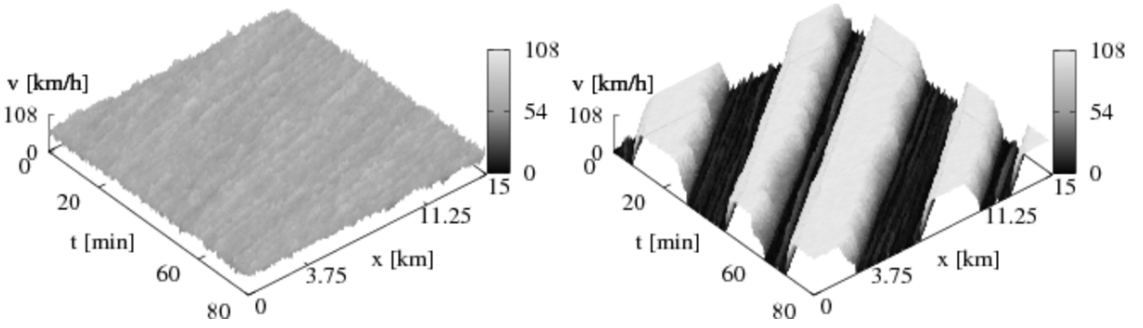

Figure 5.4: **Left:** Space-time plot of the synchronized phase of the periodic system. The initial density is $\rho = 29\,\text{veh/km}$. **Right:** Space-time plot of the congested phase of the periodic system. The initial density is $\rho = 53\,\text{veh/km}$.

arise to the brake-light cascades of the BL model (cf. Sec. 3.1.3) that are required for the emergence of the synchronized traffic.
In the presence of limited deceleration capabilities, the model is not intrinsically accident-free. Crashes may happen when fast vehicles reach a density wave of slow driving or even stopped vehicles. This is analyzed in greater detail in Sec. 5.5.

5.1.1 Basic Features

In this section the basic features of the model by Lee *et al.* are analyzed and the important features are traced back to the model parameters.
Some of the parameters – already utilized in [107, 108] – that are part of the update algorithm can be connected to empirical facts. The length of a cell is set to 1.5 m which leads to a velocity discretization of 5.4 km/h. Since one simulation step corresponds to one second, the acceleration capability is $a = 1\,\text{cell/time-step}^2 = 1.5\,\text{m/sec}^2$, which is of the same magnitude as a comfortable acceleration of about $\sim 1\,\text{m/sec}^2$ [61]. As the length of one vehicle in a compact jam is about 7.5 m this is applied to the length of cars: $l = 5\,\text{cells}$. The dawdling parameter p_d controls the magnitude of the maximum flow and $p_0 = 0.32$ is motivated by the upstream velocity of a wide moving jam. The maximum velocity is set to

$v_{\max} = 20\,\text{cells/time-step} = 108\,\text{km/h}$. Further, the following model parameters are used in the simulations of this thesis, if not explicitly stated otherwise: $D = 2\,\text{cells/time-step}^2$, $v_{\text{fast}} = 19\,\text{cells/time-step}$, $t_{\text{safe}} = 3\,\text{sec}$, $g_{\text{add}} = 4\,\text{cells}$, and $v_{\text{slow}} = 5\,\text{cells/time-step}$.
That this parameter choice is meaningful is justified in this section by a good accordance with empirical facts: The width of the synchronized traffic is calibrated by v_{slow}, the cut-off of the time-headway distribution is governed by t_{safe}, and the value of the flow in synchronized traffic is mainly affected by g_{add}.
The simulation parameters of the analyzed systems are as follows if not stated otherwise: The system length is $L = 10{,}000\,\text{cells}$ and the data is measured after a relaxation time of $T_{\text{relax}} = 30{,}000$ time-steps for $T_{\text{measure}} = 20{,}000$ steps.
Figure 5.3 shows space-time plots of a periodic system. The different traffic states can be distinguished very easily. In the left of Fig. 5.3 the homogeneous free flow is shown. Nearly all vehicles are driving with their maximum velocity. Fluctuations are very scarce and the vehicles drive unhindered. With increasing density a transition to synchronized traffic can be seen. First a mixed state emerges wherein synchronized traffic and free flow exist in parallel (Fig. 5.3 right). The synchronized traffic shows much lower velocities than the free-flow, $\langle v_{\text{synchro}} \rangle \approx 54 - 75\,\text{km/h}$ vs. $\langle v_{\text{free}} \rangle \approx 105\,\text{km/h}$. Note, the travel velocity of the synchronized region is not constant but changes with varying densities. The density range in which the free-flow coexists with the synchronized traffic is depending on the system length. Increasing the density further the regions of synchronized traffic get broader and the whole system is governed by synchronized traffic (left part of Fig. 5.4). The velocity in this example is about $v \approx 50\,\text{km/h}$ which is much slower than the maximum velocity. This state becomes unstable at higher densities and wide moving jams emerge that are separated from each other by free flow regions (right of Fig. 5.4). The existence of these parallel jams is required as a model property. It is evoked by the slow to start rule that was introduced first in the VDR model. To measure this velocity a periodic system is initialized via mega-jam and the density autocorrelation is measured. The system length divided by the time-difference of the peaks of the autocorrelation give $v_{\text{jam}} = -14.3\,\text{km/h}$ [139]. The velocity is in good accordance with empirical data, i.e., $v_{\text{jam,emp}} \approx -15\,\text{km/h}$. It is adjusted by the proper choice of p_0. The transfer from the synchronized traffic to congested traffic of wide moving jams is more elaborately studied in Sec. 2.2.3.
A very important hint, whether the model reproduces the empirical observations and the characteristics of traffic flow, gives the comparison of the locally measured fundamental diagram (Fig. 5.5) with the empirical one (Fig. 2.3). It shows that the model reproduces the three different traffic patterns very well. At low densities $\rho < 20\,\text{veh/km}$ the free-flow branch is visible. The vehicles do not interfere with each other and the slope is only dependent on the maximum velocity of the vehicles whereas the randomization parameter for fast driving vehicles affects the maximum flow $J_{\max}$. It coincides with the empirical findings. In empirical fundamental diagrams of roads with no speed limit the slope of the free-flow branch is not exactly constant but changes to a convex form for very high fluxes. This is not reproduced here as the maximum velocity is the same for all vehicles and it is not distributed. The flow reaches $J_{\max} \approx 2500\,\text{veh/h}$ which is also quantitatively in good agreement with empirical data. Note in the simulations a strict speed limit is applied and thus the results are compared to empirical data where a speed limit is in force as well.
In the two-dimensional region with $\rho > 20\,\text{veh/km}$ and $J > 1500\,\text{veh/h}$ the region of synchronized traffic is visible. The quite high flows at mid densities are similar to that of the empirical fundamental diagram. Nevertheless, the points are not so scattered and the

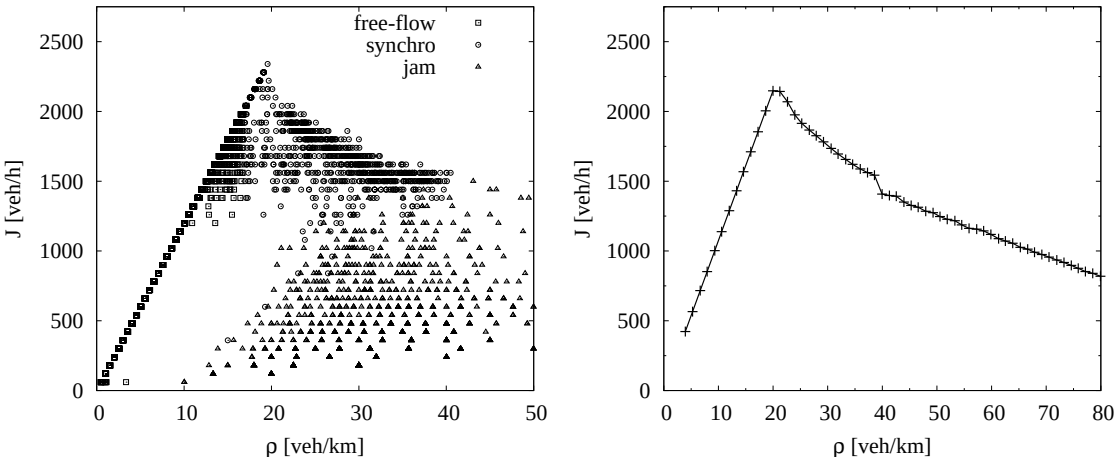

Figure 5.5: **Left:** Local fundamental diagram of a periodic system. Free-flow, synchronized traffic and congested traffic of wide moving jams can be seen. The system length is $L = 10{,}000$ cells and the data is measured after a relaxation time of $T_{\text{relax}} = 30{,}000$ time-steps for $T_{\text{measure}} = 20{,}000$ time-steps. **Right:** Global fundamental diagram of a periodic system. The free-flow traffic shows a linear slope up to $\rho = 20\,\text{veh/km}$. The synchronized traffic governs the density interval between $\rho = 20\,\text{veh/km}$ and $\rho = 40\,\text{veh/km}$. The flow is higher than in the region of wide moving jams that follows for higher densities. The drop of the flow is clearly visible at $\rho = 40\,\text{veh/km}$. The parameter are the same as for the local fundamental diagram.

variance is smaller compared to reality.
The scatter plot between $J = 0\,\text{veh/h}$ and $J < 50\,\text{veh/h}$ corresponds to the measurements in the region of wide moving jams. The variance of the scattering is in particular depending on v_{slow}, which is discussed in Sec. 5.4.3.
The global fundamental diagram (cf. Fig. 5.5) shows the different traffic states as well. Beside the free-flow branch at low densities the region of synchronized traffic shows up between $\rho \approx 20\,\text{veh/km}$ and $\rho \approx 40\,\text{veh/km}$. The flow is significantly higher than for the wide-moving jams that follow for higher densities. This fundamental diagram and in particular the characteristics of the synchronized region will be the reference in further analyses of the different model parameters and their influence on the formation of synchronized traffic.
The outflow out of a jam $J_{\text{out}} \approx 1900\,\text{veh/h}$ which is of the same magnitude as the empirically measured value of $J_{\text{out,emp}} \approx 1{,}800\,\text{veh/h}$ is in good agreement to reality as well. It can easily be triggered by a suitable choice of p_{d} and p_0.
Note the broadness of the synchronized region is not only depending on the model parameters – as discussed in Sec. 5.4 – but also on the simulation time and the system length. Furthermore, the existence of the synchronized traffic is depending on the initialization of the system. Only if the road is homogeneously initialized synchronized traffic emerges. Otherwise, if initialized with a mega jam, wide moving jams govern the whole congested traffic.

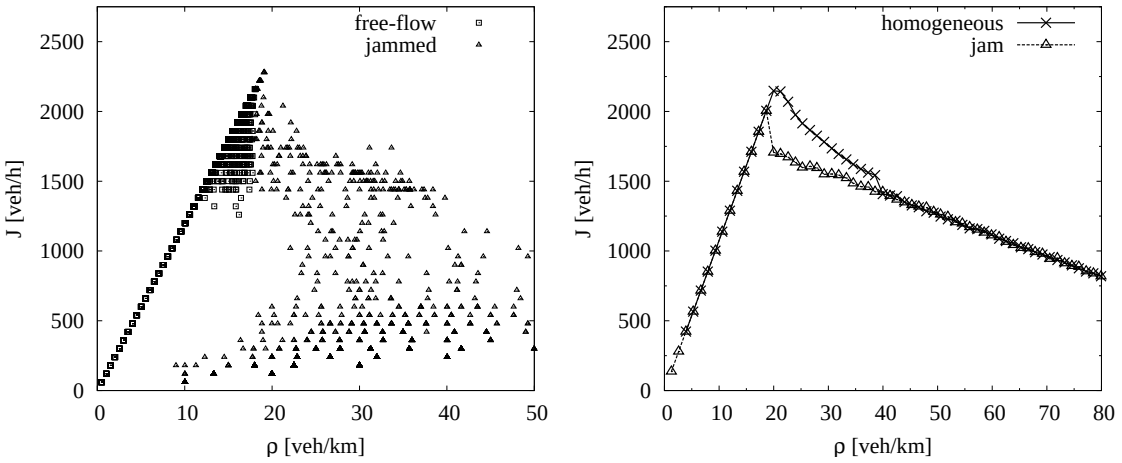

Figure 5.6: **Left:** Local fundamental diagram of a periodic system initialized by a mega jam. Free-flow and the regime of wide moving jams are shown. Synchronized traffic appears very seldom. **Right:** Global fundamental diagram of a periodic system initialized by a mega jam. For simpler comparison the diagram of the homogeneously initialized system is plotted as well. The synchronized regime between $\rho = 20\,\text{veh/km}$ and $\rho = 40\,\text{veh/km}$ is missing if the system is initialized with a mega jam.

5.1.2 System Initialization

Initializing the periodic system with a mega jam shows the metastability of the synchronized traffic. The hysteresis of the region of synchronized traffic as discussed in Sec. 2.2.3 should become visible in the dynamics of the system especially in the fundamental diagram. As shown in Fig. 5.6 left and Fig. 5.6 right the differences with regard to the homogeneously initialized system are obvious. In the local fundamental diagram the two-dimensional region of synchronized traffic is hardly to distinguish. Only a few data points with flows higher than that of the congested branch are visible. Even more explicit are the results in the global fundamental diagram. The synchronized region is no longer present but the state of wide moving jams governs the whole congested traffic. This results in a nearly straight slope of the diagram for high densities. No synchronized traffic can be observed. These results underline that the synchronized traffic is metastable in the whole region but has long-living states in a certain density interval (see Sec. 5.3). Wide moving jams do not resolve and build synchronized traffic. In contrast the density must be reduced to ρ_{out} to reestablish synchronized traffic.
The distribution of the driver's attitude in the steady state should also show differences if the system is not initialized homogeneously as the attitude is crucial for the evolution of the different traffic states (cf. Sec. 5.4.1).

5.2 Comparison with Empirical Single-Vehicle Data

In Chapter 4 the importance to validate any physical model by comparison with empirical data was emphasized. Each model should reproduce the main features qualitatively and quantitatively as accurately as possible. Thus, in this section empirically gathered single-

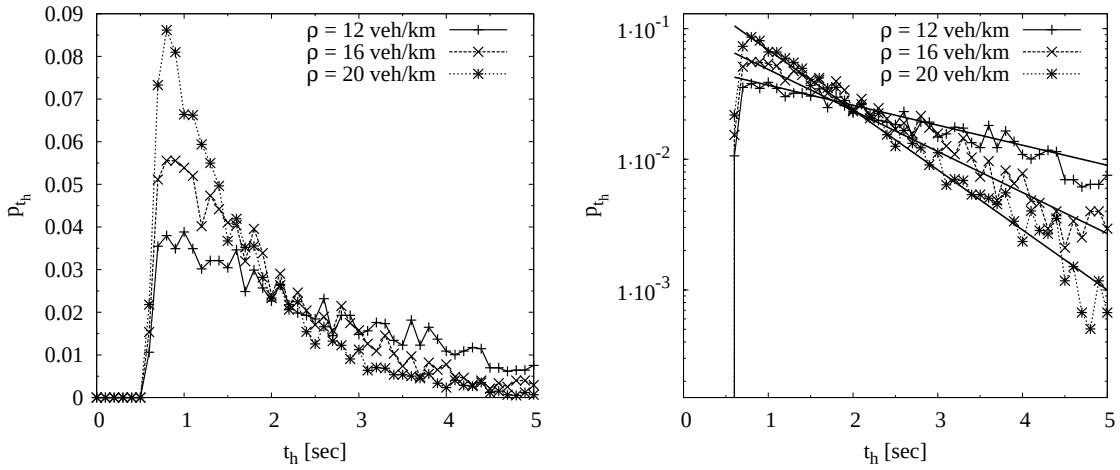

Figure 5.7: **Left:** Time-headway distribution in the free-flow phase. Time-headways shorter than 1 sec are reproduced. The value of the maximum p_{t_h} as well as its position is in very good agreement to the empirical data. **Right:** Logarithmic plot of p_{t_h} for three densities. The linear slope of the distribution shows the exponential decay of the background signal. The empirical data show the same dependence.

vehicle data are compared with the results of the simulations. Especially, the conformance of the time headway distribution is analyzed as this could not be reproduced by the BL model. Because the autocorrelation represents another characteristic feature of vehicular traffic to distinguish the different traffic states occurring in reality, it is compared with experimental results as well.

5.2.1 Time-Headway Distribution

The simulation results are at first compared to the empirical time headway distributions. The bin size of the histogram is set to $t = 0.1\,\mathrm{sec}$. The distribution p_{t_h} for the different density regimes are well reproduced. The comparison of the numerical results measured in free flow (Fig. 5.7) with the empirical data (see Fig. 4.1) shows a very good agreement. The maximum of the time headway distribution is not depending on the density but is always slightly below $t_\mathrm{h} = 1\,\mathrm{sec}$. The maximum value is also qualitatively and quantitatively in very good accordance with the empirical data. For instance, $p_{t_\mathrm{h}}(\rho = 12\,\mathrm{veh/km}) \approx 0.09$ is consistent with $p^{\mathrm{emp}}_{t_\mathrm{h}}(occ = 5, \ldots, 10\%) \approx 0.09$ of the empirical data[2] (cf. Fig. 4.2). The results for other densities are in good agreement as well. As in reality the histogram decreases exponentially. This behavior is also in very good accordance with the empirical data qualitatively and quantitatively. The reason for this good correspondence is given by the attitude of the vehicles in free flow. Here, the vehicles benefit from the reduced safety criterion as nearly all vehicles drive optimistically. Thus, the vehicles can underestimate their safety distance and follow each other with a very small gap and the time headways can reach very low values. The lower limit is mainly affected by t_safe (see Sec. 5.4.5). The

[2]Note the empirical data are plotted with respect to the occupation. Thus, $occ = 5\% \approx \rho = 6.7$ and $occ = 10\% \approx 13.3\,\mathrm{veh/km}$ if the maximum density is $\rho_\mathrm{max} = 133\,\mathrm{veh/km}$.

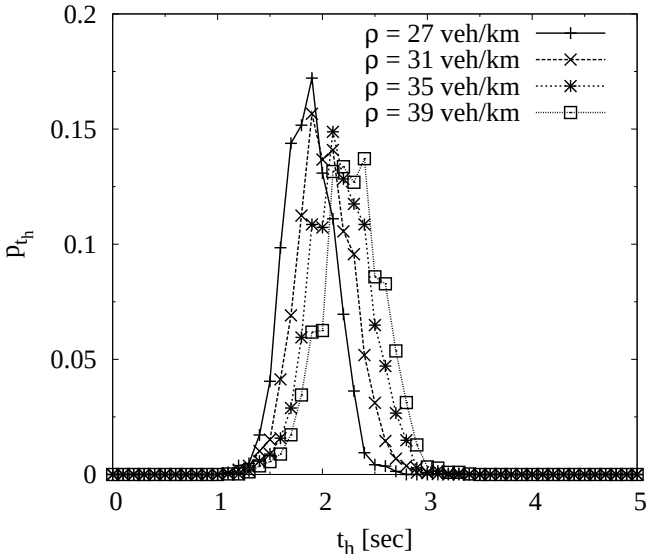

Figure 5.8: Time-headway distribution in the synchronized phase. No time headways shorter than one second are detected, but most are measured around $t_\mathrm{h} \approx 2\,\mathrm{sec}$.

origin of these short time headways can be found in the formation of platoons of very fast vehicles that are driving behind each other typically with very small distances. About three to four vehicles form one platoon. These platoons are separated from each other by larger gaps that absorb emerging fluctuations and thus keep the flow stable nevertheless. The good accordance of the time headway distribution p_{t_h} with the empirical findings is underlined by the slope of the background signal of the probability distribution. The time headways of undisturbed vehicles can be described by so-called *random headway states*. They yield an exponential decay of p_{t_h} [116] that is given by

$$p_{t_\mathrm{h}} = \frac{1}{\tau'}\, e^{-t_\mathrm{h}/\tau} \tag{5.10}$$

where $\tau \propto J^{-1}$ is the inverse flow and $\tau' \approx \tau/\nu$ with ν the number of bins in an interval of 1 sec, which is 10 here. The simulation results (Fig. 5.7) are in very good accordance with the empirical data [131]. They show an exponential dependence of the probability distribution with a slope getting larger for higher densities. This shows that the modeling approach that the drivers underestimate their safety distance and hence build platoons of fast driving vehicles with low distances seems to be correct and thus explains the existence of very short time headways.
These findings are in much better agreement than that of the BL model where short time headways result from a fraction of faster vehicles [91].
It is important to stress that the short time headways are an *intrinsic* effect of this model. For example in the BL model short time headways are provoked by fast driving vehicles [91][3].
The consistency of the distribution in synchronized traffic is not as good as that in the

[3]Note the peaks mentioned in [131] are the results of a software error of the detecting devices so that multiples of 0.9 sec were exaggerated.

free-flow. In the simulation (Fig. 5.8) the maximum is detected at $t_\mathrm{h} \approx 2\,\mathrm{sec}$ and the curve is spread far less than the empirical data (cf. Fig. 4.2). The reason for the very narrow distribution lies in the strong coupling of the vehicles in the synchronized traffic. They tend to adapt the velocity of their leaders and thus fluctuations in the velocity are small. Stronger disturbances arise only if a vehicle changes its attitude and has to brake therefore.
In contrast to the results in [107] time headways lower than one second could not be detected in the simulations of synchronized traffic. The lower limit is located at $t_\mathrm{h} \approx 1.1\,\mathrm{sec}$ and the upper at about $t_\mathrm{h} \approx 2.8\,\mathrm{sec}$. The empirical data show time headways as short as $t_\mathrm{h} \approx 0.8\,\mathrm{sec}$. This is a consequence of the majority of vehicles being pessimistic and therefore driving at quite large distances behind each other in the stationary state. Shorter distances appear in simulations of two-lane traffic if vehicles merge into the lane. These vehicles disturb the very homogeneous flow so that short time headways appear (see Sec. 6.1.2). Here the distribution is spread wider, too. This hints at the importance of the lane changes for a realistic description on the microscopic level.
The origin of the differences between the results in this thesis and those of [107] can be traced back to the measurement method used. If the calculation of time headways would be based on the net distance

$$t_\mathrm{h} = \frac{gap_n}{v_n} \tag{5.11}$$

with $gap_n = x_{n+1} - x_n - l_n$ between the vehicles, its distribution would be similar to that of [107].
A look at the time headways in free-flow can illustrate that. In free flow most of the vehicles drive with $v = 20\,\mathrm{cells/time\text{-}step}$. If now the time headway is calculated following Eq. (5.11) the length of the vehicle which is set to $l = 5\,\mathrm{cells}$ is neglected in contrast to the calculation method in (Eq. 2.9). Therein the front of the vehicles is regarded. Thus, the time headway is shifted to a smaller value, e.g., by $t_\mathrm{shift} = \frac{l}{v} = \frac{5\,\mathrm{cells}}{20\,\mathrm{cells/time\text{-}step}} = 0.25\,\mathrm{sec}$, which corresponds to the difference between the two measurement methods. The same holds for the time headway distribution of the synchronized traffic where a common velocity is $v = 10\,\mathrm{cells/time\text{-}step}$. The distribution now would be moved by $t_\mathrm{shift} = 0.2\,\mathrm{sec}$ so that time headways lower than 1 second are frequent. But as stated above, the measurement method of the detectors is reproduced as realistic as possible and thus this method is chosen for comparing simulation results with reality.

5.2.2 Correlation

The analysis of the empirical data of the synchronized traffic showed that the vehicle-vehicle correlation of the velocity and the gap of the single-vehicle data are characteristic [88]. Furthermore, the autocorrelation of the time-aggregated measurements of the flow, the velocity, and the density should vanish for all time-steps greater than one minute [130]. Thence, the model's behavior concerning these correlations is analyzed in this section.
As shown in the left of Fig. 5.9 strong vehicle-vehicle correlations $\mathcal{N}_v$ of the velocity can be measured. This is in good agreement with the empirical data. The latter just shows longer ranging correlations, i.e., up to higher n. The gaps of succeeding vehicles are only slightly correlated (right of Fig. 5.9). For $n = 1$ it is about $\mathcal{N}_{gap} \approx 0.2$ and decays slowly for higher n which is in good accordance with empirical results as well. Although the

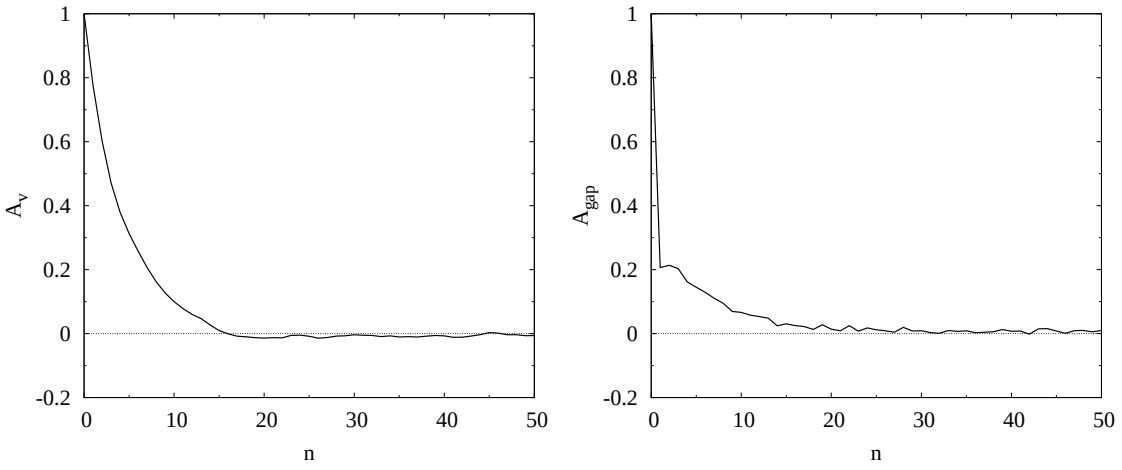

Figure 5.9: **Left:** Vehicle-vehicle correlation $\mathcal{N}_v$ of the velocities of n succeeding vehicles. The periodic system is initialized with $\rho = 27\,\text{veh/km}$. The correlation of the velocity is obvious. **Right:** Vehicle-vehicle correlation $\mathcal{N}_{gap}$ of the gaps of n succeeding vehicles of the same system. The value of the correlation drops immediately to $\mathcal{N}_{gap} \approx 0.2$ and decreases further for higher n.

velocities are strongly correlated, the gaps vary significantly. Therefore, no platoons can be observed. Accounting for the time-aggregated data the autocorrelation $\mathcal{A}$ of the flow vanishes as claimed. This holds for the velocity and the density as well. It shows that with respect to the autocorrelation of the vehicles and the time-aggregated data the model approach shows a realistic behavior and describes the synchronized traffic accurately.

5.2.3 Gap Distribution

The net gap distribution is particularly important with regard to the avoidance of unsafe configurations or the dissolving of these in systems where the intrinsic dynamics is disturbed by inserted vehicles. It happens there that short gaps occur in the free-flow that are not found in the steady state of the undisturbed system. To differentiate between these artificially short gaps and the intrinsic minimal gaps a close look at the gap distribution for low densities in the regime of free-flow traffic is taken. In Fig. 5.10 the gap distribution for initial densities in the range $\rho = 13\,\text{veh/km}$ and $\rho = 19\,\text{veh/km}$ is shown. One sees clearly, that gaps lower than $gap = 9\,\text{cells}$ are really uncommon whereas gaps smaller than 8 cells are not measured at all (see inset of Fig. 5.10). Only approximately 0.3% of the measured gaps are of size 8 cells. For a $gap = 9\,\text{cells}$ the frequency rises drastically to a value of $N_{gap=9} \approx 2\%$ for $\rho = 13\,\text{veh/km}$ and $N_{gap=9} \approx 3.5\%$ for $\rho = 19\,\text{veh/km}$. The maximum is measured between $gap = 10\,\text{cells}$ and $gap = 14\,\text{cells}$ depending on the density. For larger gaps the frequency declines exponentially according to the random headway states already mentioned in Sec. 5.2.1.
This result is used in Sec. 5.6.2 where the model is adapted so that it can be used in two-lane traffic without introducing additional accidents. The calculation of γ if $v_{n+2} \geq v_{\text{fast}}$ is changed and a lower limit of the gap between two following vehicles is applied so that additional accidents as a result of lane changes are avoided.

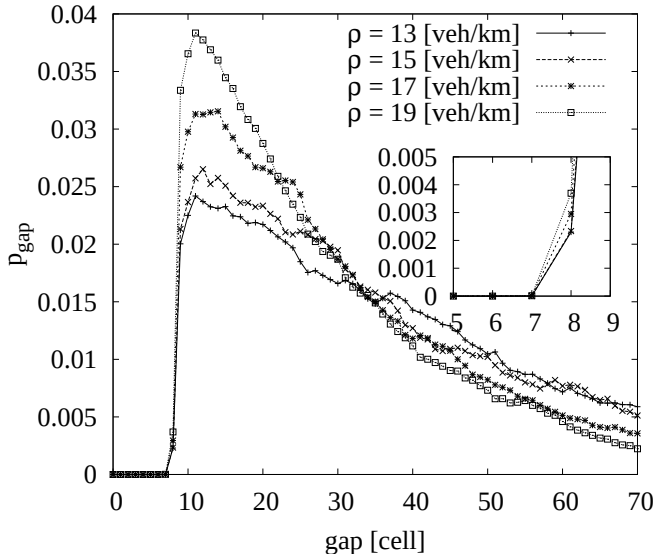

Figure 5.10: Gap distribution for densities between $\rho = 13\,\text{veh/km}$ and $\rho = 19\,\text{veh/km}$. The distribution is cut-off at $gap = 8\,\text{cells}$. The maximum is reached at $gap = 10\,\text{cells}$ and the background signal decreases exponentially. **Inset:** Magnification of the gap distribution for small gaps. Headways smaller than 8 cells rarely occur.

5.2.4 Optimal-Velocity Function

The velocity-distance relation, also called optimal-velocity function, is the next measure discussed here. The simulation results are depicted in Fig. 5.11 for free-flow and synchronized traffic. The agreement of the results in free-flow with empirical findings is very good. The velocity is independent from the distance and all vehicles can drive with the maximum velocity. The possibility for the vehicles to fall below the safety distance when driving optimistically allows for the high velocities also for very small distances.
The agreement of the optimal-velocity function in synchronized traffic is not so good. Whereas the empirical optimal-velocity function increases fast and adopts a distance independent value already for small gaps, the simulation results show a more complex dependence of the velocity on the distance for low to mid distances. A distance independent velocity is reached for large gaps. For example, in the density interval $35\,\text{veh/km} \leq \rho \leq 40\,\text{veh/km}$ the velocity is constant for small distances $\rho < 15\,\text{veh/km}$ and increases for distances between $gap \approx 15\,\text{m}$ and $gap \approx 30\,\text{m}$. For higher densities the velocity becomes independent from the distance, i.e., $v \approx 50\,\text{km/h}$. Compared to the empirical findings the velocities for larger gaps are higher: 50 km/h in the simulations for $35\,\text{veh/km} \leq \rho \leq 40\,\text{veh/km}$ vs. 40 km/h in the empirical data.
The reason for the non constant relation lies in the attitude of the vehicles. Very short headways at high velocities are only allowed for optimistic vehicles but in synchronized traffic a majority is pessimistic. Thus, the velocity is smaller. With larger distances the difference between the driving behavior of both attitudes becomes smaller and thus the vehicles drive with the same velocity despite their attitude. This leads to a larger velocity. Note for $22\,\text{veh/km} \leq \rho \leq 24\,\text{veh/km}$ free-flow and synchronized traffic coexist. Thus, it

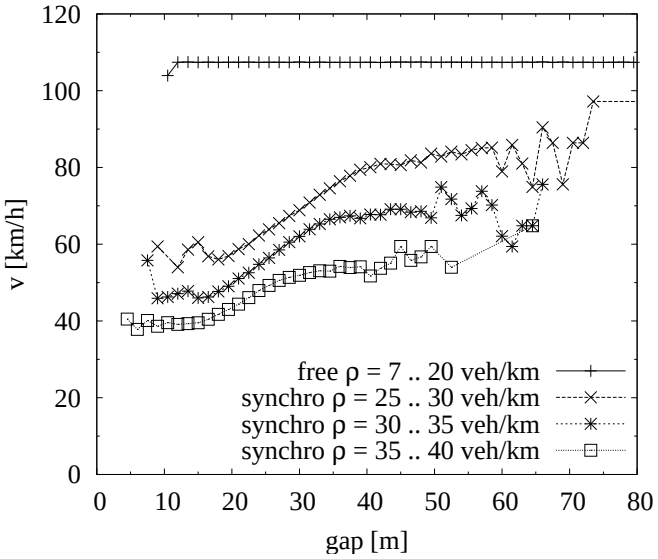

Figure 5.11: Optimal-velocity function. In free-flow the velocity is independent from the distance and all vehicles can drive with the maximum velocity. A distance independent velocity is reached in synchronized traffic at higher distances. At low gaps the velocity rises with larger distances. Here, the different gaps that are acceptable by optimistic and pessimistic drivers are relevant.

is important to distinguish the data points and use only these from synchronized traffic in the calculation.

5.3 Life-Time of Synchronized Traffic

The investigations of the empirical characteristics of synchronized traffic (cf. Sec. 2.2.3) show that it is metastable in a certain density regime. Local perturbations may rise and form a wide moving jam. The reproduction of this property by the model of Lee *et al.* is therefore necessary and has to be proven. Thus, the life-time of the synchronized regime is analyzed in the periodic single-lane system.
The numerical investigations qualitatively reflect this characteristic. Depending on the initial density, the synchronized traffic collapses more or less likely and forms separated compact jams and free-flow. An example is shown in the left part of Fig. 5.12. After $T_{\text{jam}} = 68{,}735\,\text{sec}$ – this time corresponds to the number of update steps performed in the simulation – for the first time a vehicle was detected that has stopped. This stopped vehicle is the result of a local perturbation getting larger so that it has to stop.
The life-time is defined as the time until the first vehicle has stopped completely. The system is initialized as usual as homogeneously as possible. A lower time-limit is set to $T_{\text{min}} = 5000\,\text{sec}$ after the start of the simulation so that synchronized traffic is established in the system and a standing vehicle can be interpreted as a consequence of a collapse. This prevents or at least reduces the probability of a misinterpretation of vehicles still standing because of the initialization where the vehicles are initialized as usual with $v_{\text{init}} = 0\,\text{cell/time-step}$. The upper limit is the maximum simulation time which was set to $T_{\text{sim}} = 5 \cdot 10^6\,\text{sec}$.

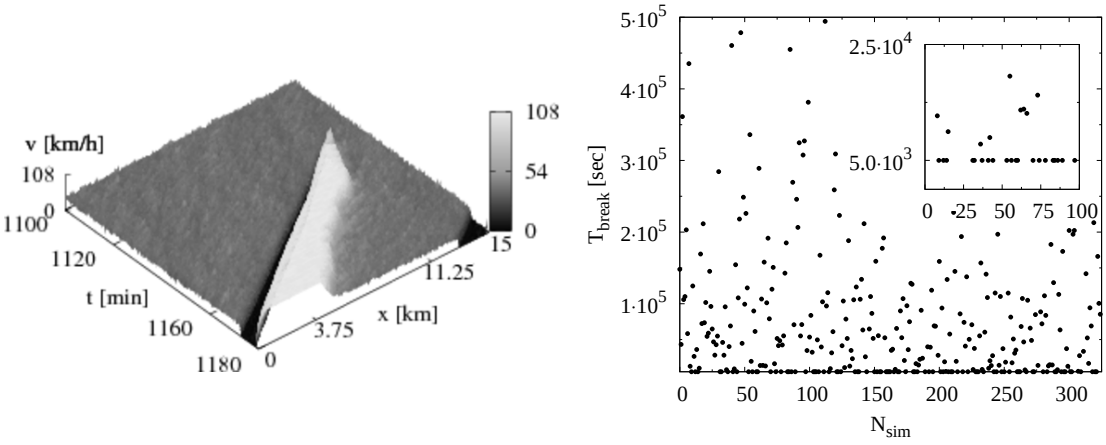

Figure 5.12: **Left:** Example for transition from the synchronized phase to the jammed phase in a periodic system. The first vehicle stopped at a simulated time of $T_{\text{jam}} = 68{,}735\,\text{sec} \approx 1{,}145$ min. The parameters are $\rho = 41\,\text{veh/km}$ and $L = 10{,}000\,\text{cells} = 15\,\text{km}$. **Right:** Life-time of the synchronized state. The time-step when the first stopped vehicle was detected in each of 325 simulations for $\rho = 41\,\text{veh/km}$ is shown. The great variation of the breakdown times is obvious. Note the data points at the bottom of the diagram have a breakdown time that is lower than the minimal measuring time $T_{\text{min}} = 5{,}000\,\text{sec}$. T_{min} denotes the time after that a breakdown is counted. Thus, the minimal time is accounted for these simulations. The ratio in how many simulations a stopped vehicle is detected with respect to the simulation time is shown in Fig. 5.13 below.

For each initialization density up to 325 simulation runs were made depending on the magnitude of the variance of the jam events – the time the first vehicle has stopped. For the lower as well as the upper density limit of the observed region 120 simulation runs where accomplished. At mid densities at $\rho \approx 38\,\text{veh/km}$, where the variance of the events is greatest, the maximum number of simulations where made. The resulting jam events are exemplarily shown in Fig. 5.12 right for $\rho = 38\,\text{veh/km}$. The measurement points are widely scattered so that the large standard deviation of 104,835 sec is not surprising. The arithmetic mean is 84,099 sec and the variance $10^{10}\,\text{sec}^2$.
As mentioned above, the life-time of the synchronized traffic strongly depends on the global density the system is initialized with. In Fig. 5.13 the arithmetic means of the breakdown times T_{break} for each density are depicted in a logarithmic plot. At low densities of the synchronized regime with up to $\rho \approx 35\,\text{veh/km}$ the traffic is stable in the scope of the simulations. All simulation runs have reached the maximum simulation time without any detected stopped vehicle so that the probability for a jam is zero. At higher densities above $\rho \approx 43\,\text{veh/km}$, which correspond to the high-density part of the synchronized region, the situation has totally changed. In this region a breakdown may occur very fast within hundreds of seconds and the probability for this event becomes one. Therefore, the global fundamental diagram that was calculated after a relaxation time of 10,000 sec hints at jammed traffic in this region.
The most interesting density interval in this context is between $\rho = 36\,\text{veh/km}$ and $\rho =$

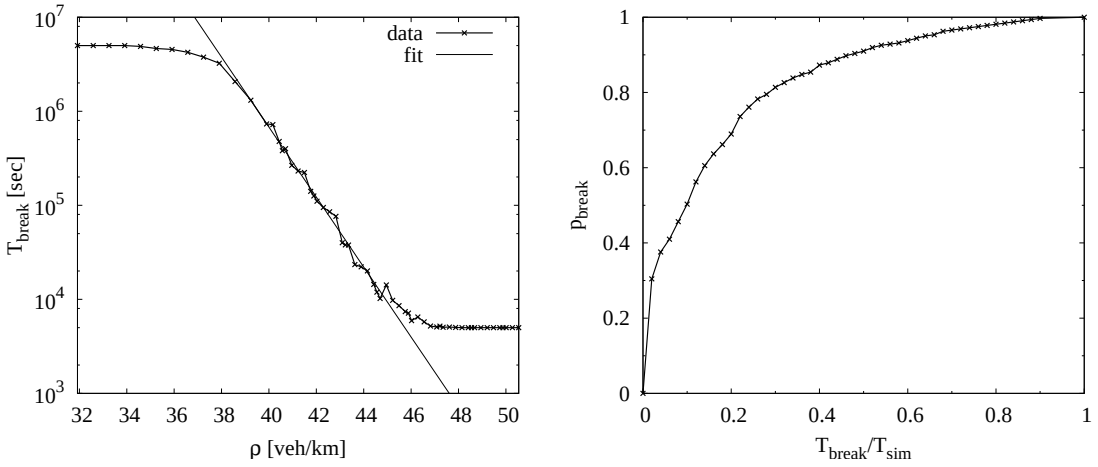

Figure 5.13: **Left:** Log-plot for the time dependence of the transition between synchronized traffic and wide moving jams in a single-lane periodic system. The arithmetic means of the simulations for each density are depicted in a logarithmic plot. The exponential decay is obvious. For large densities the graph converges to $5,000$ sec, which is the start time of the measurement. **Right:** Probability for the occurrence of a jam with respect to the corresponding time-step of the simulation for $\rho = 38$ veh/km. In all simulations a jam event was detected.

42 veh/km, which corresponds to the higher density part of the synchronized regime (see Fig. 5.5). Here, a more complex dynamics is supposed. The logarithmic plot of the mean life-time of the synchronized traffic shows the interesting properties. In this density interval the time-step at which the system collapses is varying very strongly as mentioned above.
Here, the decay of the mean life-times with respect to the initial density is of special interest. The measures in the logarithmic plot are all on a straight line. To proof this visual impression the natural logarithm of the mean life-times in the relevant density interval $\rho = 38\,\text{veh/km} \leq \rho \leq \rho = 48\,\text{veh/km}$ is calculated. The y-intercept a and the slope b can easily be calculated via linear regression. As a result one finds the linear function $T^{\ln}_{\text{break}}(\rho) = a + b \cdot \rho$ with $a = 47.7$ and $b = -0.114\,\text{km/veh}$ is given. Further, $e^{T^{\ln}_{\text{break}}(\rho)} = e^{a+b\cdot\rho}$ gives the exponential fit for the decay of the life-times $T_{\text{break}}(\rho) = 5.24 \cdot 10^{20} \cdot e^{-0.114\cdot\rho}$.
To proof the linear relation the "Pearson correlation coefficient" $r_{\vartheta,\psi}$ (Eq. 5.12) was calculated additionally.
It is a good measure to describe the strength and the direction of the linear relationship between two variables, i.e., whether the data points are scattered or lie on a straight line

$$r_{\vartheta,\psi} = \frac{\sum_{i=1}^{N}(\vartheta_i - \langle\vartheta\rangle)(\psi_i - \langle\psi\rangle)}{\sqrt{\sum_{i=1}^{N}(\vartheta_i - \langle\vartheta\rangle)^2}\sqrt{\sum_{i=1}^{N}(\psi_i - \langle\psi\rangle)^2}}. \tag{5.12}$$

The value $r_{\vartheta,\psi}$ lies between -1 and 1, inclusive. It takes a value 1 independent of the magnitude of the slope when the data points lie on a perfect straight line with positive slope, with ϑ and ψ increasing together. If $r_{\vartheta,\psi}$ equals -1 the data points lie on a perfect

line with negative slope. A value of $r_{\vartheta,\psi} = 1$ is called a "complete positive correlation" and $r_{\vartheta,\psi} = -1$ a "complete negative correlation". A value near 0 indicates that the variables are uncorrelated.
In this context the Pearson correlation coefficient $r_{T^{\ln}_{\text{break}},\rho}$ is relevant. Thus, the pairs of quantities $(T^{\ln}_{\text{break,i}}, \rho_i), i = 1, \ldots, N$ are used where N is the total number of data points. The mean $\langle\rho\rangle$ is calculated over all ρ_i's and $\langle T^{\ln}_{\text{break}}\rangle$ over all $T^{\ln}_{\text{break,i}}$'s.
The calculated value $r_{T^{\ln}_{\text{break}},\rho} = 0.998$ is very close to one which underlines the linear relation in the logarithmic plot and thus the exponential decay of the life-times.
Note, for initial densities lower than $\rho = 39\,\text{veh/km}$ the probability for a jam event during the simulations becomes smaller than one. For $\rho = 39\,\text{veh/km}$ the probability becomes $p_{\text{jam}} = 0.968$ and for $\rho = 38\,\text{veh/km}$ one finds $p_{\text{jam}} = 0.864$. For densities $\rho < 33\,\text{veh/km}$ the probability for the emergence of a jam decreases very fast, i.e., faster than exponentially[4] and approaches zero. Thus, the measurements for $\rho < 38\,\text{veh/km}$ are not used in the calculation of the linear regression. The same holds for initial densities larger than $\rho = 48\,\text{veh/km}$ as most simulations already show jammed traffic at the beginning of the measurement after 5000 sec.
Figure 5.13 shows the probability that a jam occurs in dependence on the relative simulation time $T_{\text{jam}}/T_{\text{sim}}$. This shows that the probability of a jam event decreases with increasing simulation time.
It is important to note that the dependence of the life-times of the synchronized traffic in the periodic system shows a different decay than the synchronized traffic in an open system in the vicinity of an on-ramp. In the latter the probability of a local perturbation that leads to a jam is depending on the density inside the synchronized region. This is as well indirectly controlled by the inflow rate from the ramp when keeping the flow onto the main road constant. The decay of the life-times is faster than exponential. This is not surprising as beside the intrinsic fluctuations of the synchronized traffic it is additionally perturbed by every inserted vehicle so that the traffic collapse more likely. In other words, the synchronized traffic is very stable in a wide density interval, but a breakdown can be induced by a extrinsic disturbance. See Sec. 7.1 for a detailed analysis on this topic. Therein, also empirical findings concerning the life-time are discussed.

5.4 Model Parameters

In the last sections, it was shown that the results of the simulations are in very good agreement with the empirical findings despite the fact that they were gathered at a two-lane section of the highway network. But in order to get a deeper insight into the model dynamics the influence of the parameters is investigated. So, in the next subsections the parameter set is analyzed systematically. At first, the attitude of the drivers is discussed with respect to the simulation results. It has the most crucial influence on the internal dynamics of the model. This is followed by the analysis of the parameters g_{add}, v_{slow}, and t_{safe}. They affect the synchronized traffic and the time-headway distribution in free-flow.

5.4.1 Attitude

As stated in the introduction of this chapter, the human factor is an essential part of the dynamics of the model by Lee *et al.*. Thus, it is important to understand which type of

[4] In a log-plot the slope is negative and convex.

drivers are governing the different density regions. It is obvious that optimistic drivers are dominating the free flow region. For higher densities the distribution of pessimistic and optimistic drivers is not clear. Therefore, the distribution of the optimistic and pessimistic drivers is analyzed in the periodic system that is initialized homogeneously. Afterwards the same is applied to a periodic system that is initialized by a compact jam. In the latter, the hysteretic properties of the synchronized traffic (see Sec. 2.2.3) become visible.
Note, the differences in the dynamics of the optimistic and the pessimistic vehicles are very small for very slowly driving vehicles. The additional gap for pessimistic vehicles vanishes if the velocity reaches the magnitude of g_{add}.
In order to determine which part of the calculation of γ leads to an optimistic attitude it is divided into two parts referred by γ_{first}:

$$\gamma_{\text{first}} = \begin{cases} 0, & \text{for } v_n^t \leq v_{n+1}^t \leq v_{n+2}^t, \\ 1, & \text{otherwise,} \end{cases} \tag{5.13}$$

and by γ_{second}

$$\gamma_{\text{second}} = \begin{cases} 0, & \text{for } v_{n+2}^t \geq v_{\text{fast}}, \\ 1, & \text{otherwise.} \end{cases} \tag{5.14}$$

These definitions follow the two reasons for a driver to act optimistic: He drives in a platoon of equally fast vehicles, γ_{first}, or the next but one vehicle is speeding away with high a velocity, γ_{second}.
Note, in general the two parts of the definition of γ do not exclude each other. On the contrary, in the majority of the cases if $\gamma_{\text{second}} = 0$ – optimistic attitude – γ_{first} equals zero as well.

Attitude in Homogeneously Initialized Systems

In the homogeneous system one finds an optimistic-pessimistic ratio as it is depicted in Fig. 5.14.
The relation of the attitude plot (Fig. 5.14, left part) to the different traffic states that can be seen in the fundamental diagram are obvious. In the free-flow region the system is dominated by optimistic drivers. In most cases both definitions of γ force an optimistic attitude. In the free-flow approximately 100% of the drivers are optimistic because of γ_{first}. The almost unhindered vehicles drive at least with v_{fast} and thus are optimistic. But also $\gamma_{\text{second}} = 0$ for about 80% of the vehicles. Platoons of equally fast vehicles are build that are only broken if a vehicle dawdles and drives with $v_n = v_{\text{fast}}$. In synchronized traffic between $\rho \approx 20\,\text{veh/km}$ and $\rho \approx 41\,\text{veh/km}$ only slightly more drivers are pessimistic than optimistic. But for all of these holds $\gamma_{\text{first}} = 0$. According to the properties of synchronized traffic the vehicles drive with nearly the same velocity (Sec. 5.2.2) and thus the precondition for γ_{first} is often satisfied while vehicles driving with v_{fast} are not found and thus $\gamma_{\text{second}} = 1$.
At higher densities the number of optimistic vehicles rises again. About 60% of the vehicles are optimistic because of γ_{first}. In this density regime the dynamics is governed by wide moving jams and free-flow in-between. Inside the compact jams most vehicles are standing and "drive" with the same velocity and have mostly an optimistic attitude $\gamma_{\text{jam}} = 0$. The fact that not all vehicles are optimistic shows that the standing vehicles are intercepted

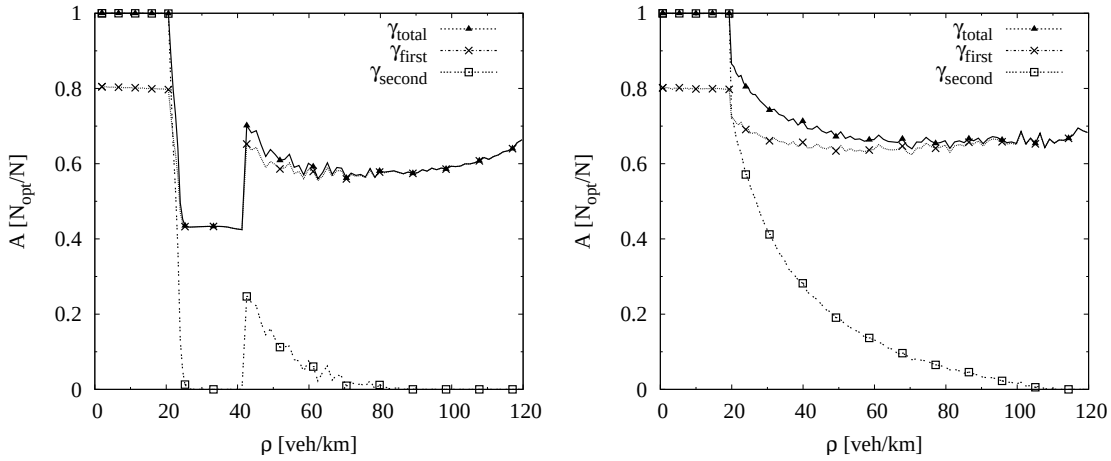

Figure 5.14: **Left:** The total ratio of optimistic vehicles in a periodic system is depicted. Additionally the values for γ_{first} and γ_{second} are plotted. The system is initialized homogeneously. In free-flow below $\rho \approx 20\,\text{veh/km}$ all vehicles are optimistic. In the synchronized regime about 40% of the drivers have an optimistic attitude. All because of γ_{first}. The number rises again for larger ρ. **Right:** The ratio of optimistic vehicles in a periodic system is depicted. The system is initialized with a mega jam. The characteristic distribution of optimistic vehicles in the range of synchronized traffic in the homogeneous system is missing.

by driving vehicles. Another part of the optimistic vehicles is contributed by vehicles that escape the jam. Their predecessors have already accelerated that satisfies the condition for $\gamma_{\text{first}} = 0$.
Additionally, there are optimistic vehicles at densities of 40 veh/km to 67 veh/km because of γ_{second}. Here, the free-flow region between the compact jams reaches an expansion that is large enough so that the vehicles that escape the jam can reach v_{fast}. Note this is a consequence of $\gamma_{\text{first}} = 0$. Otherwise the vehicles would only reach velocities lower than v_{fast} as the larger safety distance they have to adhere to would prevent further acceleration up to v_{fast}. This is discussed in Sec. 5.4.2 in greater detail. At the upper limit of the density range the number of optimistic vehicles reaches 100% as all vehicles are stopped and they are optimistic therefore.
The conditions for optimistic driving fulfill two different tasks. The first one, namely γ_{first}, governs the regime of synchronized traffic, but is important as well in dense traffic especially at very high densities. Here, the optimistic driving is indispensable for the development of wide moving jams in-between free-flow regions. Otherwise, jams would alternate with synchronized traffic (see Sec. 5.6.1). γ_{second} is clearly governing free-flow allowing short time headways and stable free-flow as dawdling does not always lead to an attitude change.

Attitude with Jam Initialization

The fraction of optimistic drivers with respect to the density shows a different characteristic if the system is initialized by a mega jam. Whereas no differences between the two

initialization methods can be found in the high density region they become obvious in the density region of the synchronized traffic and – less clearly – in the free-flow region. In the latter the predominance of the optimistic vehicles is shifted to lower densities. In the homogeneously initialized system nearly all vehicles are optimistic till $\rho \approx 21\,\text{veh/km}$ in contrast to $\rho \approx 19\,\text{veh/km}$ otherwise. This can be explained by the metastability of the free-flow branch and the well known hysteresis effect.
The differences in the synchronized density region are far more drastic. The reduced number of optimistic vehicles between $\rho \approx 21\,\text{veh/km}$ and $\rho \approx 41\,\text{veh/km}$ has vanished. A synchronized region can no longer be identified but the free-flow region passes rather smoothly into the jammed regime. Now the slope of the fraction of optimistic vehicles that is already present in the homogeneous system proceeds to smaller densities. In dense traffic the differences are small again.
This supports the result that the system is metastable in the synchronized regime. As a consequence the fundamental diagram shows a hysteresis in the synchronized traffic. The attitude shows a similar hysteresis as well.
The metastability was further analyzed in Sec. 5.3.
The strong influence of γ_{first} and γ_{second}, respectively, justifies a more detailed analysis of the dynamics of the model if only either of these two parts is used to estimate γ. This is done in the following subsection 5.4.2.

5.4.2 Reduction of the Attitude

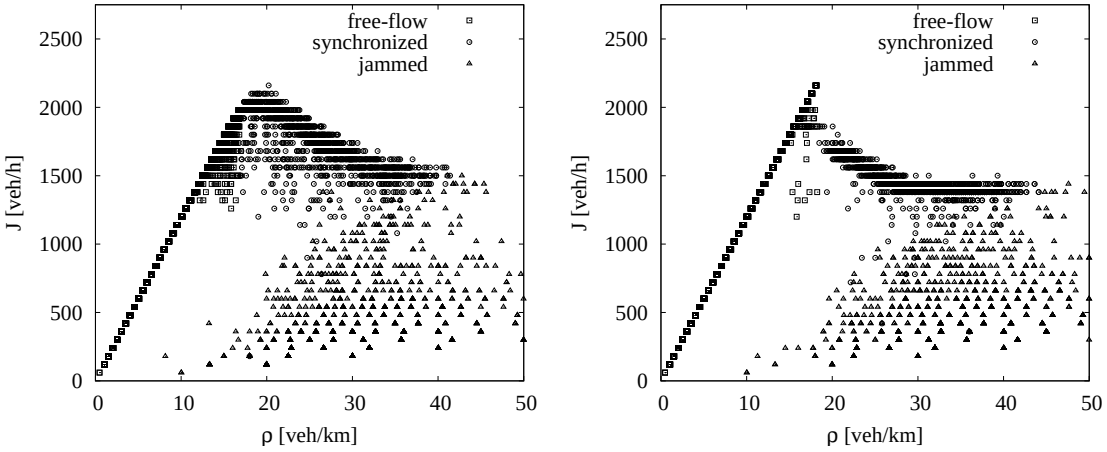

Figure 5.15: **Left:** Local fundamental diagram for $\gamma = \gamma_{\text{first}}$. The high fluxes of the free-flow branch are missing. The free-flow region goes smoothly over into the synchronized region. **Right:** The analog local fundamental diagram for $\gamma = \gamma_{\text{second}}$. One finds a broad region of synchronized traffic and high flows of the free-flow branch. Free-flow and synchronized traffic are clearly separated.

To further analyze the influence of γ_{first} and γ_{second} the local fundamental diagrams of the model in which the calculation of γ is limited to γ_{first} and γ_{second}, respectively, are shown in Fig. 5.15 left and right, respectively.
If only γ_{first} characterizes the attitude of the driver the differences to the unmodified model in the local fundamental diagram appear for densities $\rho > 18\,\text{veh/km}$. The free-

flow branch is no longer separated from the synchronized region but smoothly runs into it. The synchronized regime is now a broad linearly decreasing region for $20\,\text{veh/km} \leq \rho \leq 41\,\text{veh/km}$. The high-flow branch is missing and therefore the very short time headways below 1 sec.
These time headways appear if only γ_{second} is used for the calculation of γ (Fig. 5.15). This underlines the necessity of γ_{second} for the realistic mapping of the free-flow. However, the synchronized region has a different shape now. The flow in this region is smaller and the region now consists of a linearly decreasing and a nearly vertical region at higher densities. Note the existence of vehicles driving optimistically is not a requirement for synchronized traffic. This is shown in the following section 5.6.1.

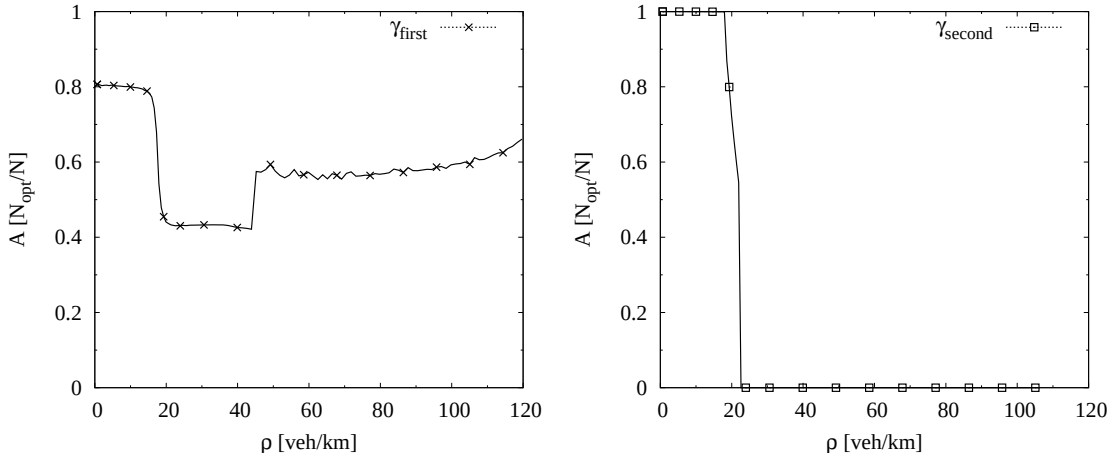

Figure 5.16: **Left:** The distribution of the attitude for a homogeneously initialized system when only γ_{first} is valid. At all densities optimistic and pessimistic vehicles can be found. The curve is similar to the original model. **Right:** The same diagram for a system initialized if only γ_{second} is applied. In the free-flow region still 100% of the vehicles are optimistic. At higher densities there are strong discrepancies to the original model formulation. No optimistic vehicles appear at densities larger than $\rho = 21\,\text{veh/km}$.

Another remarking feature is the slope of the attitude distribution in the two cases. If only γ_{first} is regarded (Fig. 5.16 left side) there are only minimal differences to the characteristic of γ_{first} in the unadapted model (Fig. 5.14 left). The region where most drivers are optimistic – which corresponds to the free-flow regime – ends earlier at $\rho \approx 18\,\text{veh/km}$ in contrast to $\rho \approx 21\,\text{veh/km}$. The region of most drivers being optimistic is also smaller if only γ_{second} is active (Fig. 5.16 right).
Thus, the probability that a vehicle is optimistic is obviously increased if γ_{first} and γ_{second} are valid simultaneously which is true in the unmodified model. This means, if $\gamma_{\text{first}} = 0$ more vehicles are optimistic due to γ_{second} as well and vice verse and the upper limit of the region where nearly 100% of the vehicles are optimistic reaches higher densities. Therefore, the high fluxes can be reached and they are stabilized.
Further, there are strong differences at the lower limit of the congested branch with $\rho = 40\,\text{veh/km} \leq \rho \leq \rho = 80\,\text{veh/km}$ if only γ_{second} is valid. In contrast to the complete model no optimistic drivers appear in this density region. This can be explained by the fact that it is not possible for the vehicles to reach v_{fast} since the spatial headways are

short and all vehicles keep driving pessimistically. In the original model optimistic drivers may appear at densities above 41 veh/km as a consequence of γ_{first}. Because γ_{first} may be 0 – optimistic – also at low velocities optimistic drivers may establish and so smaller headways and higher velocities may be reached when the vehicles accelerate unhindered. If the densities are lower than $\rho \approx 80$ veh/km, velocities $v \geq v_{\text{fast}}$ can be achieved and γ_{second} yields optimistic drivers.
Concluding, the discussion of the influence of γ_{first} and γ_{second} shows that the interplay of both rules stabilize the optimistic driving of the vehicles and this interplay is essential to describe the attitude of the driver and the dynamics of the model. Both are crucial for the realistic reproduction of real-world effects by the dynamics of the model. Here, γ_{second} allows for short time headways in the free-flow, i.e., platoons of vehicles driving with very short distances. Thus, the observed underestimation of the safety distance results in very high fluxes and in time headways shorter than 0.6 sec (see Sec. 5.2.1).
The number of optimistic vehicles in free-flow basing on each part of the definition of γ supports the emergence of optimistic vehicles of the other kind. If $\gamma_{\text{second}} = 0$ holds for more vehicles, it is more likely that $\gamma_{\text{first}} = 0$ is valid as well and vice verse. This leads to a shift of the upper density limit of the free-flow region to higher values of ρ and thus to very high fluxes.
In dense traffic the mechanism is similar. Here, the occurrence of vehicles with $\gamma_{\text{first}} = 0$ supports the emergence of vehicles with $\gamma_{\text{second}} = 0$. The consequence are optimistic vehicles because of γ_{second} in the original model.

5.4.3 Randomization

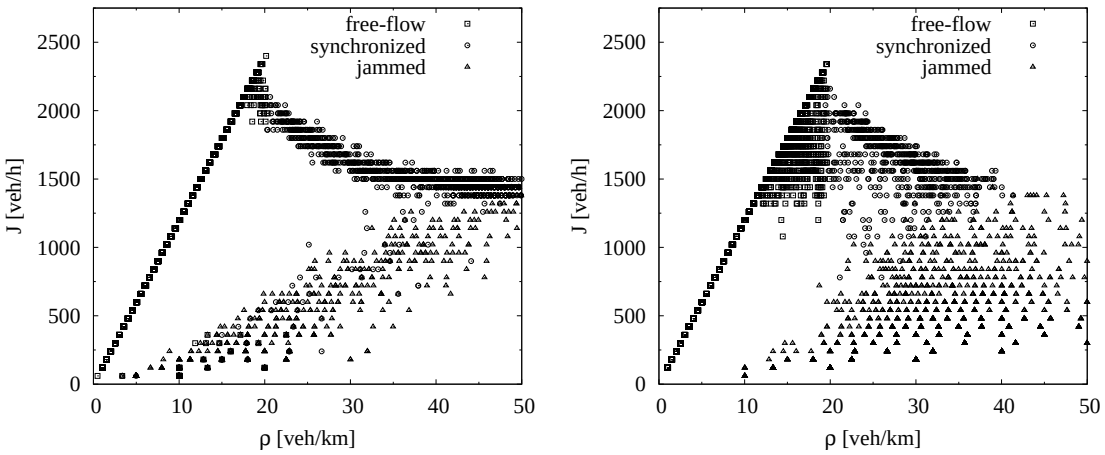

Figure 5.17: **Left:** Local fundamental diagram with $v_{\text{slow}} = 1$. The region of synchronized traffic is extended to higher densities and the measurements at dense traffic are sparsely scattered. **Right:** Local fundamental diagram with $v_{\text{slow}} = 7$. The synchronized region is less extended than for $v_{\text{slow}} = 1$ and the measures of the dense traffic are widely scattered.

The introduction of an extended velocity dependent randomization into the model has an immense influence on the dynamics in the high density region. To illustrate this the calculation of the dawdling parameter p is changed. In detail v_{slow} – the upper limit at which

the dawdling parameter increases – is changed to values between $v_{\text{slow}} = 1\,\text{cell/time-step}$ and $v_{\text{slow}} = 7\,\text{cells/time-step}$. The first case – $v_{\text{slow}} = 1\,\text{cell/time-step}$ – means that the dawdling parameter is calculated directly following [9]. Only stopped vehicles dawdle with a higher probability which leads to a strong separation of the jammed and free-flow traffic. The comparison of the local fundamental diagram with that of the unchanged model with $v_{\text{slow}} = 5\,\text{cells/time-step}$ (Fig. 5.5, left) reveals the differences (see Fig. 5.17, left). If $v_{\text{slow}} = 1\,\text{cell/time-step}$, the congested branch is much less scattered than for higher values of v_{slow} and decreases nearly linearly. This hints at very compact jams with few disturbances and a strong separation between jams and free-flow traffic. Only a few vehicles are in the transition region that account for the spread data points. Additionally, for small v_{slow} synchronized traffic emerges at lower flows than for large v_{slow}.
If a high value is assigned to v_{slow}, e.g., $v_{\text{slow}} = 7\,\text{cells/time-step}$ (see Fig. 5.17, right), the data are much wider scattered in the high density regime. This is very similar to the results from the original parameter $v_{\text{slow}} = 5\,\text{cells/time-step}$ and differences are hardly to be identified in the local fundamental diagram. Thus, a different method has to be applied in order to exhibit the differences. So, the "Pearson correlation coefficient" $r_{\vartheta,\psi}$ (Eq. 5.12) is calculated. In the current context the association between the flow J and the density ρ is of special interest. Note, this coefficient must not be confused with the cross-correlation between J and ρ.
For this analysis only data are selected that do not belong to the free-flow branch nor synchronized flow. To assure this the flow is limited to a maximum of 1450 veh/h. Table 5.1 summarizes the coefficients $r_{\rho,J}$ for the jammed traffic with respect to v_{slow}.

$v_{\text{slow}}\,[\,\text{cell/time-step}\,]$	$r_{\rho,J}$
1	0.92
2	0.73
3	0.51
4	0.41
5	0.38
6	0.37
7	0.36

Table 5.1: Linear correlation coefficient $r_{\rho,J}$ for the measurements of the high density regime. For $v_{\text{slow}} = 1$ the correlation is high. The data points build an ascending line. The coefficient of the free-flow branch is in all cases $r^{\text{free}}_{\rho,J} = 0.99$ which means they lie on an almost perfect straight line. Note, this coefficient must not be confused with the cross-correlation between J and ρ.

The results underline the visual impression of the local fundamental diagram. For $v_{\text{slow}} = 1\,\text{cell/time-step}$ the correlation coefficient is near to one. This indicates a clear linear relation between flow and density for dense traffic. For comparison, the coefficient for the free-flow branch is even higher $r^{\text{free}}_{\rho,J} = 0.99$. For larger v_{slow}, $r_{\rho,J}$ decreases fast and adopts a small constant value for $v_{\text{slow}} \geq 4\,\text{cells/time-step}$. For large values of v_{slow} a linear correlation is very weak. The similar values $r_{\rho,J}$ for $v_{\text{slow}} = 4, \ldots, 7\,\text{cells/time-step}$ correlate with the small differences found in the local fundamental diagrams.
The global fundamental diagram supports this impression as well. It is plotted in Fig. 5.18 for different values of v_{slow}. It visualizes the dependency of the width of the synchronized

region and allows for the comparison with the original model with $v_{\text{slow}} = 5\,\text{cells/time-step}$. If a higher value is assigned to v_{slow} the upper limit approaches lower densities. Otherwise, if v_{slow} decreases to a lower value the synchronized flow is stabilized and establishes at much higher densities. Note the influence of lower values of v_{slow} is more significant than for values $v_{\text{slow}} \geq 5\,\text{cells/time-step}$.
Two different processes are responsible for these properties. On the one hand, the width of the synchronized region is depending on the strength of the effective dawdling parameter. For larger v_{slow} the dawdling probability is higher for velocities that appear in synchronized traffic as these reach v_{slow}. Thus, it is more likely that a disturbance leads to a breakdown of the synchronized traffic and therefore a wide moving jam establishes more likely. If v_{slow} is low all vehicles dawdle with the lower dawdling probability p_{d}, thus more seldom, which stabilizes the synchronized traffic.
On the other hand, the scattering of the data points and the separation between synchronized traffic and wide moving jams in the fundamental diagram depends on the number of vehicles that have an enlarged dawdling parameter. Even more important is the strong differences between the individual values of p_v, i.e., the differences between the p-bins. They are larger for low v_{slow} than for large ones as the Δp_v decrease monotonically with higher v_{slow}: $\Delta p_v = (p_0 - p_{\text{d}})/v_{\text{slow}}$. For example, if $v_{\text{slow}} = 1\,\text{cell/time-step}$, $\Delta p_v = 0.105$ whereas for $v_{\text{slow}} = 7\,\text{cells/time-step}$, $\Delta p_v = 0.03$. Thus, whereas it is of minor importance with respect to p_v whether the velocity is one cell per step smaller or larger for high v_{slow}, it gets crucial for low ones. This leads to a strong separation between synchronized traffic and wide moving jams and less scattered data points in the local fundamental diagram.
Note, for $\lim_{v_{\text{slow}} \to 0} p(v) = p_{\text{d}}$ there is no slow-to-start rule in the velocity update. Just the same randomization is applied for all velocities and the strict separation between free-flow and compact jams vanishes.
Summarizing, v_{slow} triggers the scattering of the data for high densities and affects the

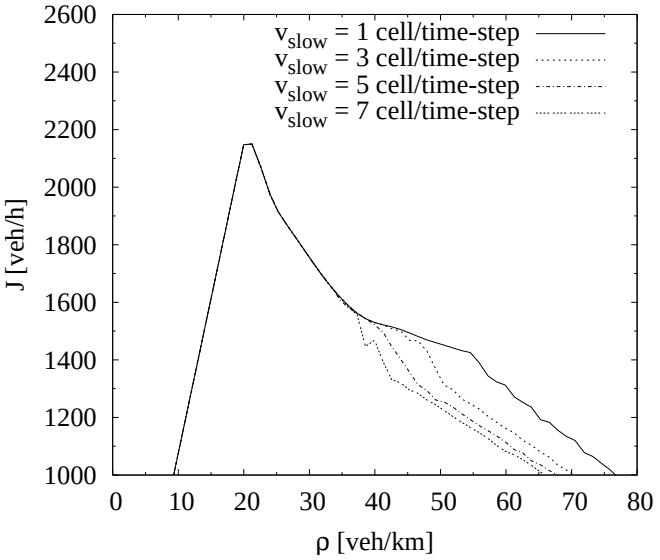

Figure 5.18: Global fundamental diagrams of a periodic system with varying v_{slow}. The higher v_{slow} gets the smaller is the synchronized region. The upper limit is shifted from a higher to a lower value.

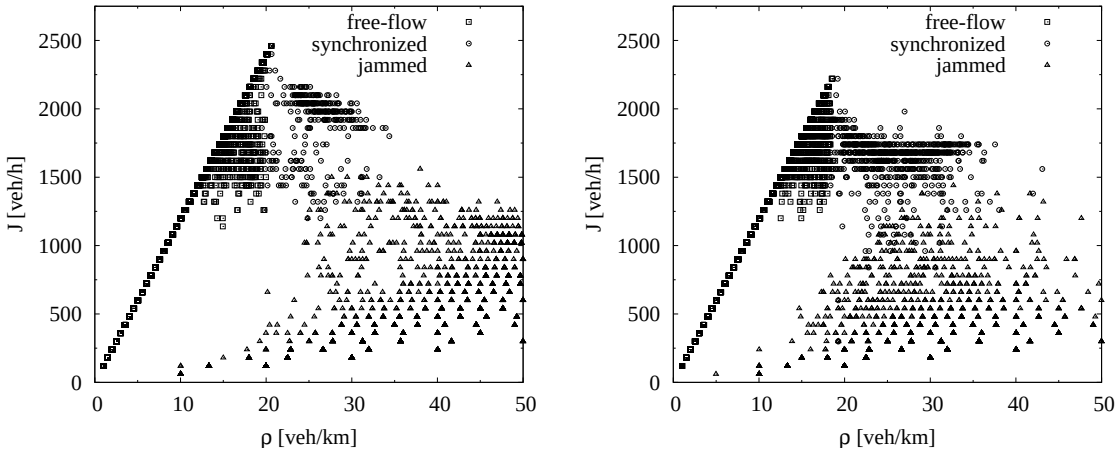

Figure 5.19: **Left:** Local fundamental diagram for $g_{\text{add}} = 2$ cells. The region of synchronized traffic is much smaller and higher flows are reached than in the system with $g_{\text{add}} = 4$ cells. **Right:** Local fundamental diagram for $g_{\text{add}} = 6$ cells. The shape of the synchronized region is different compared to the diagrams for $g_{\text{add}} = 2$ and $g_{\text{add}} = 4$. The synchronized traffic forms a horizontal region.

density regime in which synchronized traffic appears. Small v_{slow} lead do less scattered data in the local fundamental diagram and to a broader synchronized regime. Otherwise, the collapse of the synchronized traffic for high densities is more likely for high values of v_{slow} and governs a smaller region in the global fundamental diagram.

5.4.4 Influence of the Additional Safety Gap

The next parameter to be analyzed is the additional gap g_{add}. This parameter puts an additional safety gap between the vehicles if they drive pessimistically and the velocity is smaller than two times of g_{add}. If the velocity is smaller than g_{add} this factor is not applied at all. Thus, it is only important for pessimistic vehicles driving at higher velocities smaller than v_{fast} and faster than g_{add}. So, this is relevant especially for vehicles driving in synchronized traffic and it can be expected that the size of the synchronized region changes if g_{add} is varied.
This expectation is fulfilled in two aspects that a look at the fundamental diagrams – local as well as global – in Figs. 5.19 right and left and Fig. 5.20 reveals: on the one hand the height of the flux changes and on the other hand the extension of the synchronized region varies. Note that g_{add} only influences pessimistic vehicles.
The local fundamental diagrams show the great differences to the model with the original parameter set. If a small value is chosen for g_{add}, e.g., $g_{\text{add}} = 2$ cells (left part of Fig. 5.19), the synchronized region is shifted to higher flows and its extension is reduced. Contrary, for higher additional gaps, here $g_{\text{add}} = 7$ cells (Fig. 5.19), lower fluxes are measured in the region of synchronized traffic. Further, the shape of the synchronized regime is changed. It forms a horizontal band and the upper limit is shifted to higher densities. The global fundamental diagram underlines the results.
For low values of g_{add} higher fluxes are reached in the synchronized region than for higher values of g_{add}. The flow in general as well as the maximum flow is higher. The higher fluxes

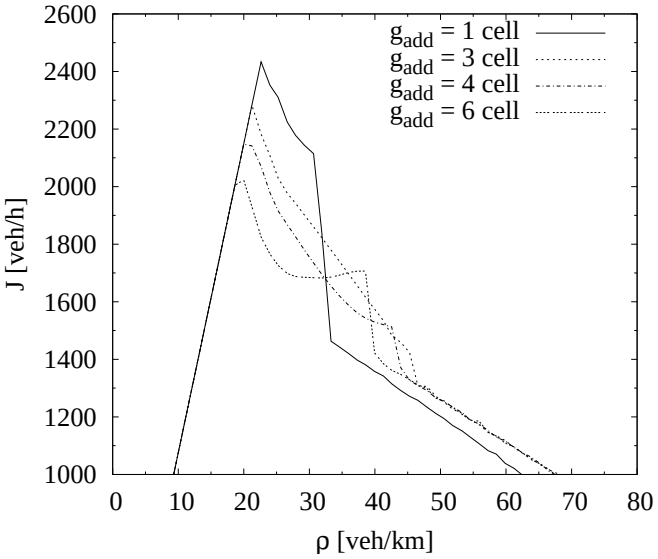

Figure 5.20: Global fundamental diagram for different g_{add}. For low values of g_{add} higher fluxes are reached in the synchronized region. The higher fluxes are obviously the result of the lower safety distance between the vehicles. On the contrary, for higher values of g_{add} the flow decreases.

are obviously the result of the lower safety distance between the vehicles. As g_{add} only affects pessimistic vehicles, these must contribute more to the total flow. The pessimistic vehicles accept shorter headways and thus the mean velocity gets higher and so does the flow. The differences between optimistic and pessimistic vehicles is reduced.. If g_{add} is increased the headway increases linearly and thus the velocity of the pessimistic vehicles decreases. Therefore, the flow decreases as well.
The extension of the synchronized regime also depends on g_{add} as stated above. For low g_{add} the upper limit is at lower densities and approaches a minimum at about $\rho \approx 32\,\text{veh/km}$. For large ones it approaches $\rho \approx 45\,\text{veh/km}$. The shift of the upper limit to lower densities is a consequence of the larger "buffers" between the vehicles.
If a vehicle is in the pessimistic state, which is valid for about 40% in the synchronized region for $g_{\text{add}} = 4\,\text{cells}$ (see Fig. 5.14), the additional gap becomes important and a "spatial buffer" between the vehicles is build. If this buffer is small because of a small g_{add}, it is more likely that a fluctuation is large enough to provoke a breakdown in the synchronized region. Note that in synchronized traffic one finds that the vehicles switch from optimistic to pessimistic driving which is an additional source of fluctuations. In contrast, if a high value is chosen for g_{add}, the influence is different. The velocity fluctuations are easily absorbed and the fluctuations lead less often to the emergence of wide moving jams.
The influence of g_{add} is also visible in the time headway distribution. For $g_{\text{add}} = 1\,\text{cell}$ the maximum is at $t_{\text{h}} \approx 1.5\,\text{sec}$ and time headways lower than 1 sec are detected which is consistent with the high fluxes found for low g_{add}. If g_{add} is larger, e.g., $g_{\text{add}} = 8\,\text{cells}$, the maximum is found at $t_{\text{h}} = 2\,\text{sec}$. The width of the distribution is approximately the same for all g_{add}.
Summarizing, even small fluctuations are not effectively absorbed for low g_{add} so that a collapse is more likely to happen. In contrast, large g_{add} form larger spacings in front of

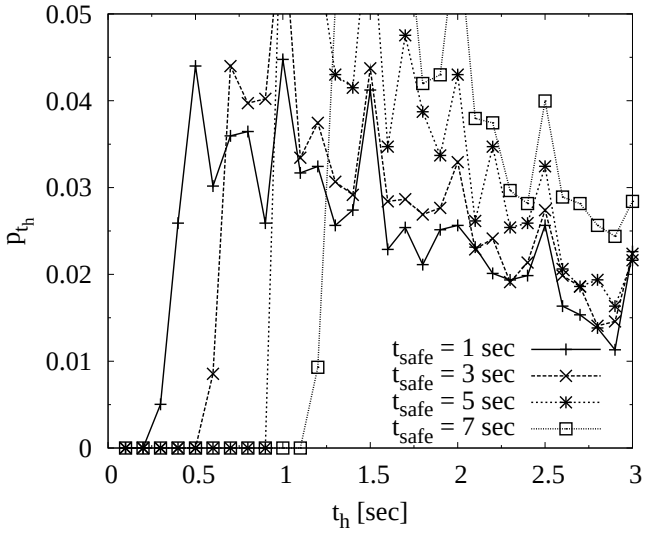

Figure 5.21: Lower cut-off of the time headway distribution p_{t_h} in free-flow traffic depending on t_safe is shown. For all curves the initial density of the periodic system was set to $\rho = 13\,\mathrm{veh/km}$. The lower t_safe is chosen the lower is the cut-off time of the time headway distribution.

the pessimistic vehicles. Hence, the probability that a fluctuation increases seriously is much lower as it is absorbed more likely.

5.4.5 Investigation of t_safe

As stated above the main role of t_safe is the calculation of the safe velocity in the optimistic case and therefore it is especially important in free-flow traffic. It is the decisive factor for the lower cut-off of the time headway distribution in free-flow. The dependence is exemplarily depicted in Fig. 5.21 for an initial density of $\rho = 13\,\mathrm{veh/km}$ and $t_\mathrm{safe} = 1, \ldots, 7\,\mathrm{sec}$. Depending on the value of t_safe one sees clearly strong differences in the simulation results. For low values the lower limit approaches zero but does not reach it due to the additional safety gap and the finite length of the vehicles. The theoretical minimum of t_h is $t_\mathrm{h} = \frac{5\,\mathrm{m/sec}}{20\,\mathrm{m}} = 0.25\,\mathrm{sec}$. The lower limit – also influenced by the interval length of the histogram which is set to $t = 0.1\,\mathrm{sec}$ – is $t_\mathrm{low} = 0.3\,\mathrm{sec}$. This cut-off time was also found in empirical data (cf. Fig. 4.1). It is obvious that such short time headways which are below the reaction time of the driver are very dangerous and these drivers take a very high risk as they would definitively be unable to avoid an accident in case of a sudden obstacle. In addition to the smaller time headways the accident probability rises drastically in the simulations, too. This is somehow in accordance with reality. If the drivers validate their safety only for the duration of their reaction time or even shorter, it is self-evident that the probability for an accident rises.
If t_safe is enlarged the cut-off rises as well and approaches an upper limit of $t_\mathrm{high} = 2\,\mathrm{sec}$. Keeping in mind that for a high value of t_safe driving optimistically gets more and more similar to driving pessimistically, this result is not surprising. The model shows for high t_safe the same lower limit of the time headway distribution as the model without optimistic

drivers (see Sec. 5.6.1 and in particular Fig. 5.28).
Regarding the fundamental diagram the variation of t_{safe} does not influence the slope seriously and is therefore not important at all, especially not for synchronized traffic. The latter is controlled by other parameters, namely g_{add} and v_{slow}.

5.5 Accidents

The last section showed that the model by Lee *et al.* is able to reproduce the complex structure of synchronized traffic and the platoon formation in the free-flow. But as stated above, the original model is not accident free which necessitates an in-depth analysis of the mechanisms that are the reasons for the accidents. This is in particular important for the development of a sophisticated lane change algorithm.
In [107] it is mentioned that the model may suffer from accidents if vehicles are inserted at an on-ramp carelessly. The analysis in this thesis show that this is not the only reason for accidents. A crash may also occur in a periodic system that is initialized as claimed in [107]. Thus, for two-lane traffic or the introduction of on-ramps the model has to be adapted.
To determine the reasons for the accidents, in the next subsection some scenarios are depicted which show the processes of the emerging accidents and that the cause for the accidents lies in the determination of the attitude. In all simulations accidents are handled as follows: If a vehicles crashes into its leader, the normal update is applied in the next time-steps. This means that both vehicles move according to the update algorithm whereas the causer of the accident will decelerate in general. After some time-steps the accident configuration will resolve if the hit vehicle accelerates again or continues to drive.

5.5.1 Accidents' Reasons

The key to a safe one-lane model is based on a more careful determination of γ. Simulations show that two different scenarios lead to a dangerous configuration. First, if all three vehicles that are involved in the calculation of γ drive optimistically with the same velocity. Second, if the velocity difference between v_{n+1} and v_{n+2} is too high. This means that one can distinguish between accidents that are caused by the – too – optimistic attitude of the driver due to the first part of the determination of γ or the second part – γ_{first} and γ_{second}, respectively. Thus, for each case accident configurations are discussed that show the mechanism that leads to such dangerous situations.
For the described accident types the important state variables are summarized in form of a table. The values are shown for the vehicles n, $n+1$ and $n+2$ for the preceding time-steps $t-T, t-T+1, .., t-2, t-1, t$. The accident occurs in time-step t and vehicle n is responsible for the crash, i.e., hits its predecessor. The values of time-step $t-T$ are given in the first row of the table and the ones of time-step $t-T+1$ in the second row. The following rows show the values of the next time-steps and end with the values of time-step t. Important state variables of each vehicle are x_n, v_n, g_n, $\tilde{c}_n$, $\tilde{v}_n$, and γ_n, as these are the parameters that are the basis to calculate the velocity and that show the occurrence of an accident. The most important parameters are also visualized in two plots. One shows the chronological sequence of the state variables of the vehicles n that causes the accident, the other plots the trajectories of the involved vehicles n and $n+1$.

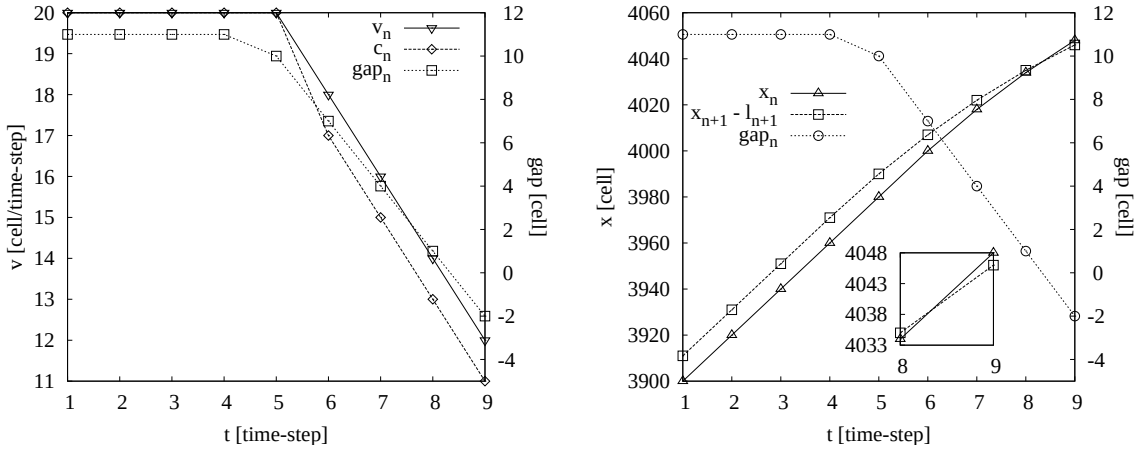

Figure 5.22: Accident example for a configuration of vehicles driving in a platoon with constant velocity. **Left:** The velocity v_n and safe velocity $\tilde{c}_n$ – denoted as c_n in the diagram – of the accident car are plotted together with its gap_n. The accident happens after time-step 8 when the gap becomes negative. **Right:** Trajectory of the two vehicles of an exemplary configuration that are driving with constant velocity in a platoon. The trajectories cross each other after time-step 8 that means an accident has happened.

Influence of γ_{first} on the Accidents

In case that γ_{first} lets the driver be optimistic, two characteristic examples of accidents that were detected during the simulations are discussed in this section. The first shows the important parameters of three vehicles driving in a row with constant velocity. In the second example the vehicles accelerate simultaneously still driving behind each other.
A typical configuration of the first type is shown in Fig. 5.22 and in Tab. 5.2. In the beginning the accident car n is driving in a platoon of vehicles all driving with the same velocity v until the vehicles $n+1$ and $n+2$ decelerate in step $t-4$ as the vehicles downstream begin to decelerate one time-step before. But vehicle n continues to drive with velocity $v_n = v_{\text{platoon}}$ so that in the next time-step a discrepancy between $\tilde{v}_n$ and $\tilde{c}_n$ emerges. This means that vehicle n is not able to decelerate fast enough. If vehicle $n+1$ continues to decelerate as strongly as possible in the following seconds this discrepancy remains and vehicle n continues to approach vehicle $n+1$. In the end these two vehicles have a cell overlap which means that an accident has happened.
The second example shows a platoon of vehicles accelerating in parallel so that each of them drives with the same velocity $v_n = v_{\text{platoon}}$. Vehicle n continues to accelerate in step $t-5$ while the other two change their attitude and start to decelerate. Vehicle n is no longer able to reach its safe velocity $\tilde{c}_n$. In formal parlance, the difference between the reachable velocity and the safe velocity $\tilde{v} - \tilde{c} > 0$.
These are typical examples for the two scenarios that for themselves or a mixture of both lead to a dangerous situations that might end up in an accident. The general mechanism is the same for both. Vehicle n drives in a platoon of at least 3 vehicles and all of them drive with the same velocity. The anticipation horizon is 2 vehicles. The leading vehicles are forced to decelerate in one time-step because of the traffic situation in front of them. The

x_n	3900	3920	3940	3960	3980	4000	4018	4034	4048
v_n	20	20	20	20	20	18	16	14	12
gap_n	11	11	11	11	10	7	4	1	**-2**
$\tilde{c}_n$	20	20	20	20	20	17	15	13	11
$\tilde{v}_n$	20	20	20	20	20	18	16	14	12
γ_n	0	0	0	0	0	1	1	1	1
x_{n+1}	3916	3936	3956	3976	3995	4012	4027	4040	4051
v_{n+1}	20	20	20	19	17	15	13	11	9
gap_{n+1}	9	9	9	8	8	8	8	9	9
$\tilde{c}_{n+1}$	20	20	20	19	17	15	13	12	10
$\tilde{v}_{n+1}$	20	20	20	19	17	15	13	12	10
γ_{n+1}	0	0	0	0	1	1	1	1	1
x_{n+2}	3930	3950	3970	3989	4008	4025	4040	4054	4066
v_{n+2}	20	20	19	19	17	15	14	12	10
gap_{n+2}	28	28	28	28	26	24	23	21	19
$\tilde{c}_{n+2}$	20	20	20	19	17	15	14	12	10
$\tilde{v}_{n+2}$	20	20	20	19	17	15	14	12	10
γ_{n+2}	0	0	1	1	1	1	1	1	1

Table 5.2: Single vehicle data of the accident example plotted in Fig. 5.22 left and right.

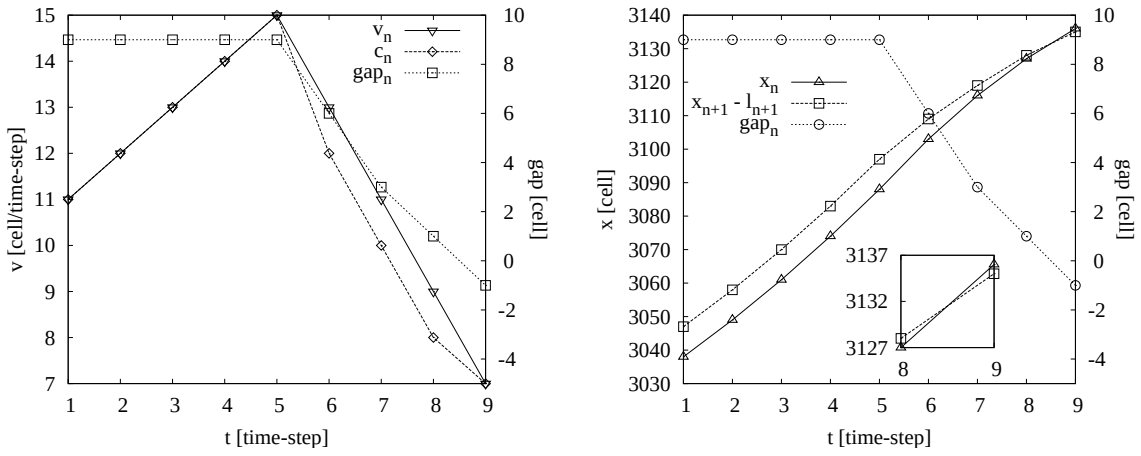

Figure 5.23: Accident example for a configuration of vehicles driving in a platoon and accelerating simultaneously. **Left:** The velocity v_n and safe velocity $\tilde{c}_n$ of the accident car – denoted as c_n in the diagram – are plotted together with its gap_n. The accident happens after time-step 8 when the gap becomes negative. **Right:** Trajectory of the two vehicles of an exemplary configuration that are driving in a platoon and accelerate simultaneously. The trajectories cross each other after time-step 8 that means an accident has happened.

x_n	3038	3049	3061	3074	3088	3103	3116	3127	3136
v_n	11	12	13	14	15	13	11	9	7
gap_n	9	9	9	9	9	6	3	1	**-1**
$\tilde{c}_n$	11	12	13	14	15	12	10	8	7
$\tilde{v}_n$	11	12	13	14	15	13	11	9	8
γ_n	0	0	0	0	0	1	1	1	1
x_{n+1}	3052	3063	3075	3088	3102	3114	3124	3133	3142
v_{n+1}	11	12	13	14	12	10	9	7	5
gap_{n+1}	10	10	10	10	10	10	10	9	7
$\tilde{c}_{n+1}$	11	12	13	14	12	11	9	7	5
$\tilde{v}_{n+1}$	11	12	13	14	12	11	9	7	5
γ_{n+1}	0	0	0	0	1	1	1	1	1
x_{n+2}	3067	3078	3090	3103	3117	3129	3139	3147	3156
v_{n+2}	11	12	13	14	12	10	8	9	9
gap_{n+2}	13	13	13	13	12	11	10	12	12
$\tilde{c}_{n+2}$	11	12	13	14	12	10	8	9	9
$\tilde{v}_{n+2}$	11	12	13	14	12	10	8	9	9
γ_{n+2}	0	0	0	0	1	1	1	0	0

Table 5.3: Single vehicle data of the accident example plotted in Fig. 5.23 left and right.

driver of vehicle n notices the deceleration of its leaders one step too late. In the following cascade of decelerations the distance between the vehicles gets consistently smaller as all vehicles decelerate as strongly as possible. In the end vehicle n crashes into its leader.
It is important to note that a higher deceleration capability does not prevent such accidents but it would just decrease the accident frequency.

Influence of γ_{second} on the Accidents

The reason for accidents that result from an optimistic attitude assigned by γ_{second} is completely different. Here, the accidents are provoked by a large speed difference between the vehicles n and $n+1$. The following Fig. 5.24 and Tab. 5.4 shows an – arranged – example that describes such an accident. This configuration does not appear in the periodic system in the stationary state but it will become important if vehicles are inserted. This is eminent in case of two-lane traffic as well as in a system with an on-ramp (see Secs. 5.7, 6.1, and 7.1).
Here, the vehicles are arranged so that the last car of this configuration will hit its predecessor after some time-steps. The configuration in the beginning consists of a stopped vehicle at position $x_n = 0$, another stopped vehicle at $x_{n+1} = 41$, and a vehicle speeding away. The exact parameters of the latter are not important since only the velocity of the speeding vehicle has to be higher or equal to v_{fast}. As the next but one vehicle of vehicle n is driving very fast optimistic attitude is assigned to the driver of vehicle n and it accelerates till step $t-2$. Then, the minimal distance for optimistic drivers becomes valid and the vehicle decelerates – too late – and hits its leader. This example is the minimal configuration for such an accident in the sense that vehicle n reaches a velocity that is too fast that the safety gap triggers an emergency brake that is sufficient to prevent an

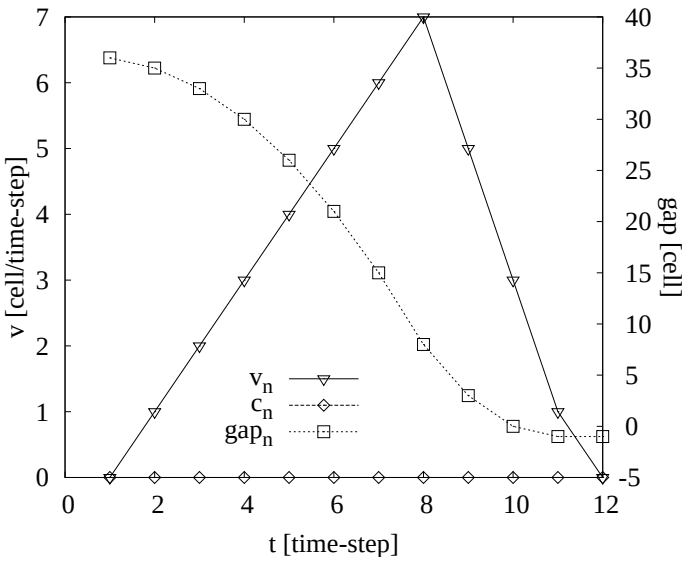

Figure 5.24: Example for an accident because of a slow driving vehicle. The velocity v_n and safe velocity $\tilde{c}_n$ – denoted as c_n in the diagram – of the accident car are plotted together with its *gap*. The accident happens after time-step 10.

accident. If a larger initial distance between vehicle n and $n+1$ is be chosen the accident would be more drastic, i.e., the overlap of the vehicles would be larger or the rear vehicle would "overtake" the leader.
As this configuration is a totally unrealistic behavior on a single-lane road the model will be adapted for the analysis of scenarios where vehicles are inserted into the system and such configurations could appear. Note, that even if these configurations emerge it is very unlikely that a vehicle dawdles several consecutive time-steps and therefore the situation becomes dangerous. Typically a vehicle whose leader speeds away would accelerate as the gap gets larger. In this example the randomization parameter was set to $p_{v=0} = 0.31$. The probability to dawdle for 9 sec is then $p^9_{v=0} = 2.6 \cdot 10^{-5}$.
Additionally, an accident scenario that is closely connected to that described in the previous section is based on an optimistic driver that is at least as fast as the next but one vehicle. If this vehicle continues to drive at $v_{\max}$ or accelerates to its maximum velocity when vehicle $n+2$ has begun to react on some leading vehicle, which has decelerated, vehicle n might have missed the right time to decelerate as well. The following cascade of decelerations may then lead to an accident as in the dangerous situations caused by a too optimistic driver relying on $\gamma_{\text{first}} = 0$.

Conclusion

Summarizing, critical situations emerge – spoken in the sense of the model philosophy – at the transition between optimistic and pessimistic driving as the vehicle that suffers from the accident reacts with an offset of one time step.
Two mechanisms are responsible for the emergence of an accident: First, if a platoon of equally fast vehicles approaches slower ones so that the leader of the platoon has to brake. Then it might happen that the last vehicle is not able to react on the deceleration and

x_n	1	3	6	10	15	21	28	33	36	37
v_n	1	2	3	4	5	6	7	5	3	1
gap_n	35	33	30	26	21	15	8	3	0	**-1**
$\tilde{c}_n$	2	3	4	5	6	7	5	3	0	0
$\tilde{v}_n$	2	3	4	5	6	7	5	3	1	0
γ_n	0	0	0	0	0	0	0	0	0	0
x_{n+1}	41	41	41	41	41	41	41	41	41	41
v_{n+1}	0	0	0	0	0	0	0	0	0	0
gap_{n+1}	190	209	228	247	266	285	304	323	342	361
$\tilde{c}_{n+1}$	1	1	1	1	1	1	1	1	1	1
$\tilde{v}_{n+1}$	1	1	1	1	1	1	1	1	1	1
γ_{n+1}	0	0	0	0	0	0	0	0	0	0
x_{n+2}	236	255	274	293	312	331	350	369	388	407
v_{n+2}	19	19	19	19	19	19	19	19	19	19
gap_{n+2}	119	138	157	176	195	214	233	252	271	290
$\tilde{c}_{n+2}$	19	19	19	19	19	19	19	19	19	19
$\tilde{v}_{n+2}$	19	19	19	19	19	19	19	19	19	19
γ_{n+2}	0	0	0	0	0	0	0	0	0	0

Table 5.4: Single vehicle data of the accident example plotted in Fig. 5.24.

cannot reach its safe velocity anymore.
The second accident scenario does, as stated before, not appear in the stationary state of the periodic system. But for realistic simulation topologies, e.g., an on-ramp with slow vehicles entering the main carriageway it gets relevant. Thus, little changes have to be implemented in the update mechanism for the two-lane model (see Secs. 5.6.2 and 6.1).

5.5.2 Accident Frequency

A strong hint at the relevance of these accidents for the overall dynamics of the system is given by the frequency in which accidents happen. Therefore, a periodic system is simulated and the accidents are recorded. Each accident is counted once even if two vehicles overlap for more than one subsequent simulation step. The accident situation resolves automatically if the hit vehicle accelerates again or continues to drive.
Two different measurement approaches are followed in this section. In the first case, the simulations were repeated several times, in the second case, a very long simulation run was made and repeated up to 20 times. In the former approach each simulation run consists of 100,000 time-steps and the system had a length of 10,000 sites. This simulation was done 20 times for all densities between $\rho = 0\,\text{veh/km}$ and $\rho = 105\,\text{veh/km}$ with a density interval of $\Delta\rho \approx 0.75\,\text{veh/km}$ so that the total measure time was $2,000,000$ time-steps. In the latter single long simulation runs of 100,000,000 time-steps were accomplished at the densities around the maximum accident frequencies computed by the first method.
First, the results of the multiple short simulations are discussed, which are shown in the left part of Fig. 5.25. In the low density region, i.e., free-flow, no accidents could be detected. Here, the vehicles are not forced to decelerate but drive optimistically (see Sec. 5.4.1) with a velocity of $v_n \geq v_{\text{fast}}$. This is different for the synchronized region in

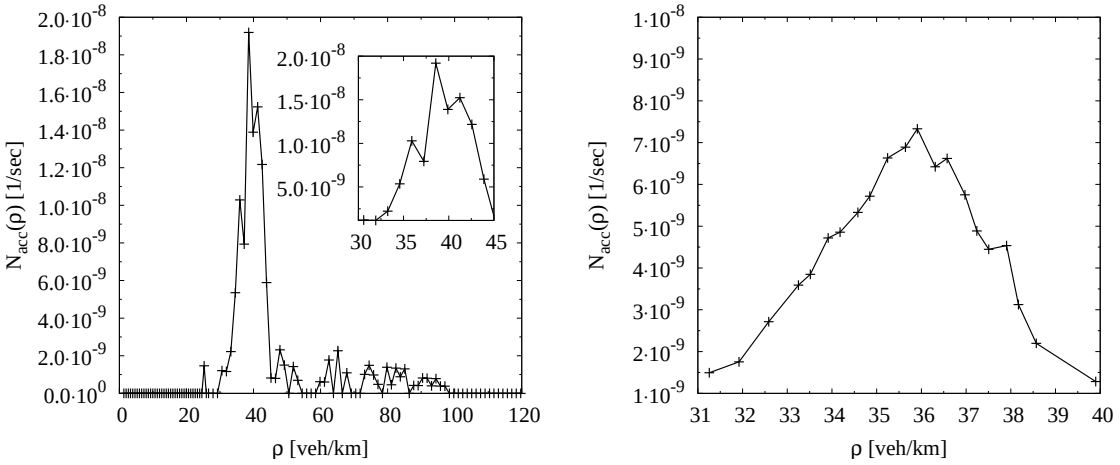

Figure 5.25: **Left:** The accident frequency in a periodic system. For each density the ratio is the mean of 20 simulation runs of 100,000 time-steps. The maximum accident frequency is at $\rho = 39\,\text{veh/km}$. Here, approx $N_{\text{acc}} = 2.0 \cdot 10^{-8} 1/\,\text{sec}$ accidents happen each time step. This means a vehicle has an accident every $5 \cdot 10^7$ time-steps. The inset shows the region of the maximum accident frequency. Right: The accident frequency acquired differently. The accidents were recorded for every density in 20 simulations over 100,000,000 time-steps.

which accidents are found especially between $\rho \approx 33\,\text{veh/km}$ and $\rho \approx 43\,\text{veh/km}$. In dense traffic up to $\rho \approx 100\,\text{veh/km}$ some accidents are detected. For even higher densities the accidents vanish as the distance between the vehicles get to small.
The density at which most accidents happen correlates with the upper density limit of the region of synchronized traffic at $\rho \approx 40\,\text{veh/km}$ as revealed by a comparison with the global fundamental diagram in Fig. 5.5. The highest accident rates occur at $\rho \approx 39\,\text{veh/km}$. At this density the probability to have an accident in one time-step is $N_{\text{acc}}(\rho) \approx 2 \cdot 10^{-8} 1/\,\text{sec}$. In other words, every $5 \cdot 10^7$ time-steps a vehicle has an accident on average. The synchronized traffic is characterized by vehicles driving behind each other with more or less the same velocity. This is exactly the configuration in which the dangerous or hazardous situations emerge. Additionally, the spatial headway gets smaller when the density approaches the upper density limit of the synchronized region. Thus, the probability that a dangerous situation results in an accident is higher there than at lower densities. The "spatial buffer" between the vehicles is smaller and therefore dangerous situations are less likely to be absorbed and transferred into safe configurations. This happens if the leader of the vehicle in danger of an accident accelerates again or at least stops to decelerate. It is important to note that about 40% of the drivers are optimistic in the synchronized region. This means that 2/5 of the vehicles may underestimate their safety distance and all vehicles that collide with their leader are optimistic at the beginning of the deceleration cascade. The fact that only optimistic vehicles exceed their safe velocity will be illustrated in Appendix A.
The second method, the long simulation runs show different results which are depicted in the right part of Fig. 5.25. These simulations are restricted to the interesting densities of the synchronized traffic in which most accidents happen. The highest accident rates occur between $\rho \approx 34\,\text{veh/km}$ and $\rho \approx 38\,\text{veh/km}$. The maximum is reached at $\rho = 35.25\,\text{veh/km}$

with an accident probability of $N_{\text{acc}}(\rho) \approx 7.5 \cdot 10^{-9} 1/\,\text{sec}$ which is 30 times smaller than the maximum frequency calculated in the multiple short simulations.
Thus, there must exist two mechanisms or configurations that give rise to the emergence of accidents. At first, the traffic state in which the accidents happens must be identified for both methods.
The discrepancy between the accident frequency measured with both methods is the result of two different processes. On the one hand, most accidents happen in synchronized traffic as stated above. But Sec. 5.3 will show that synchronized traffic has a limited life-time which gets smaller when the density rises. So, most accidents are detected in the beginning of the simulations before the synchronized flow breaks down. Using the first method in every simulation run the traffic is synchronized in the beginning and therefore the accident probability is relatively high and the time the synchronized traffic governs the system is of the order of the total simulation time. In contrast, in the long simulation runs in the beginning synchronized traffic dominates the system, but that collapses at a time which is small compared to the total simulation time. Hence, the mean number of accidents is smaller. This is underlined by the fact that in the first approach a relevant number of accidents is detected for densities larger than $\rho \approx 40\,\text{veh/km}$ which is not the case for the long simulation runs where only a negligible number of accidents are measured. Here, the formerly homogeneously initialized traffic passes over to the state of wide moving jams very fast and the dangerous situations that evolve in synchronized traffic are not relevant for the long simulations. The higher accident probability because of the smaller spatial headways at the upper end of the synchronized region works against the shorter interval in which the traffic in the system is synchronized. This moves the maximum accident frequency to smaller densities.
To support this argumentation a look at the life-time of the synchronized traffic is beneficial (Fig. 5.13). If the best fit straight line therein is continued to lower densities, one gets exactly a mean life-time for $\rho \approx 36\,\text{veh/km}$ that is of the order of the simulation time in the long simulations. For higher densities the life-time decreases rapidly, so does the number of accidents in the long simulations.
In the region of very long living synchronized traffic with $\rho \leq 35\,\text{veh/km}$ the frequencies measured by both methods are of the same order. In short as well as in long simulations synchronized traffic is the relevant state for the whole simulation as the mean life-time is much longer even than the simulation times of the long simulation runs.
Note most accidents are found in synchronized traffic and are not the consequence of fast vehicles that approach jammed traffic.
Concluding, in a periodic single-lane system these accidents are not relevant as they appear very seldomly and resolve automatically by the model dynamics. At $\rho = 39\,\text{veh/km}$ a vehicle has in the mean an accident every $5 \cdot 10^7$ time-steps. Further, the procedure to deal with the accidents does not influence the dynamics of the vehicles following the crashed one therefore the accidents have no side-effects. Nevertheless, the development of an adapted model that does not exhibit accidents should proof that the usage of a limited deceleration probability allows for an accident free model.

5.5.3 Concept of Proof

Some other models like the optimal velocity models [3, 4, 5, 6] and especially the discretized version [54] are known not to be collision free if special initial conditions are applied. But especially in discrete models where analytical approaches are very limited

the verification that no accidents occur is a very difficult task. This is also true for the presented model. A look at the inequality (5.1) reveals the complexity of the velocity update that is in the end the decisive function. Neither the simplification of this equation gives more insight (Eq. 5.2). The inequality cannot be transformed to a simpler form.
Therefore, a new approach to proof whether accidents could happen or not is proposed. It shows that the simplified model without optimistic vehicles is collision free. To validate this the states of the vehicles are systematically investigated to find out whether these are safe states or if they may lead to an accident.
First, a state vector $\underline{s}_n$ is defined that describes the state of a vehicle completely. In general, $\underline{s}_n$ consists of the position, the velocity, the length, and additional parameters $\tilde{s}_n$ depending on the special model: $\underline{s}_n := (x_n, v_n, l_n, \tilde{s}_n)$. The state of the system is then given by $S := (\underline{s}_1, \ldots, \underline{s}_N)$ and $\mathfrak{S}$ denotes the set of all possible states S. Next, those states are categorized in state classes $\overline{S}_{k,K}$ which contain only some vehicles that fulfill specific preconditions, e.g., "in the state class are those vehicles that have the same velocity v_n". From these class set collections are derived that are identified by slightly less strict requirements, e.g., "in this state class set are all classes that require from their elements that they have a velocity in a defined interval $[v_1, v_2]$".
Now the time evolution is analyzed: A time evolution operator $\mathfrak{T}$ is defined that transfers every state to another state which is interpreted as a time evolution, i.e., the state S^t at time t evolves into state S^{t+1} at time $t+1$. Using this operator one generates all states that can evolve out of the input states, and, analogous, returns for a given set of states a set of all states that can evolve into one of the input states. States that show the characteristics of a collision are named *collision-states*. Thus, if one also assumes that the cellular automaton only depends on a local environment, an algorithm can be introduced that calculates the history of any arbitrary state class. These are reduced to the history of a single state class with length 1, i.e. a class consisting of just one state, which is called an *atomic history* and are collected in a database for fast access. The number of state classes is then reduced by collecting all state classes that can be put into one state class set by assigning it a multi-value interval on the velocity or gap.
Implementing this algorithm in C++ and applying this to the model by Lee *et al.* one generates state classes for all collision states that can evolve out of non-collision states and feeds the history algorithm with all those state classes. The returned collections of state class sets were merged and again sent through the algorithm. The program stops when the algorithm does not return any results, thus no history for the input states exists, in which case we would have proven that there exists a non-empty set of safe states and the model is collision-free except for a finite set of unsafe initial conditions.
As a test case optimistic driving behavior was not allowed by excluding all state classes with $\gamma_1^t = 0$ from the atomic history database. Then for any collision state the history was a cascade of states where the following car was braking with full capacities all the time. After some iterations v_1^{t-1} would have needed to be larger than $v_{\max}$ in order to comply with the model rules. Since this is not possible, all those cascades were finite and the program halted. Not surprisingly, we proved that the Lee model, restricted to defensive driving behavior, is collision-free.
However, with allowing optimistic behavior, the velocities of the following car do not strive to higher values with backward moving time, but may oscillate. Of course, the program does not halt which leads to the conclusion that the model is not collision-free. The proof for collisions out of important, meaningful initial conditions is given by the observations

of collisions in our simulations. Despite the simplifications and optimizations put into the algorithms, determining the sets of all collision states $\mathfrak{S}_c$, unsafe states $\mathfrak{S}_u$, and safe states $\mathfrak{S}_s$ is hard and practically impossible, since the whole graph has to be traversed.
Theoretically it would be possible to modify the program in order to output the probability of collisions by assigning a weight to every edge in the automaton's evolution graph according to the evolution probability. However, to calculate the overall probably of collisions, again the whole graph would have to be traversed. For a formal description of this methodology see Appendix A.

5.6 Accident Avoidance and Modified Models

Due to the nature of the collisions observed in the original model a change in the definition of γ_n is needed to make it more reliable for simulations. Therefore, different strategies are shown in the next sections.
In order to illuminate the influence of γ the simplified model without optimistic drivers is discussed, which is accident free as shown in Sec. 5.5.3.
In general, there are two triggers – without introducing a hard-core repulsion – that are reasonable to reduce the accident frequency or even to remove all accidents. At first, the calculation of γ is changed so that dangerous situations are avoided. Second, the acceleration capability A is reduced if the vehicles drive in a platoon.

5.6.1 Simplified Model

The simplest approach to adapt the model so that no accidents happen is the original model without optimistic drivers. An analysis is also interesting to clarify the origin of the different features of the unchanged model.
In this simplified model the human factor is removed from the model. Its features especially at higher densities are different from that of the unmodified model. Especially, the synchronized phase is stabilized. This means one finds synchronized traffic in a much broader density region. However, in free-flow one does not find very high fluxes anymore.

Model Definition

As mentioned above the simplified version of the model is changed with respect to the original model by removing the human effect. The optimistic driving that would allow smaller distances between the vehicles when the neighborhood is estimated optimistically is given up. This means the core of the model, the summation which calculates the velocity of each vehicle, is changed. Instead of summing up to $\tau_{\mathrm{f}}(c_n^{t+1})$ and $\tau_{\mathrm{l}}(v_{n+1}^t)$, respectively, the upper limits are now the velocity v divided by the deceleration capability D. Thus, the limits are c_n^{t+1}/D and v_{n+1}^t/D, so that Eq. (5.1) changes to:

$$x_n^t + \Delta_n + \sum_{i=0}^{c_n^{t+1}/D} \left[c_n^{t+1} - D \cdot i\right] \quad \leq \quad x_{n+1}^t + \sum_{i=1}^{v_{n+1}^t/D} \left[v_{n+1}^t - D \cdot i\right]. \tag{5.15}$$

The remaining update simplifies to

$$\Delta = L + \max\{0, \min\{g_{\mathrm{add}}, v_n^t - g_{\mathrm{add}}\}\} \tag{5.16}$$

and

$$p = \max\{p_{\mathrm{d}}, p_0 - v_n^t \cdot (p_0 - p_{\mathrm{d}})/v_{\mathrm{slow}}\}, \tag{5.17}$$

$$\tilde{c}_n^{t+1} = \max\{c_n^{t+1} \mid c_n^{t+1} \text{ satisfies Eq. (5.15) and (5.16)}\}, \tag{5.18}$$

$$\tilde{v}_n^{t+1} = \max\{0, v_n^t + a, \max\{0, v_n^t - D, \tilde{c}_n^{t+1}\}\}, \tag{5.19}$$

$$v_n^{t+1} = \max\{0, v_n^t - D, \tilde{v}_n^{t+1} - \eta\}, \text{ where } \eta = 1 \text{ if rand}() < p \text{ or } 0 \text{ otherwise}, \tag{5.20}$$

$$x_n^{t+1} = x_n^t + v_n^{t+1}. \tag{5.21}$$

Results

The simulations show that some features of traffic at intermediate and higher densities are reproduced qualitatively correct but the differences to the original model are relevant.
Figure 5.26 left shows suitable space-time plots of a periodic system. The system length is $L = 10{,}000$ cells and the data is measured after a relaxation time of $T_{\mathrm{relax}} = 30{,}000$ time-steps for $T_{\mathrm{measure}} = 20{,}000$ steps as usual.
The space-time plots for $\rho = 13$ veh/km and $\rho = 29$ veh/km show the same characteristics as those of the unmodified model and no differences are obvious. In contrast, the discrepancies at the other densities are serious. For $\rho = 23$ veh/km (Fig. 5.26) synchronized traffic governs the whole system that does no longer coexist with free-flow. Even more drastic are the differences at high densities exemplarily shown for $\rho = 53$ veh/km in Fig. 5.26 right. Wide moving jams coexist with synchronized traffic but not with free-flow.

The fundamental diagram underlines the great differences in the dynamics of this model variant compared to the original model. The free-flow branch is now cut at $J \approx 1900$ veh/h. This is a direct consequence of the missing short time distances that are allowed for optimistically driving vehicles. In particular, in the free-flow region all vehicles drive optimistic in the original model and thus the high flows can emerge (cf. discussion in Sec. 5.4.1). At

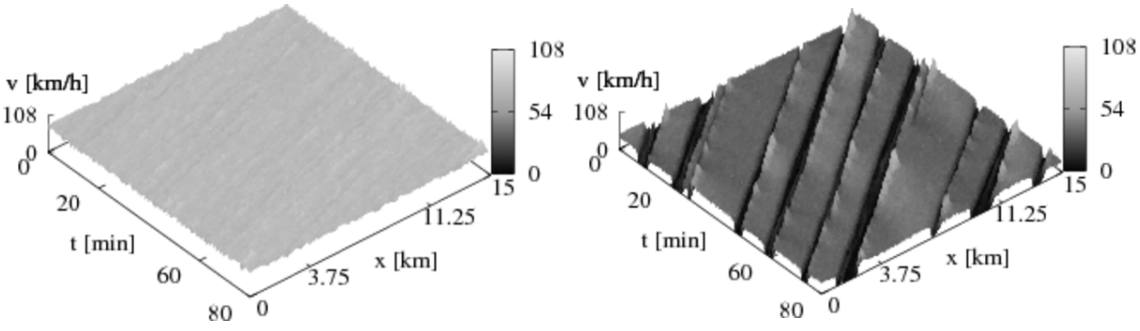

Figure 5.26: Model without optimistic driving: **Left:** Space-time plot of the synchronized traffic in the periodic system at a density of $\rho = 23$ veh/km. The synchronized traffic coexists no longer with free-flow but governs the whole system. **Right:** Space-time plot of the congested state of the periodic system. The initial density is $\rho = 53$ veh/km. Free-flow is absent in contrast to the original model.

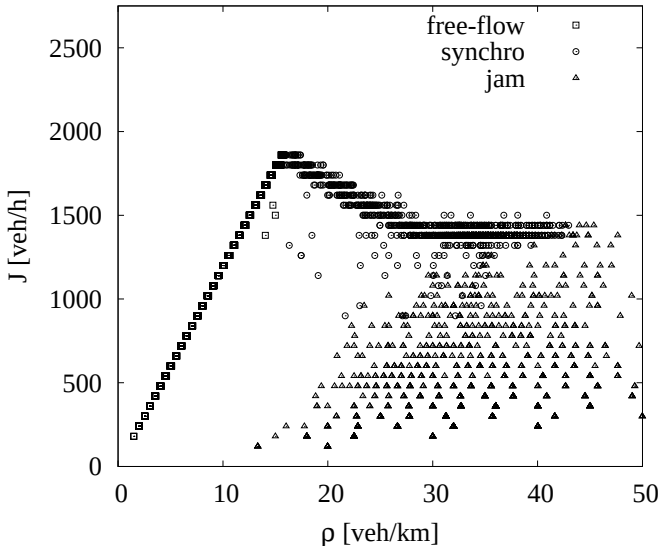

Figure 5.27: Local fundamental diagram of a periodic system of the simplified model. High fluxes in free-flow are missing but the region of synchronized traffic is extended.

higher densities the model shows the same dynamics as the model with γ reduced to the second part γ_{second} (cf. 5.4.2).
The time headway distribution changes drastically compared to the original model. The short time headways below one second do not appear anymore. In contrast the maximum is shifted to larger times. In the free flow the minimal headway is located slightly below 2 sec. Nevertheless, the background signal decreases exponentially according to the empirical data. In synchronized traffic the distribution is shifted to higher times as well. The maximums lie between 2 sec and 2.5 sec and the distributions are narrower than in the original model. All vehicles adapt the velocity of their leader and the distance keeps constant. The dawdling has no longer the side-effect of stronger fluctuations when a vehicle has to change its attitude because of a dawdling predecessor. Therefore, the distributions are very narrow. This underlines that the short time headways that can be seen in the original model are based on the optimistic driving strategy that underestimates the safety-distance (Sec. 5.4.2) not only in free-flow but also in synchronized traffic.
The homogeneity is underlined by the life-time of the synchronized traffic. An analysis analog to Sec. 5.3 shows that the synchronized state is more stable. A life-time $T_{\text{break}} = 1 \cdot 10^5$ is achieved at $\rho \approx 40\,\text{veh/km}$ vs. $\rho \approx 43\,\text{veh/km}$ in the original and the simple model, respectively. Nevertheless, the slope of the life-time is qualitatively the same. It decreases exponentially as well.
The results show that adding the "human factor" to the model leads to the characteristic performance in the free flow regime with high fluxes and short time headways. In synchronized traffic the human factor is responsible for two effects. First, optimistic vehicles are the source of relevant perturbations and thus destabilize the synchronized traffic. The likeliness of a disruption is not only affected by the dawdling of the vehicle and the velocity reduction itself but especially determined by the – possible – change of the attitude of the two next vehicles following a dawdling vehicle. This follows as the precondition

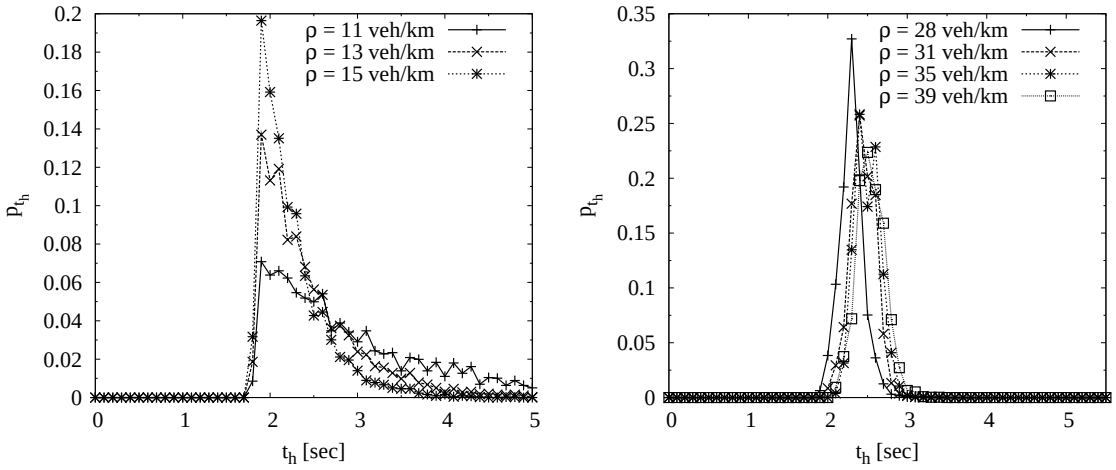

Figure 5.28: Model without optimistic attitude: **Left:** Time-headway distribution p_{t_h} in the free-flow phase. Time-headways shorter than 1 sec are not reproduced, but the background signal decreases exponentially like the empirical data. **Right:** Time-headway distribution in the synchronized phase. Compared to the original model the distribution is shifted to larger times and is very narrow.

for optimistic driving, i.e., $v_n^t \leq v_{n+1}^t \leq v_{n+2}^t$ may no longer be valid. Thus, the stricter driving rules for pessimistic vehicles are applied. The now pessimistic vehicles must in general enlarge their gap to their leaders. This disturbance propagates than upstream. (see Sec. 5.1 for the discussion of the influence of dawdling on the calculation of γ). Second, analog to the free-flow, time headways are shifted to lower values by the optimistic vehicles that accept the short distances. In very dense traffic the human-factor leads to a strong separation. Without it, free-flow regions evolve in-between compact jams which is not the case for the simplified model.
These original model and simplified model are two extremes regarding the dynamics in dense traffic. The former shows free-flow and wide moving jams whereas in the latter synchronized traffic is disturbed by compact jams. In the next section a model approach is presented that shows all three states at high densities.

5.6.2 Safe Models

The discussion in Sec. 5.5 showed that special configurations of the vehicles are the source of the emergence of accidents, i.e., a platoon of vehicles driving with the same velocity. Using these information and the results of the discussion of the simplified model in the previous section different modified models are introduced and analyzed in this section.

Restricted Optimism

To prevent the dangerous situations described in Sec. 5.5 of the first type which are thought to be related to γ_{first} the second '$\leq$' sign in $v_n^t \leq v_{n+1}^t \leq v_{n+2}^t$ is changed to '$<$':

$$\gamma_{\text{first,safe}} = \begin{cases} 0, & \text{for } v_n^t \leq v_{n+1}^t < v_{n+2}^t, \\ 1, & \text{otherwise.} \end{cases} \tag{5.22}$$

The accidents due to a large velocity difference – γ_{first} – are in general eliminated by a lower limit of the difference between v_n and v_{n+1}.

$$\gamma_{\text{second,safe}} = \begin{cases} 0, & \text{for } v_{n+2}^t \geq v_{\text{fast}} \text{ and } v_n^t - v_{n+1}^t \leq D, \\ 1, & \text{otherwise.} \end{cases} \tag{5.23}$$

Additionally, it is needed to add a stronger connection between each vehicle n and its next but one leader $n+2$. This is done by the introduction of a brake-light b_n. It denotes whether the vehicle has reduced its velocity because of its surrounding, but not because of dawdling (i.e. in the randomization step). In detail the state of the brake-light is determined by

$$b_n^t = \begin{cases} 1, & \text{for } \tilde{v}_n^{t+1} < v_n^t, \\ 0, & \text{otherwise.} \end{cases} \tag{5.24}$$

Note, that the brake-light has not the same role as in [91]. Here, it provides a way to communicate the presence of an obstacle and therefore a possible change of the optimistic state to the following cars. So each vehicle is able to sense a critical situation early enough. The parameter γ is now determined considering also the state of the brake-light of the $n+2$th vehicle as well:

$$\gamma_n^t = \begin{cases} 0, & \text{for } b_{n+2}^t = 0 \\ & \text{and } (v_n^t \leq v_{n+1}^t < v_{n+2}^t \text{ or } (v_{n+2}^t \geq v_{\text{fast}} \text{ and } v_n^t - v_{n+1}^t \leq D)), \\ 1, & \text{otherwise.} \end{cases} \tag{5.25}$$

The remaining update is unchanged.
The change in the definition of γ has desired influence on the emergence of accidents. In the scope of the simulations no accidents can be detected. The great difficulties to prove this apart from numerical investigations is elaborately shown in Sec. 5.5.3 for the simplified original model. Here the introduced brake-light makes it even more complicated as this parameter has to be taken into account as well.

Modification Frequency In order to determine the influence of the changes made here on the original model, it is calculated how often the new rules are applied and lead to a different result in the update. This means that it is counted how often a changed γ (see Eq. 5.25) has been used leading to a different result as the one used in the unmodified model. The ratio is measured for $\Delta\gamma_{eff}$, $\Delta\gamma_{\text{first}}$, and $\Delta\gamma_{\text{second}}$ that correspond to the total number of changes, the changes because of γ_{first} and because of γ_{second}, respectively. The result is shown in Fig. 5.29.
In the free flow region the fraction of vehicles with a changed γ is about $\Delta\gamma_{eff} \approx 0$ per car and second. Only γ_{second} is slightly above zero. In the synchronized region no changes of γ are detected. That means that the influence of the changed rules is very low in both

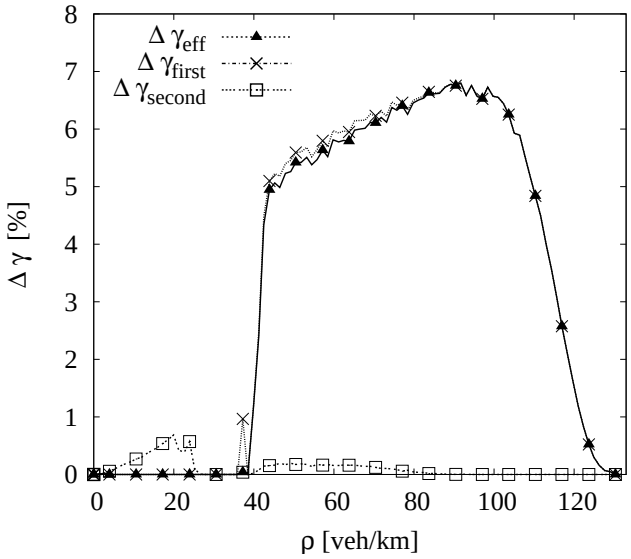

Figure 5.29: Percentage of vehicles that have a changed attitude γ because of the modifications in the model. Most changes are in dense traffic whereas in free-flow and synchronized traffic the number is very low.

regimes. At higher densities above $\rho \approx 40\,\text{veh/km}$ the number jumps to $\Delta\gamma_{eff} \approx 5\%$. At $\rho \approx 90\,\text{veh/km}$ it reaches a maximum of about $\Delta\gamma_{eff} \approx 7\%$. Beginning at $\rho \approx 105\,\text{veh/km}$ the number drops again and approaches 0 for very dense traffic.
These results show that differences in the dynamics between this model and the original model are to be expected in particular in the high-density region. A more detailed discussion in the next subsection analyzes the distinctions.

Results The dynamics of the model is still capable to reproduce the important empirically measured features of traffic flow. This is shown in the local (Fig. 5.30) as well as in the global fundamental diagram (Fig. 5.30). High fluxes and synchronized traffic are reproduced. Also in dense traffic the fundamental diagram shows no obvious differences to the unchanged model.
But the discussion of the changed attitude resulting from the differences in the definition of γ hints at a differing dynamics at higher densities. A look at a space-time plot in the high density region then reveals the differences to the original model (see Fig. 5.31). In contrast to the original model a stabilized synchronized traffic can be found at the expense off free-flow and jammed traffic. There is no longer a separation between free-flow and jammed traffic at high densities but one now finds all three traffic states in the system in parallel. Free-flow – jam outflow – is followed by a region of synchronized traffic that is again followed by a compact jam. The boundary between free-flow and synchronized traffic is not straight but the width of the synchronized region varies notable and in this region additional jams may emerge.
The adaptation of the update algorithm, namely the calculation of γ, stabilizes the synchronized traffic. Comparing this with the results of the simplified model shows similarities (Sec. 5.6.1). The number of optimistic vehicles is reduced especially in the synchronized traffic. Similar to the simplified model pessimistic vehicles encourage the emergence

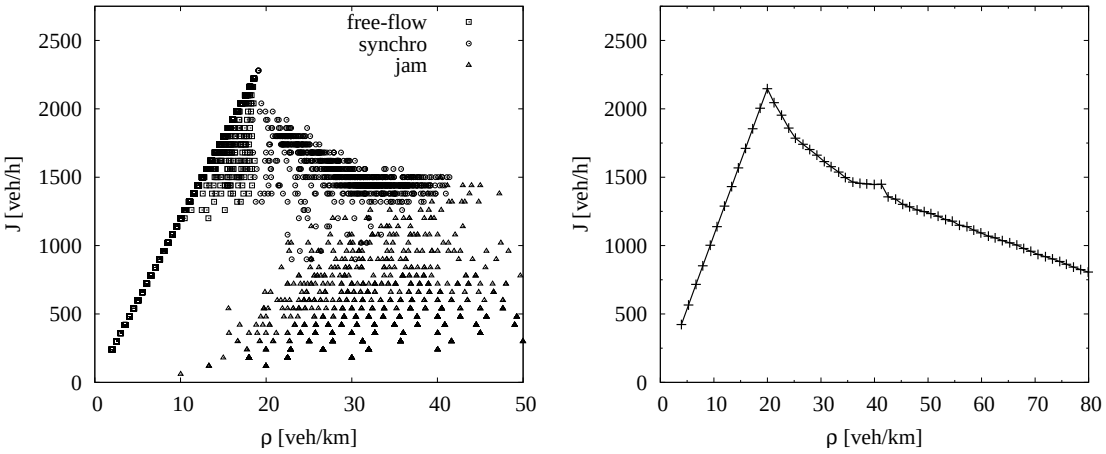

Figure 5.30: Results of the model with restricted optimism: **Left:** Local fundamental diagram. Differences to the unmodified model can hardly be found. **Right:** Global fundamental diagram. The diagram is very similar to that of the unmodified model as well.

and the stability of synchronized traffic. In this model the number of pessimistic vehicles is reduced compared to the original model but these vehicles still exist. Thus, this model stands between the original model and the simplified model.
The regime of synchronized traffic passes downstream into jammed traffic. Here, the boundary is straight and a clear separation is given. The inner structure of the jams do not differ from that of the original model. Thus, the dynamics of this model lies between that of the original and the simplified model.
Summarizing, the simplified model shows that the number of pessimistic vehicles is important for the synchronized traffic. The more vehicles are driving pessimistically the more stable is the synchronized traffic. The vehicles tend to drive with approximately the same velocity. Optimistic vehicles are always "in danger" to loose their optimistic attitude and thus are sources of strong disturbances (see Sec. 5.1 for the discussion of the influence of dawdling on the calculation of γ).

Restricted Acceleration

A different approach to overcome the deficiencies resulting from the platoon formation that may lead to accidents in the original model is presented now. The idea is to tighten the acceleration limitation for vehicles that are driving in a constellation described in Sec. 5.5. In contrast to the previous subsection the rear vehicles' acceleration capability is limited to avoid dangerous situations.
In detail a binary variable π_n is defined which indicates whether a vehicle is driving in a platoon of vehicles driving with the same velocity or not. This rule is softened in such a way that a vehicle is called to drive in a platoon as well if the next but one vehicle drives one speed step faster. In this configuration the vehicle's acceleration capability $A_{\mathrm{n,tmp}}$ is temporarily set to 0:

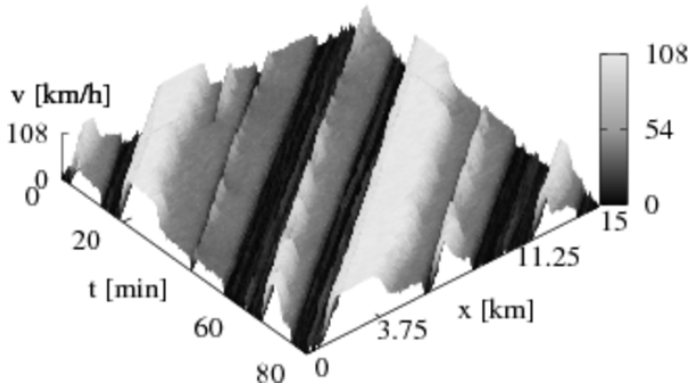

Figure 5.31: Space-time plot of the jammed phase in a periodic system of the "safe" model. The initial density is $\rho = 53\,\text{veh/km}$. Synchronized traffic establishes between compact jams and the free-flow traffic. Thereby free-flow traffic ($v = 100, \ldots, 108\,\text{km/h}$) is followed upstream by synchronized flow ($v = 30, \ldots, 50\,\text{km/h}$) that goes over to a compact jam ($v = 0, \ldots, 16\,\text{veh/km}$) which is again followed by free-flow traffic and so on.

$$\pi_n = \begin{cases} 1, & \text{if } v_n = v_{n+1} \text{ and } (v_{n+1} = v_{n+2} \text{ or } v_{n+1} = v_{n+2} - 1), \\ 0, & \text{else.} \end{cases} \tag{5.26}$$

$$A_{\text{n,tmp}} = \begin{cases} 0, & \text{if } \pi_n = 1 \text{ and } v_n = v_{n+1}, \\ a, & \text{else.} \end{cases} \tag{5.27}$$

The acceleration step is adjusted:

$$\tilde{v}_n^{t+1} = \max\{0, v_n^t + A_{\text{n,tmp}}, \max\{0, v_n^t - D, \tilde{c_n}^{t+1}\}\}. \tag{5.28}$$

The calculation of γ follows the approach in Sec. 5.6.2. Here, as well the maximum speed difference between vehicle n and $n+1$ is limited in the second part of the calculation of the attitude.
The characteristics of this model approach lie between that of the original model and that with restricted attitude. In free-flow and synchronized traffic only small differences can be determined. In dense traffic wide moving jams and free-flow are still interfered by synchronized traffic but the extension of this region is much smaller.

Unlimited Deceleration

Another approach to prevent all accidents is to replace the limited deceleration capability D with an unrealistic unlimited braking of the vehicle. This is not unproblematic at all and not in the spirit of the model. This becomes clear if one looks at the feedback such an unlimited braking might have on the dynamics of the succeeding vehicles. As all vehicles rely on the steady motion of the other vehicles a stronger braking act might push the following car into an unexpected situation as well. The safe distance the follower keeps to its leader might now be too small and unsafe. Thus, the follower is also in an unsafe configuration that would provoke emergency braking.

Because of the very small accident frequency (see Sec. 5.5.2) and the very limited impact of the accidents on the dynamics of the system the further analyses of the single-lane system are based on an only slightly adapted model. This is presented in the next subsection.

Adapted Model for Multi-Lane Traffic

The discussions of the model by Lee *et al.* in Sec. 5.1 itself and the different variants that were introduced in the sections 5.6.1 and 5.6.2 show that the ingredients can not be restricted so that the model is "safe" and the dynamics still reproduces all the important features the original approach does. But with respect to two-lane traffic on the one hand and more complex topologies on the other hand for the further analyses another sophisticated approach is introduced. It combines the comprehensive dynamical features and takes into account vehicle configurations that do not appear in the periodic system in the stationary state but in the presence of extrinsic disturbances.
The update algorithm and especially the calculation of γ is changed so that no additional accidents are provoked because of vehicles changing their lane. This leads to a different computing of γ:

$$\gamma_n^t = \begin{cases} 0, & v_n^t \leq v_{n+1}^t \leq v_{n+2}^t \text{ or} \\ & (v_{n+2}^t \geq v_{\text{fast}} \text{ and } v_n^t - v_{n+1}^t < D \text{ and } gap_n > 8) \\ 1, & \text{otherwise.} \end{cases} \tag{5.29}$$

The remaining update is unchanged. The limitation for fast optimistic vehicles in free-flow to have at least a distance of $gap_n = 8$ cells to their leader is the result of the analysis of the gap distribution in Sec. 5.2.3. This value is the lower cutoff that can be measured in free-flow. After the lane change during which the changing vehicle orients itself on its leader and accepts a small gap the driver keeps pessimistic until the distance reaches the normally accepted value again. The second adaptation, that γ_{second} results in an optimistic state prevents the accidents discussed in Sec. 5.5.1, i.e., a very fast vehicle approaches a slow one that has just entered the street or has changed to the lane in the preceding time-step.
The changes in the definition of the model dynamics hardly influence the macroscopic and microscopic results but avoid accidents caused by inflowing vehicles or lane changes. The dynamics of the model is still capable to reproduce the traffic patterns observed empirically as well as the short time headways in the free flow phase and synchronized traffic. The dynamics at high densities is not affected unlike the simplified model or the model with restricted optimism.

5.7 Open Systems

Up to now only periodic systems were considered which is undoubtedly a simplification of the reality. Every real network is build from a combination of shorter or longer sections with open boundaries. These are connected by junctions and intersections. Thus, it is needed that a suitable algorithm exists that deals with the special necessities open systems have.
This means, the modeling of open systems in particular the insertion of the vehicles needs to be well considered and must be done with care.

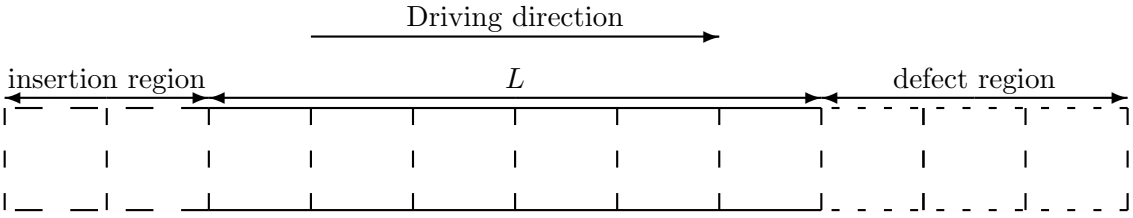

Figure 5.32: Sketch of the system with open boundaries used in this section. The insertion region is on the right end of the system. The defect region is attached to the end of the measurement region of length L.

Because of the missing hardcore repulsion accidents would appear if the cars are inserted in a naive manner. Moreover, it is important to reach all flows that occur in the periodic model. To ensure that, an intelligent input algorithm is needed. As analyzed in [8] high flows encountered in the periodic system require a more complex input strategy. In the NaSch model [9] this was done by an input buffer. Instead of just putting a new vehicle into the first cell of the system (if that is empty) – what would be the naive approach – the vehicles are inserted with respect to the first car in the system. A similar approach is thus applied here. First, the velocity v_{n_1} of the last vehicle n_1 in the system is determined and applied to the vehicle n_0 to be inserted. Then it is set at position x_{n_0} into a buffer in front of the system with at least a distance d_{n_0} then the safety is checked for vehicle n_0: $\tilde{v}_{n_0} \leq v_{n_1}$. If this test is positive, the vehicle will be inserted at this position. Otherwise, the distance is enlarged by 1 and the test is repeated until it does not fail in the end:

$$\begin{aligned} &v_{n_0} = v_{n_1} \\ &\text{WHILE } (\tilde{v}_{n_0} < v_{n_1}) \quad \{ \\ &\qquad x_{n_0} = x_{n_0} - 1; \\ &\qquad \text{CALCULATE } \tilde{v}_{n_0}; \\ &\} \end{aligned} \tag{5.30}$$

Finally, the update algorithm is applied to the inserted car in the next step. If the vehicle does not reach a position inside the system it is eliminated at the beginning of the following simulation step. Whether the newly inserted vehicle is optimistic or not is specified by the normal algorithm. The net inflow rate is therefore just the number of vehicles that have accomplished to enter the main road per time interval. In all simulations presented in this thesis the vehicles are inserted with constant time headways. Only if in the preceding time-step no vehicle could be inserted, the insertion is tried again. The time lag is then simply the reciprocal inflow rate.
The reduction of the outflow is not as simple as it is in other cellular automaton models. The outflow cannot be reduced just by closing the end of the system. Thus, a more complex approach must ensure the reduced outflow and also avoid accidents. This can only be achieved indirectly by a localized defect. This is in detail discussed in Sec. 7.2. Thus, the right boundary is realized by a region in which a speed limit is applied. If a vehicle leaves this region it is removed.
In detail, the system is divided into three sections. The first part is used for the insertion of the vehicles as described above. In the mid part, which has a length $L = 10{,}000\,\text{m}$, the

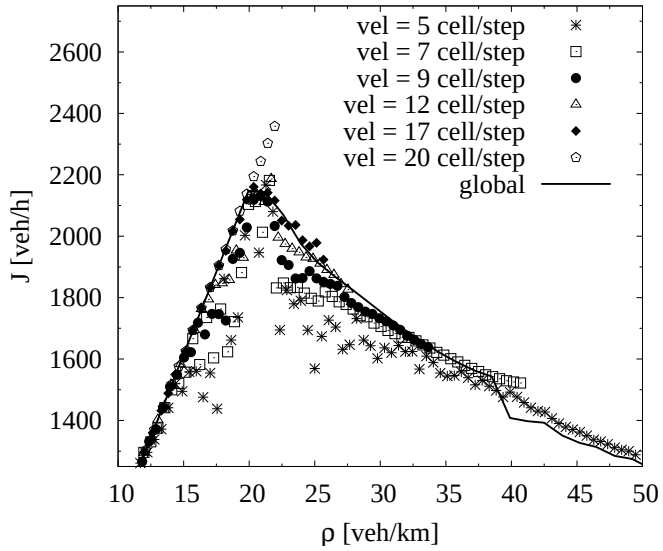

Figure 5.33: Comparison between the fundamental diagram of the street with open and periodic boundaries, respectively. The latter serves as the reference system. If the outflow is reduced appropriately by varying the speed limit all parts of the fundamental diagram of the periodic system are found in the open system as well.

vehicles can drive unhindered whereas in the last part a speed limit is applied. Figure 5.32 visualizes the configuration. To calculate a global fundamental diagram the flow and the density in the mid part is measured. The global fundamental diagram of a periodic system of the same length is used as a reference. The results are depicted in Fig. 5.33. If the outflow is reduced appropriately all parts of the fundamental diagram of the periodic system are found in the open system as well, i.e., all traffic states of the periodic system are reproduced by the open one. Even the maximum flow in free-flow is reproduced. Thus, by the approach used in this thesis it is ensured that all fluxes can be reproduced in the open system. Further, this means that for appropriate speed limits the system is governed by free-flow, synchronized traffic, and wide moving jams. This assumption is proven in Sec. 7.2.1.

5.8 Conclusion

This section showed that the model approach by Lee *et al.* is very promising as it is in good accordance with the empirical findings on a microscopic and macroscopic level. The extensive validation with empirical data showed this.
The particular model features are summarized in the following. It was shown that the fundamental diagram is in very good accordance with the empirical findings. All three traffic states are reproduced well. At low densities the free-flow branch is reproduced. The slope is nearly constant which is a direct consequence of the single class of vehicles used in the simulations.
The good reproduction of the free-flow region is not limited to macroscopic features. The degree of realism on the microscopic level is convincing as well. For example, the time

headway distribution and the optimal velocity function show very good compliance with the real world data.
At higher densities the synchronized traffic is reproduced qualitatively well. It forms the two-dimensional region in the local fundamental diagram which corresponds to the empirical data, but the region is less widely scattered. Nevertheless, the hysteretic dynamics is found as well. The synchronized regime is unstable in a wide density region and the traffic can collapse so that a wide moving jam is created that does not resolve anymore. At the lower density limit the synchronized states are long-living. Concerning single-vehicle data, the time headway distribution is reproduced not so well. It will be shown in the following chapter, that the additional influence of lane changes in two-lane traffic will improve this result.
An important attribute that distinguishes the synchronized traffic from the other states is the behavior of the vehicle-vehicle correlation. In accordance with empirical results it was pointed out that the velocities of consecutive vehicles are correlated. The other state variables show only very small or no correlation. Further, the autocorrelation vanishes if time-aggregated data is observed. This satisfies the requirements given by the empirical findings.
The third traffic state, i.e., the regime of wide moving jams, is also reproduced with a high degree of realism. The emergence of parallel jams in congested traffic at high densities shows that this traffic state is reproduced. In summary, the model approach by Lee *et al.* that is based upon limited deceleration on the one hand and human overreaction on the other forms a model that fulfills many prerequisites to simulate vehicular traffic in great detail. Thus, this can form the basis for the modeling of more complex topologies and thus for more elaborate applications, primarily two-lane traffic.
In addition to the model validation the model parameters were analyzed extensively. The most important parameter to influence the model dynamics is the attitude of the drivers. The ratio of optimistic vehicles follows the attributes of the global fundamental diagram and thus the characteristics of the different traffic patterns. Therefore the attitude distribution is a measure for the type of traffic that is present in the system and clearly separates free-flow from synchronized traffic and wide moving jams. The metastability of the synchronized traffic is mapped by the different fractions of optimistic drivers. If the system is initialized homogeneously the synchronized region clearly separates from the other traffic states. This is different if the street is initialized by a mega jam.
The other model parameters affect mainly the synchronized traffic.
Moreover, especially in synchronized traffic accidents were detected. Critical situations emerge – spoken in the sense of the model philosophy – at the transition between optimistic and pessimistic driving. These situations may happen if a platoon of faster driving vehicles approaches slower vehicles. The second accident scenario does, as stated before, not appear in the stationary state of the periodic system, but it gets relevant if realistic simulation topologies are considered, e.g., an on-ramp with slow vehicles entering the main carriageway. This analysis is especially important with respect to the development of a lane changing algorithm. Thus, changes have to be implemented in the update mechanism for the two-lane model (see Secs. 5.6.2 and 6.1).
Nevertheless, in a periodic single-lane system the accidents are not relevant. They appear very seldom and resolve automatically by the model dynamics. Further, the procedure to deal with the accidents does not influence the dynamics of the vehicles following the crashed one. Therefore, the accidents have no side-effects.

Nevertheless, the development of an accident free model limited deceleration probability is possible as the "simplified model" with reduced complexity, i.e, without optimistic vehicles shows.
The approaches for a further "safe" model show nearly the same features as the original model in free-flow and synchronized traffic. Differences become visible in the single-vehicle data. For example, the time headway distribution is shifted to larger times. In dense traffic the differences are more drastic. A sequence of all three traffic states is formed: Synchronized traffic establishes between compact jams and the free-flow traffic. Thereby free-flow traffic is followed upstream by synchronized flow that goes over to a compact jam which is again followed by free-flow traffic. Thus, the characteristics of the "safe" model are between the unchanged and the simplified model. In the former wide moving jams are separated from free-flow in the high density region whereas in the latter synchronized traffic and wide moving jams alternate.
The adapted model for two-lane traffic shows the same properties as the original model. The differences hardly influence any vehicle as the configurations that lead to a different attitude are very improbable.
The discussion of open systems showed that using an elaborate insertion algorithm all flows even the high fluxes in free-flow can be reached. Because of the limited deceleration capability no simple outflow reduction can be implemented, but a defect region with limited maximum velocity controls the outflow. The whole global fundamental diagram of the periodic system could be reproduced.
The model has reached such a degree of realism in reproducing the macroscopic features of traffic flow as well as the microscopic ones that it can serve as the basis for an elaborate two-lane model. Nevertheless, it has to be modified to be robust enough and to handle inserted vehicles and thus simulate complex topologies, e.g., traffic networks.

6 Multi-lane Traffic: Extension of the Model by Lee *et al.*

6.1 Two-Lane Traffic

The simulation of single-lane highway traffic is an important task to get a first but deep look inside the properties of a model for vehicular traffic. But to simulate more complex and realistic traffic situations, at least two more research fields have to be discussed.
First, vehicular traffic is not only disturbed by internal fluctuations but also by external factors like, e.g., construction areas, local speed limits, or on-ramps and off-ramps. Thus, the simulation of a network requires that the peculiarities that are found in it are taken into consideration, too. This objective is discussed in the next chapter.
Second, the usual highway is not just a single-lane road but it has at least two lanes on which the traffic flows. This has direct consequences on the validation of the model: It is an important fact that all empirical data are collected on multi-lane sections of the highway network. Thus, it is not sufficient that a single-lane model reproduces the empirical data qualitatively and quantitatively correct, but the two-lane approach has to be considered and its agreement with the empirical findings has to be validated as well. For example, the time headway distribution of the synchronized traffic of the single-lane approach is not in good agreement with the empirical data. The results of this chapter hint at the importance of the lane changes for this feature as the resulting time headways are in very good accordance. Additionally, the two-lane approach has to fulfill further requirements. The number of lane changes empirically found and their dependence on the density has to be reproduced. The coupling of these two lanes must also be taken into account by the means of lane changing rules.
In order to achieve this aim, much research was done to extend the knowledge of the mechanisms of two-lane traffic, especially, as the simulation of large traffic networks [124] became more important. In the beginning these were based on the NaSch model like the simulation of the inner city of Duisburg [34] or the Dallas/Fort-Worth region [146]. They simulate the traffic on a complex network which consists of multi-lane roads, on and off-ramps and intersections. The simulations require an accurate reproduction of the mentioned mechanisms especially the lane changes. Thus, a simple approach was needed to formulate the reasons for a driver to change the lane and ensure his safety in the formulation of a cellular automaton. But it turned out, that even in the NaSch model it is a crucial task to mimic the behavior and the safety restriction so that they are in accordance with the empirical findings.
Additionally, the number of investigations concerning multi-lane traffic is rather small. Only a few empirical results are available [17, 19, 44, 159] so that a proper formulation of a set of lane changing rules is difficult. However, the few empirical data have to be taken into account to get deeper knowledge of the most important features and mechanisms for a good simulation approach.
One important characteristic is the number of lane changes that strongly depends on the

traffic density. It should rise with increasing density, reach its maximum roughly at the maximum flow and decrease again. Even at high densities lane changes can be observed. The German peculiar feature that the right lane should be preferred leads to a phenomenon of a lane usage inversion that is counterintuitive to the law. The distribution of the density becomes asymmetric: It was found that the density on the left lane is higher than on the right lane [94, 111, 159]. Without this limitation the flow is in general evenly distributed on all lanes [17, 19, 44].
These investigations led to several two-lane extensions [22, 119, 120, 127, 147, 167, 168] for the NaSch model that can reproduce the lane usage inversion, but the realistic mapping of the number of lane changes was still a problem. The approach using cellular automata has another shortcoming if one introduces different kinds of vehicles. Plugs are formed that can govern the dynamics of the whole system [90].
A detailed analysis of the mechanisms that is needed for the realistic reproduction of the two-lane characteristics can be found in [93]. Therein the BL model is extended by a lane-changing algorithm that shows good agreements with the empirical results. The number of lane changes with respect to the density was reproduced as well as the lane usage inversion for the asymmetric approach. The introduction of anticipation reduced the problematic plug formation as well.
This model currently serves as the simulation kernel of the simulation of the highway network of North Rhine-Westphalia which is the basis for the web service *autobahn.nrw.de* [134]. It provides the simulation results on the Internet since 2001. The next stage of expansion will replace it by the model by Lee *et al.*. The extensions discussed in this thesis thus will provide a significant improvement as the degree of realism rises. Moreover, road works as well as ramp metering algorithms have to be included into the simulation framework in the future, which is only possible with a suitable and a carefully adapted model.
That the model by Lee *et al.* is indeed a promising candidate for such a challenge was shown by the discussion in the previous chapter. It is capable to simulate single-lane vehicular traffic in a very detailed and exact way if slight changes are made. It reproduces the empirical facts gathered on multi-lane roads in a detailed manner. The reproduction is not limited to global features but covers single-vehicle data as well.
However, because of some difficulties that arouse when the traffic is disturbed extrinsically the adaptation to multi-lane traffic is not easy. For example, accidents (see Sec. 5.5) happen in the single-lane system and additional ones will occur if the lane change procedure is performed carelessly. Therefore, a detailed analysis was performed to discover the origin of dangerous situations. Without this knowledge a two-lane extension of the model would be unusable. The results are the basis for the model adaptation and especially the formulation of the lane-changing algorithm.
The combination of an intelligent lane change algorithm that takes the limited deceleration into account and the adapted model ensures that additional accidents resulting from the lane changes are avoided. The dangerous situations that are known from the analysis of the single-lane model are considered and a lane change is disallowed if such a configuration emerges.
Therefore, the enhanced model (Sec. 5.6.2) is utilized and builds the basis for a generic lane change algorithm. Thus, the model by Lee *et al.* is extended in this chapter to a two-lane model that can not only be used to simulate complex topologies as addressed above but might also be applied to the analysis of control mechanisms like ramp metering. Therefore, the mentioned empirical results should be reproduced as well as the complex

structures of synchronized traffic at defects like on-ramps [73]. Special attention is payed to the reproduction of the different synchronized traffic patterns. These are regarded to be important ingredients for realistic simulation of highway traffic especially if scenarios like on-ramps are taken into account. This is analyzed in the next chapter but at first the basic two-lane characteristics are presented and compared to the empirical data.

6.1.1 Lane Changing Rules

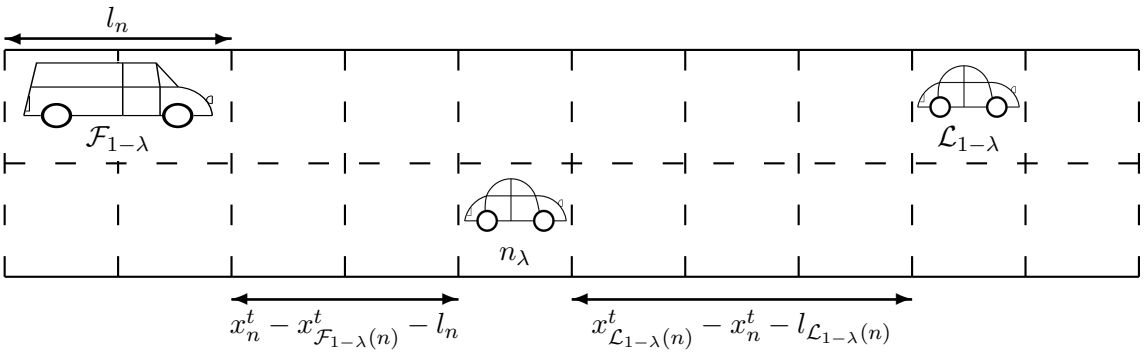

Figure 6.1: Nomenclature in the lane change algorithm. $\mathcal{F}_{1-\lambda}(n)$ is the follower of the concerned vehicle n_λ on the destination lane, $\mathcal{L}_{1-\lambda}(n)$ is the leader. $x^t_{\mathcal{F}_{1-\lambda}(n)}$ is the corresponding position of the follower, $x^t_{\mathcal{L}_{1-\lambda}(n)}$ that of the leader. l_n is the length of the vehicle.

The approach discussed here has to take into account the exceptional properties of the single-lane model. Here, it is especially important to keep in mind that a hardcore repulsion is missing. Moreover, the lane changes have to take into account safety rules in the sense of not interfering with cars on the other lane, but also avoiding accidents in the process of lane changing.
This means, lane changes must explicitly be done under the consideration of the safety of all participating vehicles very accurately and thus might disallow any lane change in situations when the limited deceleration capability takes effect (cf. 7.1.7). This might appear as a drawback of this model approach. But considering what kind of lane changes are possible, e.g., in the BL model, the advantages become clear. For example, the safety criterion of the lane change of the two-lane extension considered by Knospe for the BL model [93] is formulated as follows:

$$(d_{\mathcal{L}}^{\text{eff}} \geq v) \text{ and } (d_{\mathcal{F}} \geq v_{\mathcal{F}}),$$

where $\mathcal{F}$ and $\mathcal{L}$ denote the state variables of the following and the leading vehicle on the destination lane, respectively, vehicle $d_{\mathcal{L}}^{\text{eff}} = d_{\mathcal{L}} + \max(v_{\text{anti}} - g_{\text{add}}, 0)$ is the *effective* gap to the leading vehicle on the destination lane and $v_{\text{anti}} = \min(gap, v_{\mathcal{L}})$ the proposed velocity of the leader in the update step.
This approach allows for slowly driving vehicles or even stopped vehicles to change the lane in cases where this is obviously not safe and thus not realistic. For example, if a stopped vehicle wants to change the lane and would get in front of a vehicle driving with its maximum velocity, this is still allowed if the distance equals the velocity of the follower.

Thus, this fast driving vehicle has to brake unrealistically strong from $v_{\max}$ to zero in one time-step. This shows that the introduction of a limited deceleration capability does not only lead to more realistic driving in the single-lane system but seems to be essential for a realistic lane change procedure.
As mentioned above, the velocity calculation and therefore the determination of the security of the lane change does not only depend on the gap and the velocity of the involved vehicles but it requires the calculation of inequality Eq. 5.1. Thus, one has to follow a different approach with a virtual lane change process. This means that the changing vehicle is virtually set to its destination lane. Then the velocity can be calculated and thus the security of the involved vehicles is determined in an intermediate update-step. Following this approach and stating it in greater detail the lane-changing rules are described in this section.
Note that in this thesis symmetric lane changes are considered. These do qualitatively show the important features of the two-lane dynamics. For asymmetric lane changing rules please refer to [93]. Therein an extensive discussion on the main attributes and mechanisms of asymmetric lane changing rules is given.
In the two-lane model each time-step is separated into two sub-steps [21]. In the first step for each vehicle it is decided whether it will change lane in the current time-step. In the second step the normal one-lane model update is applied to each of the two lanes.
The basic idea behind the two-lane model is using the condition for $\tilde{v}_n^{t+1}$ to determine the safety of a possible lane change. In each time-step it is checked whether the vehicle is able to drive with the safe velocity if it changes lane. It is also checked whether the follower on the destination lane would be able to drive safely. The parameter $\beta \in \{0, \ldots, D\}$ controls how much the follower may be constrained. For $\beta = 0$ only smooth lane changes are allowed where the follower is not forced to brake at all, while at $\beta = D$ even decelerations with maximum braking capability are acceptable. These conditions constitute a *security criterion* and determine whether a vehicle *is able* to change lanes without obstructing vehicles on the destination lane or even provoking a dangerous situation.
A vehicle *intends* to change lane only if a *mobility criterion* is satisfied. For the symmetric two-lane model this means that the vehicle can drive faster on the destination lane than on its current lane. This is determined by calculating $\tilde{v}_n^{t+1}$ on the current lane and then virtually changing the vehicle to the other lane, calculating $\tilde{v}_n^{t+1}$ again and comparing these two.
According to [159] a lane change in real life takes up to $t_{\text{lc}} = 3$ seconds in time. If this is utilized in a strict manner the security criterion must hold for at least three time-steps until a positive mobility criterion can trigger the vehicle to actually change the lane. For each vehicle a new variable ϑ_n^t is introduced that is initially $\vartheta_n^0 = 0$ and acts as a counter for time-steps in which the security and the mobility criterion is valid.
To formally describe the update rules of the model, $\lambda_n^t \in \{0, 1\}$ denotes the lane used by vehicle n at time t, i.e., if a vehicle is on lane λ, $1 - \lambda$ is the other lane. $\mathcal{F}_\lambda(n)$ denotes the follower and $\mathcal{L}_\lambda(n)$ the leader of the vehicle n on lane λ. Some state variables are calculated for a vehicle virtually changing the lane. In this case, a second subscript is used to specify the lane. Thus, $\tilde{v}_{n,\lambda}^{t+1}$ means "$\tilde{v}_n^{t+1}$, if the vehicle would be on lane λ". Figure 6.1 describes the used parameters.
The update rules of the two-lane model are themselves separated in two sub-steps.
First it is checked whether the vehicle would benefit from a lane change, i.e., whether the mobility criterion is satisfied:

$$\tilde{v}^{t+1}_{n,1-\lambda^t_n} > \tilde{v}^{t+1}_{n,\lambda^t_n}. \tag{6.1}$$

This means a vehicle tends to change its lane if the velocity it can reach on the destination lane is higher than that on its origin lane. The velocity updates during the mobility check are performed deterministically so that no artificial lane changes are made if the vehicle on the origin lane dawdles.
To ensure a safe lane change the security criterion has to be valid as well:

$$x^t_n - x^t_{\mathcal{F}_{1-\lambda^t_n}(n)} > l + g_{\text{safe}} \tag{6.2}$$

$$x^t_{\mathcal{L}_{1-\lambda^t_n}(n)} - x^t_n > l + g_{\text{safe}} \tag{6.3}$$

$$v^t_n - D \leq \tilde{v}^{t+1}_{n,1-\lambda^t_n} \tag{6.4}$$

$$v^t_{\mathcal{F}_{1-\lambda^t_n}(n)} - \beta \leq \tilde{v}^{t+1}_{\mathcal{F}_{1-\lambda^t_n}(n)}. \tag{6.5}$$

Here, g_{safe} denotes an optional security gap which becomes important at higher densities where the gap between the vehicles approaches zero.
If, as the result, a safe lane change would be possible (and is wanted) ϑ_n is increased

$$\vartheta^{t+1}_n = \vartheta^t_n + 1, \tag{6.6}$$

and it is checked whether the conditions Eq. (6.1) and Eq. (6.2) did hold t_{lc} times. If this is true, the lane is changed:

$$(\lambda^{t+1}_n = 1 - \lambda^t_n \text{ and } \vartheta^{t+1}_n \geq t_{\text{lc}}) \tag{6.7}$$

$$\text{or } \lambda^{t+1}_n = \lambda^t_n \text{ otherwise.} \tag{6.8}$$

If the lane change was successful the counter ϑ_n is reset:

$$\vartheta^{t+1}_n = 0 \text{ if } \lambda^{t+1}_n \neq \lambda^t_n. \tag{6.9}$$

Note that t_{lc} is important for the number of lane changes N_{lc}.

Symmetric Lane Change Including Driver's Attitude

To increase the efficiency of the implementation of the two-lane model another variant is discussed here, which might be crucial in some cases. The determination whether a vehicle tends to change the lane is coupled with two velocity updates for the changing vehicle, one on the origin lane and one on the destination lane. In the sense of the human factor introduced in the single-lane model it is plausible to involve the attitude of the driver into the mobility criterion (Eq. 6.1.1). Thus, the mobility criterion is enhanced by a term that takes into account the attitude of the driver:

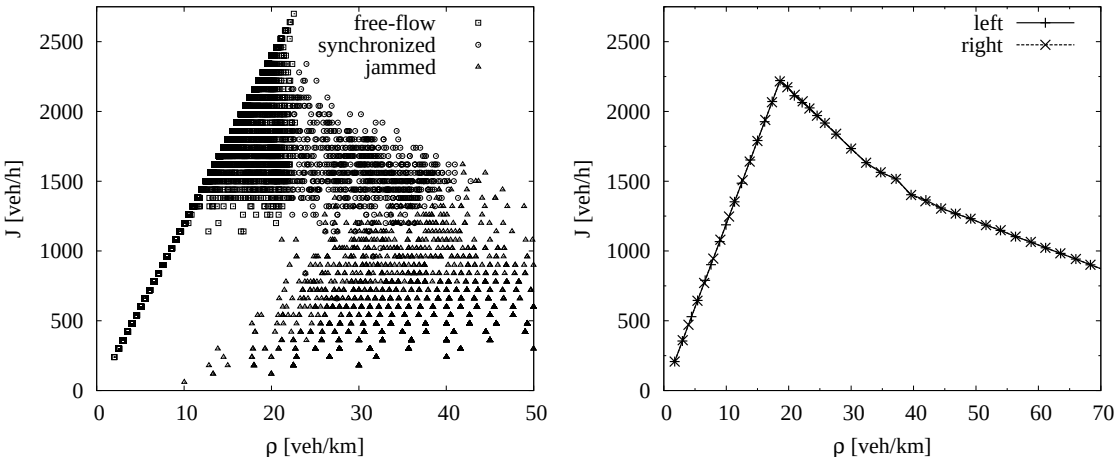

Figure 6.2: **Left:** Fundamental diagram of the left lane of a periodic two-lane system. The synchronized region is much more scattered than in the single-lane system and therefore in better accordance with the empirical findings. **Right:** Global fundamental diagram of the two lanes of a periodic two-lane system. The data points of both lanes are congruent. The differences to the single-lane system are marginal. The flow on each lane is slightly higher: $J_{\text{one}} \approx 2150\,\text{veh/h}$ vs. $J_{\text{two}} \approx 2280\,\text{veh/h}$.

$$(\gamma_n = 1 \text{ or } v_n = 0)$$

and

$$\tilde{v}^{t+1}_{n,1-\lambda^t_n} > \tilde{v}^{t+1}_{n,\lambda^t_n}.$$

This means that vehicles that are optimistic and have not stopped are not allowed to change the lane. In every simulation step at least two velocity updates are saved.
Note, in free-flow the lane change rate is approx 0, as nearly all vehicles drive optimistic. This changes if different types of vehicles, namely trucks with a reduced maximum velocity, are integrated. Nevertheless, the efficiency of the algorithm becomes in particular important in dense traffic where many vehicles have to be processed.
The restriction that the test on the drivers attitude is only applied to vehicles that still drive, allows optimistic vehicles in a compact jam to change the lane.
The features of this approach qualitatively correspond to those of the original model. Only slight quantitative differences in the number of lane changes are observed, i.e., the frequency is a little bit lower.

6.1.2 Basic Features and Model Validation

First, some basic dynamic features of the periodic two-lane system are described that show the main capabilities of this approach.

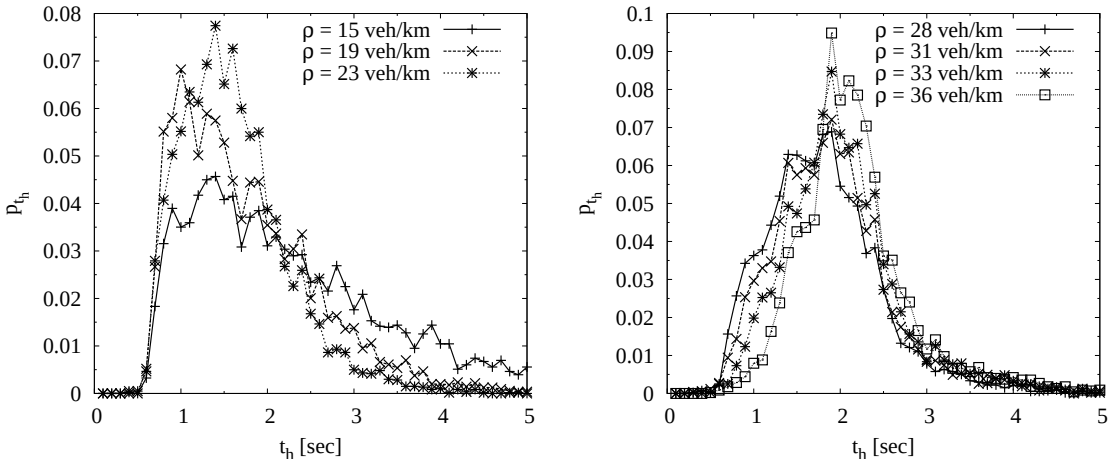

Figure 6.3: **Left:** Time-headway distribution of the symmetric two lane model in free-flow. The differences to the single-lane results are hardly to distinguish. **Right:** Time headway distribution of the synchronized flow. Headways below one second are detected very frequently. This is also found in the empirical data. Furthermore, the curve is shifted to longer times for increasing densities.

The local fundamental diagram of the periodic system of the left lane in the left of Fig. 6.2 shows the basic characteristics that have been already seen in the single-lane simulations. But there are some differences, especially the larger variance of the data points in the synchronized region. The measures cover a greater area than in the single-lane system, i.e., between $18\,\text{veh/km} \leq \rho \leq 42\,\text{veh/km}$ and $1300\,\text{veh/h} \leq J \leq 2250\,\text{veh/h}$. This is in much better agreement with the two-lane empirical empirical data. The lane changes disturb the very homogeneous traffic that is found in the single-lane system (Sec. 5.1.1).
A look at the global fundamental diagram of both lanes does not reveal any surprises. The flow is evenly distributed to both lanes so that no differences in the curves can be observed. For $\rho \leq 18\,\text{veh/km}$ free-flow emerges. Synchronized traffic is formed for $19\,\text{veh/km} \leq \rho \leq 42\,\text{veh/km}$. The BL model shows a similar characteristic. Just the upper limit of the synchronized regime is shifted slightly to smaller densities [93].
Further, the traffic state is almost always synchronized between the two lanes. Especially, if a breakdown appears at one lane, it is transferred to the other lane immediately. Thus, the traffic state is the same on both lanes. Compared to the results of the single-lane system, the maximum flow is higher: $J_{\text{one}} \approx 2150\,\text{veh/h}$ vs. $J_{\text{two}} \approx 2280\,\text{veh/h}$. The shape and the extension of the synchronized region are almost identical to the single-lane case. The upper limit of the synchronized region is slightly shifted to higher densities. Here, the vehicles can avoid disturbances by a lane change. The benefit from this maneuver is larger than the drawback of the disturbance by the changing vehicles.
Moreover, the space-time plots show the same characteristics as the single-lane system. All states are reproduced by the simulations.
Quite drastic differences between the results of the single-lane system (cf. Figs. 5.7 left and 5.8) and the two-lane one (Figs. 6.3 left and right) are found in the time headway distribution p_{t_h}. The time headway distribution in free-flow traffic is only slightly different (Fig. 6.3 left). Even here many headways lower than one second are found and the lower

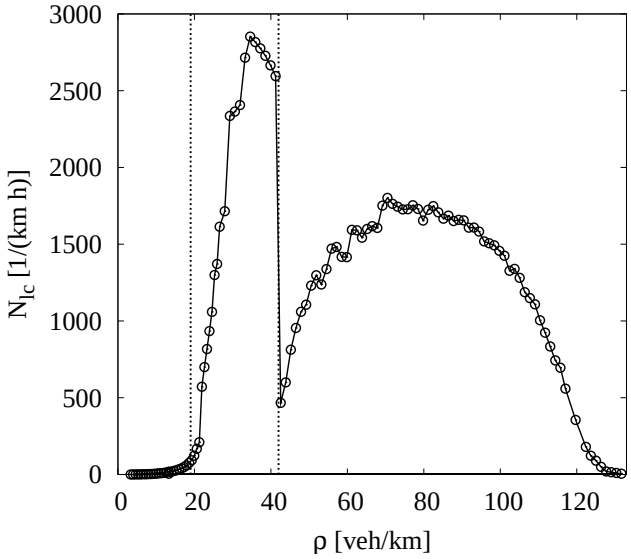

Figure 6.4: Number of lane changes in the symmetric model. The lane change time t_{lc} is set to 1 sec. The different states according to the global fundamental diagram are indicated by the vertical lines. From left to right: free-flow, synchronized traffic, and wide moving jams.

cut-off is at $t_{\mathrm{h}} = 0.5\,\mathrm{sec}$. The maximum values are $t_{\mathrm{h,max}}^{\mathrm{single}} \approx 0.09$ vs. $t_{\mathrm{h,max}}^{\mathrm{two}} \approx 0.08$ for the single-lane and the two-lane system, respectively, which means that just the maximum is a little bit lower but of the same order. The lane changing process disturbs the very homogeneous traffic and a broader range of time headways is observed. These results are qualitatively and quantitatively in very good agreement with the empirical data (see Fig. 4.2).

Compared to the single-lane system the results for the synchronized traffic are different. The time headway distribution shows a much better agreement with the empirical findings in the synchronized traffic. The empirically observed short time headways below one second are present now. As shown in the right part of Fig. 6.3 time headways down to $t_{\mathrm{h}} = 0.5\,\mathrm{sec}$ appear. This corresponds to the cut-off time found in the empirical data. Additionally, the distribution is much broader. Note the empirical data were also measured on a multi-lane road. Headways up to $t_{\mathrm{h}} \approx 3\,\mathrm{sec}$ occur in the empirical data as well as in the simulation results. Only the maximum is slightly shifted to higher times in the simulations.

The process of lane-changing seems to play an important role for the occurrence of short time headways in the synchronized traffic. It is shown on the next pages that many lane changes are found especially in the synchronized region.

It is an important result, that the time headway distribution for the two-lane model matches the empirical data better than the single-lane model especially in the synchronized traffic state.

Number of Lane Changes

The diagram in Fig. 6.4 shows the number of lane changes of the symmetric model with respect to the density. One sees, that at very low densities only a negligible number of vehicles change the lane. This is not in accordance with the empirical data. The reason for this is the very uniform velocity distribution. All vehicles drive nearly with the same velocity, i.e., the maximum velocity $v_{n,\max}$ is identical for all vehicles. In reality, on the one hand, the velocities of the vehicles are Gaussian distributed and, on the other hand, slower vehicles disturb the homogeneous flow. These slow vehicles provoke lane changes at very low densities. If trucks are introduced in the simulations, lane changes are forced even in the lower density limit (cf. 6.2). At higher densities above $\rho \approx 20\,\mathrm{veh/km}$, which corresponds to the upper limit of the free-flow region the number rises dramatically. Here, the vehicle interaction in free-flow is no longer negligible. The maximum in the synchronized regime is found at $\rho_{N_{\max}} \approx 37\,\mathrm{veh/km}$. Then the number of lane changes decreases slightly until $\rho \approx 40\,\mathrm{veh/km}$, the upper limit of the synchronized regime, where it drops down to about $N_{\mathrm{lc}} \approx 500\frac{1}{\mathrm{km\,h}}$. The system is now in the state of wide moving jams. A few compact jams mix with free-flow. The latter governs most of the street and thus the tendency to change the lane is low. At higher densities the number rises again and reaches about $N_{\mathrm{lc}} \approx 1750\frac{1}{\mathrm{km\,h}}$. The interaction between the vehicles is very high now and enough space on the destination lane is available. The latter reduces when even higher densities are reached. The number of lane changes decreases again and approaches 0 for a completely congested road.
The large number of lane changes in the synchronized traffic in the simulations hint at the importance of the lane changing process for the synchronization of the traffic on the different lanes [97] in general and in particular of the synchronized traffic. Thus, the coupling of the two lanes bases on the lane changes.
There are two parameters responsible for the lane change frequency. The influence of the value of β – the degree a vehicle is allowed to hinder the following vehicle on the destination lane in the process of lane-changing – is beside t_{lc} the second important parameter. But the influence of β is fundamentally different than that of t_{lc}. The latter may lead to a configuration where the security criterion is fulfilled once but not t_{lc}-times and therefore a lane change is permitted. In contrast, a situation may emerge in which the vehicle that wants to change the lane may never accomplish the security criterion. This occurs if the difference between the velocities of the involved vehicles is too high. For example, synchronized flow that is induced by the on-ramp (cf. Sec. 7.1) on the right lane is transferred to the left lane spontaneously. This is different for a jam of standing vehicles that may reside on the right lane and the flow on the left keeps high or even rises as approaching vehicles try to avoid the jam on the right lane. An example for this situation is given in Sec. 7.1.7.
A further effect of the lane changes in free flow is their influence on the establishing of synchronized flow as the lane changes may encourage it. If the changing car forces its successor on the destination lane to change its attitude to pessimistic, this stabilizes synchronized flow as discussed in Sec. 5.6.1. In other words, if the lane change is very smooth, no synchronized flow will be formed but free flow with very low time headways will be stable until the lane changing vehicles are numerous enough or their velocity provokes braking. Braking can be forced because of different reasons. The first and most obvious mechanism is that a slower vehicle changes to the front of a faster vehicle. The disturbed vehicle must brake if the velocity difference is large enough. This holds true for optimistic

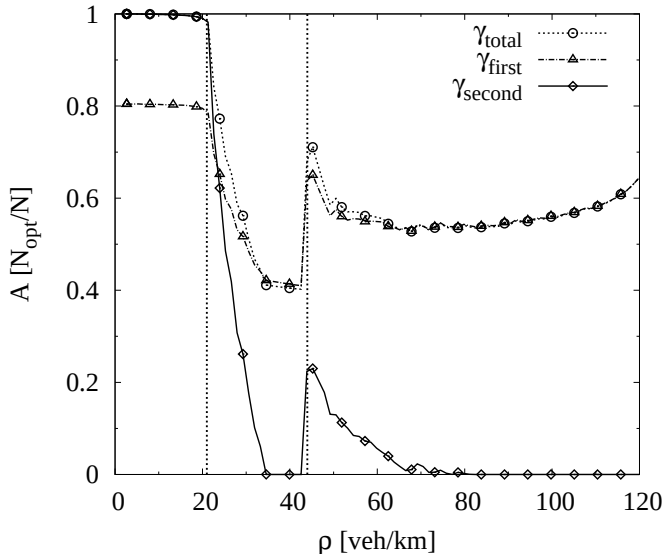

Figure 6.5: Attitude of the drivers in the two-lane system. The fraction of optimistic drivers is shown for the γ, γ_{first}, and γ_{second}. The slope is different to the single-lane system. In free-flow nearly all vehicles are optimistic. In contrast to the single-lane system the number of optimistic vehicles decreases more slowly at the beginning of the synchronized region and does not drop immediately at the boundary between free-flow and synchronized traffic.

as well as pessimistic vehicles. A different mechanism only affects optimistic vehicles. A similar effect is discussed in Sec. 5.1. In that section after the description of the update rules the effect of a dawdling vehicle on its successors is analyzed. As stated there the dawdling of a vehicle may not only provoke a deceleration of its follower but may also force him to change his attitude from optimistic to pessimistic. The same effect may be valid for vehicles that have changed the lane. Their follower might be affected alike. Therefore, lane changes can stabilize or even induce synchronized traffic. The mechanism is as follows. If the changing vehicle disturbs the free flow, vehicles on the destination lane may be forced to leave their optimistic state and change to pessimistic attitude. Thus, as stated in Secs. 5.6.2 and 5.6.1 pessimistic vehicles stabilize synchronized traffic or in this case synchronized traffic arises from free flow.
As stated above, two parameters affect the lane changing behavior. On the one hand, the degree the following vehicle may be disturbed determined by β and, on the other hand, the lane change time t_{lc}. Thus, the influence of these parameters is discussed in the following sections. But first, a closer look is taken at the characteristics of γ in the two-lane system. The huge influence of the attitude γ on the dynamics of the single-lane system makes it necessary.

Attitude

The fraction of optimistic vehicles in the two-lane system is shown in Fig. 6.5. The similarities to the results of the single-lane system (see Fig. 5.14) are obvious. The number of optimistic vehicles shows the same characteristics in free-flow and in the region of

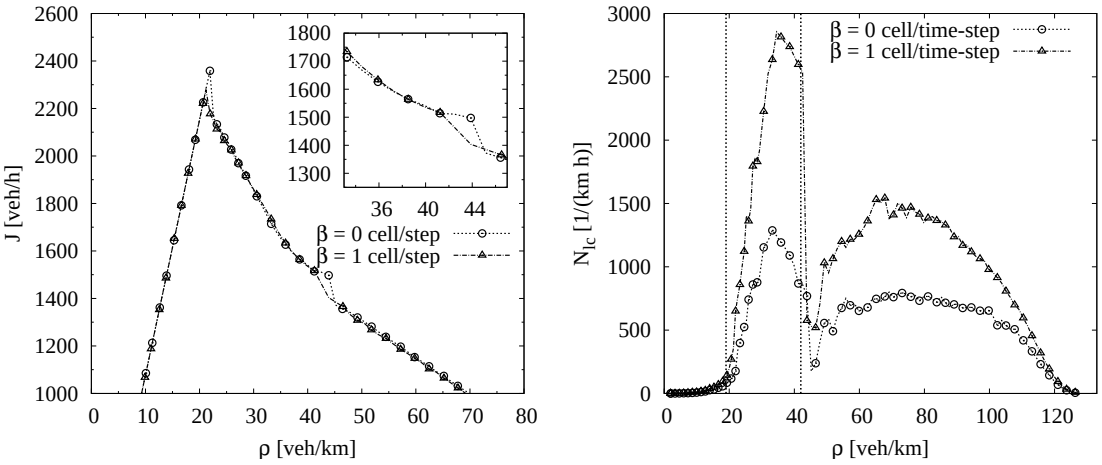

Figure 6.6: Dependence of the two-lane dynamics on β. The lane change time t_{lc} is set to 1 sec. **Left:** Global fundamental diagram depending on β. A difference emerges at the upper density limit of the synchronized regime. Synchronized traffic establishes for larger ρ if $\beta = 0$ cell/time-step. **Right:** Number of lane changes in the symmetric model. The different states according to the global fundamental diagram are indicated by the vertical lines. From left to right: free-flow, synchronized traffic, and wide moving jams. The number of lane changes is more than twice as high if $\beta = 1$ cell/time-step.

wide moving jams not only qualitatively but also quantitatively. Differences appear in synchronized traffic. The number of optimistic drivers does not drop at the boundary to free-flow but decreases much more slowly. The plateau found in the single-lane system is build for $32\,\mathrm{veh/km} \leq \rho \leq 42\,\mathrm{veh/km}$.
The slower decrease is a result of the opportunity for the vehicles to avoid becoming pessimistic by the lane change. Therefore, the total number of optimistic vehicles is larger than in the single-lane case until the free-space becomes limited and makes the lane change difficult, i.e., the plateau is reached. Note, the number of lane changes is correlated to the number of pessimistic vehicles as the comparison with Fig. 6.4 reveals. The increase of the number of lane changes is in the same density interval as the decrease of the number of optimistic drivers.
Thus, although the attitude is not explicitly used in the lane changing algorithm, it is more likely that a pessimistic vehicle benefits from a lane change. This shows again that the attitude of the drivers is of main importance for the model dynamics also in the two-lane system.

Dependence on β

The influence of β – the degree a following vehicle may be hindered during the lane change – on the fundamental diagram (right part of Fig. 6.6) is rather small. The free-flow branch as well as the regime of wide moving jams are congruent for $\beta = 0, 1$ cell/time-step. The maximum flow that is reached in free-flow is higher if $\beta = 0$ cell/time-step. It reaches approx 2400 veh/h vs. $J \approx 2320$ veh/h for $\beta = 1$ cell/time-step.
The independence on the choice of β is true for most of the region of synchronized traffic.

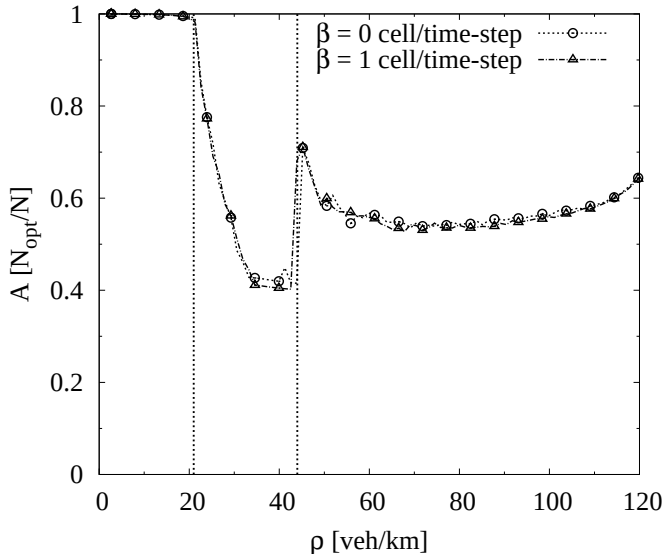

Figure 6.7: Attitude of the drivers depending on β. The upper limit of the synchronized regime is shifted to higher densities if $\beta = 0$. Furthermore, the fraction of optimistic vehicles is approximately 2% larger for $\beta = 0$. The hindrance by the lane changes lead to more pessimistic vehicles. The lane change time t_{lc} is set to 1 sec.

Differences are found only at the upper density limit of the synchronized region which is shifted to higher densities for $\beta = 0$ cell/time-step. For $\beta = 0$ cell/time-step the limit is located at $\rho \approx 44$ veh/km vs. $\rho \approx 42$ veh/km for $\beta = 1$ cell/time-step.
This means that free-flow traffic is less stable for very high flows and synchronized traffic is build at lower densities if the lane changes are uncooperative. The same argumentation holds for synchronized traffic. It is less stable at high densities if the interference of the vehicles is high. This is an obvious result as a more aggressive lane change provokes decelerations by the following traffic and thus disturbs the intrinsically homogeneous synchronized traffic. After the relaxation time of the simulation run wide moving jams have emerged for $\beta = 1$ cell/time-step. Thus, perturbations by the lane changes are not compensated by the avoidance of obstacles.
The number of lane changes shows a stronger dependence on the value of β. In Fig. 6.6 the relation is depicted. In the figure the traffic states are roughly delimited by vertical lines. In free-flow the discrepancies are negligible. In both cases the number of lane changes is very low. For $\rho > 20$ veh/km the differences become relevant. For $\beta = 0$ cell/time-step the maximum number of lane changes is reached at $\rho = 32$ veh/km. $1300 \frac{1}{\mathrm{km\,h}}$ are detected. The number is more than twice as high for $\beta = 1$ cell/time-step. At $\rho \approx 35$ veh/km the number of lane changes is about $2800 \frac{1}{\mathrm{km\,h}}$. This discrepancy is the result of the passive and cooperative lane change for $\beta = 0$ cell/time-step and the more aggressive uncooperative changing for $\beta = 1$ cell/time-step. In the latter more vehicle configurations lead to a positive security criterion as the speed interval of the follower at which a lane change is allowed is by 1 cell/time-step larger. This becomes more important if the disturbance of the system is biased for example by vehicles entering from an on-ramp. Then the speed difference between the lanes may become very large and a lane change is only possible if

a vehicle is permitted to hinder another one. If this is not allowed or the hindrance is not strong enough the lanes may decouple (see 7.1.7).
The dependence of β on γ is small like for the global fundamental diagram (Fig. 6.2). The upper limit of the synchronized regime is shifted to higher densities if $\beta = 0$. Furthermore, the fraction of optimistic vehicles is approximately 2% larger for $\beta = 0$ in accordance with the fundamental diagram. The hindrance by the lane changes lead to more pessimistic vehicles. In the density interval of the free-flow no differences can be found in contrast to the fundamental diagram.

Lane Change Time

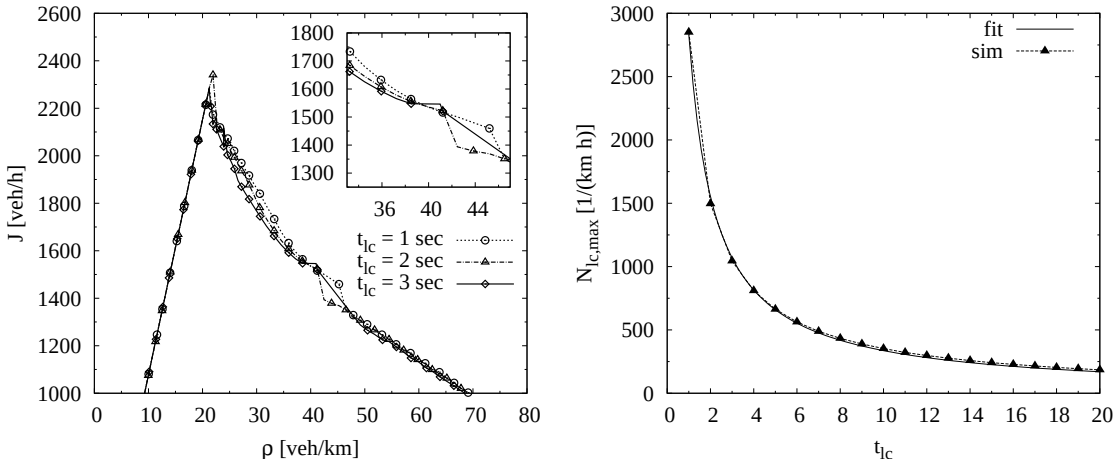

Figure 6.8: **Left:** Global fundamental diagram depending on t_{lc}. The maximum flow is higher for $t_{\mathrm{lc}} = 2\,\mathrm{sec}$. **Right:** The maximum number of lane changes N_{lc} with respect to the lane change time t_{lc}. The maximum decreases like $\frac{1}{1+a \cdot t_{\mathrm{lc}}}$.

The time a vehicle needs to change the lane is in most models set to the same time as the update of the velocity, i.e., one time-step. It is stated in [159] that the mean time a driver needs is for a complete lane change is longer, i.e., times about $t_{\mathrm{lc}} = 3\,\mathrm{sec}$ are denoted for the whole maneuver. This parameter can be related to the need of the drivers for safety when changing the lane. He checks the neighborhood during this time and changes the lane not until his desire is fulfilled.
The dependence of the fundamental diagram (Fig. 6.8) on the lane change time is small in free-flow and the regime of wide moving jams. In the former the maximum flow is slightly reliant on the particular choice of t_{lc}. The highest flow is reached with $t_{\mathrm{lc}} = 2\,\mathrm{sec}$. With this value the benefit of the lane changes overcomes the disadvantages given by two concurring processes: On the one hand, the disturbance by the lane change [24] and, on the other hand, the possibility of a vehicle to evade an obstacle. For $t_{\mathrm{lc}} = 1\,\mathrm{sec}$ the perturbations are more important. For $t_{\mathrm{lc}} = 3\,\mathrm{sec}$ the capability to change the lane is too low so that no positive effect is found. This is different in synchronized traffic. Here, the highest flow is reached for $t_{\mathrm{lc}} = 1\,\mathrm{sec}$. It decreases for higher t_{lc}. Thus, the lane changes lead to a better performance of the system. In addition, the choice affects the upper limit of the synchronized traffic. Here, again the easier a lane change is the more stable is the

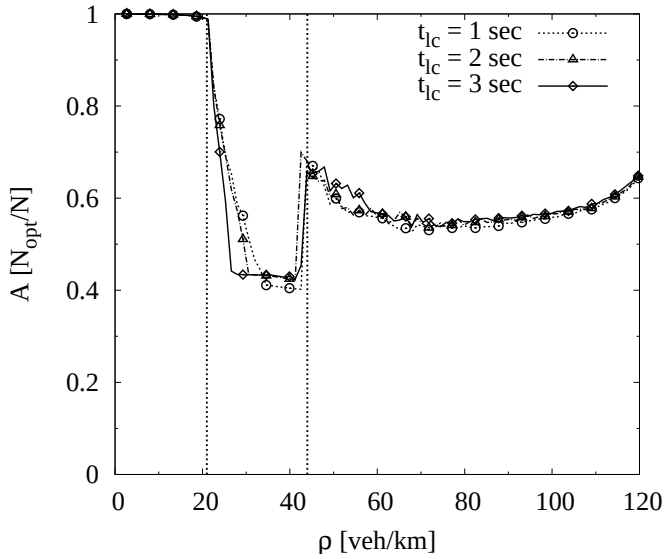

Figure 6.9: The attitude depending on the lane change time t_{lc}. β is set to 1 sec. The region of synchronized traffic is split if $t_{\mathrm{lc}} = 1$. The plateau that is formed in the single-lane system is smaller and the lower boundary is shifted to higher densities. For increasing t_{lc} the slope approaches that of the single-lane system.

synchronized traffic. In the regime of wide moving jams no differences appear with respect to the lane change time.

t_{lc} is especially important for the number of lane changes N_{lc}. The relation is shown in Fig. 6.8. At short lane change times one sees that about 2750 lane changes per kilometer and hour occur. For higher values of t_{lc} the lane change rate decreases exponentially and reaches a value of about 200 lane changes per kilometer and hour. The lane change times can nicely be fit to $N_{\mathrm{lc}}(t_{\mathrm{lc}}) = 1.61 \cdot 10^4/(1+4.69 \cdot t_{\mathrm{lc}})$. The measures lie on the fitting curve nearly perfectly. The reason for the decrease lies obviously in the decreasing probability to find a fitting gap in t_{lc} succeeding time-steps. However, for the sake of simplicity the leading vehicle on the destination lane is not traced so that the gap may be behind different vehicles in each time-step. This value can be used in the simulations to trigger the number of lane changes.

The attitude of the drivers is also affected by the lane changes as the discussion in Sec. 6.1.2 showed. The region of synchronized traffic is split into two parts. For low densities the fraction of optimistic vehicles decreases more slowly than in the single-lane system and the plateau is formed later. Thus, the lane changes lead to more optimistic drivers in the synchronized traffic for lower densities. Figure 6.9 now shows that this effect is reduced if the lane changes become more seldom. For $t_{\mathrm{lc}} = 1\,\mathrm{sec}$ the lower limit is at $\rho = 32\,\mathrm{veh/km}$, for $t_{\mathrm{lc}} = 2\,\mathrm{sec}$ it is $\rho = 30\,\mathrm{veh/km}$, and for $t_{\mathrm{lc}} = 3\,\mathrm{sec}$ the number of optimistic vehicles decreases fast and the slope approaches that of the single-lane system. This is also true for the value of the fraction. For $t_{\mathrm{lc}} = 1\,\mathrm{sec}$ the number of optimistic vehicles in the plateau is by 2% lower than for higher t_{lc}.

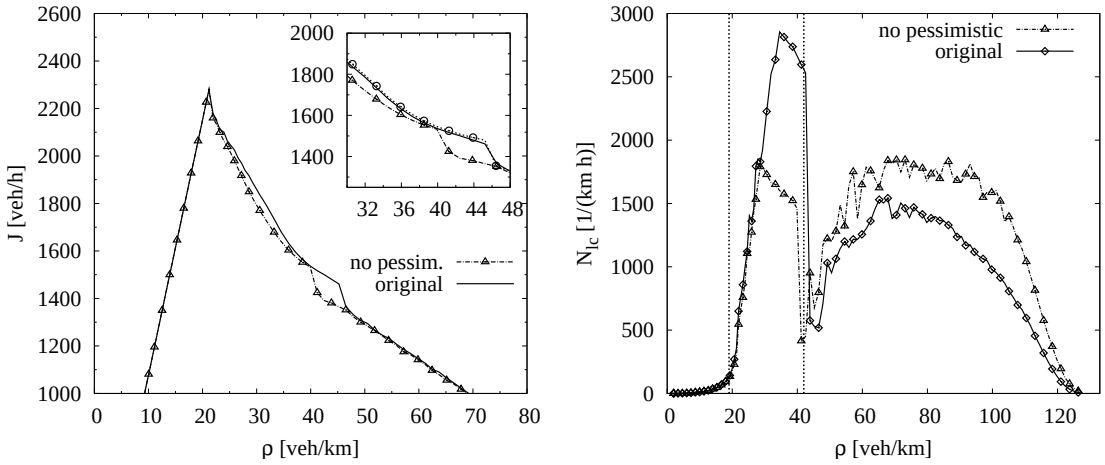

Figure 6.10: Dependence of the two-lane dynamics on γ. The lane changes are forbidden for pessimistic drivers (denoted as "no pessimistic" in the figure). The lane change time t_{lc} is set to 1 sec. The results of the original model are shown as well. The three traffic states are indicated by vertical lines. From left to right: free-flow, synchronized traffic, and wide moving jams. **Left:** Global fundamental diagram depending on γ. In each case the flow of the left lane is shown. The flow in synchronized traffic is lower and the region ends at lower densities if no pessimistic drivers change the lane. **Right:** Number of lane changes in the symmetric model depending on γ. The different states according to the global fundamental diagram are indicated by the vertical lines. The number of lane changes is lower if no pessimistic drivers change the lane.

Dependence on γ

The attitude of the vehicles is an important factor in the single-lane dynamics. It affects the high-density limit of free-flow and determines whether synchronized traffic or wide moving jams establishes in dense traffic. Thus, it can be expected that the influence on the dynamics of two-lane systems is high if pessimistic vehicles are not allowed to change the lane. Thus, in the following a scenario is discussed in which the lane changes are forbidden for pessimistic drivers denoted in the figures as "no pessimistic".
Note, that the influence of γ on the lane changing behavior is different than that of t_{lc} and β. It does not affect the vehicles on the destination lane as β does nor is it dependent on the evolution of the configuration of the vehicles on the destination lane like t_{lc}. However, it allows or forbids a lane change directly independent from the vehicles on the destination lane.
The results of the analysis are depicted in Fig. 6.10. On the left the global fundamental diagram is depicted. It shows again only little dependence on the particular parameter selection. Free-flow and wide moving jams are independent whether a vehicle is allowed to change the lane or not as the comparison with the fundamental diagram of the original model shows. Differences arise only in synchronized traffic. On the one hand, the flow is slightly lower if pessimistic vehicles are not allowed to change the lane. On the other hand, the region of synchronized traffic ends at lower densities if no pessimistic vehicles change

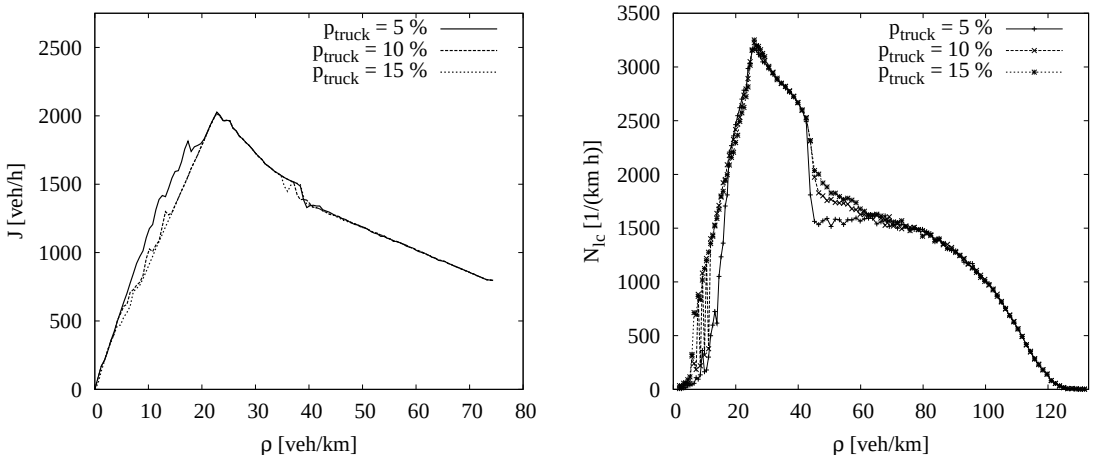

Figure 6.11: **Left:** The fundamental diagram of the right lane for a symmetric system with different fractions of trucks. These are allowed to overtake. The influence on the free flow branch is depending on the fraction of trucks. For little fractions the influence is rather small. Up to high fluxes the influence is negligible for $p_{\text{trucks}} = 5\%$. **Right:** Number of lane changes with different fractions of trucks. Lane changes at very low densities are found here. The slow trucks stimulate the drivers of the cars to change the lane more frequent to evade the hindrances.

the lane. Both effects are based on the inferior ability of the vehicles to avoid obstacles that mainly result in a pessimistic attitude of the vehicles which are not allowed to change the lane. Thus, the flow is reduced as lower velocities are adopted by the pessimistic vehicles and the stability of the synchronized traffic is reduced as perturbations cannot be avoided by a lane change.
The lane change frequency (Fig. 6.10) is stronger affected by the restriction of the lane change. For $\rho < 27\,\text{veh/km}$ the number of lane changes is equal for the original model and that in which pessimistic vehicles are not allowed to change the lane. In free-flow traffic no pessimistic vehicles exist and thus no change is to be expected. For higher densities more vehicles change the lane if pessimistic ones are allowed to change as well. In the other case the number decreases slightly. In the regime of wide moving jams the frequencies are similar again.

6.2 Introduction of Trucks

Since the normal vehicular traffic is not as homogeneous as supposed in the simulations presented up to now, the next step to reach more realism is to include slower driving vehicles that represent trucks in reality.
In a single-lane system the influence of slow vehicles is obvious. Since overtaking is not possible, these slow vehicles form dynamic defects that control the dynamics [35, 36, 100, 102]. In contrast to this the influence of slow vehicles on a two-lane system is not so obvious. Despite the ability to pass other vehicles the influence is rather significant. In particular, for cellular automaton models of multi-lane traffic it is well understood that the formation of plugs may lead to a confined dynamics as the system is governed by the slow

vehicles [22, 52, 127]. Behind these slow ones a platoon is formed by the other vehicles and the velocity is determined by the slow leading vehicle. In the NaSch model for two-lane traffic one slow driving vehicle is sufficient to govern the dynamics of the whole two-lane system [90]. Introducing anticipation these effects can be reduced notable [90].
Thus, it is important to investigate how the two-lane model proposed here is influenced by slow driving vehicles. These "trucks" are modeled as vehicles which have a reduced maximum velocity $v_{\mathrm{max,slow}} = 15\,\mathrm{km/h}$. The length of the trucks is for the sake of simplicity the same for the faster vehicles, the cars.
For the simulations the γ-calculation (Eq. 5.3) has to be precised. Since v_{fast} is not equal for all vehicles anymore, the individual fast velocity has to be applied: $v_{\mathrm{n,fast}} = v_{n,\mathrm{max}} - 1$.
As stated above the fundamental diagram gives insight into the differences. This is shown in Fig. 6.11. for the right lane for a symmetric system with different fractions of trucks which are allowed to overtake. It can clearly be seen that the influence on the free flow branch is depending on the fraction of trucks. For little fractions $p_{\mathrm{trucks}} = 5\%$ the influence is rather small especially at very low densities where no differences to the undisturbed fundamental diagram can be observed. Towards higher densities the influence is no longer negligible. At about $\rho \approx 18\,\mathrm{veh/km}$ the slow vehicles get dominant and determine the flux. The slope of free-flow branch becomes lower and corresponds now to the maximum velocity of the slow vehicles. The vehicle interaction results in a lower mean velocity $\langle v \rangle$ and also the cars cannot reach velocities faster than $v_{\mathrm{max,slow}}$. For a higher fraction of slow vehicles the influence gets more important and dominates the system even at very low densities. For $p_{\mathrm{trucks}} = 15\%$ the trucks already dominate at $\rho \approx 8\,\mathrm{veh/km}$. The results are quite comparable to those of the two-lane BL model. In the BL model [90] the anticipation of the predecessor's velocity allows for short distances during the lane change. The anticipation has a similar function in that model with respect to the lane change than the optimistic vehicles in the model by Lee *et al.*. The safety distance is not calculated as rigid as, e.g., in the NaSch model where the influence on the dynamics of single slow vehicles is much stronger [90].
The reason for this dependence on the truck fraction is that the fast cars can evade the slower ones by changing the lane or not. This is possible if the number of trucks is considerably low and the density is not too high. Lane changes become less easy or are even no longer possible if the flow reaches the maximum flow J_{max} and the free space gets fewer. Then the safe lane changes are less likely and the trucks govern the system dynamics also if these are not numerous.
Nevertheless, it is an important result that the known deficiency of several model approaches, amongst them cellular automaton models, regarding the formation of plugs do not occur in this model approach. The vehicles are allowed to accept very low distance headways down to the additional gap g_{safe} when they change the lane and thus the difficulties arising from the big amount of free space on the destination lane [90] are not given here for a low number of trucks.
The influence of the trucks can also be seen in the number of lane changes that are made. This is depicted in Fig. 6.11 for the same lorry fractions as in the fundamental diagram. The differences to the undisturbed system (cf. Fig. 6.4) can especially be seen at very low densities. Whereas for $p_{\mathrm{trucks}} = 5\%$ only negligible differences exist this changes for larger fractions. For $p_{\mathrm{trucks}} = 15\%$ the differences get obvious as despite the low density the number of lane changes reaches $N_{\mathrm{lc}} \approx 1000 \frac{1}{\mathrm{km\,h}}$ for $\rho = 10\,\mathrm{veh/km}$. This is much higher than in the undisturbed system and in better agreement with the empirical data

that indicate a non-vanishing number also for low densities. Note, the empirical data were collected on a highway section where a part of vehicles were trucks. This is simply a consequence of the stronger vehicle interaction. A lane change is more often promising for the fast vehicles as they can evade the slower trucks and pass them.
Another density region in which the number of lane changes differs from the undisturbed system begins after the upper limit of the synchronized region at $\rho \approx 42\,\mathrm{veh/h}$. For all truck-fractions the number of lane changes does not drop as in the homogeneous system. In the free-flow region between the wide moving jams the same mechanism like at low densities takes effect. It is again beneficial for fast cars to pass the slow trucks. This effect is stronger for higher truck-fractions. Above $\rho \approx 60\,\mathrm{veh/km}$ the lane change rates become equal to the system with homogeneous vehicles.
These results are qualitatively in accordance with the results of the two-lane BL model [94]. Lane changes happen at low densities in both models. In the BL model the maximum of the lane changes is reached at slightly lower densities than in the model discussed here. They keep high until $\rho \approx 40\,\mathrm{veh/km}$ which is the region of synchronized traffic. For higher densities in both models the number decreases slowly and approaches 0 for a fully jammed street.

6.3 Conclusion

The results of this chapter show that the extended model reproduces multi-lane traffic with a high degree of realism. In this context it is very important to note that all empirical data available is gathered on multi-lane roads. Data from single-lane highways are not obtainable simply as these do not exist as independent highway sections. The only single-lane segments are short parallel lanes or curves that are additionally disturbed by intersections. Therefore, the validation of a model for vehicular highway traffic is always limited if just a single-lane approach is considered. The results that are found by the comparison of the two-lane model with empirical data underline this impression: The local fundamental diagram is in better agreement than the single-lane one. Whereas the free-flow branch is reproduced equally accurate as in the single-lane case, the results concerning synchronized traffic are convincing. The two-dimensional region of the synchronized traffic is much wider scattered and agrees much better with the empirical data. Further, the time headway distribution shows a better agreement with the empirical data in the two-lane model than in the single-lane one. In free-flow the very good qualitative and quantitative agreement with the empirical data of the single-lane model is confirmed. In synchronized traffic the agreement is very good in contrast to the single-lane results. Now time headways shorter than one second are found frequently in accordance with the empirical findings. This underlines that the empirical data have to be compared with a two-lane model to cover all influences on the dynamics.
The empirical findings that are specific for two-lane traffic are reproduced as well. Special concern was laid on the reproduction of the lane change frequency. Depending whether trucks are implemented or not, most lane changes are in the region of synchronized or free-flow traffic. A similar behavior was found for the BL model [93].
The lane changing dynamics is mainly controlled by two parameters that determined whether a vehicle is allowed to change the lane or not. On the one hand, β is the degree the follower on the destination lane is hindered. On the other hand, the lane change time t_{lc} sets the number of successive positive security tests that have to be fulfilled for a

lane change. Considering the global fundamental diagram, both parameters hardly affect the free-flow branch and the regime of wide moving jams. Only the synchronized traffic depends on the particular parameter value. This is not surprising as most lane changes are in this region. If β is chosen such a way that the follower may not be hindered synchronized traffic reaches up to higher density values than if a hindrance is allowed. This is obviously the result of the stronger interference of the traffic on the destination lane which makes a collapse more likely. The lane change time t_{lc} leads to a slightly higher flow in the synchronized region if it is set to 1. All vehicles can easily evade obstacles by changing the lane. Higher values of t_{lc} reduce this flexibility and reduce the overall flow as the vehicles stick to their lane. The influence on the lane change frequency is much stronger. If the vehicles may hinder succeeding vehicles the number of lane changes is more than doubled compared to completely passive lane changes, i.e., during which no other vehicle is interfered. The lane change time t_{lc} influences the number of lane changes drastically as well.
The introduction of trucks – from the physical point of view they represent particle wise defects – changes the model dynamics especially in free-flow. The flow therein is depending on the fraction of trucks but the rigid influence trucks have on many other model approaches is not found. For example in the NaSch model one truck is sufficient to form a plug that governs the dynamics of the whole system. The results of this thesis show a much smaller influence of the slow vehicles on the system dynamic. For small fractions just the upper limit of the free-flow branch is cut and all vehicles adapt the velocity of the slow vehicles.
Thus, the analysis showed that two concurring processes are responsible for the dynamics of the two-lane system: On the one hand, a lane change can arouse a perturbation and thus reduce the capacity. On the other hand, by a lane change a vehicle can evade an obstacle and thus reduce the disturbances on its lane.
One question arises from the uncooperative implementation of the lane change algorithm. Here, the changing vehicles force the ones on the destination lane to adapt their driving behavior according to the changing vehicle. A totally different approach could introduce a turn signal so that the traffic on the destination lane is prepared. These vehicles can readapt their driving strategy and avoid hard braking maneuvers and make room for the changing vehicle. Another benefit would be the less drastic influence of the lane change time. The vehicles on the destination lane can adapt their velocity and give the changing vehicles time enough to do the lane change.

7 Defects

Defects or bottlenecks are known to be the reason for most interferences in highway traffic in contrast to undisturbed parts of the highways: Congestions build upstream of, e.g., on-ramps or lane reductions. Therefore, the analysis of the traffic at these bottlenecks especially at an on-ramp is very reasonable. In particular, the complex features that can be seen in real world traffic in the vicinity of an on-ramp are important to understand so that this knowledge can be applied to increase the efficiency of on-ramps for example by means of ramp metering procedures.
The general influence of on-ramps was subject of many studies [50, 67, 73, 106, 109]. In particular, the classification of the traffic states that emerge in dense traffic at an on-ramp was extensively investigated (see [50, 53, 73, 110]). The states are mainly classified by the spatiotemporal structure of the states near the on-ramps and abstracted as a function of the flows in a complex phase diagram. Moreover, much research was done in the field of traffic simulation [56, 56, 77] and especially of cellular automaton models [20, 28, 81, 94]. Other perturbations like lane reductions are of great interest as well [27].
This holds true for the influence of defects like speed limits in general and its relation to on-ramps as well. These are under discussion since the first approaches to simulate highway traffic were proposed.
In order to classify the type of the defect, one has to distinguish between two different kinds: First, particle-wise disorder where deviating parameters are assigned to a part of the *vehicles* and, second, space-wise disorder where the defect is connected to the *sites*.
An example for the former is the assignment of different time independent randomization parameters that determine the dawdling probability to every vehicle. This leads to exotic phenomena [90, 102] like the formation of platoons behind the slowest vehicles. An interesting example is the disordered ASEP where the particle hopping rates are time-independent random variables. It has a remarkable similarity to the "Bose-Einstein-Condensation" [35, 36, 101]. In the low density phase a finite fraction of empty cells agglomerate before the slowest vehicles – they condensate in such a "Bose-Einstein-like condensed" state, however in real space and not in momentum space. In the high density phase the "bosons" are thinly spread over all states. Note, a boson in this sense is an empty cell and its state is determined by the state of its preceding cell. Several general phenomena in this context were reviewed by Krug [100]. Similar effects are achieved if different maximum velocities are assigned to the vehicles [12, 13, 14, 15, 22]. "Coherent moving blocks" are build at higher densities as it becomes more difficult to overtake for the faster vehicles [52]. A detailed analysis of the plug-formation is made in [90]. For more information see Sec. 6.2.
The second class of defects are associated to the sites of the road. In the simplest case a point defect [87] is introduced – an impurity assigned to a single site at which a vehicle needs more time to proceed than at the other sites. This impurity leads to an upper cut-off in the flux. It is strongly connected to the TASEP with one site that has a lower hopping probability than all other sites [62, 63]. In the fundamental diagram a typical wide interval of constant flow emerges. A semi-phenomenological theory for the NaSch model

with $v_{\max} = 1$ describes the limited flow assuming the steady state to be phase-segregated (for more details see [21]).
With respect to cellular automaton models some other approaches to parametrize the defect were introduced. In [89, 139, 150] localized defects have been investigated where the defect sites have a higher dawdling parameter than the other sites. Csahok and Vicsek [26] made a similar approach and related the defect sites with a smaller permeability than the rest of the system. Emmerich and Rank [32] have chosen the other obvious parameter of the cellular automaton models to form a defect. They assigned a smaller maximum velocity to the vehicles when these reside in the defect region. It is important to note that no conceptual differences where found between single site defects and extended defects.
With respect to the application of a simulation model and its degree of realism, it is of main interest for the analysis of a traffic model that it is capable to reproduce the "defects" that are present in every real road network. These are not only on-ramps and speed limits but also road works, lane reductions, and lane additions. Whereas the on-ramps, speed limits, and lane reductions can simply be implemented directly, the mapping of road works might be connected to a more defensive driving that is modeled by a higher dawdling probability. Hence, the model by Lee *et al.* with the introduced two-lane extension presented in this thesis is analyzed with respect to different defects keeping in mind the main aim to apply it in an on-line traffic simulation [134]. First, the basic features of the single-lane model with open-boundary conditions and an on-ramp are discussed in this section. After the insertion algorithm that serves as the on-ramp is described, the resulting traffic patterns are shown for a single-lane system as well as for the two-lane street. It is shown that the different traffic patterns – in particular the different forms of synchronized traffic – are reproduced in both cases.
Different approaches to describe the influence of the parameter of the on-ramp on the dynamics follow. These are the investigation of the life-time of the synchronized traffic with respect to different insertion algorithms and the collection of the resulting traffic states in a phase diagram.
The connection to other defects is established by the analysis of a velocity defect, i.e., a speed limit. This influences the traffic states in a quite comparable manner.

7.1 Modeling of On-Ramps

A straightforward approach to implement an on-ramp is to search the largest gap in the region of the on-ramp and insert a new car into this clearance with a velocity slightly below the speed of the leader. More complex solutions perform a real lane change process. That means the on-ramp is simulated in the same way as the main road but all vehicles on it intend to change the lane to the main road.
A more elaborate approach divides the acceleration lane into three sections. The partition is based on the results of the analysis of video recordings. Each section has a special function: acceleration, orientation, and changing to the main road:

1. Acceleration: The vehicle accelerates and tries to adapt its velocity to the speed of the vehicles on the right lane of the main road.

2. Orientation: The vehicle searches a suitable gap on the right lane and adapts its acceleration behavior, so that it reaches this gap.

3. Lane-changing: This section is the area in which the real lane change is performed.

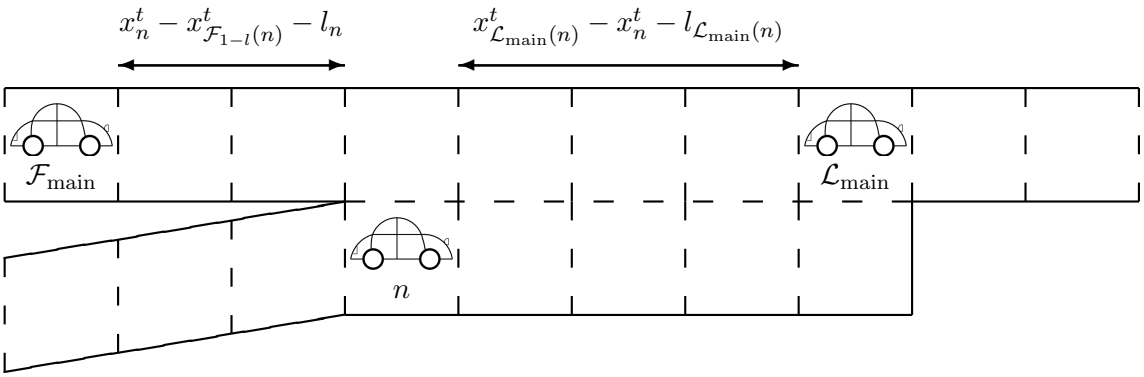

Figure 7.1: Sketch of a single-lane road with an on-ramp that shows the configuration of the involved vehicles.

This partitioning is valid for simple junctions. For more complex ones, e.g., intersections, the division into three parts has to be enhanced. Two important results are the observed adaptation to the velocity of the vehicles on the main road and the search for a suitable gap. These facts are utilized in the simplified approach used in this chapter. For a detailed analysis of this approach, of the driving behavior of the inflowing vehicles and the classification of the different section types on the basis of satellite pictures see [117].
Another important and typical strategy of the drivers was identified during the analysis of video recordings. Vehicles try to clear the right lane if a vehicle is on the acceleration lane. However, this is carried out only up to a certain density. After that a short-term lane change is rather rare.
For the sake of simplicity and to focus the analysis in this chapter on the main problems, the approach to insert vehicles at the on-ramp is based on a simple algorithm. Here, at first the largest gap in the region of the on-ramp at the main carriage way is determined. In the second step it is checked whether the following and the inserted car are able to reach their safe velocity in the step after the insertion.
As mentioned before, the original model reacts sensitively to the initialization of the simulated system. This gets even more important if vehicles are inserted from outside into the system as it is done in open systems and at an on-ramp. The insertion algorithm for the on-ramp described in [107, 108] is not sufficient. It is noted therein that accidents may emerge if vehicles are inserted not carefully enough. Therefore, the insertion algorithm is adapted taking into account the results of the accident discussion (Sec. 5.5), the adapted model for the two-lane system (Sec. 5.6.2), and that of the two-lane system (Sec. 6.1). In detail the input algorithm looks as follows.

Vehicle Insertion Strategy

First, in the region of the on-ramp that vehicle is determined which has the largest gap between itself and its predecessor. In the next step it is verified whether the center of this region is also in the region of the on-ramp. In other words, only a part of the clearance overlaps with the on-ramp as long as the center is inside the merging region. If this is true, the vehicle is inserted into the system with its center set to the position of the middle of

the gap. Simply inserting the car in the middle of the largest gap would produce insertions outside the ramp region. But note, the insertion must be made with respect to certain security criteria that will be introduced below.
This complex algorithm is used to ensure that the effective length of the region in which the vehicles can be inserted is equal to the defined length of the on-ramp. The length of the ramp is important for the magnitude of the disturbance of the system dynamics. Concerning the systematic use of this algorithm in an application that simulates a real world network one has to be certain that the dimensions of the merging region between the ramp and the main carriageway is mapped correctly, especially as the construction of the simulation network is done automatically on the basis of a geo referenced digital map [134].
In the second step of the vehicle insertion it is verified that the lane change is safe for all involved vehicles in analogy to the algorithm for two-lane traffic (Eq. 6.2 in Sec. 6.1).
In detail, a virtual vehicle is created and its velocity v_n is set to a fraction of the leader's speed on the main road $\mathcal{L}_{\text{main}}$

$$v_n = v_{\mathcal{L}_{\text{main}}} \cdot K, \tag{7.1}$$

where K is a parameter that is in general set to $K = 0.7$ following [107, 108]. This models the in general lower velocity of the entering vehicles. Note, that the velocity has a significant influence on the traffic patterns that establish upstream of the on-ramp. A detailed analysis hereof is made in Sec. 7.1.3. The vehicle n is now inserted – virtually – into the street. Then it is checked if this and the previous vehicle $n_{\mathcal{F}_{\text{main}}}$ can reach their safe velocity:

$$x_n^t - x_{\mathcal{F}_{\text{main}}(n)}^t > l_n, \tag{7.2}$$
$$x_{\mathcal{L}_{\text{main}}(n)}^t - x_n^t > l_{\mathcal{L}_{\text{main}}(n)}, \tag{7.3}$$
$$v_n^t - D \leq \tilde{v}_{n,\text{main}}^{t+1}, \tag{7.4}$$
$$v_{\mathcal{F}_{\text{main}}(n)}^t - \beta \leq \tilde{v}_{\mathcal{F}_{\text{main}}(n)}^{t+1}. \tag{7.5}$$

The parameters are chosen in analogy to the security criterion of the lane change algorithm (Eq. 6.2). β represents the degree the follower may be forced to brake to reach its safe velocity in the next step, $\mathcal{L}_{\text{main}}$ and $\mathcal{F}_{\text{main}}$ indicate the state variable of the predecessor and the successor on the main road, and D is the standard braking capability. Scenarios, in which the following car is hindered so that it has to brake too hard, may lead to an unstable situation as the further following vehicles trust in the steadily driving behavior of the leader. This is especially valid for platoons of optimistic vehicles (see Sec. 5.5). In contrast to the lane-changing algorithm of Sec. 6.1 an additional safety gap g_{add} is not part of this algorithm as the intention to enter the main carriageway is obviously stronger than in a normal lane change process and the driver takes less respect for the other vehicles.
Unless stated otherwise, the vehicles are inserted with constant frequency and time lag which is simply the reciprocal inflow rate. The inflow rates of the main road and of the on-ramp are denoted as J_{main} and J_{ramp}. The total system length is set to 25,000 cells = 37,5 km. The relevant section of length $L = 10{,}000$ cells = 15 km including the on-ramp that begins at 13.5 km is cut out and displayed in space-time plots. The length of an

on-ramp is set to $L_{\text{ramp}} = 400\,\text{cells} = 0.6\,\text{km}$, which is the standard length of a simple on-ramp in the highway network of North-Rhine Westphalia. The simulation time is $10{,}000\,\text{sec} \approx 3.8\,\text{h}$ after a relaxation period of the same duration. If not stated otherwise, the follower on the main road may be hindered slightly, i.e., $\beta = 1\,\text{cell/time-step}$.

7.1.1 Single-Lane System

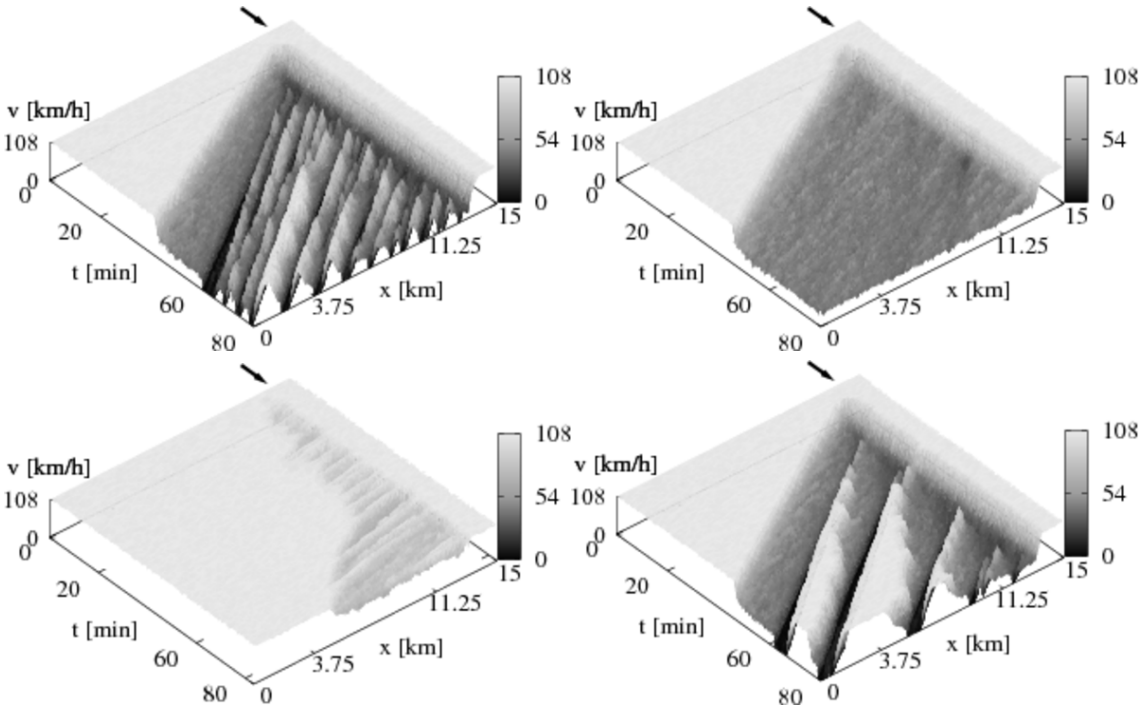

Figure 7.2: Space-time plots of the different synchronized traffic states of an open system in the vicinity of an on-ramp. The states are from top left to down right: general pattern, widening synchronized pattern, and moving synchronized pattern. At the bottom right the pinch effect is visualized. The arrow denotes the position of the on-ramp.

First the effects of an on-ramp on the traffic on the main carriage way of a single-lane system are recapitulated as discussed in [107]. These form the basis for further analyses and comparisons not only in the single-lane system but also on a two-lane road.
The different types of synchronized traffic that are known [73] are reproduced in the simulations. Figure 7.2 shows exemplarily moving synchronized traffic, widening synchronized traffic, and the general pattern as well as a local perturbation that leads to a compact jam – the pinch effect. Localized synchronized traffic is reproduced as well.
The different patterns of synchronized traffic are characterized by their spatiotemporal structure. Widening synchronized and localized patterns are pinned at the on-ramp. This means, that the downstream end of the synchronized region sticks at the on-ramp. Widening synchronized traffic grows depending on the inflow and the upstream boundary moves with constant velocity upstream. The region of localized synchronized traffic does not grow but its upstream boundary oscillates around a maximum value. In contrast

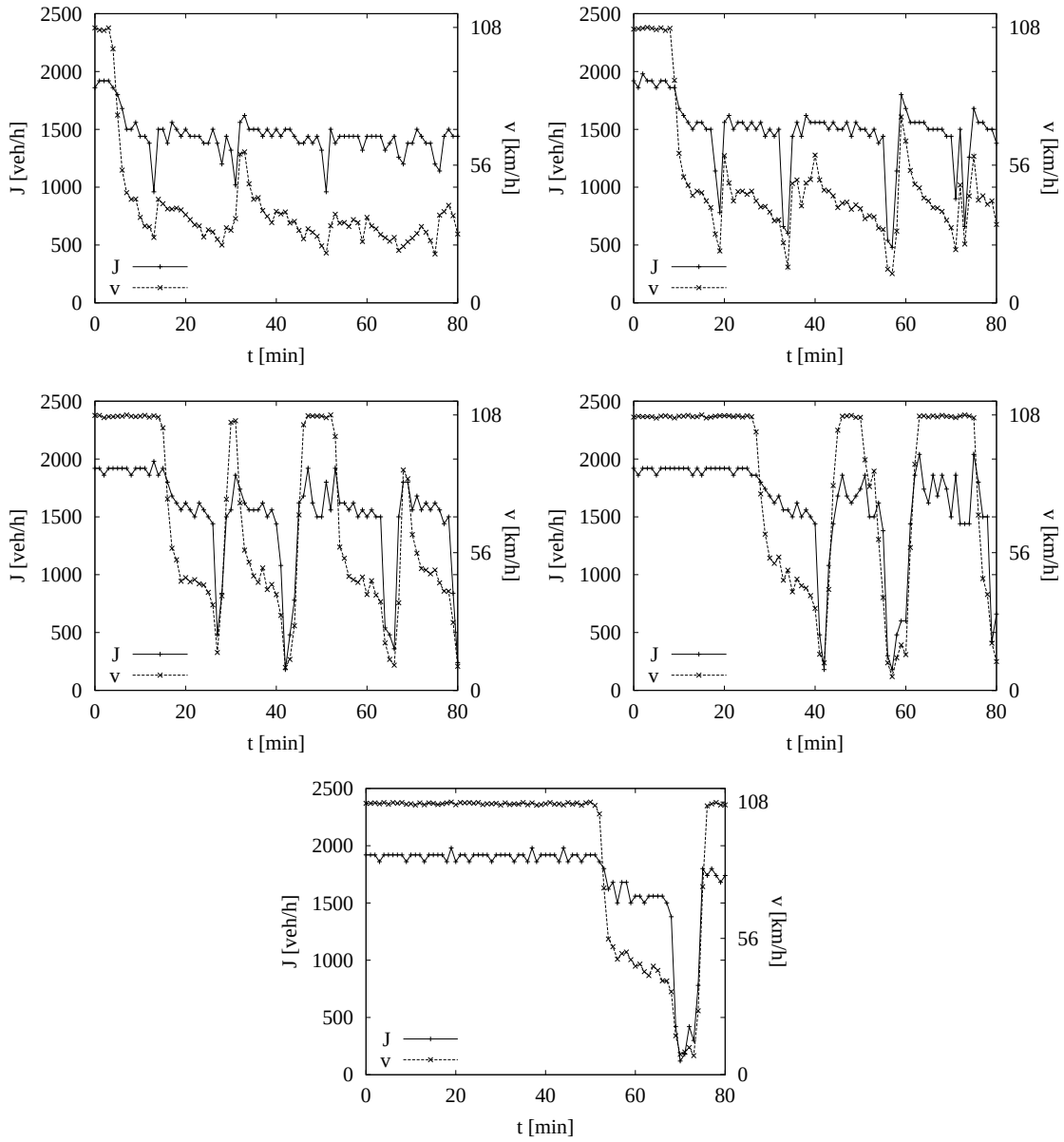

Figure 7.3: Velocity and flow time series of the main road of a single-lane open system in the vicinity of an on-ramp that captures the dynamics of the pinch effect shown in Fig. 7.2 bottom left. The detector positions are from top left to the bottom: $x_{\text{det}} = 12.75\,\text{km}$, $x_{\text{det}} = 11.25\,\text{km}$, $x_{\text{det}} = 9\,\text{km}$, $x_{\text{det}} = 5.25\,\text{km}$ and $x_{\text{det}} = -2.25\,\text{km}$.

moving synchronized traffic detaches from the on-ramp and moves upstream. Free-flow is build between the waves of synchronized traffic.
A further difference between widening and moving synchronized traffic beside the internal structure is the form of the boundary to the free-flow region. The boundary between widening synchronized traffic and free-flow is a straight line and moves upstream – for each inflow rate at the main carriage way – with constant speed. In contrast the boundary

of moving synchronized traffic shows a different behavior. The boundary is bent and fluctuates as can be seen in Fig. 7.2 bottom right.
The time-series of the minute averaged flow and velocity at different locations are additionally shown in Fig. 7.3 for the pinch effect depicted in Fig. 7.2, bottom left. This visualizes the emergence of the jam and its upstream propagation. Starting from top left, one can see synchronized traffic with high flux and low mean velocity near the on-ramp. In the next pictures at larger distances small narrow jams form merging out of small perturbations. Their amplitude rises and far upstream from the on-ramp only a few wide moving jams survive.

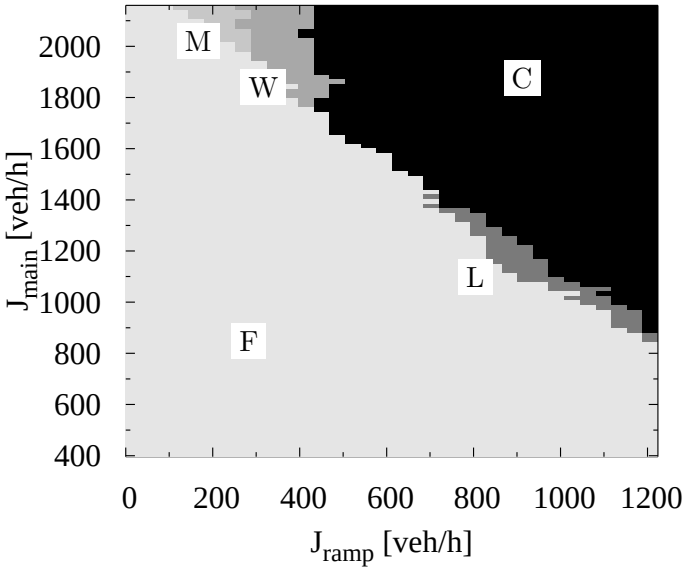

Figure 7.4: State diagram of the single-lane system with an on-ramp. The resulting regions stand for the different traffic states: "C" denotes the region of wide moving jams, "W" the widening synchronized traffic, "M" stands for moving synchronized traffic and "L" marks the region of localized synchronized traffic. The free-flow regime is hinted at by "F". The resulting diagram is comparable to those shown in [73, 74, 77, 81].

In Fig. 7.4 the general appearances of the different traffic states are collected in a diagram whose composition mimics a phase diagram. The various regions are qualitatively different which evokes the term "phase" in the description of the diagram. The x-axis shows the inflow at the on-ramp J_{ramp}. On the y-axis the flow J_{main} on the main road is depicted. The resulting areas stand for the different traffic states: "C" denotes the region of compact jams, "W" the widening synchronized traffic, "M" stands for moving synchronized traffic and "L" marks the region of localized synchronized traffic. The free-flow regime is hinted at by "F". The resulting phase diagram is, as stated in [107, 108], comparable to those shown in [73, 74, 77, 81]. All the proposed traffic patterns are reproduced in good accordance to the empirical findings.
Since the empirical data were collected on a multi-lane highway [73, 74], the reproduction of the traffic states should not only be limited to single-lane simulations but their existence must be verified for two-lane traffic, too. This is done in Sec. 7.1.6.

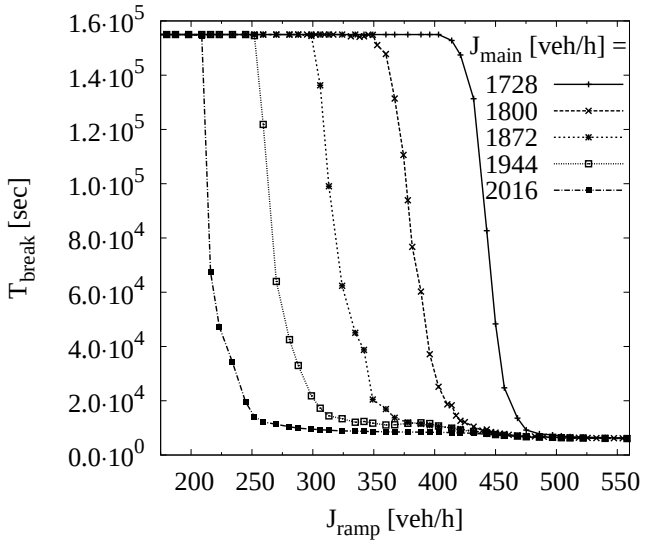

Figure 7.5: Time dependence of the breakdown for different inflow rates at the on-ramp. The mean life-time, the time until the traffic collapses, is strongly depending on the inflows J_{main} and J_{ramp}. The inflow rates are chosen such a way that the region of widening synchronized traffic is traversed. The slope as well as the width of the region where both synchronized traffic and wide moving jams occur is equal for all rated thus the mechanism is universal.

Note, the boundaries of the specific regions of the traffic states are not strict but in general both adjacent states can emerge at the limiting flow rates. The state that has developed at the end of most simulations is shown in the diagram. This means, if a jam has emerged, the state is classified as general pattern. Otherwise, if synchronized traffic is governing the system, the according classification of the synchronized pattern is applied. In the phase diagram that pattern is depicted that has occurred most often. This is especially important for the boundary between widening and localized synchronized traffic on the one hand and the regime of the general pattern on the other hand. At these boundaries the traffic is not stable and whether the synchronized flow remains or the local perturbations get strong enough to form a seed for a wide moving jam is stochastic. Thus, it is worthwhile to analyze the life-time of the synchronized traffic with respect to the inflow rates. This is the topic of the next section. The analysis shows that the life-time is varying very strongly for the parameters of the boundary states and the variance of the life-times is very high.

7.1.2 Life-Time of Synchronized Traffic at an On-ramp

As described in Sec. 2.2.3 the pinch-effect – a local perturbation that forms a breakdown of the traffic and thus a widening jam is triggered upstream of an on-ramp – leads to the establishing of a wide moving jam in the synchronized traffic upstream of the on-ramp. Since the traffic collapse is clearly a random process, the time-dependence of its occurrence as well as the question whether the synchronized traffic is stable or at least very long-living at certain inflow rates is of great interest. Special importance arises with respect to the optimization of the on-ramp inflow by means of ramp metering algorithms.

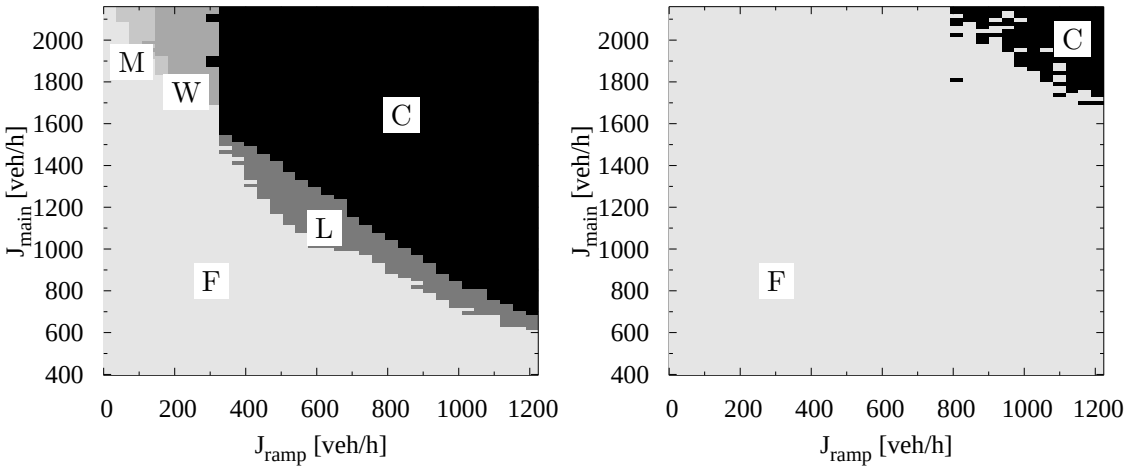

Figure 7.6: Phase diagram of the emergent traffic states at an on-ramp for different insertion velocities that are calculated by multiplying the leaders velocity $v_{\mathcal{L}_{\text{main}}}$ with K. **Left:** $K = 0.5$. All five patterns are formed. **Right:** $K = 0.9$. Only two states emerge: free-flow and general pattern. Synchronized traffic is not formed or dissolves to wide moving jams very fast so that it does not appear in the state diagram.

Thus, a detailed analysis of the dependence of the life-time of the synchronized traffic on the inflow rates at the on-ramp and the main road is valuable. The results are depicted in Fig. 7.5. For different flows on the main road $J_{\text{main}} = 1728, 1899, \ldots, 2016\,\text{veh/h}$ the inflow from the on-ramp is varied between $J_{\text{ramp}} = 180, \ldots, 560\,\text{veh/h}$ and the mean life-time of the synchronized traffic is drawn. Note, the inflow rates are chosen such a way that the widening synchronized region is traversed (see Fig. 7.4). For each flow pair J_{main} and J_{ramp} the mean is build from up to 250 simulations. The number is reduced for very high and very low inflows as the standard deviation is very low there in contrast to the transfer region, in which synchronized traffic or wide moving jams can be detected at the end of a simulation. Here, the standard deviation can reach $\text{dev}_{T_{\text{break}}} \approx 5.4 \cdot 10^5$. The transfer region is about $\Delta J \approx 50\,\text{veh/h}$ wide. This value is independent of the flow on the main road. This is also true for the slope of the function which means that the characteristic decay of the life-time is independent from a special density region and thus universal for widening synchronized traffic.
The decay of the life-time is faster than the decay of the life-times of the synchronized traffic in the periodic system. In a log-plot the slope is negative and convex and thus the life-time decreases faster than exponentially. This is obviously the result of the additional disturbance of the inserted vehicle. Whereas in the periodic system the brake-down results from internal fluctuations, in the vicinity of an on-ramp the inserted vehicle perturbs the traffic so that both processes lead to a higher brake-down probability.

7.1.3 Insertion Velocity

Section 7.1.1 shows the basic features of the open system with an on-ramp. But as noted in the description of the insertion algorithm in Secs. 7.1 and 7.1.2, the velocity which is

applied to the inserted vehicles is important with respect to the traffic state that emerges on the main carriageway. The velocity is triggered following Eq. (7.1) with the factor K which is multiplied by the velocity of the leading vehicle on the main road. Thus, a different value is applied to K and the changes are analyzed.
These differences are best seen in the phase diagrams for various insertion velocities. Two examples, one for a lower $K = 0.5$ and one for a higher insertion velocity, i.e., $K = 0.9$, are shown in Fig. 7.6. The differences are significant. The phase diagram for the low insertion velocity shows qualitatively the same characteristics as the one depicted in the introducing section 7.1 of the on-ramps (cf. Fig. 7.4). All the proposed types of synchronized traffic can be found. Not only widening and moving but also localized synchronized traffic and the general pattern govern a wide part of the phase space. Compared to the phase diagram with $K = 0.7$, which is depicted in Fig. 7.4, the regions of synchronized traffic govern a larger part of the phase space in case of $K = 0.5$. If the velocity is set close to that of the main road the state diagram looks completely different. This is shown exemplarily for $K = 0.9$ in Fig. 7.6 right. Synchronized traffic is no longer present.
Thus, it is more likely that synchronized traffic is established if the velocity difference between the inserted vehicle and the ones on the main carriageway is higher. The reason for this is in the range of the disturbance. It is important to keep in mind, that the determination of the attitude has an interaction range of two vehicles. If an inserted vehicle is driving slowly and the density is quite high it will in general influence at least two succeeding vehicles. Both vehicles will change their attitude if they have not already driven pessimistically. If only the direct follower changes its attitude the next vehicle would at least have to react on this by keeping its distance and thus decelerate as well. The number of pessimistic vehicles, which stabilize synchronized traffic, rises. Whether the interference of these two following vehicles proceeds upstream and is not absorbed by, e.g., a sufficient large gap, is strongly depending on the strength of the disturbance which means how strong the vehicles have to brake. If $K \to 1$ the vehicles hardly have to brake. Hence, at lower insertion velocities the emergence of synchronized traffic is more probable. Concluding, the range of the disturbance due to an inserted vehicle and therefore the formation of synchronized traffic is directly depending on the velocity difference. If the difference is rather large, it influences more vehicles that have to brake and the emergence of synchronized traffic is more likely.
A further difference lies in the position of the boundary of the particular traffic states. With respect to the diagram with $K = 0.7$ these are shifted to lower values of J_{main} and J_{ramp}. This is not surprising as lower velocities are equivalent with stronger disturbances and thus with a higher probability for a full breakdown of the traffic or the emergence of synchronized traffic.
The appearance of the phase diagram for the high insertion velocity is totally different (Fig. 7.6 right). No synchronized traffic formes at all. One finds only two traffic states, free-flow and the general pattern. Additionally the boundary is moved to higher values of J_{main} and J_{ramp} and it is less easy to define. This is indicated in the diagram by the alternating states – free flow was more often detected in the simulations than jams inside the region of general patterns. If the velocities of the inserted vehicles and that on the main road are barely different no pessimistic vehicles arise, but the traffic collapses immediately if the density gets too high.
Another effect can be observed for very low values of K. If the velocity difference is too large it is possible that the security criterion is never fulfilled and thus no vehicles can

enter the main road. This reflects the behavior of a very defensive driver who does not use the on-ramp to accelerate but has to stop as it seems to be unsafe to enter the main road. This is similar to the discussion in Sec. 7.1.7 where high velocity differences between the lanes on a two-lane road are analyzed.
These investigations show that the velocity difference between the merging vehicles and that on the main carriageway is of fundamental importance with respect to the emergent traffic states and therefore crucial for the stability of the traffic. This is important especially with respect to ramp metering procedures.

7.1.4 Insertion Algorithm

The capacity of an on-ramp is also affected by the temporal distribution in which the cars enter the main road. Are they evenly distributed, do they have constant time differences, or do they enter in short platoons? To determine the influence of the insertion strategy onto the system dynamics, three scenarios are simulated to show that the insertion strategy has a strong influence on the system dynamics and thus is a proper way to improve the efficiency of an on-ramp.
To compare the different approaches a scenario of a single-lane road with an on-ramp is simulated. The flow on the main carriageway is kept constant at $J_{\text{main}} = 1{,}800\,\text{veh/h}$ and the inflow J_{ramp} on the on-ramp is set to a value between $J_{\text{ramp,min}} = 250\,\text{veh/h}$ and $J_{\text{ramp,max}} = 500\,\text{veh/h}$. The phase diagram in Fig. 7.4 reveals that both inflows, that of the main carriageway and that of the on-ramp, are chosen so that for low to high inflows from the on-ramp first free-flow arises then the regime of widening synchronized traffic is traversed and at high inflows the regime of the general pattern is hit.
The insertion itself is the same for all strategies and follows the approach discussed in Sec. 7.1. In few words a vehicle is inserted in the largest gap in the merging region if it does not compromise the other vehicles. The length of the merging area is set to $L_{\text{merge}} = 600\,\text{m}$ and $K = 0.7$ so that the velocity of the inserted vehicles is $v_n = v_{\mathcal{L}_{\text{main}}} \cdot 0.7$.

Random Insertion

The first strategy that is analyzed is an on-ramp that is not controlled at all which means that the vehicles are entering the on-ramp at random time headways.

Evenly Distributed Insertion

The second approach controls the inflow. According to the inflow rate J_{ramp} a temporal gap between two inserted cars is calculated $t_{gap} = \frac{1}{J_{\text{ramp}}}$ and at the beginning of each of these intervals a vehicle is inserted into the main carriageway. This is the strategy used in Sec. 7.1.

Platoon Insertion

The third procedure is similar to the evenly distributed insertion but here two vehicles enter the main road in a platoon. The temporal gap is doubled – $t_{gap} = 2 \cdot \frac{1}{J_{\text{ramp}}}$ – so that the mean inflow keeps constant.

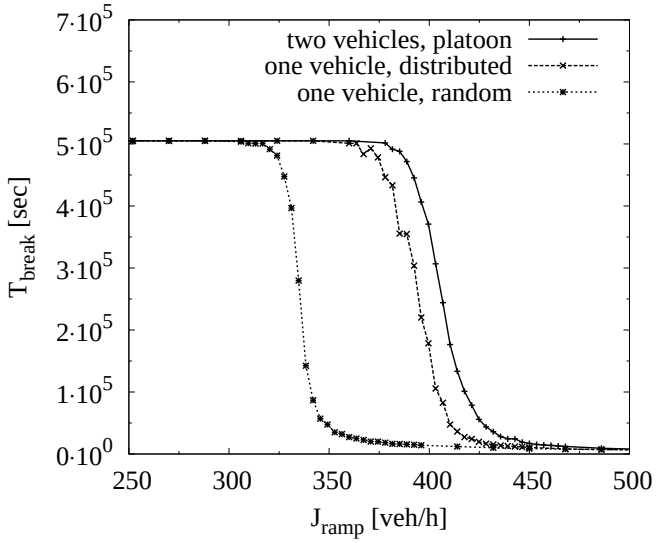

Figure 7.7: Time dependence of the breakdown for insertion algorithms. The inflow rate on the main carriageway is kept constant and that of the on-ramp is varied. The capacity of the on-ramp is lowest if the vehicles are inserted with random headways. If they are filled in with constant time headway – denoted as "one vehicle, distributed" –, more vehicles can be inserted until the traffic collapses. Further, it is a superior approach if two-vehicles are inserted in succeeding time-steps. The latter is labeled "two vehicles, platoon".

Results

The interesting and fundamental differences in the resulting capacity of the on-ramp are depicted in Fig. 7.7. The simulation time is set to $T_{\text{sim}} = 5 \cdot 10^5$ sec. The first vehicles are inserted at the on-ramp after 5000 time-steps. The breakdown time is averaged over 100 simulation runs at the boundaries and over 700 simulations in the interesting region. If no stopped vehicle is detected until the simulation end the breakdown time is set to this maximum time. The inflow from the on-ramp is in general varied by $\Delta J = 36\,\text{veh/h}$. In the transfer region the interval length is reduced to $\Delta J = 7\,\text{veh/h}$. The capacity is determined by the maximum number of vehicles that are inserted and the traffic does not collapse. It is very different for the particular insertion algorithms.
The capacity of the on-ramp is lowest if the vehicles are inserted with random headways. The traffic breaks down if the flow onto the on-ramp reaches $J_{\text{ramp}} \approx 340\,\text{veh/h}$. With this strategy it is likely that several vehicles are inserted with very short time headways or in succeeding time-steps. Each of the vehicles increases the disturbance aroused by the preceding vehicles. A collapse becomes more likely and thus the capacity of the on-ramp is very limited. If the vehicles are forced to enter the main road more thoughtfully, the capacity can easily be risen. This is shown by the two other insertion algorithms.
If they are filled in with constant time headway – denoted as "one vehicle, distributed" in Fig. 7.7 –, more vehicles can be inserted before the traffic collapses. Nearly $J_{\text{ramp}} \approx 400\,\text{veh/h}$ can safely be inserted without provoking a fast breakdown of the synchronized traffic. The disturbance aroused by one vehicle is very likely to be solved when the next

vehicle is inserted. Thus, the perturbation by the preceding vehicle is not boosted. Each insertion can be interpreted as a single event.
The step in the curve at $J_{\text{ramp}} \approx 385$ veh/h can be explained by the high standard deviation in the breakdown times. It reaches $\text{dev}_{T_{\text{break}}} \approx 1.8 \cdot 10^5$.
An even higher capacity can be reached if two vehicles are inserted in succeeding time-steps. This is labeled "two vehicles, platoon" in the figure. The curve is shifted by $\Delta J_{\text{ramp}} \approx 10$ veh/h to higher flows. This means, the inflow from the ramp can be 10 veh/h higher before the same breakdown time is measured.
The superiority of the two-vehicle algorithm compared to the single-vehicle ones is a result of two screening processes. Lets now look at a slightly more general scenario. In reality it is not clear which vehicle enters the main road first. The simulations presented above were limited to the latter one but the other case is discussed here as well.
In the beginning the order is analyzed, in which the downstream vehicle enters the main road at first. This vehicle will now produce a disturbance in the traffic on the main road. The vehicles behind it have to brake in general as the entering vehicle is driving slower. The traffic becomes more dense upstream the on-ramp. However, downstream of the entering vehicle vacant space emerges as the vehicles in front keep on driving unchanged. If now a second vehicle enters the main road upstream of the first one, it will disturb the traffic flow as well but the perturbation can resolve or at least be weakened by the vacancy the first vehicle has produced.
In the second case – the downstream vehicle enters first – another mechanism reduces the effective perturbation. The downstream vehicle produces the typical disturbance. This will move upstream. If the second vehicle enters the main road upstream of the perturbation it will itself disturb the traffic and thus screens the first one.
Thus, if two vehicles enter the main road in one cycle it is likely that the two inflowing vehicles do effectively produce less than two disturbances – in the ideal case only one. Thus, the likeliness for the emergence of wide moving jams is reduced significantly. Nevertheless, this simple approaches do require intelligent drivers that use the whole length of the on-ramp to merge into the traffic on the main road and do not use the same spacing.
Nevertheless, the superiority of the platoon insertion is reduced again as the vehicles that have entered the main road accepted a small spatial headway to their leaders. The gap is afterwards enlarged during the normal velocity update (see Sec. 5.2.3) so that the followers might have to brake in the next time-steps, too.
It is interesting to note, that the slope of the curves is very similar for all three insertion procedures and the standard deviation is of the same magnitude. This shows that the process of a breakdown is only depending on the magnitude of the disturbance and the synchronized flow breaks down with the same universal mechanism. Note that the decrease of T_{break} is faster than the breakdown time of the synchronized flow in a periodic system (cf. 5.3). This is not surprising as in the latter only the internal fluctuations may arouse a perturbation. In the case of the on-ramp one also has an external factor, the disturbance by the inserted vehicle. All in all the synchronized traffic is less stable in the vicinity of an on-ramp, but it is very valuable to make an effort to optimize the inflow at the on-ramp.

7.1.5 Time Scales and the Connection to Ramp Metering Algorithms

The metastability and thus the life-time of the synchronized traffic has to be reviewed concerning two different time scales. First, with respect to the model dynamics and second, with respect to real applications.

The first case is of theoretical interest as the functional formulation of the dependence may lead to a better understanding of the internal process and shows in this case that there exists a simple functional interdependence. This is also true for the second case, but in addition it is important to keep in mind that the high inflows during a day are limited to durations of several minutes to a few hours. Thus, it is fundamental to evaluate the life-time of the metastable states in the context of ramp metering procedures. The usual ramp metering algorithms do not take into account synchronized traffic and its metastability nor the stochasticity of the traffic collapse. However, it is valuable to estimate the breakdown probability so that one can judge the likeliness of a breakdown at a given inflow rate and take a risk of jam emergence.

The "ALINEA" algorithm [135, 136], an integral controller, is the most frequently used algorithm for the ramp metering in North-Rhine Westphalia to stabilize free-flow. It calculates the time of circulation with which the traffic lights operate. The resulting algorithm is $J_{\text{ramp}}^{t+1} = J_{\text{ramp}}^{t} + K_r(occ_{\text{opt}} - occ^t)$. Here, J_{ramp}^{t} is the flow on the on-ramp at time t, occ_t the measured occupation of the cross section downstream of the ramp, occ_{opt} the "optimal occupation" of the cross section and K[1] a correction factor for the inflow from the ramp. The equation gives the planned inflow from the ramp J_{ramp}^{t+1} in the next time interval. The reciprocal is then the time of circulation of the traffic light at the on-ramp. The main aim of this procedure is to adjust the flow from the on-ramp so that the optimal occupation on the main road is reached.

Additionally a hysteresis procedure is used to reduce flickering and generate a smoother steering. Hysteresis means in this context that a circulation time ΔT_1 is set for a measured $J_{\text{ramp}}^{\text{on}}$ and the circulation time is reset to the former value for $J_{\text{ramp}}^{\text{off}}$ with $J_{\text{ramp}}^{\text{on}} > J_{\text{ramp}}^{\text{off}}$. It is needed as the steering parameter as the ALINEA time changes significantly in very short times. The main challenge is the calibration of the optimal occupation occ_{opt}. This parameter is therefore frequently changed by the responsible authority.

One problem of this algorithm is that it assumes an optimal occupation whose existence is questionable. Traffic collapses are random processes so that no objective optimal occupation exists. The empirical results [76, 112, 137] underline that.

A totally different approach should take into account the phase-diagram that is measured at an on-ramp. The inflow from the on-ramp should be used to control the state that is formed at the on-ramp. Thus, it can be reduced if the flow on the main carriageway approaches values that are close to the boundary values between the synchronized, e.g., widening synchronized traffic, and wide moving jams.

In a second step one has to decide how much risk one wants to take that nonetheless the traffic collapses. This means one has to decide which regions in the state-diagram are acceptable with respect to the jam probability. This becomes important if the duration of the heavy traffic is of the order of the life-time or shorter. It is important to consider that the boundary region is limited and the difference between the life-times in a small inflow interval are huge.

Recent approaches try to take the probabilistic property into account [18, 76, 79, 112, 175]. In addition, in this publications a functional relation for the jam probability is formulated despite the limited empirical data [112, 137].

In addition to the metastability of the traffic, an important aspect is the velocity of the entering vehicles. On the one hand, the position of the particular traffic states is depending on the inflow velocity. Thus, it is important to take the speed difference into

[1] Typical values used in North Rhine-Westphalia are $K = 65, \ldots, 85$ and $occ_{\text{opt}} = 19, \ldots, 25$.

account when the capacity of the ramp is determined. On the other hand, the simulations hint at a different mechanism if the velocities of the entering vehicles are of the same order than the speed of the vehicles on the main road. The latter have not to break because of the disturbing vehicles and synchronized traffic is not stable or is not formed at all. Here, it might be valuable to stabilize free-flow and not synchronized traffic.

7.1.6 Two-Lane System

Reproducing the correct synchronized traffic not only in a single-lane system but also on a two-lane road is really a complex task. The vehicles that change the lane are always a source of disturbance and thus the transfer of the different patterns of the synchronized state is not obvious. This means it is not clear whether the traffic patterns are transferred from one lane to the other and in addition are stable in spite of the lane changes.
Nevertheless, the formulation of the symmetric lane changing rules in Sec. 6.1 perform this task. This is shown in Fig. 7.8. The known characteristics (cf. Sec. 7.1.1) are well reproduced. From top to bottom general pattern, wide-moving jams, moving synchronized pattern, and the pinch effect are shown. The latter shows the emergence of two jams in widening synchronized traffic whereas the second is build in the upstream region of the first jam. This underlines the existence of parallel jams in synchronized traffic as well. The plots of both lanes are almost identical as the traffic state is transferred from one lane to the other almost immediately.
The internal structure of the general pattern that is shown in the top of Fig. 7.2 is depicted in Fig. 7.9. For different locations the minute averages of the flow and the velocity are drawn. The characteristics are qualitatively the same as in the singe-lane system. Small narrow jams are formed near the on-ramp. They are almost immediately transferred from one lane to the other. Some of them grow and form wide moving jams. Far away from the on-ramp only several jams survive and move upstream. This property is in accordance with the empirical findings.
At the detector at $x_{\text{det}} = 12.75\,\text{km}$ – in the top row – a peak in the flow on the left lane appears at $t \approx 22\,\text{min}$. At the same time a narrow jam emerges on the right lane. Here, vehicles evade the disturbance on the right lane and change to the left one.
It is important to note that the capability of the two-lane approach to reproduce the different traffic patterns does not depend on a specially chosen parameter set, neither of the two-lane algorithm nor the insertion procedure, but it is stable with respect to them. Different parameters just control the peculiarity of the different states.
The state-diagram (Fig. 7.10) of the two-lane system shows qualitatively the same properties as the single-lane system (Sec. 7.1.1) and the empirical data [73]. The boundaries between the different regimes are just displaced. Whereas in the single-lane system the lower limit of the region of the general pattern lies at flows on the main road of about $J_{\text{ramp}} \approx 450\,\text{veh/h}$ it is now moved to a higher value $J_{\text{ramp}} \approx 1100\,\text{veh/h}$ for $J_{\text{main}} = 2000\,\text{veh/h}$. The reason for this is that inflowing vehicles still disturb the traffic on the right lane of the main road but now the vehicles have the opportunity to change the lane. The update algorithm takes into account the next two vehicles' velocities. Thus, if a vehicle enters the main road – it has a lower velocity as its surrounding vehicles as defined in the insertion algorithm (Sec. 7.1) –, the following vehicles detect the worse neighborhood and evade to the left lane as long as the maximum capacity of both lanes is not reached. The inflowing vehicles are distributed to both lanes and the disturbance is absorbed for higher inflow rates. This is qualitatively in good accordance to reality [73, 74].

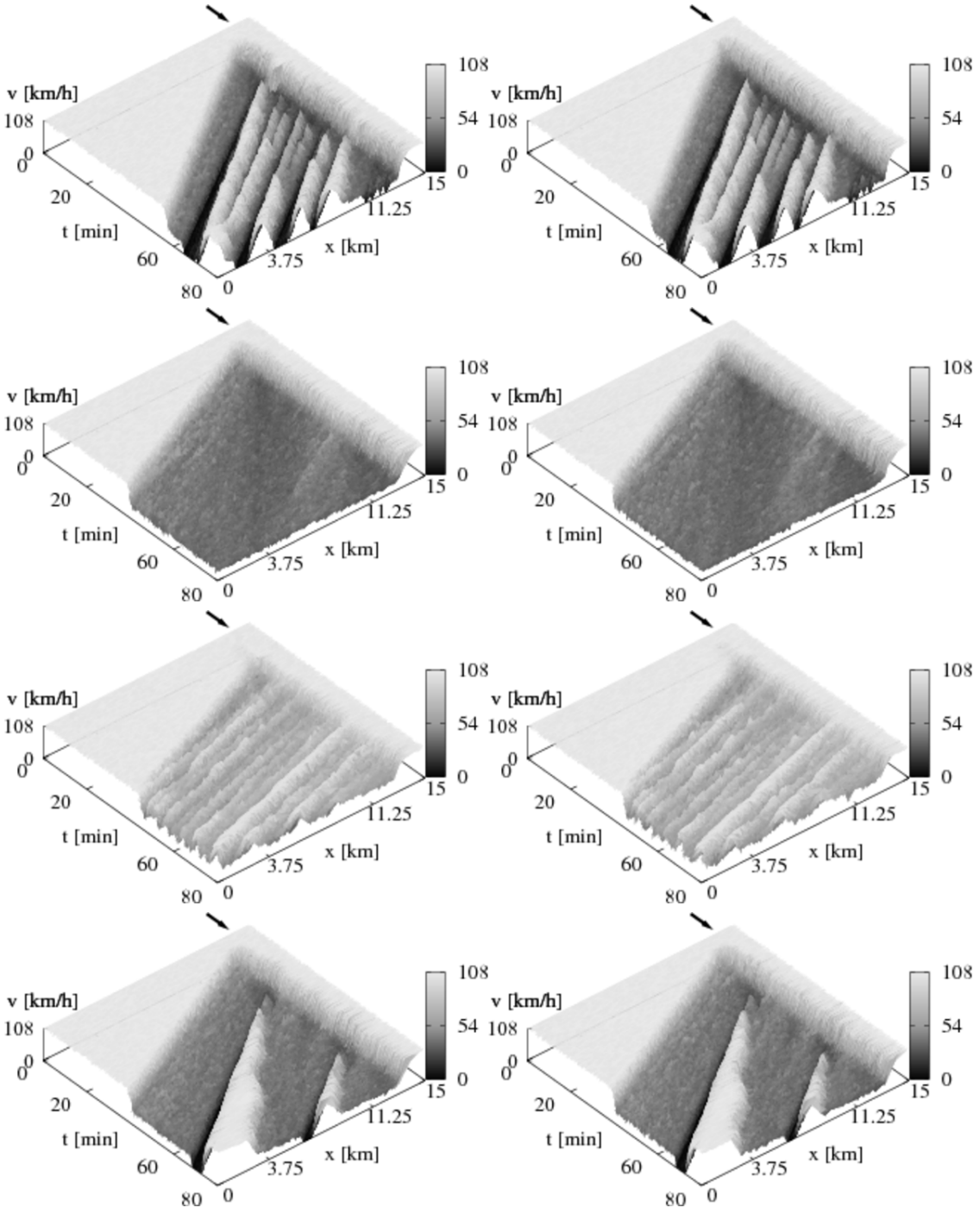

Figure 7.8: Different traffic states at an on-ramp for a two-lane road. From top to bottom: general pattern, widening synchronized traffic, and moving synchronized traffic. The left column shows the left lane and the right column the corresponding right lane. At the bottom the pinch effect is depicted. The plots of both lanes are almost identical. The traffic state is transferred from one lane to the other immediately.

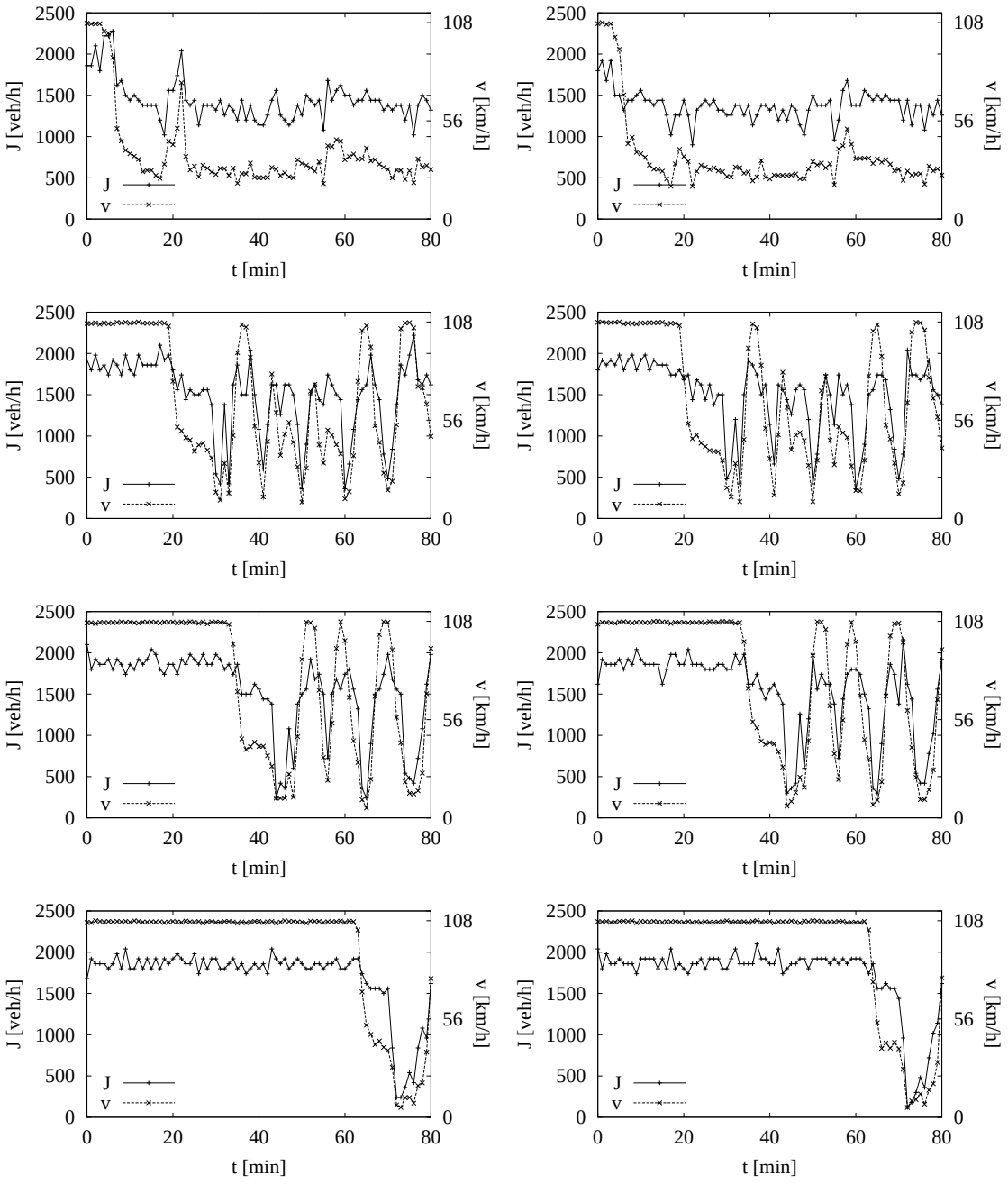

Figure 7.9: Velocity and flow time series of the left (left column) and right (right column) lane of an open system in the vicinity of an on-ramp. The dynamics of the general pattern shown in Fig. 7.2 top are captures here. The slope of the curves is almost identical for both lanes. In the top a peak in the flow on the left lane appears at $t \approx 22\,\mathrm{min}$. At the same time a narrow jam emerges on the right lane. Here, vehicles evade the disturbance on the right lane and change to the left one. The detector positions are top down: $x_{\mathrm{det}} = 12.75\,\mathrm{km}$, $x_{\mathrm{det}} = 9\,\mathrm{km}$, $x_{\mathrm{det}} = 5.25\,\mathrm{km}$ and $x_{\mathrm{det}} = -2.25\,\mathrm{km}$.

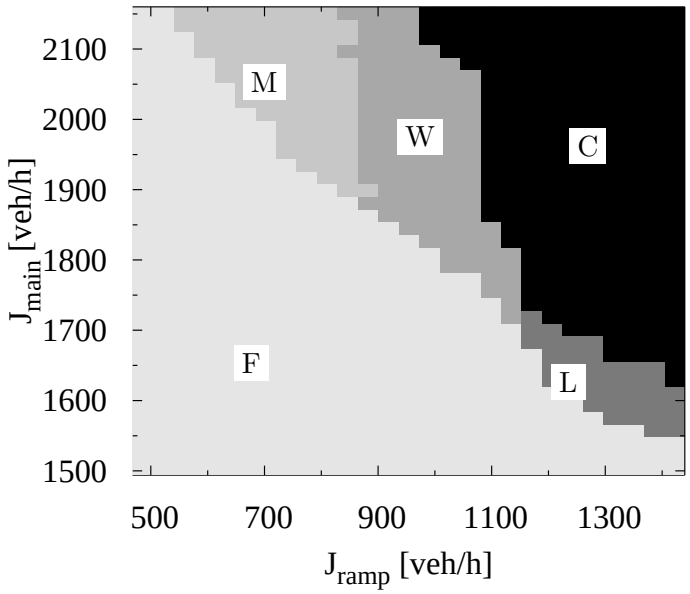

Figure 7.10: The phase diagram of the two-lane system with an on-ramp. The similarities to the single-lane pendant are obvious. All proposed variants of synchronized traffic are reproduced and are in good agreement with the empirical findings [73].

The boundary between localized synchronized pattern and the general pattern shows the same characteristics as in the single-lane system apart from a shift to higher flows on the main road.
Note, as already stated in the discussion of the single-lane system, the boundaries of the particular regions are not strict but in general both adjacent states can emerge at the limiting flow rates. The simulation times are of the magnitude of the life-time of the synchronized traffic. Thus, this is caused by the metastability of the synchronized traffic (see Sec. 7.1.2). Nevertheless, only a limited number of simulations can be performed despite of the very high variance of the life-time at the boundaries. Thus, the resolution which traffic pattern emerges is limited.
Nevertheless, one important property of the model is required to ensure the transfer of the traffic state from one lane to the other. The "coupling" of the lanes is depending on the lane change time and the degree of hindrance of the other vehicles during the lane change.

7.1.7 (De-)Coupled Lanes

Up to now it is supposed that the traffic state is transferred from one lane to the other of the two-lane road. This means that the state that emerges at one lane is transferred to the other lane and both lanes show the same state. This is in general what is found empirically. But if the disturbance at one lane is very rigid and appears suddenly the smooth transfer could not be realized.
The important parameters that control whether a lane change is possible at all are t_{lc} and β – the duration of a lane change and the strength of the interference of the follower on the destination lane. These affect in the first instance the lane change frequency.

The latter function is analyzed in Sec. 6.1.2. The former gets important if the velocity of the vehicle that tends to change the lane is much slower than that of the vehicles on the destination lane. This configuration does not occur often in the periodic system when the traffic phases are transferred smoothly from one lane to the other, but it is important in the vicinity of an on-ramp. The cars that are inserted in the right lane disturb the system and may slowe down the vehicles on this lane. If the vehicles now want to change the lane, the probability that the security criterion is fulfilled for t_{lc} succeeding time-steps is low as the fast-driving vehicles drive past the vehicle that want to change and thus the vehicle gets stuck on the right lane. This leads to a decoupled system.

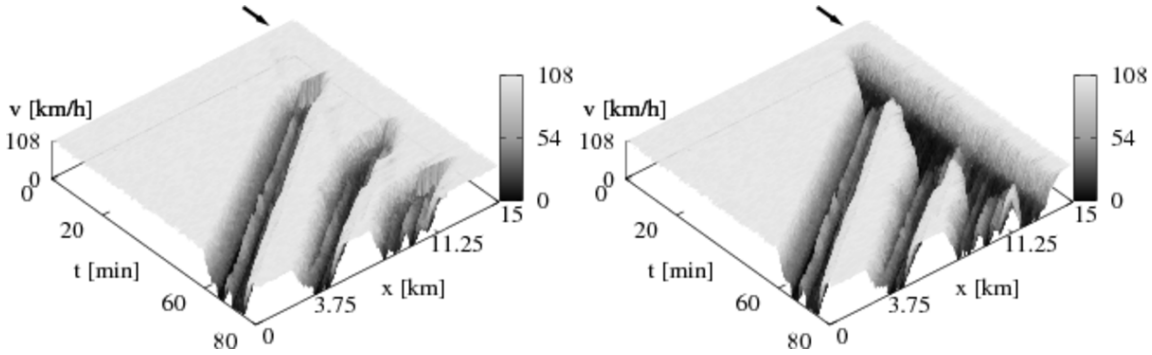

Figure 7.11: **Left:** Left lane of a decoupled system. **Right:** Right lane of a decoupled system. The traffic state is not immediately transferred from the right lane to the left one as the velocity difference between the stopped vehicles on the right lane and the vehicles on the left lane is too high. The mean velocity in the decoupled region is $\langle v \rangle = 103\,\mathrm{km/h}$ on the left lane whereas the vehicles drive with $\langle v \rangle = 15\,\mathrm{km/h}$ on the right one. The lanes are decoupled until a vehicle accomplishes to change the lane.

Thus, an on-ramp scenario is considered where the inflow is of the magnitude that in the homogeneous case, where the traffic state is smoothly transferred from the right to the left lane, widening synchronized traffic emerges. If the driver follows a cooperative behavior so that he will not hinder any vehicle on the destination lane or drives defensively, a slowly driving vehicle might not be able to change to the left lane where the vehicles are driving much faster. The resulting structure is shown in Fig. 7.11. When the inflow from the ramp is started a compact jam is induced on the right lane close to the on-ramp. Here, the vehicles drive very slow. In the next minutes free-flow keeps stable on the left lane and the jam resides on the right one. At some time a vehicle accomplishes to change from the right to the left lane and thwarts the following vehicles. The jam is transferred to the left lane. The vehicles on the right lane reach slightly higher velocities but the slower entering vehicles force the others to brake and the lanes decouple once again.
In the model approach the capability to change the lane and therefore the strength of the coupling of the two lanes is strongly depending on the parameters β and t_{lc}. Whether a lane change is successful if a vehicle wants to change its lane is determined by these two parameters. Note, that this effect is no limitation of the model approach but reflects the reality more accurately. In real world traffic the vehicles may also be trapped on one lane if the velocity difference is too large. Thus, it is a deficiency of traffic models with unlimited deceleration of the vehicles that these effects are not present. For example in the

two-lane extension of the BL model [93] a standing vehicle may change to the other lane if a vehicle driving on the other lane with maximum velocity is approaching. The safety criterion with respect to the follower is just $d_{\mathcal{F}} \geq v_{\mathcal{F}}$. Thus, this lane change would be allowed and the follower has to stop in one time-step. This obviously leads to unrealistic behavior of the vehicle dynamics.

7.2 Localized Defects

In the introduction to this chapter it is stated that the influence of further defects beside on-ramps was topic of different studies. Especially the relation between the different defect types are of great interest.
In [28] a simple model for an on-ramp in the NaSch model is presented and its impact is compared with other kinds of defects. It shows that the general influence of these two types of defects are comparable. Amongst others, it is analyzed now whether this is also true for the more complex dynamics of the model by Lee *et al.* so that the different variants of synchronized traffic that are found at an on-ramp can be retrieved in the vicinity of a local defect as well.

7.2.1 Velocity Defect

The influence of a defect caused by a region that enforces a lower maximum velocity was studied for different cellular automaton models [32]. The defect leads to a reduction of the total flow in the system and becomes visible in the fundamental diagram in a plateau with a maximum flow that is directly connected to the strength of the defect.
In contrast to the NaSch model the influence of a defect in the Lee-model is more complex. Beside the free-flow and the congested phase of stop-and-go traffic which are also reproduced by the NaSch model, synchronized traffic is observed as well in the presence of the defect.
A further difference to the models with unlimited braking arises as the maximum velocity cannot be assigned directly. To implement the defect the maximum velocity has no longer a constant value but it is now also determined by its position. The original update cycle is completed by

$$v_{n,\max}^{\text{tmp}} = \max(v_n - D, \min(v_{n,\max}, v_{\text{i,max}})), \tag{7.6}$$

where $v_{n,\max}^{\text{tmp}}$ is the temporal maximum velocity assigned to the vehicle, $v_{n,\max}$ is the maximum velocity of the vehicle and $v_{\text{i,max}}$ is the spatial maximum velocity. The temporal maximum velocity is now set with respect to the current position of the vehicle and the defect maximum velocity v_{def}.

$$v_{\text{i,max}} = \begin{cases} v_{\text{def}}, & \text{for } x_n \in \{d_{\text{begin}}, d_{\text{end}}\}, \\ v_{\max}, & \text{else.} \end{cases} \tag{7.7}$$

Note, because of the limited deceleration capability of the vehicles, the vehicles maximum velocity is just reduced by D – the maximum deceleration capability. This follows a realistic behavior of the road user who does not do an emergency brake when approaching a speed limit but they adapt the claimed velocity smoothly.
The simulations are made for in an single lane open system of length 23 km and the measure time is 10,000 sec after a relaxation of 30,000 sec.

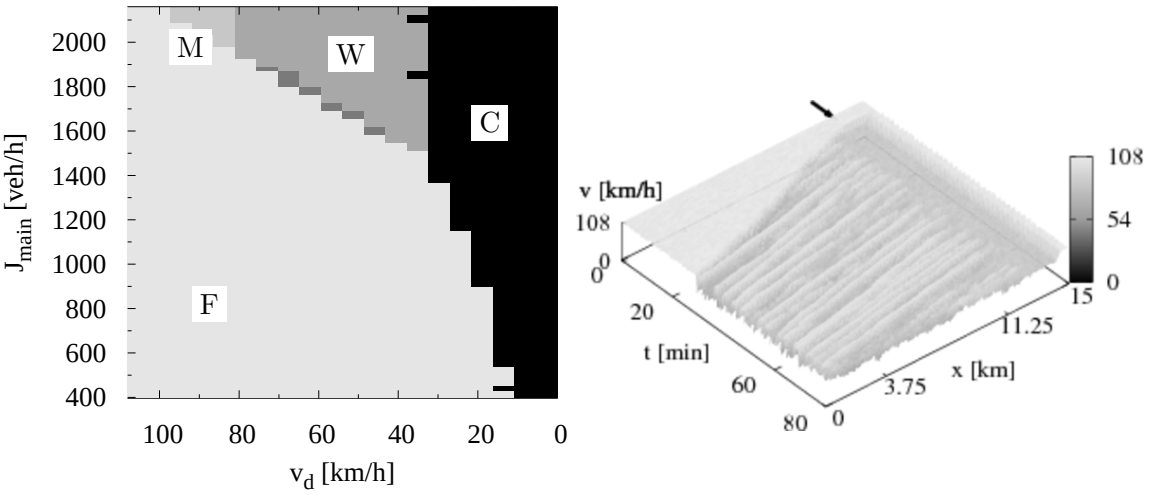

Figure 7.12: **Left:** Phase diagram of the open system with a speed limit. The states that establish are qualitatively the same as for the impact of an on-ramp. **Right:** The general influence of a velocity defect. The velocity in the region of the defect is reduced to the defect velocity $v_{\text{def}} = 16 \approx 80\,\text{km/h}$. The inflow rate onto the main road is $J_{\text{main}} = 2100\,\text{veh/h}$. The length of the street is 23 km and the upstream end is set to $-15\,\text{km}$. The beginning of the defect region at 12 km is indicated by the arrow.

7.2.2 Results

The effect of the velocity defect is different from that of simpler model approaches as the NaSch or VDR model. In these models the defect forms a seed for the formation of jams. The more complex dynamics of the model by Lee *et al.* leads to a more elaborate formation of all three traffic states. This is shown in the diagram in the left part of Fig. 7.12. At defect velocities near the maximum velocity of the vehicles there is nearly no effect. In the region of the defect the velocity is just reduced. More interesting is the dynamics at lower defect velocities. At intermediate velocities synchronized traffic depending on the flow is formed. At lower inflow rates moving synchronized traffic is build. On the right side of Fig. 7.12 this is shown exemplarily. At higher inflow rates widening synchronized can be detected. This corresponds to the emergent traffic at an on-ramp (see Fig. 7.4). In the latter also localized synchronized traffic is present that is not found at the velocity defect.
The phase diagram shows that the effect of a defect has qualitatively the same influence on the system dynamics as an on-ramp. Except for localized synchronized traffic the formation of the different traffic states is likewise. This underlines the former results that effects of on-ramps and localized defects are qualitatively equivalent.
Note, if the defect is implemented on a two-lane road, the qualitatively and quantitiatives the same results are found. This is not surprising as the lane changes do not lead to an advantage nor a disadvantage as the defect is spread over both lanes.

7.3 Conclusion

In the first part of this chapter the dynamics of the single-lane model in the vicinity of an on-ramp was recapitulated. It was shown that the single-lane model reproduces the different spatiotemporal patterns of synchronized traffic very accurately. The resulting state diagram of the single-lane system is qualitatively in good accordance with that proposed by Kerner [73].
This is in particular true for the system with two lanes. Here, the different patterns are found as well and they are in very good agreement with the empirical results that are found in the vicinity of an on-ramp. The lane changes transfer the state from one lane to the other and the states are stable despite of the disturbances by the lane changes. The different traffic patterns are just moved to higher fluxes on the main road and on the on-ramp as the vehicles can evade obstacles by changing the lane. Free-flow and synchronized traffic are still stable for higher flows. Note, the empirically observed traffic patterns are acquired on a two-lane road.
In general, the state is transferred from one lane to the other almost immediately. Nevertheless, if vehicles enter the main road from the on-ramp at a high frequency a configuration might be formed in which the vehicles from the right lane are not able to change the lane. This happens if the velocity on the right lane is reduced by the entering vehicles and the speed difference between the two lanes gets too high. It is no longer safe for the vehicles on the right lane to change to the left as the successors cannot reach their safe velocity. The lanes are decoupled. Note, this is a consequence of the limited deceleration capability and the required safe lane change.
The life-time of the synchronized traffic near an on-ramp was of special interest in this chapter. Thus, different aspects were investigated in detail.
The life-time of synchronized traffic showed a high dependence on the flow on the main road as well as on the inflow rate. The life-time decreases faster than exponentially with respect to the inflow from the ramp. Thus, the decrease is faster than in the periodic system. Obviously this is caused by the additional disturbance by the entering vehicle that adds to the internal fluctuations.
Recent approaches try to gather emirical data of the breakdown probability [18, 76, 79, 112, 175]. In addition, in this publications functional relation for the jam probability is formulated despite the limited empirical data [112, 137]. But the data are still very scarce so that additional investigations are needed.
Further, the dependence of the emergent traffic state on the insertion strategy was discussed. It was shown that a controlled inflow, i.e., the vehicles enter at fixed intervals, stabilizes the traffic on the main road so that a breakdown is less likely compared to a random insertion of the vehicles. The controlled insertion of short platoons is even more efficient. The reason for this is the screening of the disturbance by the vehicles.
The strong influence of the velocity that is assigned to the on-driving vehicles showed that this is an important factor with respect to the capacity of the road. The traffic state emerges near the on-ramp varies strongly. If the velocity difference is large, extended regions of synchronized traffic appear in the phase diagram. For lower insertion velocities the boundaries are shifted to lower inflow rates. Otherwise, if the velocities are nearly equal, no stable synchronized traffic is formed and the phase diagram consists only of free-flow and jammed traffic. The free-flow is stable till high inflow rates, but breaks down very fast if the inflow reaches a critical value.
This shows that the emergence of traffic jams in the vicinity of an on-ramp is indeed

strongly depending on the velocity the vehicles can reach on the on-ramp. There are two ways to control this. The first and obvious approach is to elongate the on-ramps so that the vehicles have more space to adjust their velocity to that of the main carriageway. The second possibility, which is slightly more complex because of side-effects, is to enforce a speed limit on the main road and adapt the velocities in such a way. The mentioned side-effect is the inherent influence of the speed-limit. That these should not be neglected is elaborately discussed in this chapter as well.
If a speed limit is assigned to a part of the road, similar effects as upstream of an on-ramp are observed. Depending on the value of the speed limit, different forms of synchronized traffic are formed upstream of the defect sites. Except for localized synchronized traffic the same traffic patterns are found as in the vicinity of an on-ramp. Thus, different kinds of defects lead to qualitatively the same influence on the emergent traffic states.

A Testing Accident Behaviour

A.1 Basic Definitions

Definition 1. *Let $N \in \mathbb{N}$ and for every $n \leq N$ let $\underline{s}_n$ be a set of information completely describing the state of a vehicle. Then $S := (\underline{s}_1, \ldots, \underline{s}_N)$ is called a* state *and $\mathfrak{S}$ denotes the set of all possible states S. Let $\mathfrak{T} : \mathfrak{S} \times \mathbb{Z} \to \mathfrak{S}, (S^t, z) \mapsto S^{t+1}$ be the* time evolution operator *that maps every state to another state which is interpreted as time evolution, i.e. the state S^t at time t evolves into state S^{t+1} at time $t+1$.[1] Let $S^0 \in \mathfrak{S}$ be the initial state, then* TSCA $:= (\mathfrak{S}, \mathfrak{T}, S^0)$ *is called a* traffic-simulating cellular automaton.
Furthermore, let $\mathfrak{E} := \left\{(S^t, S^{t+1}) \in \mathfrak{S}^2 \mid S^{t+1} = \mathfrak{T}(S^t, z), z \in \mathbb{Z}\right\}$ and $\mathfrak{G} = (\mathfrak{S}, \mathfrak{E})$ the digraph representing all possible transitions in the automaton.

Definition 1 is somewhat imprecise in defining $\underline{s}_n$. That is because the explicit definition of $\underline{s}_n$ depends on the requirements of the time evolution operator. Furthermore, depending on $\mathfrak{T}$, there might be a $\mathfrak{T}'$ that depends on a different $\underline{s}'_n$ but describes the same physics. In particular, one will start out with the following definition:

Definition 2. *For $n \leq N$ let x_n be the front bumper position of the vehicle n on the street, v_n its velocity, and l_n its length. Then $\underline{s}_n := (x_n, v_n, l_n, \tilde{s}_n)$ where $\tilde{s}_n$ is a placeholder for (arbitrary) additional properties.*

Definition 3. *A state S is called a* collision state *if and only if there exists an $n < N$ such that $x_{n+1} - x_n - l_{n+1} < 0$. A state S is called* unsafe *if there exists a path in $\mathfrak{G}$ from S to any collision state,* safe *otherwise. The sets of all collision states, unsafe states, and safe states are denoted $\mathfrak{S}_c$, $\mathfrak{S}_u$, and $\mathfrak{S}_s$, respectively.*

Definition 4. *If $\mathfrak{S}_s \neq \emptyset$ and $S^0 \in \mathfrak{S}_s$, then* TSCA *is called a* collision-free traffic-simulating cellular automaton.

A.2 Calculating the Set of Safe States

Definition 5. *An operator is defined that returns for a given set of states a set of all states that can evolve out of the input states:*

$$\begin{aligned} \mathrm{T} : \mathfrak{P}(\mathfrak{S}) &\to \mathfrak{P}(\mathfrak{S}) \\ \mathcal{S}^t \mapsto \mathcal{S}^{t+1} &:= \left\{S^{t+1} \mid \exists\, S^t \in \mathcal{S}^t, z \in \mathbb{Z} : S^{t+1} = \mathfrak{T}(S^t, z)\right\}. \end{aligned}$$

Analogous, an operator is defined that returns for a given set of states a set of all states that can evolve into one of the input states:

$$\begin{aligned} \mathrm{IT} : \mathfrak{P}(\mathfrak{S}) &\to \mathfrak{P}(\mathfrak{S}) \\ \mathcal{S}^t \mapsto \mathcal{S}^{t-1} &:= \left\{S^{t-1} \mid \exists\, S^t \in \mathcal{S}^t, z \in \mathbb{Z} : S^t = \mathfrak{T}(S^{t-1}, z)\right\}. \end{aligned}$$

[1] The additional argument z allows $\mathfrak{T}$ to return different states for the same state S^t if called with a different parameter z. Traffic models implement random perturbations leading to different S^1 each run even if started with the same S^0. This is reflected by different z values.

Theorem 1. $\mathfrak{S}_u = \bigcup_{p=0}^{\infty} \mathrm{IT}^p(\mathfrak{S}_c)$, $\mathfrak{S}_s = \mathfrak{S} \setminus \mathfrak{S}_u$.

Proof. Let S_u be an unsafe state, thus there exists a path in $\mathfrak{G}$ from S_u to any collision state. Let S_c be a collision state such that there exists a path from S_u to S_c and denote its length (number of edges) with p. $\mathrm{IT}(\mathfrak{S}_c)$ returns a set of states that are all connected to any collision state through a path of length 1. If $\mathfrak{S}$ contains every state for which exists a path of length j to any collision state and $\mathrm{IT}(\mathfrak{S})$ returns a set of states that are all connected to any state in $\mathfrak{S}$ through a path of length 1, then all states in $\mathrm{IT}(\mathfrak{S})$ are connected to any collision state through a path of length $j+1$. Therefore, by induction S_u must be element of $\mathrm{IT}^p(\mathfrak{S}_c)$ and thus element of $\mathfrak{S}_u$.
The theorem's second statement follows directly from the definition of unsafe and safe states which implies that $\mathfrak{S}_s$ and $\mathfrak{S}_u$ are disjunctive. □

Algorithm 1. *Theorem 1 provides a generic algorithm for calculating the set of safe states and thus for determining the set of valid initial states for a collision-free traffic-simulating cellular automaton:*

Input: *The set of possible states $\mathfrak{S}$, the set of collision states $\mathfrak{S}_c \subset \mathfrak{S}$, and the time evolution operator $\mathfrak{T}$.*
Output: *The set of safe states $\mathfrak{S}_s \subset \mathfrak{S}$.*

$\mathfrak{S}_u := \emptyset$
$\mathfrak{S}' := \mathfrak{S}_c$
WHILE $(\mathfrak{S}' \neq \emptyset)$ {
  $\mathfrak{S}_u := \mathfrak{S}_u \cup \mathfrak{S}'$
  $\mathfrak{S}' := \mathrm{IT}(\mathfrak{S}') \setminus \mathfrak{S}_u$
}
OUTPUT $\mathfrak{S} \setminus \mathfrak{S}_u$

However, this algorithm is practically useless since it only solves for one particular $\mathfrak{S}$ and $\mathfrak{T}$ (for a traffic model simulating a closed system there are different $\mathfrak{S}$ and $\mathfrak{T}$ for every possible vehicle density).

A.3 Introducing State Classes

In the following the fact is exploited that collisions are local properties of states. cosets of states are defined such that one can easily identify *any* state representing *any* number of vehicles that has certain local properties. Furthermore, it is assumed that the time evolution of the TSCA is local, thus $\overline{s}_n^{t+1}$ does only depend on $\left\{\overline{s}_{n-n_b}^t, \ldots, \overline{s}_{n+n_a}^t\right\}$.

Definition 6. *Let $K \in \mathbb{N}$ and for every $n \leq K$ let $\underline{s}'_n$ be a set of information completely describing the state of a vehicle.*
Then $\overline{S}_{k,K} := \left\{S = (\underline{s}_1, \ldots, \underline{s}_N) \in \mathfrak{S} \mid \underline{s}_{k+n-1} = \underline{s}'_n \text{ for all } n = 1, \ldots, K\right\}$ is called a state class *and denoted $(\underline{s}'_1, \ldots, \underline{s}'_K)_k$. The set of all such state classes is denoted $\overline{\mathfrak{S}}$. A state $S \in \overline{S}_{k,K}$ is called a state* covered by $\overline{S}_{k,K}$. *Furthermore, the* cover *of a set of state classes $\overline{\mathcal{S}}$ is the union of the covers of its elements:* $\mathrm{cover}(\overline{\mathcal{S}}) := \bigcup_{\overline{S}_{k,K} \in \overline{\mathcal{S}}} \overline{S}_{k,K}$.

Definition 7. *In the spirit of the state class approach it is defined:*

$$\begin{aligned}
\overline{\mathrm{T}} &: \mathfrak{P}(\overline{\mathfrak{S}}) \to \mathfrak{P}(\overline{\mathfrak{S}}) \\
&\overline{\mathcal{S}}^t \mapsto \overline{\mathcal{S}}^{t+1} := \left\{ \overline{S}^{t+1}_{k+n_b,K-n_b-n_a} \mid \exists\, \overline{S}^t_{k,K} \in \overline{\mathcal{S}}^t : \overline{S}^{t+1}_{k+n_b,K-n_b-n_a} = \mathrm{T}(\overline{S}^t_{k,K}) \right\}, \\
\overline{\mathrm{IT}} &: \mathfrak{P}(\overline{\mathfrak{S}}) \to \mathfrak{P}(\overline{\mathfrak{S}}) \\
&\overline{\mathcal{S}}^t \mapsto \overline{\mathcal{S}}^{t-1} := \left\{ \overline{S}^{t-1}_{k-n_b,K+n_b+n_a} \mid \exists\, \overline{S}^t_{k,K} \in \overline{\mathcal{S}}^t : \overline{S}^t_{k,K} = \mathrm{IT}(\overline{S}^{t-1}_{k-n_b,K+n_b+n_a}) \right\}.
\end{aligned}$$

Note that the state classes returned by $\overline{\mathrm{T}}$ shrink in size. Successive applications of $\overline{\mathrm{T}}$ will lead to state classes with size zero, thus covering the whole set of states. This is not surprising because any given local vehicle situation can evolve into anything if the conditions beyond that given situation are unknown. This also explains why the state classes returned by $\overline{\mathrm{IT}}$ grow in size.

Theorem 2. *With $\overline{\mathcal{S}}_c$ being a set of state classes such that* $\mathrm{cover}(\overline{\mathcal{S}}_c) = \mathfrak{S}_c$*, and* $\overline{\mathcal{S}}_u := \bigcup_{p=0}^{\infty} \overline{\mathrm{IT}}^p(\overline{\mathcal{S}}_c)$*,* $\mathfrak{S}_u = \mathrm{cover}(\overline{\mathcal{S}}_u)$.

Proof. By definition of $\overline{\mathrm{IT}}$ and IT, each state covered by the result of the $\overline{\mathrm{IT}}$ operator is connected through a path of length 1 to a state covered by the operand. Therefore, each state covered by the result of $\overline{\mathrm{IT}}^j$ is connected to a state covered by the operand through a path of length j. Thus, $\overline{\mathcal{S}}_u$ covers all states connected to any state covered by $\overline{\mathcal{S}}_c$ through a path of any length. The cover of $\overline{\mathcal{S}}_c$ is by definition $\mathfrak{S}_c$, thus the cover of $\overline{\mathcal{S}}_u$ is identical to $\mathfrak{S}_u$. □

Theorem 2 provides a more valuable result than theorem 1. The local property of a collision does not depend on the overall number of vehicles simulated by the TSCA, therefore the same $\overline{\mathcal{S}}_c$ covers different $\mathcal{S}_c$. Since the calculation of $\overline{\mathcal{S}}_u$ does not depend on the actual set of states $\mathcal{S}$ but only on the state classes, the same unique $\overline{\mathcal{S}}_u$ will provide $\mathcal{S}_u$ for different $\mathcal{S}$. Furthermore, none of the calculations depend on k (which must run from 1 to N to completely cover $\mathfrak{S}$), thus, all calculations can be done with $k = 1$ and only when calculating actual state sets such as $\mathfrak{S}_c$ or $\mathfrak{S}_u$ an iteration over k has to be done.

Definition 8. *The history of a single state class with length* 1, $\overline{\mathrm{IT}}(\{\overline{S}_{k,1}\})$ *is called an* atomic history.

Algorithm 2. *This algorithm calculates the history of an arbitrary state class. It uses* $\overline{\mathrm{IT}}$ *only to calculate atomic histories, which is a relatively easy task. They are used as building blocks to recursively assemble the history of the input state class.* $\overline{S}_{k,K}$.

Input: $\overline{S}^t_{k,K} = (\underline{s}'_1, \ldots, \underline{s}'_K)_k$

Output: $\overline{\mathrm{IT}}(\{\overline{S}^t_{k,K}\})$

IF $(K = 1)$
  OUTPUT $\overline{\mathrm{IT}}(\{\overline{S}^t_{k,K}\})$
ELSE {
  $\overline{\mathcal{S}}^{t-1} := \emptyset$
  $\overline{Si}^t_{k,1} := (\underline{s}'_1)_k$
  $\overline{Sr}^t_{k+1,K-1} := (\underline{s}'_2, \ldots, \underline{s}'_K)_{k+1}$
  $\overline{\mathcal{S}i}^{t-1} := \mathrm{IT}(\{\overline{Si}_{k,1}\})$
  $\overline{\mathcal{S}r}^{t-1} :=$ RECURSIVE CALL WITH $\overline{Sr}^t_{k+1,K-1}$
  FOR EACH $(\underline{si}'_1, \ldots, \underline{si}'_{1+n_b+n_a})_{k-n_b} \in \overline{\mathcal{S}i}^{t-1}$ {
    FOR EACH $(\underline{sr}'_1, \ldots, \underline{sr}'_{K-1+n_b+n_a})_{k+1-n_b} \in \overline{\mathcal{S}r}^{t-1}$ {
      IF $(\underline{si}'_{j+1} = \underline{sr}'_j$ FOR $j = 1, \ldots, n_b + n_a)$
        $\overline{\mathcal{S}}^{t-1} := \overline{\mathcal{S}}^{t-1} \cup \left\{(\underline{si}'_1, \underline{sr}'_1, \ldots, \underline{sr}'_{K-1+n_b+n_a})_{k-n_b}\right\}$
    }
  }
  OUTPUT $\overline{\mathcal{S}}^{t-1}$
}

A.4 Specializing to the Model by Lee *et al.*

Now the general findings are applied to the model by Lee *et al.*. The first simplification one can make exploits the homogeneity of the model. The central inequality (Eq. 5.1) does not depend on the single vehicle positions but on their differences only, thus in the definition of $\underline{s}_n$ one can replace x_n with the gap d_n, which is defined as follows.

Definition 9. *The gap between vehicle n and its leader is $d_n := x_{n+1} - x_n - l_{n+1}$.*

Corollary 1. *S is a collision state $\Leftrightarrow \exists\, n < N : d_n < 0$.*

There is no vehicle-specific length in the Lee04 model, thus $l_n = l$. The state of a vehicle reduces to $\underline{s}_n = (v_n, d_n)$, with $v_n \in [0, v_{\max}]$ and $d_n \in \mathbb{Z}$. To simplify notation, a state class is written as $\overline{S}_{k,K} = (v_1, d_1, v_2, d_2, \ldots, v_K)_k$. Note, that d_K is omitted. This is sufficient for all of our purposes and is to be read such that the state class does not state any requirements for d_K (as it does not for v_{K+1}). In the update rules, each vehicle's new velocity depends on the gap to the next vehicle and the velocities of the next two vehicles only, thus $n_b = 0$ and $n_a = 2$.

Algorithm 3. *Given the model's update rules, one can easily develop the algorithm to calculate the atomic histories.*

Input: $\overline{S}^t_{k,1} = (v^t_1)_k$
Output: $\overline{\mathrm{IT}}(\{\overline{S}^t_{k,1}\})$

$\overline{\mathcal{S}}^{t-1} := \emptyset$
FOR EACH $v_1^{t-1}, v_2^{t-1}, v_3^{t-1} \in [0, v_{\max}]$, $d_1^{t-1}, d_2^{t-1} \in \mathbb{Z}$ {
CALCULATE $\tilde{v}_1^t$ ACCORDING TO THE UPDATE RULES
IF $(v_1^t \in \{\tilde{v}_1^t, \max\{0, v_1^t - D, \tilde{v}_1^t - 1\}\})$
$\overline{\mathcal{S}}^{t-1} := \overline{\mathcal{S}}^{t-1} \cup \{(v_1^{t-1}, d_1^{t-1}, v_2^{t-1}, d_2^{t-1}, v_3^{t-1})_k\}$
}
OUTPUT $\overline{\mathcal{S}}^{t-1}$

Theorem 3. *Let $\overline{S}_{k,1} = (V)_k$ be a state class, $v_1, v_2, v_3 \in [0, v_{max}]$, and $\underline{d}_1, \overline{d}_1, d_2 \in \mathbb{Z}$ with $\underline{d}_1 \leq \overline{d}_1$. If $(v_1, \underline{d}_1, v_2, d_2, v_3)_k \in \overline{\mathrm{IT}}(\{\overline{S}_{k,K}\})$ and $(v_1, \overline{d}_1, v_2, d_2, v_3)_k \in \overline{\mathrm{IT}}(\{\overline{S}_{k,K}\})$, then $(v_1, d_1, v_2, d_2, v_3)_k \in \overline{\mathrm{IT}}(\{\overline{S}_{k,K}\})$ for $d_1 \in [\underline{d}_1, \overline{d}_1]$.*

Proof. With constant v_n^t, v_{n+1}^t and v_{n+2}^t Eq. 5.1 has the form $F(c_n^{t+1}) \leq d_n^t + G$. Since $\tilde{c}_n^{t+1}$ is defined as the maximum c_n^{t+1} that satisfies the equation, obviously $\tilde{c}_n^{t+1}$ is monotonic in d_n^t. Thus, for $\underline{d}_1 \leq d_1 \leq \overline{d}_1$ the relation $\tilde{c}_1(\underline{d}_1) \leq \tilde{c}_1(d_1) \leq \tilde{c}_1(\overline{d}_1)$ holds. In update step (iii) $\tilde{v}_n^{t+1}$ is chosen from $[v_n^t - D, v_n^t + a]$ such that $|\tilde{v}_n^{t+1} - \tilde{c}_n^{t+1}|$ is minimal. It follows, that $\tilde{v}_1(\underline{d}_1) \leq \tilde{v}_1(d_1) \leq \tilde{v}_1(\overline{d}_1)$. If $V \in \{\tilde{v}_1(\underline{d}_1), \max\{0, v_1 - D, \tilde{v}_1(\underline{d}_1) - 1\}\}$ and $V \in \{\tilde{v}_1(\overline{d}_1), \max\{0, v_1 - D, \tilde{v}_1(\overline{d}_1) - 1\}\}$, then $V \in \{\tilde{v}_1(d_1), \max\{0, v_1 - D, \tilde{v}_1(d_1) - 1\}\}$. □

It can be shown that $\tilde{c}_n^{t+1}$ also is monotonic in v_n^t, v_{n+1}^t and v_{n+2}^t. If $(\underline{v}_1, d_1, v_2, d_2, v_3)_k \in \overline{\mathrm{IT}}(\{\overline{S}_{k,K}\})$ and $(\overline{v}_1, d_1, v_2, d_2, v_3)_k \in \overline{\mathrm{IT}}(\{\overline{S}_{k,K}\})$, then $(v_1, d_1, v_2, d_2, v_3)_k \in \overline{\mathrm{IT}}(\{\overline{S}_{k,K}\})$ for $v_1 \in [\underline{v}_1, \overline{v}_1]$. Similarly for v_2 and v_3.

Theorem 4. *Let $\overline{S}_{k,1} = (V)_k$ be a state class, $v_1, v_2, v_3 \in [0, v_{max}]$, and $d_1, d_2 \in \mathbb{Z}$. If $(v_1, d_1, v_2, d_2, v_3)_k \in \overline{\mathrm{IT}}(\{\overline{S}_{k,K}\})$, then $(v_1, d_1, v_2, d_2', v_3)_k \in \overline{\mathrm{IT}}(\{\overline{S}_{k,K}\})$ for $d_2' \in \mathbb{Z}$.*

Proof. The calculation of $\tilde{c}_n^{t+1}$ does not depend on d_{n+2}^t, thus $\tilde{c}_1(d_2) = \tilde{c}_1(d_2')$. □

Definition 10. *These results enables us to identify sets of state classes by intervals:* $\overline{\mathcal{S}} = \big([\underline{v}_1, \overline{v}_1], [\underline{d}_1, \overline{d}_1], [\underline{v}_2, \overline{v}_2], [\underline{d}_2, \overline{d}_2], \ldots, [\underline{v}_K, \overline{v}_K]\big)_k :=$
$\big\{(v_1, d_1, v_2, d_2, \ldots, v_K)_k \mid v_i \in [\underline{v}_i, \overline{v}_i], d_i \in [\underline{d}_i, \overline{d}_i]$ *for* $i = 1, \ldots, K-1$ *and* $v_K \in [\underline{v}_K, \overline{v}_K]\big\}$.
Throughout, sets of such sets of state classes are called collections of state class sets.

Algorithm 4. *Furthermore, the algorithm for calculating the atomic histories can be simplified. Besides the above results it is used that $v_1^{t-1} \in [v^t - a, v^t + D]$ and that v_3^{t-1} only influences γ_1^{t-1}. Furthermore, since $\tilde{c}_1^t$ is bound to $[0, v_{max}]$, there exists a d_1 with $\tilde{c}_1^t = 0$ ($\tilde{c}_1^t = v_{max}$) such that any $d_1' < d_1$ ($d_1' > d_1$) will not change $\tilde{c}_1^t$. Therefore, the iteration of d_1^{t-1} does not need to be done over all integers, but only over a sufficiently large interval around zero. For practical reasons, all collision states are excluded from the histories since the interest lies in how the* TSCA *can evolve into collision states and not how it will evolve after a collision.*

Input: $\overline{S}^t_{k,1} = (v^t_1)_k$

Output: *A collection of state class sets* $\{\overline{\mathcal{S}}_i\}$ *such that* $\bigcup_i \overline{\mathcal{S}}_i = \overline{\mathrm{IT}}(\{\overline{S}^t_{k,1}\})$

$\overline{\mathcal{C}}^{t-1} := \emptyset$
FOR EACH $v_1^{t-1} \in [v_1^t - a, v_1^t + D] \cap [0, v_{\max}]$, $v_2^{t-1} \in [0, v_{\max}]$, $\gamma_1^{t-1} \in [0, 1]$ {
  IF $((\gamma_1^{t-1} = 0)$ AND $(v_1^{t-1} > v_2^{t-1}))$
    CONTINUE
  $D_1^{t-1} := \emptyset$
  FOR EACH $d_1^{t-1} \in [0, 200]$ {
    CALCULATE $\tilde{v}_1^t$ ACCORDING TO THE UPDATE RULES
    IF $(v_1^t \in \{\tilde{v}_1^t, \max\{0, v_1^t - D, \tilde{v}_1^t - 1\}\})$
      $D_1^{t-1} := D_1^{t-1} \cup \{d_1^{t-1}\}$
  }
  IF $(200 \in D_1^{t-1})$
    $D_1^{t-1} := [\min D_1^{t-1}, \infty[$
  IF $((\gamma_1^{t-1} = 0)$ AND $(v_1^{t-1} \leq v_2^{t-1}))$
    $V_3^{t-1} := [v_2^{t-1}, v_{\max}]$
  ELSE IF $((\gamma_1^{t-1} = 0)$ AND $(v_1^{t-1} > v_2^{t-1}))$
    $V_3^{t-1} := [v_{\text{fast}}, v_{\max}]$
  ELSE IF $((\gamma_1^{t-1} = 1)$ AND $(v_1^{t-1} \leq v_2^{t-1}))$
    $V_3^{t-1} := [0, v_2^{t-1} - 1]$
  ELSE
    $V_3^{t-1} := [0, v_{\max}]$
  $\overline{\mathcal{C}}^{t-1} := \overline{\mathcal{C}}^{t-1} \cup \left\{ \left(\{v_1^{t-1}\}, D_1^{t-1}, \{v_2^{t-1}\}, \mathbb{Z}, V_3^{t-1}\right)_k \right\}$
}
OUTPUT COMPRESS($\overline{\mathcal{C}}^{t-1}$)

Of course, the output of this algorithm is not unique.

Algorithm 5. *The COMPRESS algorithm already used above transforms a given state class set collection* $\{\overline{\mathcal{S}}_i\}$ *into another collection* $\{\overline{\mathcal{S}}'_j\}$ *such that* $\bigcup_j \mathrm{cover}(\overline{\mathcal{S}}'_j) = \bigcup_i \mathrm{cover}(\overline{\mathcal{S}}_i)$ *and* $\#\{\overline{\mathcal{S}}'_j\}$ *minimal. This optimization problem is hard, thus a heuristic method is used that first expands the whole input collection into state class set with only single-valued intervals. It then iterates over all velocities and gaps, starting from the higher indices, and collects all state class sets that can be put into one state class set by giving it a multi-value interval on the currently processed velocity or gap. This collecting process is repeated until the resulting collection does not shrink further.*

Definition 11. *Let* $\overline{\mathcal{C}} = \{(V_1, D_1, V_2, D_2, V_3)_k\}$ *be a collection of state class set and* $\overline{\mathcal{S}} = (V'_1, D'_1, V'_2)_k$ *another state classes.*
Then $\overline{\mathcal{C}} \cap \overline{\mathcal{S}} := \left\{(V_1 \cap V'_1, D_1 \cap D'_1, V_2 \cap V'_2, D_2, V_3)_k \mid (V_1, D_1, V_2, D_2, V_3)_k \in \overline{\mathcal{C}}\right\}$.

Algorithm 6. *The following algorithm is the specialization of Alg. 2 to the Lee04 model and makes use of the introduction of state class sets. The call AHIST*(v_1^t) *refers to Alg. 4 with the state class* $(v_1^t)_k$ *as input. Again, the algorithm is simplified to only return non-collision states.*

Input: $\overline{\mathcal{S}}^t = (V_1^t, D_1^t, V_2^t, D_2^t, \ldots, V_K^t)_k$; *two intervals* V_1^{t-1} *and* V_2^{t-1} *which values default to* $[0, v_{max}]$

Output: *A collection of state class sets* $\{\overline{\mathcal{S}}_i\}$ *such that* $\bigcup_i \overline{\mathcal{S}}_i = \overline{\mathrm{IT}}(\overline{\mathcal{S}}^t)$

IF $(K = 1)$
  OUTPUT $\left(\bigcup_{v_1^t \in V_1^t} \mathrm{AHIST}(v_1^t)\right) \cap (V_1^{t-1}, \mathbb{N}, V_2^{t-1})_k$
ELSE {
  $\overline{\mathcal{C}}^{t-1} := \emptyset$
  FOR EACH $v_1^t \in V_1^t$, $v_2^t \in V_2^t$ {
    $D_1^{t-1} := [\min D_1^t - v_2^t + v_1^t, \max D_1^t - v_2^t + v_1^t] \cap [0, \infty[$
    $\overline{\mathcal{S}r}^t := (\{v_2^t\}, D_2^t, V_3^t, D_3^t, \ldots, V_K^t)_{k+1}$
    $\overline{\mathcal{C}i}^{t-1} := \mathrm{COMPRESS}\left(\mathrm{AHIST}(v_1^t) \cap (V_1^{t-1}, D_1^{t-1}, V_2^{t-1})_k\right)$
    FOR EACH $\overline{\mathcal{S}i}^{t-1} = (V_1'^{t-1}, D_1'^{t-1}, V_2'^{t-1}, D_2'^{t-1}, V_3'^{t-1})_k \in \overline{\mathcal{C}i}^{t-1}$ {
      $\overline{\mathcal{C}r}^{t-1} :=$ RECURSIVE CALL WITH $\overline{\mathcal{S}r}^t, V_2'^{t-1}, V_3'^{t-1}$
      FOR EACH $\overline{\mathcal{S}r}^{t-1} = (V_2''^{t-1}, D_2''^{t-2}, \ldots, V_K''^{t-1})_{k+1} \in \overline{\mathcal{C}r}^{t-1}$
        $\overline{\mathcal{C}}^{t-1} := \overline{\mathcal{C}}^{t-1} \cup \left\{(V_1'^{t-1}, D_2'^{t-1}, V_2''^{t-1}, D_3''^{t-1}, \ldots, V_K''^{t-1})_k\right\}$
    }
  }
  OUTPUT $\overline{\mathcal{C}}^{t-1}$
}

The use of the COMPRESS algorithm is carefully chosen. Another possible application would have been to compress the result $\overline{\mathcal{C}}^{t-1}$ before outputting it or not to use it at all. However, profiling and complexity analysis showed that this use is the most efficient. The number of elements in $\overline{\mathcal{C}i}^{t-1}$ determine the number of recursions to do, thus $\#\overline{\mathcal{C}i}^{t-1}$ is an exponent in the complexity of this algorithm. Although the COMPRESS algorithm is costly, it is only used for the result of the atomic history algorithm which usually returns only small collections of state class sets and the gain in doing less recursions exceeds the cost of COMPRESS. Note that although the COMPRESS algorithm is used here to simplify the collection return by $\mathrm{AHIST}(v_1^t)$ (and filtered with $(V_1^{t-1}, D_1^{t-1}, V_2^{t-1})_k$), it is still useful to apply COMPRESS to the result of the atomic history algorithm before returning it, because this reduces the amount of atomic histories that need to be stored in the atomic history database and will speed up database searches.

A.5 Results

As already indicated, a database (MySQL) is used to store the precalculated atomic histories. The operation $\mathrm{AHIST}(v_1^t) \cap (V_1^{t-1}, D_1^{t-1}, V_2^{t-1})_k$ can be easily performed by the database. Then state classes are generated for all collision states that can evolve out of non-collision states ($d_1^t - v_2^t + v_1^t > 0$) and fed Alg. 6 with all those state classes. The returned collections of state class sets were merged and again sent through the algorithm. The program stops when the algorithm does not return any results, thus no history for the input states exists, in which case one has proven that there exists a non-empty set of safe states and the model is collision-free except for a finite set of unsafe initial conditions. First, optimistic driving behavior is not allowed by excluding all state classes with $\gamma_1^t = 0$ from the atomic history database. Then for any collision state the history was a cascade

of states where the following car was braking with full capacities all the time. After some iterations v_1^{t-1} would have needed to be larger than $v_{\max}$ in order to comply with the model rules. Since this is not possible, all those cascades were finite and the program halted. Not surprisingly, it is easily proved that the model by Lee *et al.*, restricted to defensive driving behavior, is collision-free.
However, with allowing optimistic behavior, the velocities of the following car do not strive to higher values with backward moving time, but may oscillate. Of course, the program does not halt which leads to the conclusion that the model is not collision-free. The proof for collisions out of important, meaningful initial conditions is given by the observations of collisions in our simulations. Despite the simplifications and optimizations put into the algorithms, determining the sets of all collision states $\mathfrak{S}_c$, unsafe states $\mathfrak{S}_u$, and safe states $\mathfrak{S}_s$ is hard and practically impossible, since the whole graph $\mathfrak{G}$ has to be traversed.
Theoretically it would be possible to modify the program in order to output the probability of collisions by assigning a weight to every edge in the automaton's evolution graph according to the evolution probability. However, to calculate the overall probability of collisions, again the whole graph would have to be traversed.

Bibliography

[1] Applied generics, 1999, `http://www.appliedgenerics.de`.

[2] P. Bak, C. Tang, and K. Wiesenfeld, *Self-organized criticality*, Phys. Rev. A **38** (1988), 364.

[3] M. Bando, K. Hasebe, K. Nakanishi, and A. Nakayama, *Analysis of optimal velocity model with explicit delay*, Phys. Rev. E **58** (1998), 5429.

[4] M. Bando, K. Hasebe, K. Nakanishi, A. Shibata, and Y. Sugiyama, *Phenomenological study of dynamical models of traffic flow*, J. Phys. I **5** (1995), 11.

[5] M. Bando, K. Hasebe, A. Nakayama, A. Shibata, and Y. Sugiyama, *Structure stability of congestion in traffic dynamics*, Jap. J. Indust. Appl. Math. **11** (1994), 203.

[6] M. Bando, K. Hasebe, A. Nakayama, A. Shibata, and Y. Sugiyama, *Dynamical model of traffic congestion and numerical simulation*, Phys. Rev. E **51** (1995), 1035.

[7] P. Bantay and I.M. Janosi, *Avalanche dynamics from anomalous diffusion*, Phys. Rev. Lett. **68** (1992), 2058–2061.

[8] R. Barlović, T. Huisinga, A. Schadschneider, and M. Schreckenberg, *Open boundaries in a cellular automaton model for traffic flow with metastable states*, Phys. Rev. E **66** (2002), no. 4, 046113.

[9] R. Barlović, L. Santen, A. Schadschneider, and M. Schreckenberg, *Metastable states in cellular automata for traffic flow*, Eur. Phys. J. B **5** (1998), 793–800.

[10] R. Barlović, A. Schadschneider, and M. Schreckenberg, *Random walk theory of jamming in a cellular automaton model for traffic flow*, Physica A **294** (2001), 525–538.

[11] C.L. Barrett, M. Wolinsky, and M.W. Olesen, *Emergent local control properties in particle hopping traffic simulations*, in Wolf et al. [171], pp. 169–173.

[12] E. Ben-Naim and P.L. Krapivsky, *Stationary velocity distribution in traffic flow*, Phys. Rev. E **56** (1997), 6680.

[13] E. Ben-Naim and P.L. Krapivsky, *Steady-state properties of traffic flow*, J. Phys. A **31** (1998), 8073.

[14] E. Ben-Naim and P.L. Krapivsky, *Maxwell model of traffic flows*, Phys. Rev. E **59** (1999), no. 1, 88–97.

[15] E. Ben-Naim, P.L. Krapivsky, and S. Redner, *Kinetics of clustering in traffic flows*, Phys. Rev. E **50** (1994), 822.

[16] V.J. Blue and J.L. Adler, *Flow capacities from cellular automata modelling*, in Schreckenberg and Sharma [156], pp. 115–121.

[17] M. Brackstone and M. McDonald, *The microscopic modelling of traffic flow: Weaknesses and potential developments*, in Wolf et al. [171], pp. 151–165.

[18] W. Brilon, M. Regler, and J. Geistefeld, *Zufallscharakter der Kapazität von Autobahnen und praktische Konsequenzen*, Straßenverkehrstechnik **3** (2005), 136–144, (in german).

[19] G. L. Chang and Y. M. Kao, *An empirical investigation of macroscopic lane-changing characteristics on uncongested multilane freeways*, Transp. Res. A **25** (1991), 375–389.

[20] B. Chopard, P.O. Luthi, and P.A. Queloz, *Cellular automata model for car traffic in a two-dimensional street network*, J. Phys. A **29** (1996), 2325–2336.

[21] D. Chowdhury, L. Santen, and A. Schadschneider, *Statistical physics of vehicular traffic and some related systems*, Phys. Rep. **329** (2000), 199–329.

[22] D. Chowdhury, D.E. Wolf, and M. Schreckenberg, *Particle hopping models for two-lane traffic with two kinds of vehicles: Effects of lane-changing rules*, Physica A **235** (1997), 417.

[23] R. Chrobok, A. Pottmeier, S.F. Hafstein, and M. Schreckenberg., *Traffic forecast in large scale freeway networks*, International Journal of Bifurcation and Chaos **14** (2004), no. 6, 1995–2005.

[24] B. Coifman, S. Krishnamurthy, and X. Wang, *Lane-change maneuvers consuming freeway capacity*, in Hoogendoorn et al. [58], pp. 3–14.

[25] M. Cremer and J. Ludwig, *A fast simulation model for traffic flow on the basis of boolean operations*, Math. and Comp. in Sim. **28** (1986), 297–303.

[26] Z. Csahok and T. Vicsek, *Traffic models with disorder*, J. Phys.: Condensed Matter **27** (1994), no. 16, L591.

[27] C.F. Daganzo, M.J. Cassidy, and R.L. Bertini, *Possible explanations of phase transitions in highway traffic*, Transp. Res. A **33** (1999), 365–379.

[28] G. Diedrich, L. Santen, A. Schadschneider, and J. Zittartz, *Effects of on- and off-ramps in cellular automata models for traffic flow*, IJMPC **11** (2000), 335–345.

[29] C. Domb and J.L. Lebowitz (eds.), *Phase transition and critical phenomena*, vol. 17, Academic Press, New York, 1995.

[30] L. C. Edie and R. S. Foote, *Traffic flow in tunnels*, Highway Research Board, Proc. Annu. Meet. **37** (1958), 334–344.

[31] S. El Yacoubi, B. Chopard, and S. Bandini (eds.), *Cellular automata - 7th international conference on cellular automata for research and industry, acri 2006*, Perpignan, France, Springer, Berlin Heidelberg, September 2006.

[32] H. Emmerich and E. Rank, *Investigating traffic flow in the presence of hindrances by cellular automata*, Physica A **216** (1995), no. 4, 435.

[33] J. Esser, L. Neubert, J. Wahle, and M. Schreckenberg, *Microscopic online simulation of urban traffic*, Proc. of the 14th ITS (A. Ceder, ed.), Pergamon, 1999, pp. 535–554.

[34] J. Esser and M. Schreckenberg, *Microscopic simulation of urban traffic based on cellular automata*, Int. J. of Mod. Phys. C **8** (1997), 1025–1036.

[35] M.R. Evans, *Bose-Einstein condensation in disordered exclusion models and relation to traffic flow*, Europhys. Lett. **36** (1996), no. 1, 13–18.

[36] M.R. Evans, *Exact steady states of disordered hopping particle models with parallel and ordered sequential dynamics*, J. Phys. A **30** (1997), no. 16, 5669–5685.

[37] M. Fukui, Y. Sugiyama, M. Schreckenberg, and D.E. Wolf (eds.), *Traffic and granular flow '01*, Tokyo, Springer, 2003.

[38] M. Gardner, *The fantastic combinations of john conway's new solitaire game "life"*, Sc. American **220** (1970), 120–123.

[39] M. Goldbach, A. Eidmann, and A. Kittel, *Simulation of multilane freeway traffic with detailed rules deduced from microscopic driving behavior*, Phys. Rev. E **61** (2000), R1239–1246.

[40] B. D. Greenshields, *A study of traffic capacity*, Proceedings of the Highway Research Board (Washington, D.C.), vol. 14, Highway Research Board, 1935, pp. 448–477.

[41] S.F. Hafstein, R. Chrobok, A. Pottmeier, M. Schreckenberg, and F. Mazur, *A high-resolution cellular automata traffic simulation model with application in a freeway traffic information system*, Computer-Aided Civil and Infrastructure Engineering **19** (2004), no. 5, 338–350.

[42] F.L. Hall, *Traffic stream characteristics*, Traffic Flow Theory – A state-of-the-art report (Washington D.C.), Transp. Res. Board, 1992.

[43] F.L. Hall, B.L. Allen, and M.A. Gunter, *Empirical analysis of freeway flow-density relationships*, Transp. Res. A **20** (1986), 197–210.

[44] F.L. Hall and T.N. Lam, *The characteristics of congested flow on a freeway across lanes, space and time*, Transp. Res. A **22** (1988), 45–56.

[45] D. Helbing, *Empirical traffic data and their implications for traffic modelling*, Phys. Rev. E **55** (1996), R25–R28.

[46] D. Helbing, *Modeling multi-lane traffic flow with queuing effects*, Physica A **242** (1997), 175–194.

[47] D. Helbing, *Verkehrsdynamik*, Springer, Berlin, 1997, (in german).

[48] D. Helbing, *Traffic and related self-driven many-particle systems*, Rev. Mod. Phys. **73** (2001), 1067–1141.

[49] D. Helbing, D. Batic, M. Schönhof, and M. Treiber, *Modelling widely scattered states in 'synchronized' traffic flow and possible relevance for stock market dynamics*, Physica A **303** (2002), no. 1-2, 251–260.

[50] D. Helbing, A. Hennecke, and M. Treiber, *Phase diagram of traffic states in the presence of inhomogeneities*, Phys. Rev. Lett. **82** (1999), 4360–4363.

[51] D. Helbing, H.J. Herrmann, M. Schreckenberg, and D.E. Wolf (eds.), *Traffic and granular flow '99*, Heidelberg, Springer, 2000.

[52] D. Helbing and B.A. Huberman, *Coherent moving states in highway traffic*, Nature **396** (1998), 738.

[53] D. Helbing, D. Mukamel, and G.M. Schütz, *Global phase diagram of a one-dimensional driven lattice gas*, Phys. Rev. Lett. **82** (1999), 10.

[54] D. Helbing and M. Schreckenberg, *Cellular automata simulating experimental properties of traffic flow*, Phys. Rev. E **59** (1999), 2505–2508.

[55] D. Helbing and B. Tilch, *Generalized force model of traffic dynamics*, Phys. Rev. E **58** (1998), 133.

[56] D. Helbing and M. Treiber, *Gas-kinetic-based traffic model explaining observed hysteretic phase transition*, Phys. Rev. Lett. **81** (1998), 3042–3045.

[57] R. Herman and R. W. Rothery, *Car following and steady-state flow*, Proceedings of the 2nd International Symposium on the Theory of Traffic Flow (Bonn, Germany), 1965.

[58] S.P. Hoogendoorn, S. Luding, P.H.L. Bovy, M. Schreckenberg, and D.E. Wolf (eds.), *Traffic and granular flow '03*, Berlin, Springer, 2005.

[59] B. A. Huberman and D. Helbing, *Economics-based optimization of unstable flows*, Europhys. Lett. **47** (1999), 196–202.

[60] InnovationNiedersachsen : ITS, 2001, `http://telematik.niedersachsen.de/index.php?id=13`.

[61] Institute of Transportation Engineers, Washington, DC, *Traffic Engineering Handbook*, 5 ed., 1999.

[62] S.A. Janowsky and J.L. Lebowitz, *Finite-size effects and shock fluctuations in the asymmetric, simple-exclusions process*, Phys. Rev. A **45** (1992), 618.

[63] S.A. Janowsky and J.L. Lebowitz, *Exact results for the asymmetric simple exclusion process with a blockage*, J. Stat. Phys. **77** (1994), no. 1-2, 35–51.

[64] R. Jiang and Q.-S. Wu, *Cellular automata models for synchronized traffic flow*, J. Phys. A **36** (2003), no. 2, 381–390.

[65] A. John, A. Schadschneider, D. Chowdhury, and K. Nishinari, *Collective effects in traffic on bi-directional ant trails*, Journal of Theoretical Biology **231** (2004), 279–285.

[66] O. Kaumann, K. Froese, R. Chrobok, J. Wahle, L. Neubert, and M. Schreckenberg, *On-line simulation of the freeway network of North Rhine-Westphalia*, in Helbing et al. [51], pp. 351–356.

[67] B.S. Kerner, *Experimental features of self-organization of traffic flow*, Phys. Rev. Lett. **81** (1998), 3797–3800.

[68] B.S. Kerner, *Traffic flow: Experiment and theory*, Traffic and Granular Flow '97 (Singapore) (M. Schreckenberg and D. E. Wolf, eds.), Springer, 1998, pp. 239–267.

[69] B.S. Kerner, *The physics of traffic*, Physics World **8/99** (1999), 25–30.

[70] B.S. Kerner, *Experimental features of the emergence of moving jams in free traffic flow*, J. Phys. A **33** (2000), 221–228.

[71] B.S. Kerner, *Phase transitions in traffic flow*, in Helbing et al. [51], pp. 253–282.

[72] B.S. Kerner, *Complexity of synchronized flow and related problems for basic assumptions of traffic flow theories*, Network and Spatial Economics **1** (2001), 35–76.

[73] B.S. Kerner, *Empirical macroscopic features of spatial-temporal traffic patterns at highway bottlenecks*, Phys. Rev. E **65** (2002), 046138.

[74] B.S. Kerner, *Three phase traffic theory*, in Fukui et al. [37], pp. 13–50.

[75] B.S. Kerner, *The physics of traffic*, Springer, Berlin, 2004.

[76] B.S. Kerner, *Control of spatiotemporal congested traffic patterns at highway bottlenecks*, Physica A **355** (2005), no. 2-4, 565–601.

[77] B.S. Kerner and S.L. Klenov, *A miroscopic model for phase transitions in traffic flow*, J. Phys. A **35** (2002), no. 3, L31–L43.

[78] B.S. Kerner and S.L. Klenov, *Comparison of congested pattern features at different freeway bottlenecks*, in Hoogendoorn et al. [58], pp. 141–160.

[79] B.S. Kerner and S.L. Klenov, *Probabilistic breakdown phenomenon at on-ramp bottlenecks in three-phase traffic theory: Congestion nucleation in spatially non-homogeneous traffic*, Physica A **364** (2006), 473–492.

[80] B.S. Kerner, S.L. Klenov, A. Hiller, and H. Rehborn, *Microscopic features of moving jams*, Phys. Rev. E **73** (2006), 046107.

[81] B.S. Kerner, S.L. Klenov, and D.E. Wolf, *Cellular automata approach to three-phase traffic theory*, J. Phys. A **35** (2002), no. 47, 9971–10013.

[82] B.S. Kerner, S.L. Klenov, and D.E. Wolf, *Congestion due to merging roads: Predictions of three-phase traffic theory*, in Hoogendoorn et al. [58], pp. 161–172.

[83] B.S. Kerner and P. Konhäuser, *Structure and parameters of clusters in traffic flow*, Phys. Rev. E **50** (1994), 54–83.

[84] B.S. Kerner and H. Rehborn, *Experimental features and characteristics of traffic jams*, Phys. Rev. E **53** (1996), R1297–1300.

[85] B.S. Kerner and H. Rehborn, *Experimental properties of complexity in traffic flow*, Phys. Rev. E **53** (1996), R4275–4278.

[86] B.S. Kerner and H. Rehborn, *Experimental properties of phase transitions in traffic flow*, Phys. Rev. Lett. **79** (1997), 4030–4033.

[87] P.M. Hui K.H. Chung, *Traffic flow problems in one-dimensional inhomogeous media*, J. Phys. Soc. Japan **63** (1994), no. 12, 4338–4341.

[88] W. Knospe, *Synchronized traffic: Microscopic modeling and empirical observations*, Ph.D. thesis, Universität Duisburg, Duisburg, 2002.

[89] W. Knospe, L. Santen, A. Schadschneider, and M. Schreckenberg, *Disorder effects in ca-models for traffic flow*, in Schreckenberg and Wolf [157], pp. 349–354.

[90] W. Knospe, L. Santen, A. Schadschneider, and M. Schreckenberg, *Disorder effects in cellular automata for two-lane traffic*, Physica A **265** (1999), 614–633.

[91] W. Knospe, L. Santen, A. Schadschneider, and M. Schreckenberg, *Towards a realistic microscopic description of highway traffic*, J. Phys. A **33** (2000), L477–L485.

[92] W. Knospe, L. Santen, A. Schadschneider, and M. Schreckenberg, *Human beavior as origin of traffic phases*, Phys. Rev. E **65** (2001), 015101.

[93] W. Knospe, L. Santen, A. Schadschneider, and M. Schreckenberg, *A realistic two-lane traffic model for highway traffic*, J. Phys. A **35** (2002), 3369–3388.

[94] W. Knospe, L. Santen, A. Schadschneider, and M. Schreckenberg, *Single-vehicle data of highway traffic: Microscopic description of traffic phases*, Phys. Rev. E **65** (2002), 056133.

[95] W. Knospe, L. Santen, A. Schadschneider, and M. Schreckenberg, *Empirical test for cellular automaton models of traffic flow*, Phys. Rev. E **70** (2004), 016115.

[96] A.B. Kolomeisky, G.M. Schütz, E.B. Kolomeisky, and J.P. Straley, *Phase diagram of one-dimensional driven lattice gases with open boundaries*, J. Phys. A **31** (1998), 6911–6919.

[97] M. Koshi, M. Iwasaki, and I. Ohkura, *Overview on vehicular flow characteristics*, Proc. 8th International Symposium on Transportation and Traffic Theory (Toronto), University of Toronto Press, 1983, pp. 403–426.

[98] S. Krauss, P. Wagner, and C. Gawron, *Metastable states in a microscopic model of traffic flow*, Phys. Rev. E **55** (1997), no. 5, 5597–5602.

[99] T. Kretz and M. Schreckenberg, *The F.A.S.T.-Model*, in El Yacoubi et al. [31], pp. 712–715.

[100] J. Krug, *Platoon formation as a critical phenomenon*, in Schreckenberg and Wolf [157], pp. 285–300.

[101] J. Krug and J.A. Ferrari, *Phase transitions in driven diffuse systems with random rates*, J. Phys. A **29** (1996), 465.

[102] D.V. Ktitarev, D. Chowdhury, and D.E. Wolf, *Stochastic traffic model with random deceleration probabilities: Queuing and power law gap distribution*, J. Phys. A **30** (1997), 221.

[103] R. Kühne, R. Mahnke, I. Lubashevsky, and J. Kaupužs, *Probabilistic description of traffic breakdowns*, Phys. Rev. E **65** (2002), no. 6, 066125–1–066125–13.

[104] R.D. Kühne and S. Immes, *Freeway speed distribution and acceleration noise – calculations from a stochastic continuum theory and comparison with measurements*, Proceedings of the 10th International Symposium on Transportation and Traffic Theory (New York) (N.H. Gartner and N.H.M. Wilson, eds.), Elsevier, 1987, pp. 119–137.

[105] L. D. Landau and E. M. Lifschitz, *Lehrbuch der theoretischen physik, bd.5, statistische physik*, Harri Deutsch, Ffm., 1991.

[106] H. Y. Lee, H. W. Lee, and D. Kim, *Origin of synchronized traffic flow on highways and its dynamic phase transition*, Phys. Rev. Lett. **81** (1998), no. 5, 1130–1133.

[107] H.K. Lee, R. Barlović, M. Schreckenberg, and D. Kim, *Mechanical restriction versus human overreaction triggering congested traffic states*, Phys. Rev. Lett. **92** (2004), no. 23, 238702–1–238702–4.

[108] H.K. Lee, R. Barlović, M. Schreckenberg, and D. Kim, *Pinch effect in s cellular automaton (ca) model for traffic flow*, in Hoogendoorn et al. [58], pp. 253–260.

[109] H.Y. Lee, H.W. Lee, and D. Kim, *Dynamic states of a continuum traffic equation with on-ramp*, Phys. Rev. E **59** (1999), 5101–5111.

[110] H.Y. Lee, H.W. Lee, and D. Kim, *Phase diagram of congested traffic flow: An empirical study*, Phys. Rev. E **62** (2000), 4737–4741.

[111] W. Leutzbach and F. Busch, *Spurwechselvorgänge auf dreispurigen BAB-Richtungsfahrbahnen*, Institut für Verkehrswesen, University of Karlsruhe, 1984, (in german).

[112] M. Lorenz and L. Elefteriadou, *A probabilistic approach to defining freeway capacity and breakdown*, Transp. Res. Circular (2000), 84–95.

[113] I. Lubashevsky, R. Mahnke, P. Wagner, and S. Kalenkov, *Long-lived states in synchronized traffic flow: Empirical prompt and dynamical trap model*, Phys. Rev. E **66** (2002), no. 1, 016117.

[114] S. Maerivoet and B. De Moor, *Cellular automata models of road traffic*, Phys. Rep. **419** (2005), no. 1, 1–64.

[115] J. Marro and R. Dickman (eds.), *Nonequilibrium phase transitions in lattice models*, Cambridge University Press, 1999.

[116] A.D. May, *Traffic flow fundamentals*, Prentice Hall, Englewood Cliffs, 1990.

[117] F. Mazur, *Modellierung von auffahrten und spursperrungen mittels zellularautomaten für den straßenverkehr*, Diplomarbeit, Universität Duisburg-Essen (2004), (in german).

[118] H.S. Mika, J.B. Kreer, and L.S. Yuan, *Dual-mode behaviour of freeway traffic*, Highway Research Record **279** (1969), 1–13.

[119] T. Nagatani, *Car bunching and traffic jams in cellular automaton models*, in Wolf et al. [171], pp. 57–72.

[120] T. Nagatani, *Kinetics of segregation in a two-lane highway traffic flow*, J. Phys. A **29** (1996), 6531–6542.

[121] T. Nagatani, *Stabilization and enhancement of traffic flow by next-nearest neighbor interaction*, Phys. Rev. E **60** (1999), 6395–6400.

[122] T. Nagatani, *Multiple jamming transitions in traffic flow*, Physica A **290** (2001), no. 3-4, 501–511.

[123] K. Nagel, *Particle hopping models and traffic flow theory*, Phys. Rev. E **53** (1996), 4655–4672.

[124] K. Nagel, J. Esser, and M. Rickert, *Large-scale traffic simulations for transport planning*, Ann. Rev. of Comp. Phys. VII (Singapore) (D. Stauffer, ed.), World Scientific, 2000, pp. 151–202.

[125] K. Nagel and M. Paczuski, *Emergent traffic jams*, Phys. Rev. E **51** (1995), 2909–2918.

[126] K. Nagel and M. Schreckenberg, *A cellular automaton model for freeway traffic*, J. Physique I **2** (1992), 2221–2229.

[127] K. Nagel, D. E. Wolf, P. Wagner, and P. Simon, *Two-lane traffic rules for cellular automata: A systematic approach*, Phys. Rev. E **58** (1998), 1425–1437.

[128] P. Nelson, *Synchronized traffic flow from a Lighthill-Whitham model*, Phys. Rev. E **61** (2000), no. 6, R6052–6055.

[129] L. Neubert, *Statistische Analyse von Verkehrsdaten und die Modellierung von Verkehrsfluß mittels zellularer Automaten*, Ph.D. thesis, University of Duisburg, 2000.

[130] L. Neubert, L. Santen, A. Schadschneider, and M. Schreckenberg, *Single-vehicle data of highway traffic: A statistical analysis*, Phys. Rev. E **60** (1999), no. 6, 6480–6490.

[131] L. Neubert, L. Santen, A. Schadschneider, and M. Schreckenberg, *Statistical analyses of freeway traffic*, in Helbing et al. [51], pp. 307–314.

[132] J. von Neumann and A.W. Burks, *Theory of self-reproducing automata*, Univ. of Illinois Press, Urbana, IL, 1966.

[133] K. Nishinari, Y. Kanayama, Y. Okada, P. Greulich, A. Schadschneider, and D. Chowdhury, *Stochastic modelling and experiments on intra-cellular transport of single-headed molecular motors*, in Schadschneider et al. [154], pp. 263–268.

[134] Physics of Transport and Traffic, *autobahn.nrw.de*, 2001, `http://autobahn.nrw.de`.

[135] M. Papageorgiou, H. Hadj-Salem, and J.-M. Blosseville, *Alinea: a local feedback control law for on-ramp metering.*, Transp. Res. Record **1320** (1991), 58–64.

[136] M. Papageorgiou, H. Haj-Salem, and F. Middelham, *ALINEA local ramp metering: Summary of field results.*, Transp. Res. Record **1603** (1998), 90–98.

[137] B. Persaud, S. Yagar, and R. Brownlee, *Exploration of the breakdown phenomenon in freeway traffic*, Transp. Res. Record **1634** (1998), 64–69.

[138] V. Popkov and G.M. Schütz, *Steady-state selection in driven diffusive systems with open boundaries*, Europhys. Lett **48** (1999), 257–263.

[139] A. Pottmeier, R. Barlović, W. Knospe, A. Schadschneider, and M. Schreckenberg, *Localized defects in a cellular automaton model for traffic flow with phase separation*, Physica A **308** (2002), 471–482.

[140] A. Pottmeier, R. Barlović, W. Knospe, A. Schadschneider, and M. Schreckenberg, *Localized defects in a cellular automaton model for traffic flow with phase separation*, in Fukui et al. [37], pp. 109–114.

[141] A. Pottmeier, R. Chrobok, J. Wahle, and M. Schreckenberg, *On-line simulation of large scale networks*, Operation Research Proceedings (P. Chamoni, R. Leisten, A. Martin, J. Minnemann, and H. Stadtler, eds.), Springer, 2001, pp. 311–318.

[142] A. Pottmeier, C. Thiemann, A. Schadschneider, and M. Schreckenberg, *Mechanical restriction vs. human overreaction: the modeling of synchronized two-lane traffic*, International Symposium of Transport Simulation 2006 (ISTS06) (Lausanne, Switzerland) (E. Chung, ed.), vol. 1, 2006, p. 0002.

[143] A. Pottmeier, C. Thiemann, A. Schadschneider, and M. Schreckenberg, *Mechanical restrictions versus human overreaction: Accident avoidance and two-lane traffic simulations*, in Schadschneider et al. [154], pp. 503–508.

[144] K. Preston and M. Duff (eds.), *Modern cellular automata: Theory and applications*, Plenum, 1984.

[145] N. Rajewsky, L. Santen, A. Schadschneider, and M. Schreckenberg, *The asymmetric exclusion process: Comparison of update procedures*, J. Stat. Phys. **92** (1998), 151–194.

[146] M. Rickert and K. Nagel, *Experiences with a simplified microsimulation for the Dallas/Forth-Worth area*, Int. J. of Mod. Phys. C **8** (1997), 483–503.

[147] M. Rickert, K. Nagel, M. Schreckenberg, and A. Latour, *Two lane traffic simulations using cellular automata*, Physica A **231** (1996), 534–550.

[148] S. Rosswog and P. Wagner, *Towards a macroscopic modeling of the complexity in traffic flow*, Phys. Rev. E **65** (2002), no. 3, 036106.

[149] H. H. Salem and M. Papageorgiou, *Ramp metering impact on urban corridor traffic: Field results*, Transp. Res. A **29** (1995), 303–319.

[150] L. Santen, *Numerical investigations of discrete models for traffic flow*, Ph.D. thesis, Universität zu Köln, 1999.

[151] A. Schadschneider, *The Nagel-Schreckenberg model revised*, Eur. Phys. J. B **10** (1999), 573–582.

[152] A. Schadschneider, *Bionics-inspired cellular automaton model for pedestrian dynamics*, in Fukui et al. [37], pp. 499–509.

[153] A. Schadschneider, *Cellular automaton approach to pedestrian dynamics - theory*, in Schreckenberg and Sharma [156], pp. 76–85.

[154] A. Schadschneider, T. Pöschel, R. Kühne, M. Schreckenberg, and D.E. Wolf (eds.), *Traffic and granular flow '05*, Berlin, Springer, 2007.

[155] A. Schadschneider and M. Schreckenberg, *Traffic flow models with 'slow-to-start' rules*, Ann. Phys. **6** (1997), 541–551.

[156] M. Schreckenberg and S.D. Sharma (eds.), *Pedestrian and evacuation dynamics*, Berlin Heidelberg, Springer, 2002.

[157] M. Schreckenberg and D.E. Wolf (eds.), *Traffic and granular flow '97*, Singapore, Springer, 1998.

[158] G. Schütz, *Exactly solvable models for many-body systems far from equilibrium*, Phase Transitions and Critical Phenomena (London) (C. Domb and J.L. Lebowitz, eds.), Phase Transition Phenomena, vol. 19, Academic Press, 2000, pp. 3–255.

[159] U. Sparmann, *Spurwechselvorgänge auf zweispurigen BAB-Richtungsfahrbahnen*, Forschung Straßenbau und Straßenverkehrstechnik Heft 263 (Bonn-Bad Godesberg), Bundesminister für Verkehr, 1978, (in german).

[160] D. Stauffer, *Computer simulations of cellular automata*, J. Phys. A **24** (1991), 909–927.

[161] M. Takayasu and H. Takayasu, *1/f-noise in a traffic flow model*, Fractals **1** (1993), 860–866.

[162] B. Tilch and D. Helbing, *Evaluation of single vehicle data in dependence of the vehicle-type, lane and site*, in Helbing et al. [51], pp. 333–338.

[163] E. Tomer, L. Safonov, and S. Havlin, *Presence of many stable nonhomogeneous states in an inertial car-following model*, Phys. Rev. Lett. **84** (2000), no. 2, 382–385.

[164] TomTom Mobility Solutions, 2006, `http://www.mobility.tomtom.de`.

[165] M. Treiber and D. Helbing, *Macroscopic Simulation of Widely Scattered Synchronized Traffic States*, J. Phys. A **32** (1999), L17–L23.

[166] C. Wagner, *Asymptotic solutions for a multi-anticipative car-following model*, Physica A **260** (1998), no. 1-2, 218–224.

[167] P. Wagner, *Traffic simulations using cellular automata: Comparison with reality*, in Wolf et al. [171], pp. 199–203.

[168] P. Wagner, K. Nagel, and D. E. Wolf, *Realistic multi-lane traffic rules for cellular automata*, Physica A **234** (1997), 687–698.

[169] J. Wahle, R. Chrobok, A. Pottmeier, and M. Schreckenberg, *A microscopic simulator for freeway traffic*, Networks and Spatial Economics **2** (2002), 371–386.

[170] J. Wahle, L. Neubert, and M. Schreckenberg, *A cellular automaton traffic flow model for online simulation of traffic*, Parallel Comp. **27** (2001), 719–735.

[171] D.E. Wolf, M. Schreckenberg, and A. Bachem (eds.), *Traffic and granular flow*, Singapore, World Scientific, 1996.

[172] S. Wolfram, *Theory and applications of cellular automata*, World Scientific, Singapore, 1986.

[173] S. Wolfram, *A new kind of science*, Wolfram Media, Inc, Ilinois, USA, 2002.

[174] H.M. Zhang and W.W. Recker, *On optimal freeway ramp control policies for congested traffic corridor*, Transp. Res. B **33** (1999), no. 6, 417–436.

[175] H. Zurlinden, *Ganzjahresanalyse des Verkehrsflusses als Zufallsgröße*, Schriftenreihe des Lehrstuhls for Verkehrswesen der Ruhr-Universität Bochum **26** (2003), (in german).

Summary and Outlook

The aims and the objectives of this thesis were to develop an elaborate multi-lane cellular automaton model for vehicular traffic and validate its conformance to empircal data. The analyses showed that the presented approach is capable to reproduce the macroscopic and microscopic empirical data with a high degree of realism. Thus, this model fulfills the preconditions to serve as the basis for sophisticated simulations, e.g., of realistic highway networks.
Special concern in the analysis was laid on the properties of synchronized traffic as this traffic state is still least understood. In particular, the microscopic features and the occurrence in realistic environments were analyzed with methods from statistical physics. Moreover, synchronized traffic seems to be the most important and most desirable traffic state as the capacity of the road is very high despite the high density. Further, the stability of synchronized traffic is of main interest as wide moving jams form therein in particular in the vicinity of a bottleneck, e.g., an on-ramp.
The thesis is arranged in four parts. The first part covers the theoretical background of the basic measurement methods, model approaches, and the empirical results. The first chapter provided an introduction and the outline of this thesis. This was followed by an overview of the basic measurement methods in the real world as well as in the simulations. The basic modeling concepts concerning cellular automaton models for vehicular traffic were reviewed in chapter 3. Calibration methods and the validation of single-vehicle as well as aggregated data of the simulation results based on empirical data were discussed in the next chapter. The most important facts were summarized therein and methodologies were presented to validate any simulation model for vehicular traffic.
In the second part, the empirical features, although gathered at two-lane sections of the highway, were utilized to validate the single-lane model by Lee *et al.* which built the basis for the further developments of this thesis. This model was considered in this thesis as it proposes the interesting approach to include the local neighborhood in the velocity update and as it is capable to reproduce synchronized traffic on a single-lane road.
After the basic features were recapitulated, new results concerning the comparison with empirical single-vehicle data were discussed. It was shown that the model by Lee *et al.* is in good agreement with the empirical findings. Concerning the vehicle-vehicle correlation and the autocorrelation in synchronized traffic, the model approach is in very good agreement with the empirical findings. The autocorrelation of the temporally aggregated data vanishes whereas the velocities of succeeding vehicles are correlated. The time headway distribution is reproduced very well for free-flow traffic, but the distribution in synchronized traffic is not convincing. This differs from the results in [107]. The time headway distribution of the single-lane model in the synchronized regime was not reproduced here as no headways shorter than one second were detected. This is probably based on a different measurement method. Further, the periodic single-lane system suffers from accidents in the stationary state. The accidents are a consequence of the intrinsic dynamics of the model by Lee *et al.* and not only caused by inserted vehicles as stated in [107]. Thus, the reasons for the accidents were analyzed in great detail and two mechanisms were identified.

It was shown that the formation of platoons of at least three equally fast and optimistic vehicles gives reason for accidents. If the leading vehicle changes its attitude because of its predecessors, the last vehicle of the platoon may react too late on the deceleration of the leader. It is not possible anymore to brake fast enough, i.e., the vehicle cannot reach its safe velocity because of the limited deceleration capability. Another reason for an accident, which does not appear in the stationary state of a closed single-lane system, but becomes important when vehicles are inserted into the street or the system is extended to a multi-lane road. If a slow vehicle is set in front of an optimistic vehicle with its former leader speeding away an accident becomes likely as well. The successor might get to close before the distance criterion forces him to brake and reach its safe velocity if the inserted vehicle does not accelerate but dawdles. An accident would be the consequence.
The analysis of accidents underlined that the attitude of the drivers, which determines the local neighborhood and thus the driving strategy, is the most important model parameter. The ratio of optimistic vehicles follows the attributes of the global fundamental diagram and thus the characteristics of the different traffic patterns. Therefore, the attitude distribution is a measure for the type of traffic that is present in the system as it adopts different values for the three traffic states. The metastability of the synchronized traffic as well as that of the free-flow is reflected by the different fraction of optimistic vehicles if the system is initialized appropriately, i.e., the different initialization approaches illuminates that. The other parameters affect in general the synchronized traffic: The density interval of the synchronized traffic is calibrated by v_{slow}, the cut-off of the time-headway distribution is governed by t_{safe}, and the value of the flow in synchronized traffic is mainly affected by g_{add}.
Special concern was laid on the measurement of the life-time of the synchronized traffic in the periodic system. It was shown that the life-time is strongly depending on the initial density. At lower densities the synchronized state is stable or at least very long living. For higher densities the life-time decreases exponentially. Local intrinsic perturbations form a seed for a compact jam.
Motivated by the accidents in the original model, it was modified so that the occurring dangerous configurations of the original model formulation are avoided and an accident free model despite the limited deceleration is provided. Nevertheless, the model dynamics in dense traffic is affected by the changes in the algorithm. Synchronized traffic was stabilized and the separation at high densities between wide moving jams and free-flow changed to a sequence of free-flow followed upstream by synchronized traffic and wide moving jams. The latter is again followed by free-flow. However, the findings were used to modify the original model formulation so that it is robust against the dangerous configurations that may arise by inserted vehicles. This is needed for the analysis of two-lane traffic and complex topologies. The calculation of the attitude parameter is changed so that no additional accidents appear that are caused by inserted vehicles.
However, the analysis showed the complications that arise if a limited deceleration is applied. Thus, one idea may be to introduce an "emergency brake" that is applied if stationary driving would lead to an accident, but the benefits of the limited deceleration should not be thrown away. For example, the decoupling of the two lanes if the velocity difference between them is too high is a feature that improves the model approach. Thus, in planned situations like a lane change the limited deceleration is an interesting feature that leads to a more realistic model. Otherwise, if a critical situation emerges, a higher deceleration capability may be assigned to the vehicles to avoid accidents in particular as

the value for the deceleration capability is rather small compared to real cars or trucks.
In the third part based on the modified and more robust model an extended two-lane cellular automaton model was developed. Its lane change procedure is conceptually different from former approaches in two aspects. On the one hand, the limited deceleration capability enforces an accurate consideration of the safety of the lane change. On the other hand, the criterion whether a vehicle intends to change the lane is extended to the neighborhood of the vehicles including the destination lane. It is calculated on which lane the driving situation is more promising, i.e., the velocity is higher.
The analysis of the approach led to interesting results. In general, a better agreement with the empirical data was found in the two-lane system than in the single-lane approach. This is especially remarkable, as the empirical data are always gathered at multi-lane sections of the network. The local fundamental diagram showed a much wider scattered region of synchronized traffic and the time headway distribution of the synchronized traffic showed time headways shorter than one second as proposed by the empirical findings. Thus, the lane changes are important to reproduce empirical facts qualitatively and quantitatively. Further analyses of empirical data on single-lane section are needed to verify this. Note, all empirical data that served as the reference in this study were gathered on multi-lane sections of the highway.
Further, specific attributes of the two-lane model were analyzed as well. One important characteristic is the lane change frequency. It was pointed out that the number of lane changes is in agreement with the empirical findings [159].
A very interesting result was the direct influence of the limited deceleration capability on the model dynamics of the two-lane extension. Several configurations can emerge in which a vehicle cannot change the lane as it would be too dangerous for the follower on the destination lane. This happens if the velocity difference between the lanes is too large. The two lanes may decouple: On one lane a compact jam emerges whereas on the other lane free-flow is still preserved.
In the last part, the developed two-lane model was applied to investigate the influence of two defects, an on-ramp and a velocity defect. For both defects, the single and a two-lane street with an on-ramp the empirically observed patterns of synchronized traffic were found. Thus, the two-lane approach is capable to reproduce not only the microscopic findings but also the macroscopic traffic patterns of widening, localized, and moving synchronized traffic. The pinch effect is reproduced as well in both cases. Similar results showed the analysis of a velocity defect. The same characteristic patterns of synchronized traffic were observed there. Thus, different bottlenecks show similar characteristics as already shown for cellular automaton models with less complex dynamics.
The life-time of the synchronized traffic, here especially of the widening synchronized traffic, was investigated afterwards. This led to a better understanding of the processes that lead to a breakdown of the traffic in the neighborhood of an on-ramp. It is fundamentally different from the mechanisms that result in a breakdown of synchronized traffic without extrinsic interferences as in a periodic system. The life time is shorter in the former as the intrinsic perturbations are boosted by the inserted vehicles.
The results of the life time analysis are especially important with respect to the controlling of ramp metering procedures. The currently used algorithms do not account for the existence and the stochasticity of the life-time of synchronized traffic and thus do not stabilize this traffic state by an intelligent vehicle insertion. The simulations and recent empirical findings underline that this would be promising.

Further, the understanding of the breakdown process is indispensable for realistic traffic simulations since the stability of a traffic state is one of the most important elements for a reliable traffic forecast.
In summary, the excellent reproduction of the empirical findings of the new extended two-lane model shows that it is capable to serve as a basis for the simulation of complex topologies like whole traffic networks. Thus, this approach will be implemented as the simulation kernel of autobahn.nrw.de. This raises the questions, how this model scales when large neworks like that of North Rhine-Westphalia with a length of 2,350 km are simulated and how realistic the resulting traffic information are.
Furthermore, from a practical point of view it would be interesting to investigate objectives like: How does this model perform in a large traffic network and how realistic is the resulting traffic information?

Zusammenfassung und Ausblick

Das Ziel dieser Dissertation war die Entwicklung und Validierung eines wirklichkeitsnahen Zellularautomaten-Modells für den mehrspurigen Straßenverkehr. Die Analysen in dieser Arbeit zeigten, dass das präsentierte Modell in der Lage ist, sowohl die makroskopischen als auch die mikroskopischen empirischen Daten mit einem hohen Grad an Realitätsnähe zu reproduzieren. Es erfüllt damit alle Voraussetzungen, um es als Basis für realistische Simulationen von Autobahn-Netzwerken zu verwenden.
Bei den Untersuchungen wurde insbesondere Wert auf die Eigenschaften des synchronisierten Verkehrs gelegt, weil dieser Verkehrszustand der zurzeit am wenigsten verstandene ist. Ein besonderes Augenmerk galt der Analyse der mikroskopischen Eigenschaften mit Hilfe von Methoden der statistischen Physik sowie dem Auftreten des synchronisierten Verkehrs in realistischen Umgebungen. Außerdem ist der synchronisierte Verkehr von besonderer Bedeutung und erstrebenswert, da trotz der hohen Dichte an Fahrzeugen große Flüsse erreicht werden können. Ein weiterer wichtiger Aspekt, der in dieser Arbeit behandelt wurde, ist die Stabilität bzw. die Lebensdauer des synchronisierten Verkehrs, denn gerade hier entstehen kompakte Staus, die zu vermeiden sind. Dies geschieht hauptsächlich in der Nähe von Störstellen wie z.B. Zufahrten.
Um diese Fragestellungen zu behandeln, wurde die Arbeit in vier Hauptabschnitte aufgeteilt. Im ersten Teil wurde die Arbeit in den Kontext bisheriger Forschungsergebnisse gesetzt und die theoretischen Grundlagen behandelt. Das erste Kapitel gab hierbei eine Einführung, stellte den Zusammenhang mit den Resultaten bisheriger Untersuchungen her und zeigte die Gliederung der Arbeit auf. Im zweiten Kapitel wurden sowohl die grundlegenden Messmethoden der empirischen Daten als auch der Simulationsergebnisse zusammengefasst. Außerdem wurden die wichtigsten empirischen Messergebnisse diskutiert und vorgestellt. Insbesondere wurden die Ergebnisse aus Einzelfahrzeug-Daten benutzt, um ein Konzept zur Kalibrierung und Validierung von Simulationsmodellen für den Straßenverkehr zu erstellen.
Im zweiten Teil wurden die empirischen Daten, auch wenn sie auf zweispurigen Abschnitten der Autobahn gesammelt wurden, benutzt, um das Einspur-Modell von Lee *et al.* [107, 108], das die Basis für die weitere Entwicklung innerhalb dieser Arbeit bildet, zu validieren. Dieses Modell wurde gewählt, weil es den interessanten Ansatz nutzt, die Umgebung des Fahrzeugs in die Bestimmung der Geschwindigkeit einzubinden und weil es synchronisierten Verkehr auf einspurigen Straßen reproduzieren kann.
Nachdem die in [107, 108] behandelten grundlegenden Eigenschaften des Modells kurz zusammengefasst wurden, sind neue Ergebnisse bezüglich des Vergleichs mit Einzelfahrzeug-Daten vorgestellt worden. Hierbei wurde betont, dass die Dynamik des Modells von Lee *et al.* gut mit den empirischen Ergebnissen übereinstimmt. Beispielsweise ist die Übereinstimmung der Autokorrelation und der Fahrzeug-Fahrzeug Korrelation im synchronisierten Verkehr mit den empirischen Ergebnissen sehr hoch. Während die Autokorrelation der zeitlich aggregierten Daten verschwindet, sind die Geschwindigkeiten aufeinander folgender Fahrzeuge korreliert. Aber auch die Zeitlücken-Verteilung im Freifluss wird detailliert nachgebildet. Dies gilt allerdings nicht für die Zeitlücken im synchronisierten Verkehr. Hier

werden keine Zeitlücken kleiner als eine Sekunde gemessen. Dies steht im Widerspruch zu den Ergebnissen in [107, 108], wo die empirisch gemessenen kurzen Zeitlücken gefunden wurden. Der Grund dafür ist wahrscheinlich eine unterschiedliche Messmethode.
Außerdem wurden in Rahmen der Untersuchungen zu dieser Arbeit Unfälle im stationären Zustand detektiert, und nicht nur in Systemen, in die von außen Fahrzeuge eingesetzt werden, wie in [107, 108] erwähnt. Um die Gründe für diese Unfälle zu bestimmen, wurden Fahrzeug-Konfigurationen, die zu gefährlichen Situationen führen, sehr genau untersucht. Hierbei wurden zwei unterschiedliche Mechanismen bestimmt, die bei ungünstigen Konfigurationen der Fahrzeuge zu Unfällen führen können. Die erste Konstellation sind Kolonnen von mindestens drei gleich schnellen Fahrzeugen. Unfälle können geschehen, wenn das führende Fahrzeug aufgrund der ihm vorausfahrenden Fahrzeuge bremst und das dritte Auto zu spät darauf reagieren kann. Dann ist es wegen des begrenzten Bremsvermögens nicht mehr in der Lage, eine sichere Geschwindigkeit zu erreichen. Ein weiteres Scanario, das zu Unfällen führen kann, tritt im stationären Zustand des periodischen Systems nicht auf, sondern nur, wenn Fahrzeuge von außen eingefügt werden. Ist die Geschwindigkeitsdifferenz zwischen dem eingefügten Fahrzeug und dem hinter ihm fahrenden optimistischen Fahrzeug zu groß, greift das geschwindigkeitsreduzierende Abstands-Argument zu spät und es kommt auch hier zu einem Unfall.
Die Analysen zu den Unfällen unterstreichen, dass die Einstellung des Fahrers, welche das Ergebnis der Bewertung der Umgebung ist und worauf er sein Fahrverhalten auslegt, der wichtigste Modellparameter ist. Dessen Verlauf in Abhängigkeit von der Dichte folgt genau dem des globalen Fundamentaldiagramms und charakterisiert damit auch die verschiedenen Verkehrszustände. Der Anteil der optimistischen Fahrer unterscheidet sich klar in den einzelnen Verkehrszuständen und ist damit ein Maß für den Verkehrszustand im System. Die Metastabilität wird ebenfalls in der Verteilung der optimistischen Fahrer sichtbar, wenn das System geeignet initialisiert wird, d.h., zum einen mit homogen verteilten Fahrzeugen und zum anderen mittels eines kompakten Staus. Die weiteren Modell-Parameter beeinflussen insbesondere den synchronisierten Verkehr. Das Dichteintervall, in dem synchronisierter Verkehr gefunden wird, ist von v_{slow} bestimmt, die untere Grenze der Zeitlücken durch t_{safe} und die Höhe des Flusses im synchronisierten Verkehr hauptsächlich durch g_{add}.
Ein großes Augenmerk wurde auf die Analyse der Lebensdauer des synchronisierten Verkehrs gelegt. Es wurde gezeigt, dass diese stark von der Dichte abhängt. Bei kleinen Dichten ist der synchronisierte Verkehr langlebig, während die Lebensdauer zu höheren Dichten exponentiell abnimmt.
Durch die auftretenden Unfälle motiviert, wurde das ursprüngliche Modell von Lee *u.a.* so verändert, dass Unfälle trotz des begrenzten Bremsvermögens vermieden werden können. Allerdings wurde dadurch die Dynamik des Modells bei hohen Dichten verändert. Der synchronisierte Verkehr wird stabilisiert und die im ursprünglichen Modell auftretende Aufteilung des Verkehrs in Freifluss und Stauwellen tritt nicht mehr auf, sondern der Verkehr wird nun aus allen drei Verkehrszuständen gebildet: Ein kompakter Stau wird in Fahrtrichtung von Freifluss gefolgt, der in synchronisiertem Verkehr übergeht und dem erneut ein kompakter Stau folgt. Die Ergebnisse dieser Analyse wurden genutzt, um das Original-Modell so zu modifizieren, dass es robust gegen eingefügte Fahrzeuge wird. Die Beurteilung der Umgebung wird so geändert, dass keine Unfälle aus eingefügten Fahrzeugen resultieren. Dies ist unabdingbar für Mehrspur-Verkehr und Systeme mit Zufahrten.
Die Analysen der Unfälle werfen allerdings auch die Frage auf, ob die Schwierigkeiten

umgangen werden könnten, wenn eine “Notbremsung” eingeführt wird, falls das normale Fahrverhalten zu einem Unfall geführt hätte. Andererseits sollten die Vorteile des begrenzten Bremsvermögens nicht außer Acht gelassen werden. Dies gilt beispielsweise für entkoppelte Fahrspuren, wenn der Geschwindigkeits-Unterschied zwischen den einzelnen Spuren zu groß ist. Das begrenzte Bremsvermögen ist daher ein Charakteristikum, dass in bestimmten Situationen zu einem realistischeren Fahrverhalten führt. Andererseits ist das Bremsvermögen in der Modelldefinition im Vergleich zu realen Werten gering gehalten, so dass in gefährlichen Situationen durchaus ein höherer Wert angebracht sein kann.
Im dritten Teil wurde auf der Basis des modifizierten und daher robusteren Modellansatzes ein Spurwechsel-Algorithmus entwickelt, dessen Ansatz in zwei Punkten von bisherigen Konzepten abweicht. Einerseits erfordert das begrenzte Bremsvermögen der Fahrzeuge eine genaue Beurteilung der Sicherheit des Spurwechsels. Andererseits wird bei der Entscheidung, ob sich ein Spurwechsel lohnt, auch die Zielspur in Betracht gezogen. Dass heißt, es wird geprüft, auf welcher Spur die Geschwindigkeit im nächsten Zeitschritt höher ist.
Die Analyse dieses Ansatzes führte zu interessanten Ergebnissen. Im Allgemeinen waren die Übereinstimmungen der Simulationsergebnisse mit den empirischen Daten genauer als im Einspur-Modell. Dies ist besonders bemerkenswert, da die empirischen Daten auf zweispurigen Abschnitten der Autobahn gesammelt wurden. Der zweidimensionale Bereich des synchronisierten Verkehrs im lokalen Fundamentaldiagramm nimmt einen größeren Bereich ein. Außerdem wurden auch im synchronisierten Verkehr Zeitlücken unterhalb einer Sekunde detektiert. Dies zeigt, dass die Spurwechsel ein wichtiger Faktor sind, damit die empirischen Daten qualitativ und quantitativ reproduziert werden können. Um diese Erkenntnis zu verfestigen, sind allerdings weitere Analysen von empirischen Daten auf einspurigen Straßen nötig. Alle empirischen Daten, die in dieser Arbeit verwendet wurden, sind auf zweispurigen Autobahnen gesammelt worden.
Neben den Charakteristika, die sich auf eine Spur beziehen, wurden auch für den Zweispur-Verkehr typische Eigenschaften diskutiert. Ein wichtiges Attribut ist die Spurwechselhäufigkeit. Die Analysen haben gezeigt, dass die Anzahl der Spurwechsel und deren Abhängigkeit von der Dichte mit der Empirie übereinstimmen.
Im Bezug auf die Spurwechselhäufigkeit hat das begrenzte Bremsvermögen einen direkten und interessanten Einfluss auf die Dynamik des Modells. Es können sich Fahrzeug-Konfigurationen bilden, in denen kein Spurwechsel mehr möglich ist, weil dieser zu gefährlich für das nachfolgende Fahrzeug auf der Zielspur wäre. Dies geschieht dann, wenn die Geschwindigkeits-Unterschiede zu groß sind. Die beiden Spuren sind dann entkoppelt. Während sich auf der einen Spur ein kompakter Stau bildet, hält sich auf der anderen Spur Freifluss aufrecht.
Im letzten Teil dieser Arbeit wurde das entwickelte Zweispur-Modell in realistischen Topologien eingesetzt, um den Einfluss von Störungen wie Auffahrten oder Geschwindigkeitsbegrenzungen zu untersuchen. In der Nähe von Auffahrten wurde sowohl für den Einspur-Ansatz als auch für das Zweispur-Modell die empirisch beobachteten Muster wie sich ausbreitender oder sich bewegender synchronisierter Verkehr beobachtet. Dies zeigt, dass das Zweispur-Modell nicht nur in der Lage ist, die mikroskopischen Eigenschaften des Verkehrs sehr gut nachzubilden, sondern auch die makroskopischen Strukturen sehr genau reproduziert.
Auch bei der Untersuchung der Auffahrten wurde großes Augenmerk auf die Stabilität des synchronisierten Verkehrs gelegt um ein besseres Verständnis der Vorgänge zu bekommen, die zu einem Zusammenbruch des Verkehrs führen. Es wurde gezeigt, dass der

Mechanismus, der in der Nähe einer Auffahrt zu einem Kollaps führt, ein anderer ist, als im periodischen System. Im ersten Fall nimmt die Lebensdauer schneller ab als im zweiten, da die inneren Fluktuationen durch die von außen eingesetzten Fahrzeuge verstärkt werden.
Diese Erkenntnisse zur Lebensdauer sind insbesondere im Hinblick auf Zuflussregelungen interessant. Die zurzeit benutzten Algorithmen ignorieren die Existenz von synchronisiertem Verkehr und dessen begrenzte Lebensdauer und versuchen daher nicht, diesen Verkehrszustand durch eine intelligente Regelung des Zuflusses zu stabilisieren. Die Simulationen unterstreichen jedoch, dass dies sehr aussichtsreich wäre.
Um die Ergebnisse der Untersuchungen der Auffahrten in einen allgemeineren Kontext zu stellen, wurde auch die Auswirkung einer Geschwindigkeitsbegrenzung untersucht. Auch hier wurden die typischen Strukturen des synchronisierten Verkehrs wieder gefunden. Dies zeigt, dass Defekte, wie schon für weitere Zellularautomaten-Modelle gezeigt, allgemein gültige Eigenschaften aufweisen.
Die hervorragenden Eigenschaften des vorgestellten Zweispur-Modells zeigen, dass dieser Ansatz geeignet ist, um komplexe Topologien und ganze Netzwerke zu simulieren. Aus diesem Grund wird dieses Modell den aktuellen Simulationskern von www.autobahn.nrw.de ersetzen. Hieraus ergeben sich dann interessante Fragestellungen, beispielsweise, wie das Modell bei der Simulation von Netzwerken skaliert und wie realistisch die daraus resultierenden Verkehrsinformationen sind.
Des Weiteren bildet dieses Modell, da nun auch realistischer Zweispur-Verkehr modelliert werden kann, eine sehr gute Basis für die Analyse von Algorithmen zur Zuflussregelung oder die Steuerung von variablen Geschwindigkeitsbegrenzungen.

Danksagung

An dieser Stelle möchte ich mich bei den vielen Menschen bedanken, die zum Gelingen dieser Arbeit beigetragen haben.

Mein erster Dank gebührt Herrn Prof. Dr. Michael Schreckenberg für die Betreuung der Arbeit und die Schaffung idealer Arbeitsbedingungen.

Bei Herrn Professor Dr. Andreas Schadschneider bedanke ich mich für freundschaftliche Zusammenarbeit, fachliche Anregungen und unzählige Diskussionen.

Mein weiterer Dank gilt den Mitarbeitern des gesamten Lehrstuhls Physik von Transport und Verkehr. Die gelöste Arbeitsatmosphäre hat viel zum Gelingen der Arbeit beigetragen. Besonders hervorzuheben sind Frau Dr. Dahm-Courths und Dr. Torsten Huisinga für die kurzweiligen Gespräche in den Kaffeepausen.

Für das sorgfältige Korrekturlesen des Manuskripts bedanke ich mich bei Dr. Torsten Huisinga, Prof. Dr. Andreas Schadschneider, Johannes Brügmann, Daniel Weber, Florian Mazur sowie bei Dr. Joachim Wahle und Nadine Wahle.

Ein großer Dank gebührt meinen Eltern Elisabeth und Georg sowie meinem Bruder Daniel, die mich nicht nur während meiner Ausbildung stets unterstützt haben und mich meinen Weg haben gehen lassen.

Nicht zuletzt bedanke ich mich bei meiner Freundin Eva, die mir stets ein liebevoller Ansporn war und somit ganz besonders zum Gelingen dieser Arbeit beigetragen hat.